Electronic Supplementary Material (ESI) for Journal of Materials Chemistry C.

Thieno[3,2-*b*]phosphole-based AIEgens: Facile Preparation and Dual Modulation of Solid-State Luminescence

Nils König[a], Justin Mahnke[a], Yokari Godínez-Loyola[b], Hendrik Weiske[c], Peter Lönnecke[a], Julian Appel[a], C. A. Strassert[b]* and Evamarie Hey-Hawkins[a]*

[a] Dr. Nils König, B. Sc. Justin Mahnke, Dr. Peter Lönnecke, B. Sc. Julian Appel, Prof. Dr. Dr. h.c. Evamarie Hey-Hawkins*, Leipzig University, Faculty of Chemistry and Mineralogy, Institute of Inorganic Chemistry, Johannisallee 29, 04103 Leipzig, Germany. [*] Corresponding Author, E-mail: hey@uni-leipzig.de

[b] M. Sc. Yokari Godínez-Loyola, Prof. Dr. Cristian A. Strassert*, Institut für Anorganische und Analytische Chemie, CiMiC, SoN and CeNTech, Wesfälische Wilhelms-Universität Münster, Heisenbergstraße 11, 48149 Münster, Germany. [*] Corresponding Author, E-mail: cstra_01@uni-muenster.de

[c] M. Sc. Hendrik Weiske, Wilhelm-Ostwald-Institut für Physikalische und Theoretische Chemie, Fakultät für Chemie und Mineralogie, Universität Leipzig, Linnéstraße 2, 04103 Leipzig, Germany

Table of Contents

1 Experimental Methods

1.1 General

All reactions were carried out under dry high purity nitrogen using standard SCHLENK techniques. THF was degassed and distilled from potassium. Chloroform, acetonitrile, diethyl ether, toluene, hexane (mixture of isomers) and dichloromethane were dried and degassed with a SOLVENT PURIFICATION SYSTEM SPS-800 SERIES from MBRAUN. 2,5-dibromothiophene, 2,4-dibromothiophene, phenylbronic acid, 2-thienylbronic acid, 4-biphenylboronic acid, 4-anisylboronic acid, diphenylacetylene and dichlorophenylphosphane are commercial available and were used without further purifications. LiCl was dried for 6 h at 180 °C under high vacuum. The synthesis of secondary phosphine oxides[1,2], thieno[3,2-*b*]phosphole oxides[2–4] and tosylimino phospholes[5] were carried out following the related literature. Compounds **1** and **2** were prepared according to the literature.[2] Compound **3a** has been previously reported,[2] but a novel synthetic route with higher yield is reported here (see chapter 2.2.3).

1.2 Analytics

The NMR spectra were recorded with a BRUKER AVANCE DRX 400 spectrometer (^{1}H NMR 400.13 MHz, ^{13}C NMR 100.63 MHz, ^{31}P NMR 161.98 MHz) or a BRUKER ASCEND 400 spectrometer (^{1}H NMR 400.16 MHz, ^{13}C NMR 100.63 MHz, ^{31}P NMR 161.99 MHz). For ^{1}H NMR and ^{13}C NMR spectra, TMS was used as the internal standard. The ^{31}P NMR spectra were referenced to TMS using the Ξ-scale.[6] Assignment of the configurations and chemical shifts was done using HSQC, HMQC, HMBC, COSY and NOESY techniques.

Mass spectra (ESI) were measured using a BRUKER DALTONICS ESQUIRE 3000 Plus spectrometer. High-resolution mass spectra (HRMS; ESI) were measured using a BRUKER DALTONICS IMPACT II ESI-TOF spectrometer. The FT-IR spectra were obtained with a Nicolette IS5 (ATR) from Thermo Fisher (Waltham, MA, USA) with the scan range 4000–400 cm^{-1}. Elemental analyses were obtained with a HEREAUS VARIO EL oven. The melting points were determined in glass capillaries sealed under vacuum using a GALLENKAMP apparatus and are uncorrected.

Steady-state excitation and emission spectra were recorded on a FluoTime300 spectrometer from PicoQuant equipped with a 300 W ozone-free Xe lamp (250-900 nm), a 10 W Xe flash-lamp (250-900 nm, pulse width < 10 µs) with repetition rates of 0.1 – 300 Hz, an excitation monochromator (Czerny-Turner 2.7 nm/mm dispersion, 1200 grooves/mm, blazed at 350 nm), diode lasers (pulse width < 80 ps) operated by a computer-controlled laser driver PDL-820 (repetition rate up to 80 MHz, burst mode for slow and weak decays), two emission monochromators (Czerny-Turner, selectable gratings blazed at 500 nm with 2.7 nm/mm dispersion and 1200 grooves/mm, or blazed at 1250 nm with 5.4 nm/mm dispersion and 600 grooves/mm) with adjustable slit width between 0 mm and 10 mm, Glan-Thompson polarizers for excitation (Xe-lamps) and emission, a Peltier-thermostatized sample holder (-40 °C–

105 °C), and two detectors, namely a PMA Hybrid 40 (transit time spread FWHM < 120 ps, 200 – 900 nm) and a R5509-42 NIR-photomultiplier tube (transit time spread FWHM 1.5 ns, 300-1400 nm) from Hamamatsu. Signal-to-noise ratio (optical noise) typically better than 29000:1, as measured with double monochromators in the excitation and emission light path. Steady-state spectra and fluorescence lifetimes were recorded in TCSPC mode by a PicoHarp 300 (minimum base resolution 4 ps) or MCS mode by a TimeHarp 300, where up to several ms can be detected. Emission and excitation spectra were corrected for source intensity (lamp and grating) by standard correction curves. For samples with lifetime in ns order instrument response function calibration (IRF) was performed using a diluted Ludox® solution. Lifetime analysis was performed using the commercial FluoFit software. The quality of the fit was assessed by minimizing the reduced chi squared function (χ^2) and visual inspection of the weighted residuals and their autocorrelation. For solid state, a special holder in the Front Face (FF) mode was adapted.

Luminescence quantum yields were measured with a Hamamatsu Photonics absolute PL quantum yield measurement system (C9920-02) equipped with a L9799-01 CW Xenon light source (150 W), monochromator, C7473 photonic multi-channel analyzer, integrating sphere and employing U6039-05 PLQY measurement software (Hamamatsu Photonics, Ltd., Shizuoka, Japan). All solvents used were of spectrometric grade (Uvasol®). In all measurements, round quartz cuvettes were used.

The UV/Vis spectra in reflection mode were recorded by a CARY 5000 (AGILENT) with a 150 mm diameter DRA-2500 unit (DRA: diffuse reflection accessory) and a polytetrafluoroethylene coating. The samples were embedded between a metal support and a quartz glass plate. The use of an integrating sphere in combination with a UV/Vis spectrometer in reflection position can completely reflect the light lost by diffuse reflection, by spectralon in integrating sphere and direct it to a detector. This allows absorption in reflection mode. The light absorbed by the sample cannot be detected by the detector. Luminescence spectra were recorded with an inverted confocal microscope (IX71, Olympus) fibre-coupled to a spectrometer (iHR320, synapse CCD, HORIBA JobinYvon) at 355nm photoexcitation (xenon lamp as source). The light was focused and captured in the backscatter geometry with a 10x objective (Olympus LUCPlan FLN 10x NA = 0.3).

The fully corrected fluorescence spectra, quantum yield and fluorescence lifetimes in solution were measured using a Fluoromax 4 (Horiba) equipped with a 366 nm or 254 nm laser diode and a TCSPC unit (Fluorohub, Horiba).

2 Synthesis

2.1 Synthesis of Thienylphosphine Oxides

2.1.1 Phenyl(5-bromothiophen-2-yl)phosphine Oxide (1)

Compound **1** was prepared according to the literature procedure.[2]

2.1.2 Phenyl(4-bromothiophen-2-yl)phosphine Oxide (4)

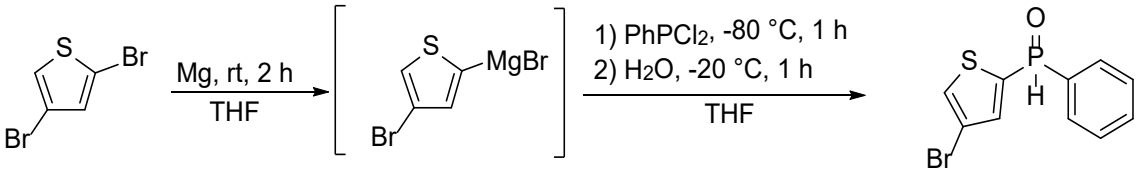

Under an argon atmosphere, a two necked SCHLENK-flask with condenser and dropping funnel was filled with magnesium turnings (1.3 eq.) and suspended in THF. The thienyl bromide (1.0 eq) was dissolved in THF and added dropwise under vigorous stirring at rt (use a water bath for constant temperature). After the complete addition of thienyl bromide, the suspension was stirred for 2 h at rt. The reaction mixture was filtered and added dropwise into a solution of $PhPCl_2$ (1.1 eq.) in THF at -80 °C. Then the orange coloured solution was allowed to warm to -20°C and H_2O was added dropwise. The solution warmed to rt and EtOAc was added. Then, the solution was washed three times with Brine and once with saturated $NaHCO_3$ solution. After that, the mixture was dried over Na_2SO_4, the solvents were completely removed and purified via flash chromatography (EtOAc).

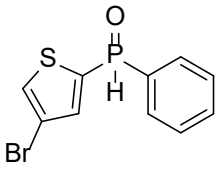

Yield: 67 % brownish oil.

***R*f** (EtOAc): 0.56.

^{1}H NMR (400 MHz, $CDCl_3$): δ = 8.23 (d, $^1J_{H\text{-}P}$ = 504.3 Hz, 1H), 7.82 – 7.72 (m, 2H), 7.67 – 7.61 (m, 1H), 7.53 (td, *J* = 7.6, 3.3 Hz, 2H), 7.39 (dd, *J* = 8.0, 1.3 Hz, 1H) ppm.

^{13}C{^{1}H} NMR (101 MHz, $CDCl_3$): ^{13}C NMR (101 MHz, $CDCl_3$) δ =137.6 (d, *J* = 10.8 Hz), 134.3 (d, $^1J_{C\text{-}P}$ = 103.5 Hz), 133.4 (d, *J* = 3.1 Hz), 131.3 (d, *J* = 4.0 Hz), 130.5 (d, *J* = 12.2 Hz), 130.4 (d, $^1J_{C\text{-}P}$ = 107.7 Hz), 129.2 (d, *J* = 13.7 Hz), 111.7 (d, *J* = 16.6 Hz) ppm.

^{31}P NMR (162 MHz, $CDCl_3$): δ = 8.8 (dq, $^1J_{P\text{-}H}$ = 504.3 Hz, $^3J_{P\text{-}H}$ =12.7 Hz) ppm.

HRMS (ESI, MeCN, pos.): *m/z* calcd for $C_{10}H_8BrOPS+H^+$: 286.9290 [*M*+H]$^+$; found: 286.9293.

2.2 Synthesis of Thiophene-Fused Phospholes

2.2.1 General Procedure *α*-Synthon (2)

Compound **2** was prepared according to the literature procedure.[2]

2.2.2 General Procedure *β*-Synthon (5)

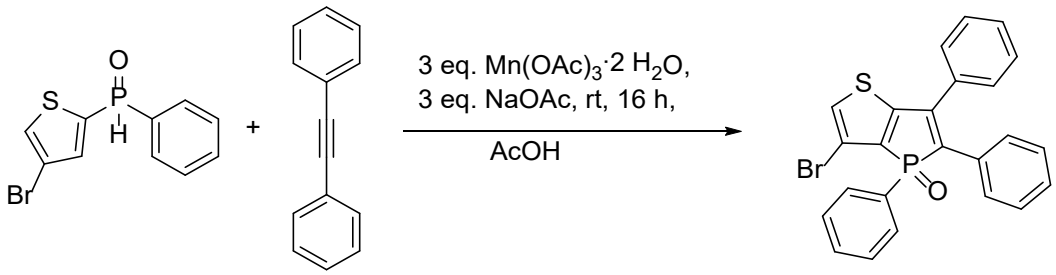

Diphenylacetylene (1.5 eq), phenyl-2-bromo-thienylphosphine oxide (1 eq.), $Mn(OAc)_3 \cdot H_2O$ (3 eq.) and NaOAc (3 eq.) were added to nitrogen purged Schlenk flask. Then AcOH was added to the mixture and stirred at rt for 16 h. The yellow or orange solution was mixed with EtOAc and washed three times with brine and once with saturated $NaHCO_3$ solution. The organic phase was dried over $MgSO_4$ and the solvent was removed under reduced pressure. The residue was purified by column chromatography (hexane/ EtOAc 1:1 to 1:3) to obtain the *β*-synthon **5** as a yellowish solid.

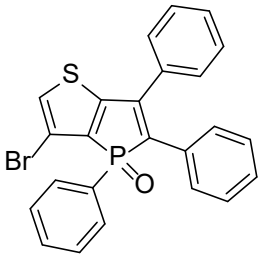

Yield: 35 % yellowish solid.

Mp.: 169–171 °C.

***R*f**(EtOAc/hexane 2:1) = 0.47.

^{1}H NMR (400 MHz, $CDCl_3$): *δ* = 7.82 (dd, *J* = 13.1, 7.6 Hz, 2H), 7.58 – 7.50 (m, 1H), 7.47 – 7.37 (m, 8H), 7.33 – 7.25 (m, 2H), 7.23 (d, *J* = 2.7 Hz, 1H), 7.19 – 7.10 (m, 3H) ppm.

^{13}C{^{1}H, ^{31}P} NMR (101 MHz, $CDCl_3$) *δ* = 156.3, 141.8, 135.2, 135.1, 133.6, 132.7, 132.6, 131.0, 129.8, 129.3, 129.1, 129.1, 128.7, 128.5, 128.4, 128.3, 126.5, 110.6 ppm.

^{31}P NMR (162 MHz, $CDCl_3$) δ = 28.6 (t, $^{3}J_{P\text{-}H}$ = 13.2 Hz) ppm.

Infrared spectrum (ATR-IR): $\tilde{\nu}$ = 3106 (w), 3054 (w), 1573 (w), 1479 (w), 1456 (w),1443 (m), 1434 (m), 1370 (s), 1303 (m), 1204 (s, P=O), 1153 (m), 1107 (m), 1067 (w), 1036 (w), 1027 (w), 1002 (w), 935 (s), 832 (m), 792 (m), 768 (s), 753 (s), 734 (s), 711 (s), 689 (s), 644 (w) 619 (m), 610 (s), 548 (s), 534 (m), 508 (s), 495 (s), 460 (m) cm^{-1}.

HRMS (ESI, MeCN, pos.): *m/z* calcd for $C_{24}H_{16}BrOPS+H^+$: 462.9916 [*M*+H]$^+$; found: 462.9918.

m/z calcd for $C_{24}H_{16}BrOPS+Na^+$: 484.9736 [*M*+Na]$^+$; found: 484.9735.

Elemental analysis: found: N 0.00%, C 62.01%, H 3.34%.

calc.: N 0.00%, C 61.88%, H 3.50%.

2.2.3 General Procedure Suzuki Coupling

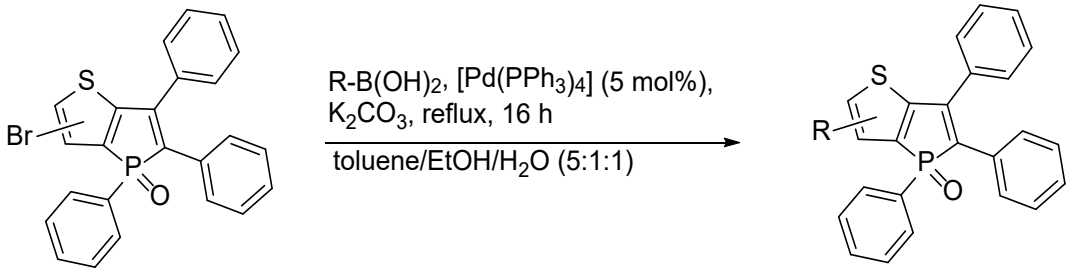

1.2 eq. arylboronic acid, 5 mol-% $[Pd(PPh_3)_4]$ and 2 eq. K_2CO_3 were added into a degassed SCHLENK flask with reflux condenser. Then, 1.0 eq. of synthon (**2** or **5**) was dissolved in toluene (5 mL/mmol) and transferred to the reaction vessel. Degassed H_2O (1 mL/mmol) and degassed EtOH (1 mL/mmol) were added to the mixture and refluxed for 16 h. After addition of EtOAc and subsequent filtration, the mixture was washed twice with saturated NaCl solution and once with H_2O. The organic phase was dried over Na_2SO_4 and then the solvent was removed under reduced pressure. The residue was purified by column chromatography (ethyl acetate/ hexane = 1:9 to 1:0, v:v). The products were precipitated with hexane and then dried under reduced pressure.

Compound **3a** is known and was previously prepared via an Mn^{III}-mediated oxidative annulation reaction between diphenylacetylene and phenyl(5-bromothiophen-2-yl)phosphine oxide, albeit in a lower yield (49% vs. 85% via Suzuki coupling reported here).[2]

3b

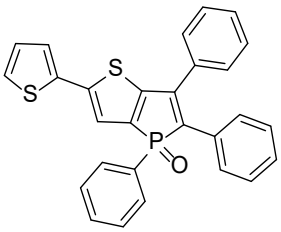

Yield: 80% orange solid.

Mp.: 200–202 °C

***R*f**(EtOAc/hexane 2:1) = 0.60.

^{1}H NMR (400 MHz, $CDCl_3$): δ = 7.72 (dd, *J* = 12.8, 7.5 Hz, 2H), 7.44 – 7.37 (m, 3H), 7.37 – 7.28 (m, 5H), 7.23 (d, *J* = 2.4 Hz, 1H), 7.19 (t, *J* = 4.6 Hz, 2H), 7.14 (d, *J* = 5.0 Hz, 1H), 7.10 – 7.01 (m, 4H), 6.91 (t, *J* = 4.4 Hz, 1H) ppm.

^{13}C{^{1}H, ^{31}P} NMR (101 MHz, $CDCl_3$) δ = 153.1, 142.5, 142.4, 136.2, 135.4, 134.2, 133.9, 132.6, 132.3, 130.8, 130.0, 129.5, 129.3, 129.0, 128.9, 128.9, 128.5, 128.4, 127.9, 125.4, 124.4, 122.0 ppm.

^{31}P NMR (162 MHz, $CDCl_3$): δ = 30.1 (t, $^3J_{P\text{-}H}$ = 12.9 Hz) ppm.

Infrared spectrum (ATR-IR): $\tilde{\nu}$ = 3104 (w), 3073 (w), 3052 (w), 2980(w), 15989 (w), 1571 (w), 1479 (w), 1438 (m), 1379 (m), 1329 (w), 1301 (w), 1271 (w), 1186 (s, P=O), 1142 (m), 1109 (s), 1079 (m), 1029 (m), 997 (m), 918 (w), 902 (w), 848 (w), 816 (m), 790 (s), 772 (s), 754 (s), 742 (s), 713 (s), 693 (s) 651 (m), 631 (m) ,605 (w), 577 (w), 548 (s), 520 (s), 512 (s), 494 (s), 470 (m) cm^{-1}.

HRMS (ESI, MeCN, pos.): *m/z* calcd for $C_{29}H_{19}OPS_2+H^+$: 467.0688 $[M+H]^+$; found: 467.0689.

Elemental analysis: found: N 0.00%, C 72.01 %, H 3.85%

calc.: N 0.00%, C 72.08%, H 4.11%.

3c

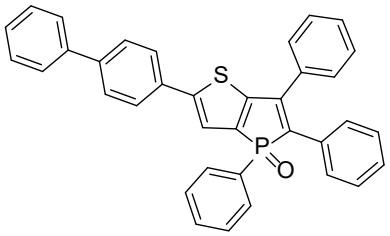

Yield: 95 % yellow solid.

Mp.: 230–232 °C.

R_f(EtOAc/hexane 2:1) = 0.71.

^{1}H NMR (400 MHz, $CDCl_3$): δ =) δ 7.81 (dd, J = 12.8, 7.6 Hz, 2H), 7.66 – 7.57 (m, 6H), 7.55 – 7.48 (m, 4H), 7.46 – 7.39 (m, 7H), 7.35 (t, J = 7.3 Hz, 1H), 7.32 – 7.26 (m, 2H), 7.19 – 7.10 (m, 3H) ppm.

^{13}C{^{1}H, ^{31}P} NMR (101 MHz, $CDCl_3$) δ = 153.8, 149.2, 142.8, 141.1, 140.1, 135.6, 134.3, 134.0, 132.78, 132.5, 132.3, 130.9, 129.5, 129.2, 129.1, 129.0, 128.9, 128.5, 128.5, 128.0, 127.7, 127.6, 126.9, 126.3, 126.1, 121.7 ppm.

^{31}P NMR (162 MHz, $CDCl_3$): δ = 30.4 (t, $^3J_{P\text{-}H}$ = 12.9 Hz) ppm.

Infrared spectrum (ATR-IR): $\tilde{\nu}$ = 3058 (w), 1591 (w), 1573 (w), 1527 (w), 1476 (w), 1437 (m), 1410 (w), 1364 (w), 1302 (w), 1194 (s, P=O), 1167 (m), 1145 (m), 1112 (s), 1069 (m), 1029 (w), 999(m), 990 (m), 910 (w), 834 (s), 792 (m), 766 (m), 750 (s), 727 (s), 716 (s), 695 (s), 650 (m), 633 (m), 613 (m) ,606 (w), 572 (w), 552 (s), 540 (s), 513 (s), 500 (s) cm^{-1}.

HRMS (ESI, MeCN, pos.): *m/z* calcd for $C_{36}H_{25}OPS+H^+$: 537.1442 [*M*+H]$^+$; found: 537.1444.

Elemental analysis: found: N 0.00%, C 80.26%, H 4.61%

calc.: N 0.00%, C 80.58%, H 4.70%.

3d

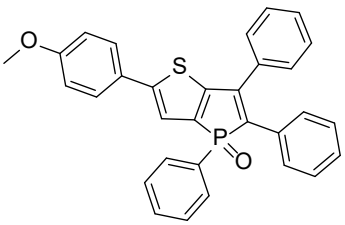

Yield: 94 % orange solid.

Mp.: 209–211 °C.

R_f(EtOAc/hexane 2:1) = 0.45.

^{1}H NMR (400 MHz, $CDCl_3$): δ = 7.90 – 7.68 (m, 2H), 7.53 – 7.46 (m, 5H), 7.44 – 7.39 (m, 5H), 7.35 (d, J = 2.4 Hz, 1H), 7.30 – 7.23 (m, 2H), 7.16 – 7.07 (m, 3H), 6.89 (d, J = 8.8 Hz, 2H), 3.82 (s, 3H, -OC**H**$_3$) ppm.

^{13}C{^{1}H, ^{31}P} NMR (101 MHz, $CDCl_3$) δ = 159.8, 152.7, 149.7, 142.9, 139.0, 135.5, 134.4, 133.4, 132.9, 132.3, 130.9, 129.7, 129.5, 129.0, 128.9, 128.5, 128.5, 127.9, 127.1, 126.3, 120.6, 114.0, 55.4 (-O**C**H$_3$) ppm.

^{31}P NMR (162 MHz, $CDCl_3$): δ = 30.5 (t, $^3J_{P\text{-}H}$ = 12.9 Hz) ppm.

Infrared spectrum (ATR-IR): $\tilde{\nu}$ = 3050 (w), 2838 (w), 1605 (m), 1571 (w), 1522 (m), 1481 (w), 1464 (w), 1438 (m), 1418 (w), 1377 (m), 1329 (w), 1307 (m), 1251 (s), 1182 (s, P=O), 1141 (m), 1111 (s), 1082 (m), 1028 (s), 997 (m), 986 (w), 928 (w), 833 (m), 813 (s), 790 (m), 772 (s), 746 (s), 713 (s), 702 (s), 695 (s) 686 (s), 659 (m), 635 (m) ,606 (w), 570 (w), 547 (s), 511 (s), 496 (s), 455 (s) cm^{-1}.

HRMS (ESI, MeCN, pos.): *m/z* calcd for $C_{31}H_{23}O_2PS+H^+$: 491.1230 [*M*+H]$^+$; found: 491.1225.

Elemental analysis: found: N 0.00%, C 75.75%, H 4.61%

calc.: N 0.00%, C 75.90%, H 4.73%.

3e

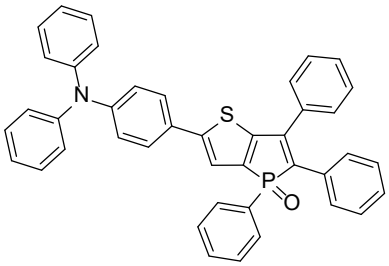

Yield: 89 % red solid.

Mp.: 210–211 °C.

R_f(EtOAc/hexane 2:1) = 0.79.

^{1}H NMR (400 MHz, $CDCl_3$): δ = 7.68 (dd, $^3J_{P,H}$ = 12.8 Hz, $^3J_{H,H}$ = 7.0 Hz, 2H), 7.45 – 7.28 (m, 8H), 7.26 (d, J = 2.5 Hz, 1H), 7.24 – 7.14 (m, 8H), 7.10 – 6.95 (m, 9H), 6.89 (d, $^3J_{H,H}$ = 8,6 Hz, 2H) ppm.

^{13}C{^{1}H, ^{31}P} NMR (101 MHz, $CDCl_3$) δ = 152.8, 149.9, 148.2, 147.4, 143.0, 135.7, 134.5, 133.6, 133.0, 132.4, 131.0, 129.9, 129.6, 129.5, 129.2, 129.1, 129.1, 128.7, 128.6, 128.0, 127.3, 126.7, 124.9, 123.6, 123.3, 120.8 ppm.

^{31}P NMR (162 MHz, $CDCl_3$): δ = 30.0 (t, $^3J_{P,H}$ = 13.1 Hz) ppm.

IR (ATR): $\tilde{\nu}$ = 3051 (w), 2963 (w), 2186 (w), 1953 (w), 1587 (m), 1508 (m), 1485 (s), 1437 (m, $\nu_{P\text{-Phenyl}}$), 1320 (m), 1285 (m), 1261 (s), 1196 (s, P=O), 1170 (s), 1148 (m), 1108 (s), 1074 (m), 1026 (m), 988 (m), 916 (w), 886 (m), 852 (m), 826 (m), 791 (s), 758 (s), 746 (m), 736 (m), 713 (s), 695 (s), 635 (m), 621 (m), 583 (m), 547 (s), 535 (m), 506 (s), 492 (s) cm^{-1}

HRMS (ESI, MeCN, pos.): *m/z* calcd for $C_{42}H_{30}OPS+H^+$: 628.1859 $[M+H]^+$; found: 628.1859

Elemental analysis: found: N 1.90 %, C 80.86 %, H 4.24 %

calc.: N 2.15 %, C 81.09 %, H 4.64 %

3f

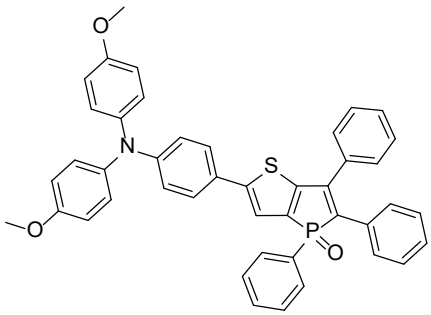

Yield: 92 % red solid.

Mp.: 247–248°C.

R_f(EtOAc/hexane 2:1) = 0.70.

^{1}H NMR (400 MHz, $CDCl_3$): δ = 7.79 (dd, J = 12.8, 7.6 Hz, 2H), 7.52 – 7.46 (m, 3H), 7.44 – 7.36 (m, 5H), 7.35 – 7.31 (m, 3H), 7.28 – 7.22 (m, 2H), 7.15 – 7.10 (m, 3H), 7.06 (d, J = 8.7 Hz, 4H), 6.91 – 6.79 (m, 6H), 3.79 (s, 6H, -OC**H**$_3$) ppm.

^{13}C{^{1}H, ^{31}P} NMR (101 MHz, $CDCl_3$) δ = 156.2, 152.0, 150.2, 148.9, 142.9, 140.2, 135.5, 134.4, 133.1, 132.9, 132.2, 130.8, 129.7, 129.4, 129.0, 128.9, 128.5, 128.4, 127.8, 127.1, 126.8, 126.3, 125.1, 120.01, 119.9, 114.8, 55.4 (-O**C**H$_3$) ppm.

^{31}P NMR (162 MHz, $CDCl_3$): δ = 30.5 (t, $^3J_{P,H}$ = 12.9 Hz) ppm.

IR (ATR): $\tilde{\nu}$ = 3059 (w), 2955 (w), 2836 (w), 1598 (m, $\nu_{C=C}$), 1503 (s), 1480 (s), 1443 (m_l), 1413 (m), 1369 (m), 1322 (m), 1286 (m), 1239 (s), 1183 (s, P=O), 1170 (s), 1103 (s), 1029 (s), 999 (m), 970 (w), 847 (m), 824 (s), 804 (m), 790(s), 768 (m), 741 (m), 711 (s), 697 (s), 689 (s), 636 (m), 607 (w), 593 (m), 576 (s), 566 (s), 514 (s), 499 (s) cm^{-1}

HRMS (ESI, MeCN, pos.): *m/z* calcd for $C_{44}H_{34}NO_3PS+H^+$: 688.2070 $[M+H]^+$; found: 688.2070

Elemental analysis: found: N 1.98 %, C 76.86 %, H 4.74 %

calc.: N 2.04 %, C 76.84 %, H 4.98 %

6a

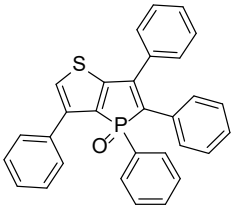

Yield: 74% yellowish solid.

Mp.: 250–252 °C.

***R*f**(EtOAc/hexane 2:1) = 0.74.

^{1}H NMR (400 MHz, $CDCl_3$): δ = 7.74 (d, *J* = 7.5 Hz, 2H), 7.60 (dd, *J* = 12.8, 7.5 Hz, 2H), 7.45 – 7.35 (m, 3H), 7.34 – 7.30 (m, 3H), 7.25 (q, *J* = 6.7 Hz, 5H), 7.21 – 7.13 (m, 3H), 7.10 – 7.01 (m, 3H) ppm.

^{13}C{^{1}H, ^{31}P} NMR (101 MHz, $CDCl_3$) δ = 156.5, 143.8, 142.5, 134.5, 134.3, 134.1, 132.9, 132.6, 132.2, 130.9, 129.5, 129.1, 128.9, 128.8, 128.6, 128.5, 128.1, 128.1, 127.6, 124.5 ppm.

^{31}P NMR (162 MHz, $CDCl_3$): δ = 30.2 (t, $^{3}J_{P,H}$ = 13.0 Hz) ppm.

IR (ATR): $\tilde{\nu}$ (cm^{-1}) = 3052 (w), 1600(w), 1478 (m), 1437 (m), 1405 (m, $\nu_{P\text{-}Phenyl}$), 1321 (w), 1303 (m), 1182 (s, $\nu_{P=O}$), 1149 (m), 1109 (s), 1071 (m), 1029 (m), 995 (m), 947 (w), 924 (m), 842 (m), 792 (m), 771 (m), 738 (s), 726 (s), 716 (m), 696 (s), 663 (m), 644 (m), 622 (m), 611 (m), 575 (s), 511 (s), 504 (s), 472 (m), 457 (m).

HRMS (ESI, MeCN, pos.): *m/z* calcd for $C_{30}H_{21}OPS+H^+$: 461.1123 $[M+H]^+$; found: 461.1129.

Elemental analysis: found: N 0.00 %, C 78.36 %, H 4.51 %.

calc.: N 0.00 %, C 78.24 %, H 4.60 %.

6b

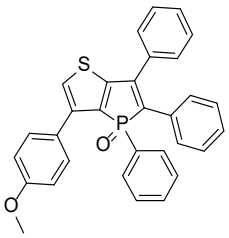

Yield: 96% yellow solid.

Mp.: 220–222 °C.

***R*f**(EtOAc/hexane 2:1) = 0.87.

^{1}H NMR (400 MHz, $CDCl_3$): δ = 7.68 (d, *J* = 8.7 Hz, 2H), 7.60 (dd, *J* = 12.7 Hz, 7.1 Hz, 2H), 7.42-7.37 (m, 1H), 7.37 (d, *J* = 3.7 Hz, 1H), 7.35-7.25 (m, 5H), 7.25-7.15 (m, 4H), 7.09-7.01 (m, 3H), 6.79 (d, *J* = 8.7 Hz, 2H), 3.70 (s, 3H, -OC**H**$_3$) ppm.

^{13}C{^{1}H, ^{31}P} NMR (101 MHz, $CDCl_3$) δ = 159.6 , 156.3, 143.5, 142.6, 134.4, 134.3, 133.0, 132.3, 132.2, 130.9, 129.5, 129.3, 129.1, 129.1, 128.9, 128.8, 128.6, 128.5, 128.0, 126.9, 123.2, 114.3, 55.3 (-O**C**H$_3$) ppm.

^{31}P NMR (162 MHz, $CDCl_3$): δ = 30.3 (t, $^{3}J_{P\text{-}H}$ = 13.0 Hz) ppm.

Infrared spectrum (ATR-IR): $\tilde{\nu}$ = 3104 (w), 3055 (w), 2996 (w), 2932 (w), 2835 (w), 1606 (w), 1573 (w), 1522 (m), 1475 (m), 1443 (m), 1435 (m, $\nu_{P\text{-}Phenyl}$), 1424 (m), 1399 (m), 1304 (w), 1287 (m), 1246 (m), 1215 (m), 1194 (s, $\nu_{P=O}$), 1181 (s), 1152 (m), 1135 (m), 1110 (m), 1075 (m), 1025 (m), 998 (m), 967 (m), 944 (m), 920 (m), 870 (w), 854 (w), 836 (s),797 (s), 791 (m), 772 (m), 757 (m), 740 (s), 714 (m), 695 (m), 664 (m), 639 (m), 622 (m), 608 (m), 583 (m), 572 (m), 527 (m), 509 (s), 499 (s), 474 (m), 459 (s) cm^{-1}.

HRMS (ESI, MeCN, pos.): *m/z* calcd for $C_{31}H_{23}O_2PS+H^+$: 491.1235 $[M+H]^+$; found: 491.1233.

Elemental analysis: found: N 0.00%, C 75.72%, H 4.85%.

calc.: N 0.00%, C 75.90%, H 4.73%.

6c

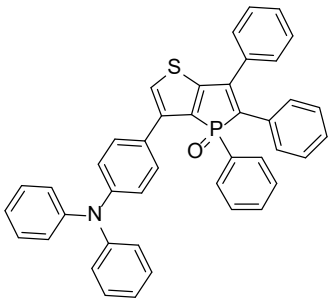

Yield: 72% yellow solid.

Mp.: 252–254 °C.

***R*f**(EtOAc/hexane 1:1) = 0.37.

^{1}H NMR (400 MHz, $CDCl_3$): δ = 7.70 (dd, J = 12.7 Hz, 7.1 Hz, 2H), 7.64 (d, J = 8.6 Hz, 2H), 7.51-7.43 (m, 2H), 7.42-7.37 (m, 4H), 7.35 (d, J = 3.2 Hz, 1H), 7.33-7.19 (m, 8H) , 7.16-7.07 (m, 3H,), 7.07-7.02 (m, 6H), 7.01 (d, J = 8.6 Hz, 2H) ppm.

^{13}C{^{1}H, ^{31}P} NMR (101 MHz, $CDCl_3$) δ = 156.2, 147.7, 147.4, 143.4, 142.5, 134.3, 134.3, 132.9, 132.4, 132.1, 130.9, 129.4, 129.3, 129.1, 128.8, 128.6, 128.4, 128.3, 128.0, 124.6, 123.3, 123.2, 123.1 ppm.

^{31}P NMR (162 MHz, $CDCl_3$): δ = 30.1 (t, $^{3}J_{P,H}$ = 12.9 Hz) ppm.

IR (ATR): $\tilde{\nu}$ (cm^{-1}) = 3053 (w), 1734(w), 1587 (m), 1522 (w), 1480 (s), 1436 (m, $\nu_{P\text{-}Phenyl}$), 1408 (m), 1328 (m), 1316 (m), 1292 (m), 1270 (s), 1179 (s, $\nu_{P=O}$), 1149 (s), 1107 (m), 1077 (m), 1029 (m), 997 (w), 967 (w), 947 (m), 921 (m), 891 (m), 839 (m), 825 (m), 791 (m), 773 (m), 747 (s), 729 (s), 716 (s), 690 (s), 665(m), 641 (m), 621 (m), 609 (s), 575 (s), 526 (s), 504 (s), 471 (m), 458 (m), 444 (m)

HRMS (ESI, MeCN, pos.): *m/z* calcd for $C_{42}H_{20}OPS+H^+$: 628.1857 $[M+H]^+$; found: 628.1860

Elemental analysis: found: N 2.11 %, C 80.57 %, H 4.44 %

calc.: N 2.23 %, C 80.36 %, H 4.60 %

2.2.4 General Procedure Sonogashira Cross-Coupling

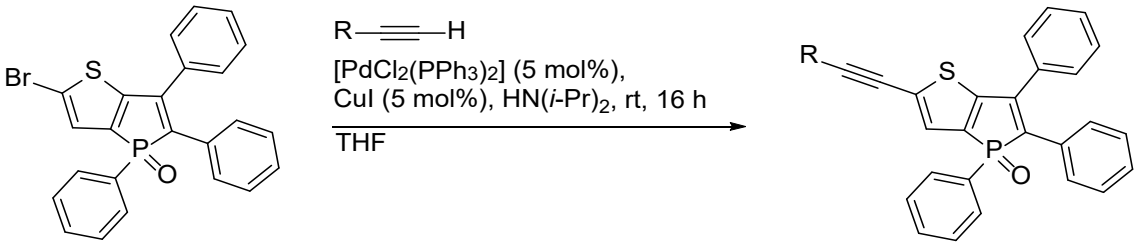

1.00 eq. of *α*-synthon **2**, 0.05 eq. of CuI, 0.05 eq. of $[PdCl_2(PPh_3)_2]$, and 1.20 eq. of arylalkyne were placed in a Schlenk flask. THF (8mL/mmol) and degassed diisopropylamine (3 mL/mmol) were added to the reaction mixture. The solution was then stirred at room temperature for 16 h, to which ethyl acetate was added and washed three times with saturated NaCl solution. The organic phase was dried over $MgSO_4$ and the solvent was removed under reduced pressure. The product was subsequently purified by column chromatography (EtOAc/hex= 1:6-1:0 (*v*:*v*)) and precipitated with hexane in an ultrasonic bath as a yellow powder.

3g

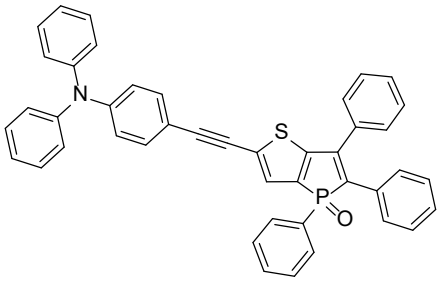

Yield: 456 mg orange solid (89%)

Mp.: 186–188 °C

R_f(EtOAc/hexane 2:1) = 0.75

^{1}H NMR (400 MHz, $CDCl_3$): δ = 7.76 (dd, J = 12.7 Hz, J = 8.4 Hz, 2H), 7.53 – 7.43 (m, 3H), 7.43 – 7.36 (m, 5H), 7.34 (d, J = 2.5 Hz, 1H), 7.30 – 7.24 (m, 7H), 7.15 – 7.08 (m, 7H), 7.08 – 7.03 (m, 3H), 6.97 (d, J = 8.7 Hz, 2H) ppm.

^{13}C{^{1}H, ^{31}P} NMR (101 MHz, $CDCl_3$) δ = 155.1, 148.6, 147.1, 142.8, 135.5, 13.6, 134.2, 132.8, 132.5, 131.0, 130.0, 129.7, 129.6, 129.4, 129.2, 129.1, 129.1, 128.8, 128.6, 128.6, 128.3, 125.4, 124.0, 121.9, 114.8, 96.5 (**C**≡C), 81.4 (**C**≡C) ppm.

^{31}P NMR (162 MHz, $CDCl_3$): δ = 29.8 (t, $^3J_{P\text{-}H}$ = 13.0 Hz) ppm.

IR (ATR): $\tilde{\nu}$ = 3055 (w), 2922 (m), 2852 (m),1890 (w), 1588(m), 1519 (m), 1481 (s), 1436 (m, $\nu_{P\text{-}Phenyl}$), 1412 (m), 1372 (m), 1324 (m), 1273 (s), 1195 (s, $\nu_{P=O}$), 1107 (m), 1074 (m), 1027 (m), 1000 (m), 918 (m), 822 (m), 791 (m), 750 (s), 712 (m), 691 (s), 634 (m), 614 (m), 553 (s), 508 (s) cm^{-1}.

HRMS (ESI, MeCN, pos.): *m/z* calcd for $C_{44}H_{30}OPS+H^+$: 652.1859 $[M+H]^+$; found: 652.1862

Elemental analysis: found: N 1.98 %, C 79.84 %, H 5.15 %

calc.: N 2.23 %, C 80.36 %, H 4.82 %

2.2.5 General Procedure Phosphole Imination

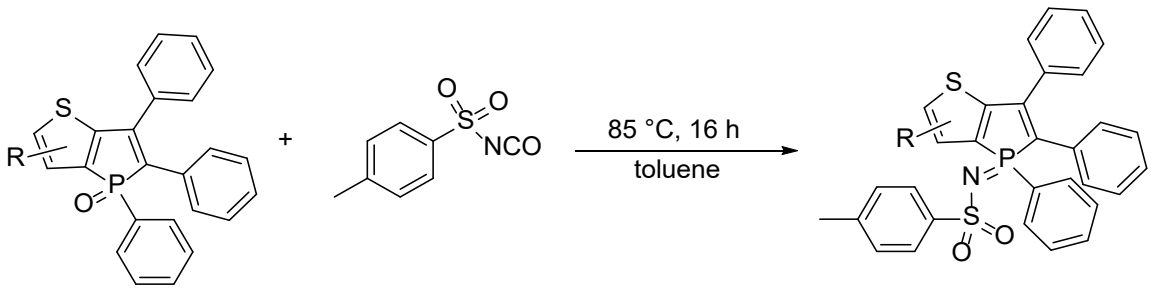

In a Schlenk flask, phosphole oxide (1 eq.) was suspended in toluene (3 mL/mmol) and TSI stock solution (1.5 eq.) in toluene was added. The reaction mixture was heated for 16 h at 85 °C. After cooling to room temperature, the solvent was completely removed and the oily residue was mixed with dry Et_2O (6 mL/mmol). The precipitate formed was filtered via filter canula and washed with dry Et_2O and *n*-pentane. After drying under reduced pressure, phosphole imines were obtained as yellow solids. Suitable crystals for X-ray analysis were obtained by recrystallization in MeCN (~3 mL/mmol) or diffusion of hexane vapour in a solution of phospholes in CH_2Cl_2 at room temperature.

7a

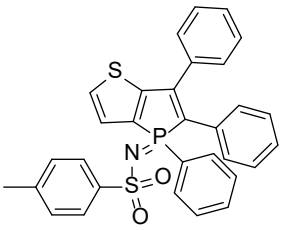

Yield: 85% yellow solid.

M.p.: 168–170 °C.

^{1}H NMR (400 MHz, $CDCl_3$): δ = 7.72 – 7.64 (m, 2H), 7.52 – 7.40 (m, 3H), 7.35 – 7.27 (m, 8H), 7.13 (dd, J = 4.9, 2.0 Hz, 1H), 7.10 – 6.98 (m, 5H), 6.95 (d, J = 8.0 Hz, 2H), 2.22 (s, -C**H$_3$**, 3H).

^{13}C{^{31}P,^{1}H} NMR (101 MHz, $CDCl_3$): δ = 156.4, 144.4, 142.5, 140.9, 133.5, 133.2, 131.9, 131.6, 131.5, 130.1, 129.8, 129.7, 129.3, 129.1, 128.9, 128.7, 128.5, 128.3, 128.2, 127.5, 125.9, 123.6, 21.3 (-**C**H$_3$) ppm.

^{31}P NMR (162 MHz, $CDCl_3$): 11.7 (t, $^{3}J_{P,H}$ = 14.5 Hz) ppm.

HR MS (ESI(+), MeCN): *m/z* für $[M+H]^+$ 538.1069; calcd. 538.1064.

IR (ATR): $\tilde{\nu}$ = 3094 (w), 3081 (w), 3061 (w), 1599 (w), 1575 (w), 1483 (w), 1438 (m), 1401 (w), 1362 (w), 1273 (s, ν_{SO2}), 1207 (w), 1187 (w), 1144 (s), 1089 (m), 1028 (w), 1000 (w), 989 (w), 901 (w), 851 (w), 806 (m), 790 (w), 761 (m), 746 (m), 731 (m), 717 (s), 691 (s), 673 (m), 652 (m), 629 (m), 604 (m), 565 (s), 550 (s), 526 (s), 498 (s), 478 (s), 466 (s) cm^{-1}.

Elemental analysis: found: N 2.84 %, C 68.76 %, H 4.33 %
calc.: N 2.61 %, C 69.26 %, H 4.50 %

7b

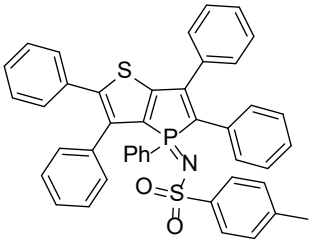

Yield: 82% yellow solid.

m.p.: 148–150 °C.

^{1}H NMR (400 MHz, $CDCl_3$) δ = 7.62 (dd, J = 14.3, 7.7 Hz, 2H), 7.51 – 7.46 (m, 2H), 7.42 (d, J = 7.9 Hz, 2H), 7.39 – 7.31 (m, 4H), 7.23 (td, J = 7.8, 3.7 Hz, 2H), 7.17 – 7.04 (m, 8H), 7.04– 6.91 (m, 7H), 6.88 (d, J = 7.9 Hz, 2H), 2.17 (s, 3H, -C**H$_3$**) ppm.

^{13}C{^{31}P,^{1}H} NMR (101 MHz, $CDCl_3$): δ = 153.6, 145.0, 144.1, 142.2, 140.6, 138.7, 133.8, 133.3, 133.0, 131.7, 131.3, 129.8, 129.6, 129.5, 129.0, 128.9, 128.7, 128.6, 128.5, 128.2, 128.1, 128.1, 128.0, 127.6, 125.9, 122.7, 21.2 (-**C**H$_3$) ppm

^{31}P NMR (162 MHz, $CDCl_3$) δ = 11.2 (t, $^{3}J_{P,H}$ = 14.4 Hz) ppm.

IR (ATR): $\tilde{\nu}$ = 3056 (w), 2970 (w), 1597 (w), 1574 (w), 1494 (w), 1439 (m), 1404 (w), 1294 (m), 1279 (s, ν_{SO2}), 1178 (w), 1144 (s), 1124 (s), 1086 (s), 1027 (w), 999 (w), 986 (w), 894 (w), 807 (m), 775 (w), 748 (s), 718 (s), 710 (s), 692 (s), 670 (s), 658 (s), 625 (m), 600 (w), 564 (s), 555 (s), 529 (m), 506 (s), 491 (s), 480 (s) cm^{-1}.

HRMS (ESI, MeCN, pos.): *m/z* calcd for $C_{43}H_{32}NO_2PS_2+H^+$: 690.1685 $[M+H]^+$; found: 690.1685.

Elemental analysis: found: N 2.13%, C 74.56%, H 4.49%
calc.: N 2.03%, C 74.87%, H 4.68%.

7c

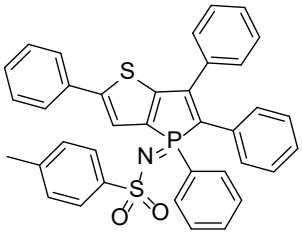

Yield: 92% yellow-orange solid.

m.p.: 134–135 °C.

^{1}H NMR (400 MHz, CD_2Cl_2) δ = 7.88 – 7.79 (m, 2H), 7.58 (d, J = 7.7 Hz, 2H), 7.54 – 7.38 (m, 12H), 7.39 – 7.33 (m, 1H), 7.30 – 7.22 (m, 2H), 7.21 – 7.12 (m, 3H), 7.08 (d, J = 2.3 Hz, 1H), 7.03 (d, J = 7.9 Hz, 2H), 2.14 (s, 3H, -C**H$_3$**) ppm.

^{13}C{^{31}P,^{1}H} NMR (101 MHz, CD_2Cl_2): δ = 154.5, 149.9, 144.9, 142.4, 141.3, 133.6, 133.4, 132.9, 131.8, 131.4, 131.2, 130.2, 129.8, 129.4, 129.2, 129.1, 129.0, 128.7, 128.6, 128.5, 128.3, 128.2, 125.9, 125.6, 123.3, 122.2, 20.8. (-**C**H$_3$) ppm

^{31}P NMR (162 MHz, CD_2Cl_2) δ = 14.3 (t, $^{3}J_{P,H}$ = 14.4 Hz) ppm.

IR (ATR): $\tilde{\nu}$ = 3066 (w), 2968 (w), 1597 (w), 1595 (w), 1479(w), 1438 (m), 1275 (s, ν_{SO2}), 1160 (m), 1137 (s), 1086 (s), 1037 (w), 998 (w), 989(w), 866 (w), 854 (m), 794 (m), 754 (m), 745 (m), 735 (m), 716 (s), 700 (s), 687 (s), 649 (m), 629 (w), 573 (w), 554 (s), 525 (m), 501 (s), 479 (s), 456 (s) cm^{-1}.

HRMS (ESI, MeCN, pos.): *m/z* calcd for $C_{37}H_{28}NO_2PS_2$+H$^+$: 614.1372 [*M*+H]$^+$; found: 614.1371.

Elemental analysis: found: N 2.26%, C 00.00 %, H 4.43%

calc.: N 2.28%, C 72.41%, H 4.60%.

7d

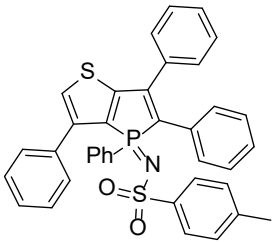

Yield: 74% yellowish solid.

m.p.: 221–223 °C.

^{1}H-NMR (MHz; $CDCl_3$): δ = 7.84 (ddd, J = 14.2, 8.3 Hz, 1.3 Hz, 2H), 7.53 (dd, J = 7.6 Hz, 2.0 Hz, 2H), 7.51-7.41 (m, 7H), 7.40 (d, J = 3.8 Hz,), 7.39-7.35 (m, 3H), 7.26-7.21 (m, 2H), 7.22-7.15 (m, 3H), 7.15-7.06 (m, 3H), 6.85 (d, J = 7.9 Hz, 2H), 2.24 (s, 3H) ppm.

^{13}C{^{31}P,^{1}H} NMR (101 MHz, $CDCl_3$): δ = 144.8, 144.5, 143.9, 143.6, 141.8, 140.7, 133.6, 133.3, 133.0, 132.8, 131.7, 131.5, 129.8, 129.7, 129.2, 129.0, 128.8, 128.6, 128.5, 128.4, 128.2, 128.0, 127.2, 125.9, 124.7, 122.4, 21.3 (**C**H$_3$).ppm.

^{31}P NMR (162 MHz; $CDCl_3$): δ = 11.1 (t, $^{3}J_{P,H}$ = 14.5 Hz) ppm.

IR (ATR): $\tilde{\nu}$ =3058 (w), 1598 (w), 1575 (w), 1475 (m), 1440 (m, $\nu_{P\text{-}Phenl}$), 1402 (m), 1291 (m), 1274 (s, ν_{SO2}), 1190 (m), 1139 (s, ν_{SO2}), 1110 (s), 1065 (s), 1027 (m), 998 (m), 950 (m), 921 (w), 849 (m), 806 (m), 771(m), 747 (s), 715 (s), 687 (s), 668 (s), 659 (s), 622 (m), 608 (m), 584 (m), 567 (s), 553 (s), 507 (s), 497 (s), 470 (s).

HRMS (ESI, MeCN, pos.): *m/z* calcd for $C_{37}H_{28}NO_2PS_2$+H$^+$: 614.1372 [*M*+H]$^+$; found: 614.1371.

Elemental analysis: found: N 2.26%, C 72.25%, H 4.73%

calc.: N 2.28%, C 72.41%, H 4.60%.

3 NMR Spectra

NMR spectra of compounds **1** (^{1}H, ^{13}C{^{1}H}, ^{31}P{^{1}H} and ^{31}P), **2** (^{1}H ,^{13}C{^{31}P, ^{1}H}, ^{31}P{^{1}H} and ^{31}P) and **3a** (^{1}H, ^{13}C{^{31}P, ^{1}H}, ^{31}P{^{1}H} and ^{31}P) have already been reported in the literature.[2]

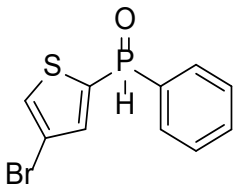

4

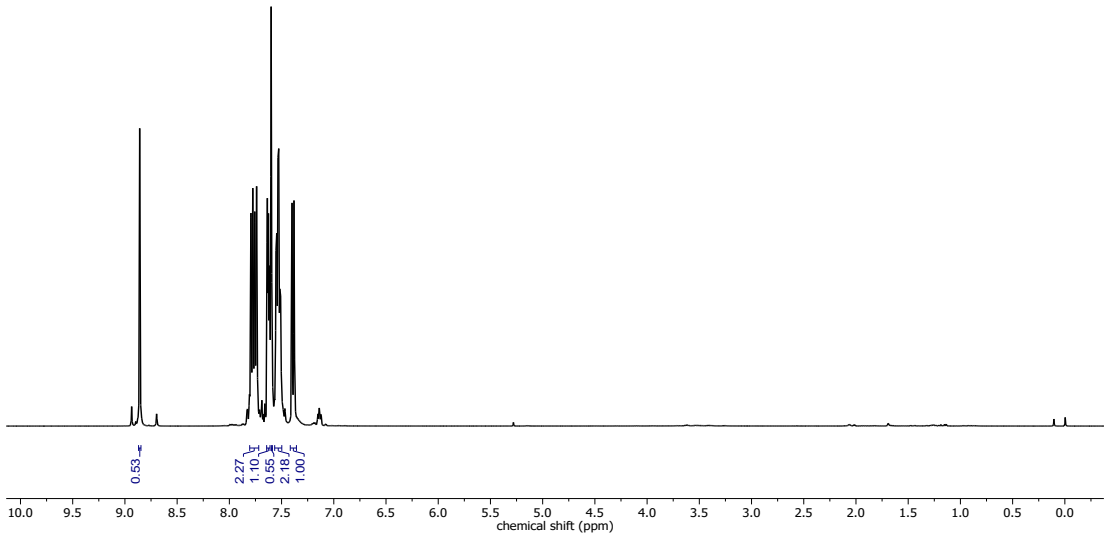

Fig S3.1: ^{1}H NMR spectrum of **4** in $CDCl_3$.

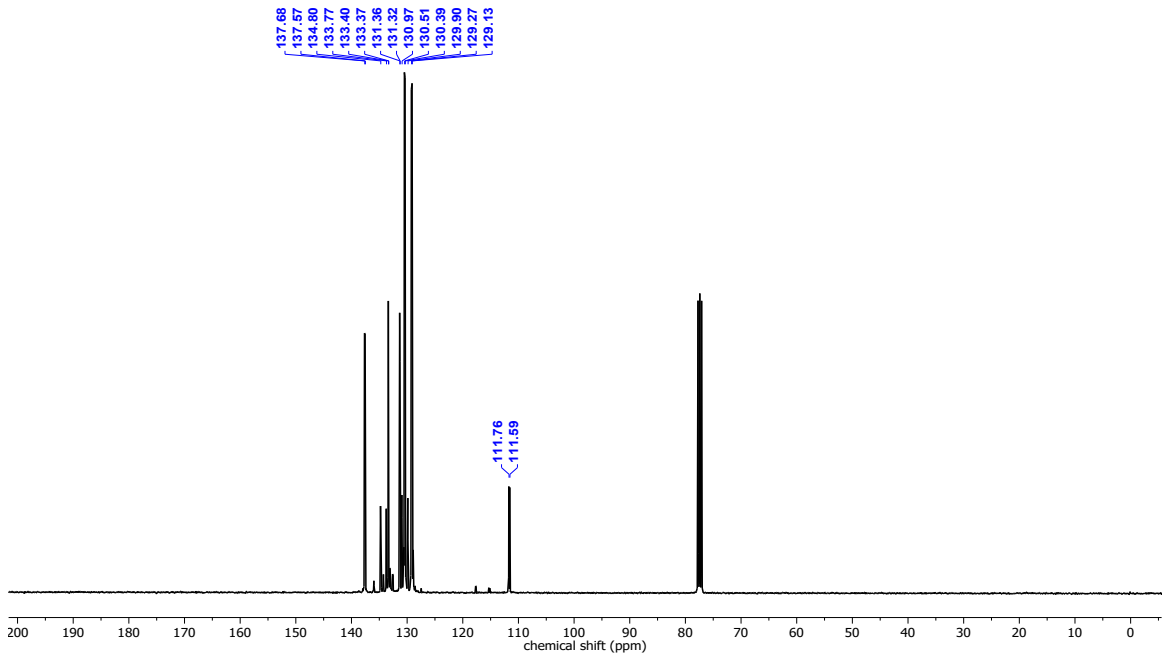

Fig S3.2: ^{13}C{^{1}H} NMR spectrum of **4** in $CDCl_3$.

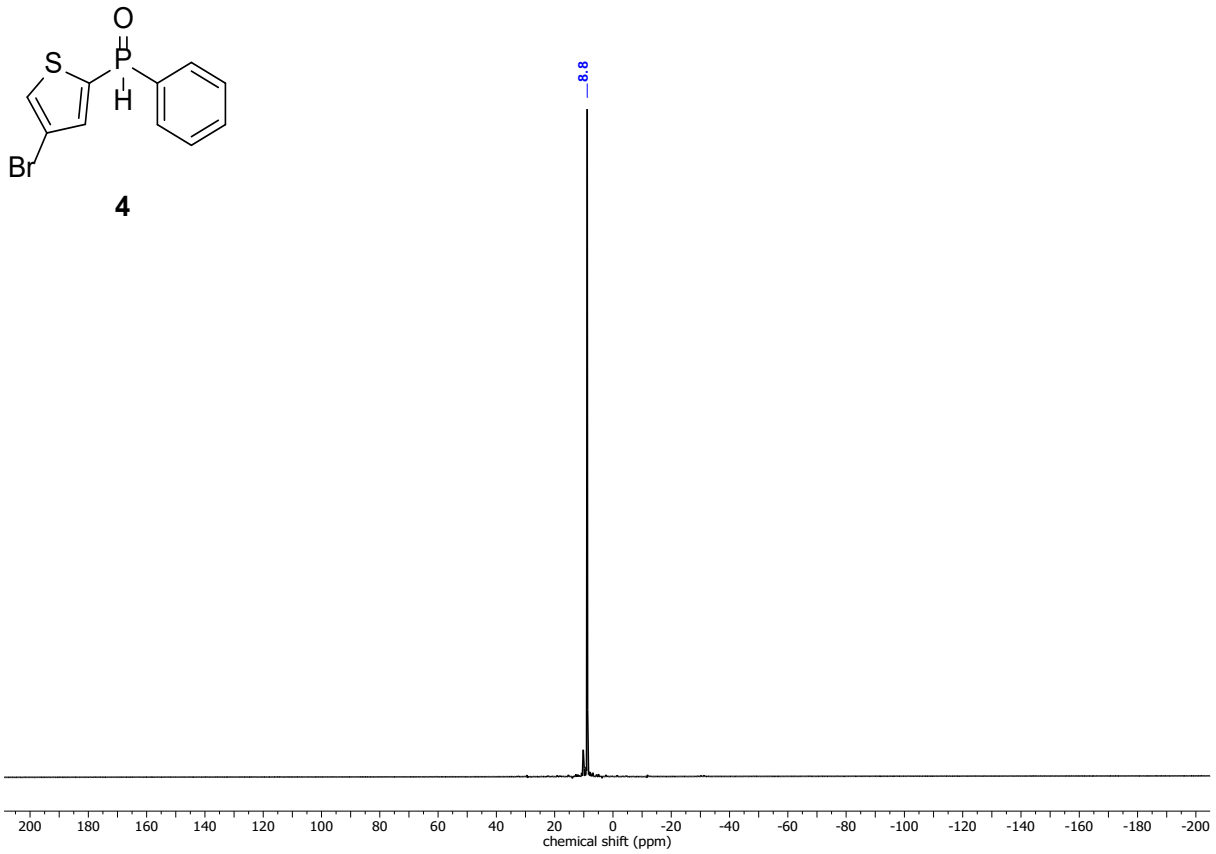

Fig S3.3: $^{31}P\{^{1}H\}$ NMR spectrum of **4** in $CDCl_3$.

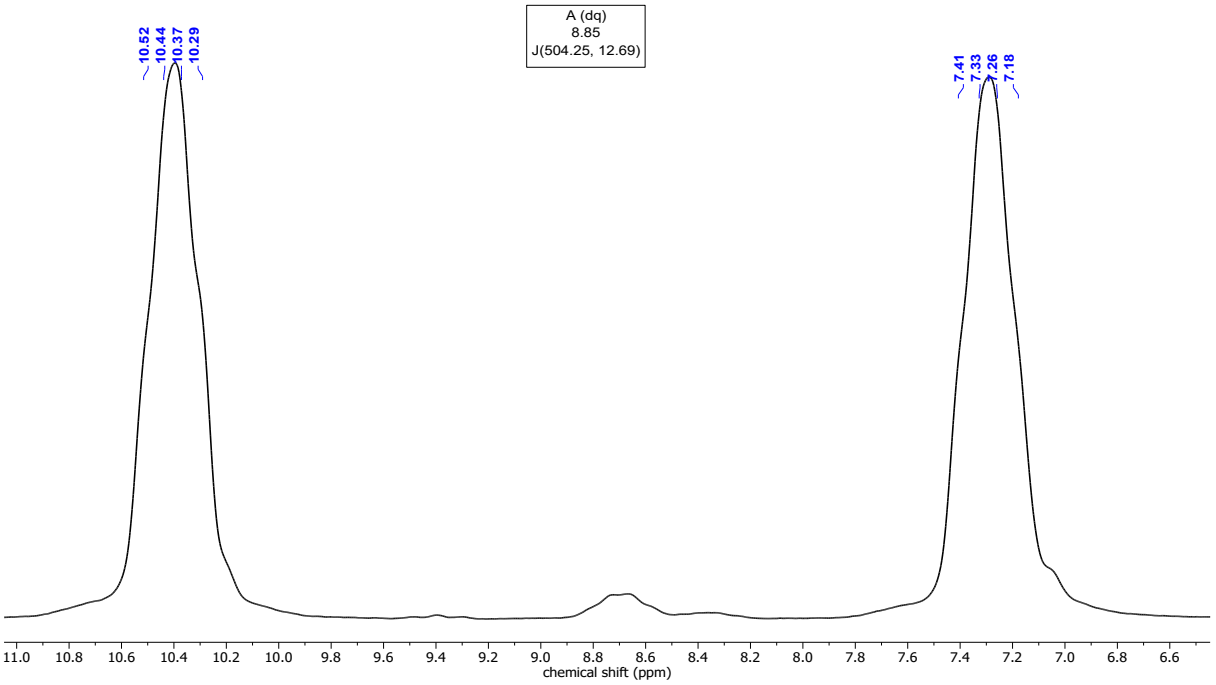

Fig 3.4: Details of the ^{31}P NMR spectrum of **4** in $CDCl_3$.

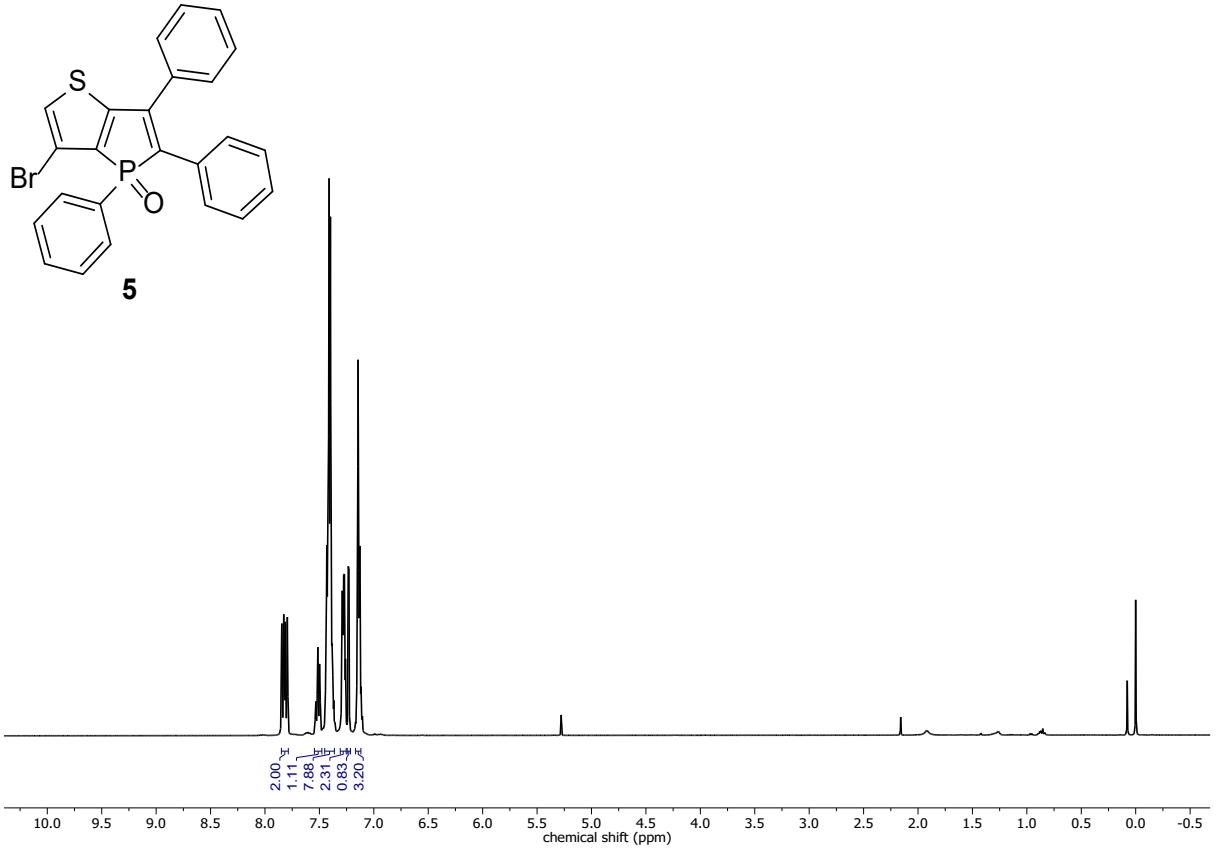

Fig S3.5: ^{1}H NMR spectrum of **5** in $CDCl_3$.

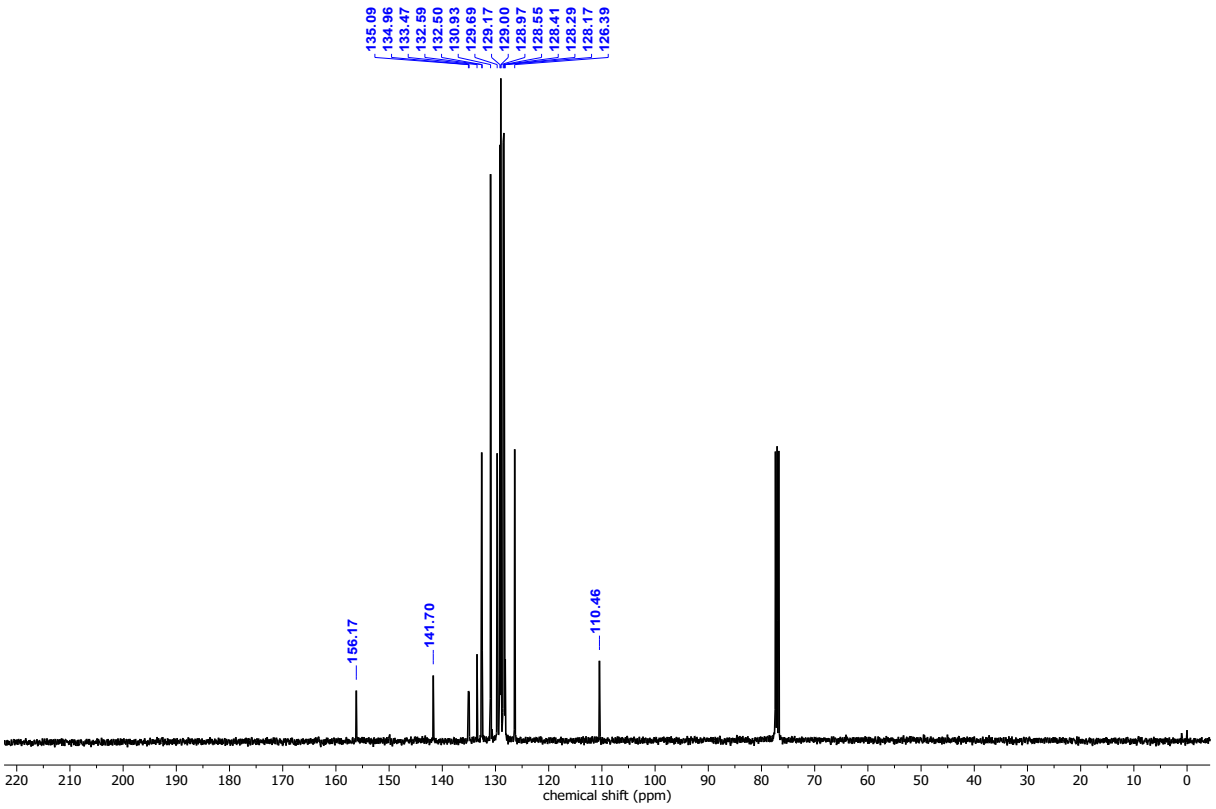

Fig S3.6: $^{13}C\{^{31}P, ^{1}H\}$ NMR spectrum of **5** in $CDCl_3$.

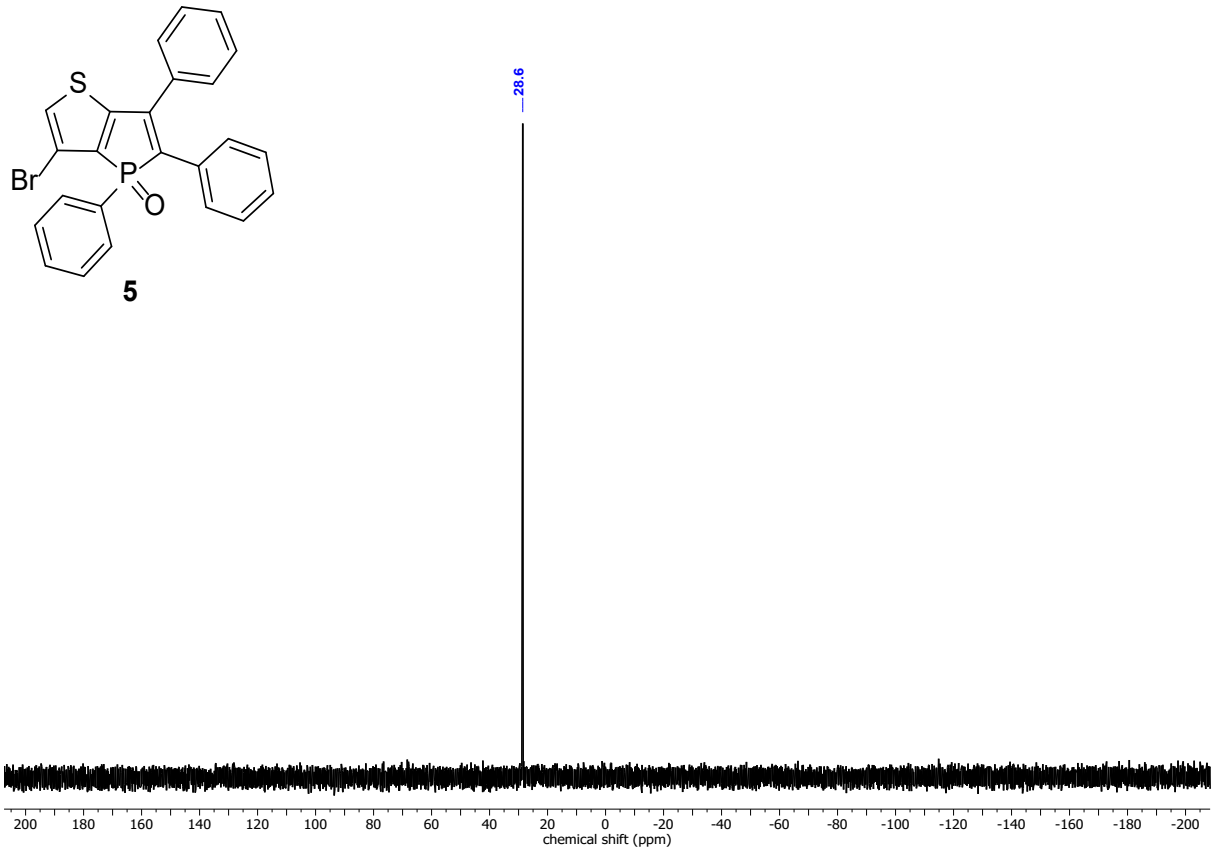

Fig S3.7: $^{31}P\{^{1}H\}$ NMR spectrum of **5** in $CDCl_3$.

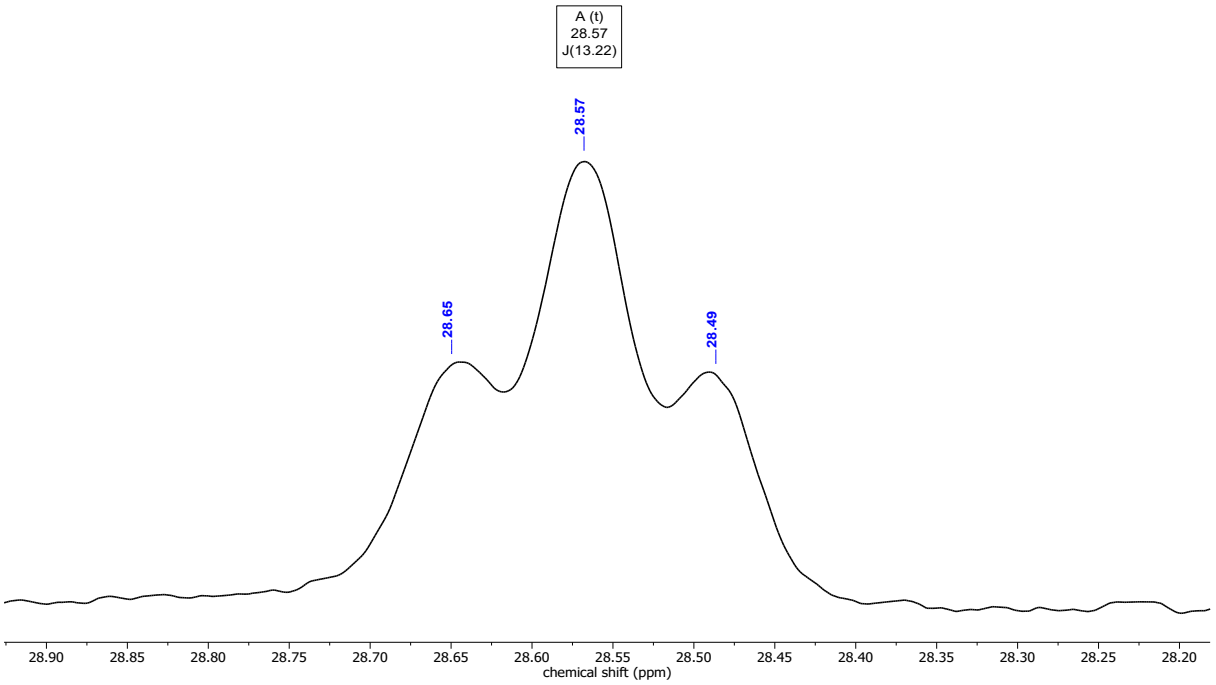

Fig S3.8: Details of the ^{31}P NMR spectrum of **5** in $CDCl_3$.

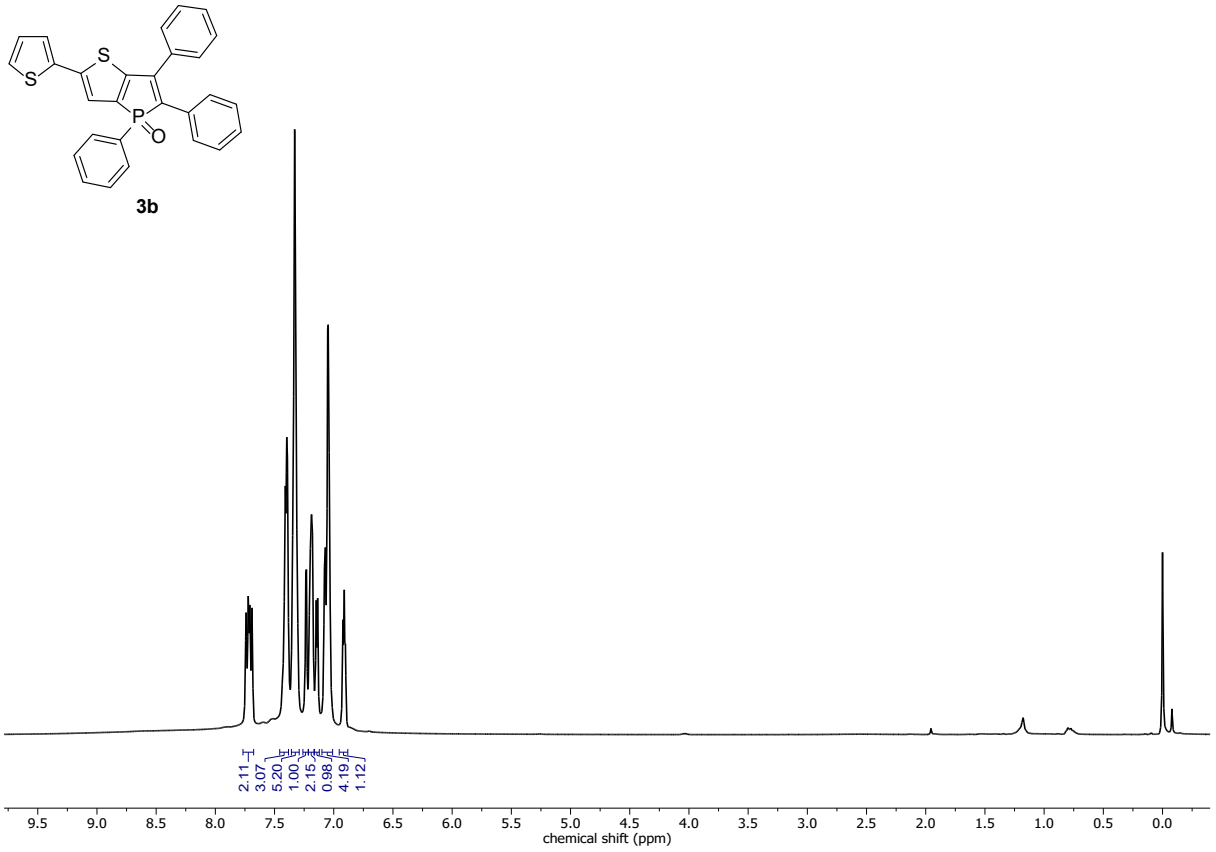

Fig S3.9: ^{1}H NMR spectrum of **3b** in $CDCl_3$.

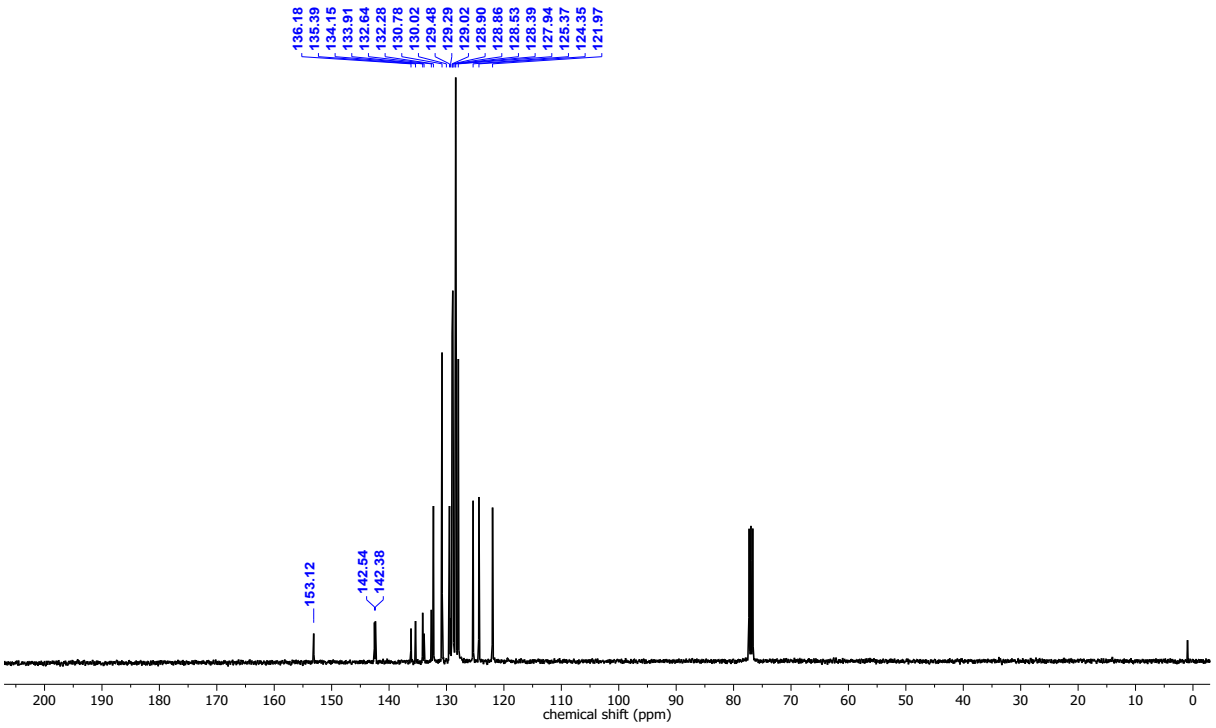

Fig S3.10: $^{13}C\{^{31}P, ^{1}H\}$ NMR spectrum of **3b** in $CDCl_3$.

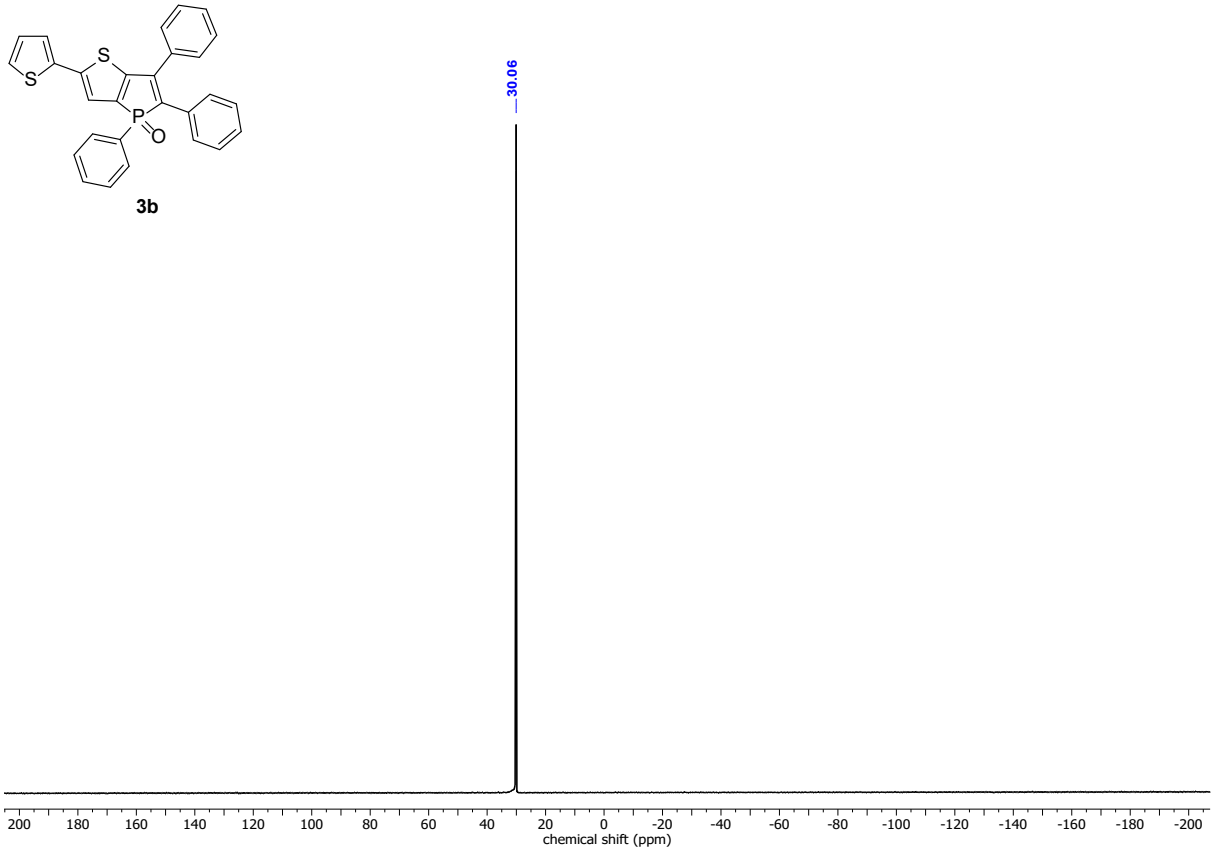

Fig S3.11: $^{31}P\{^{1}H\}$ NMR spectrum of **3b** in $CDCl_3$.

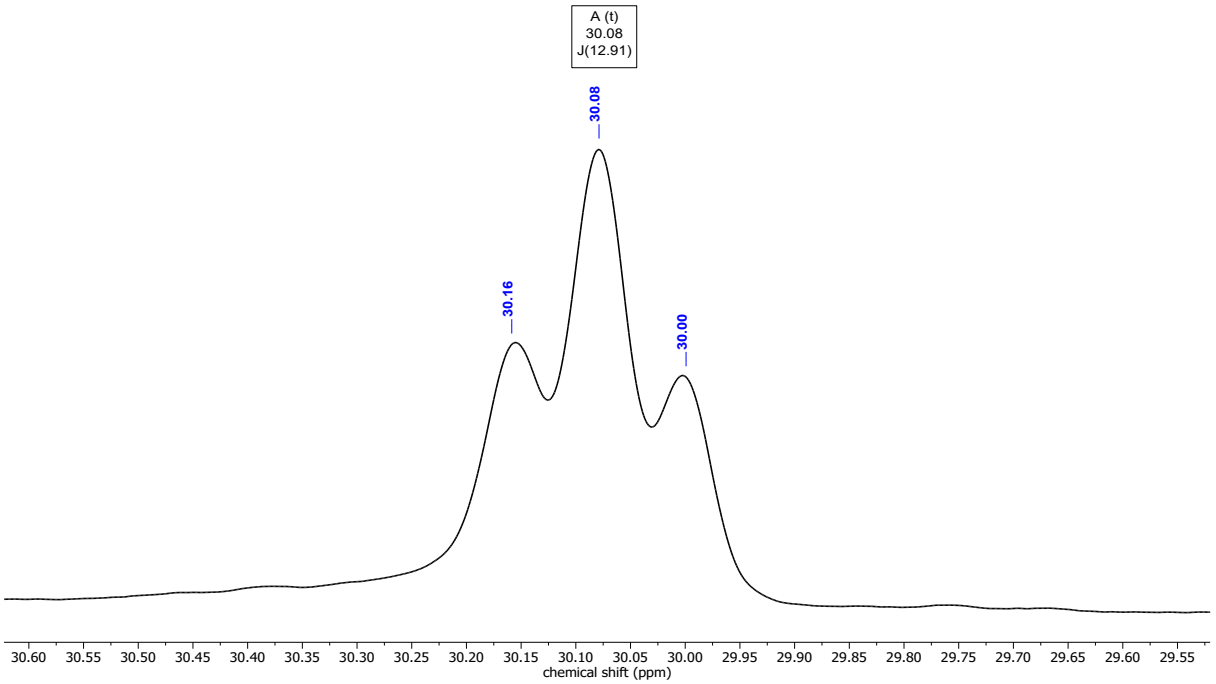

Fig S3.12: Details of the ^{31}P NMR spectrum of **3b** in $CDCl_3$.

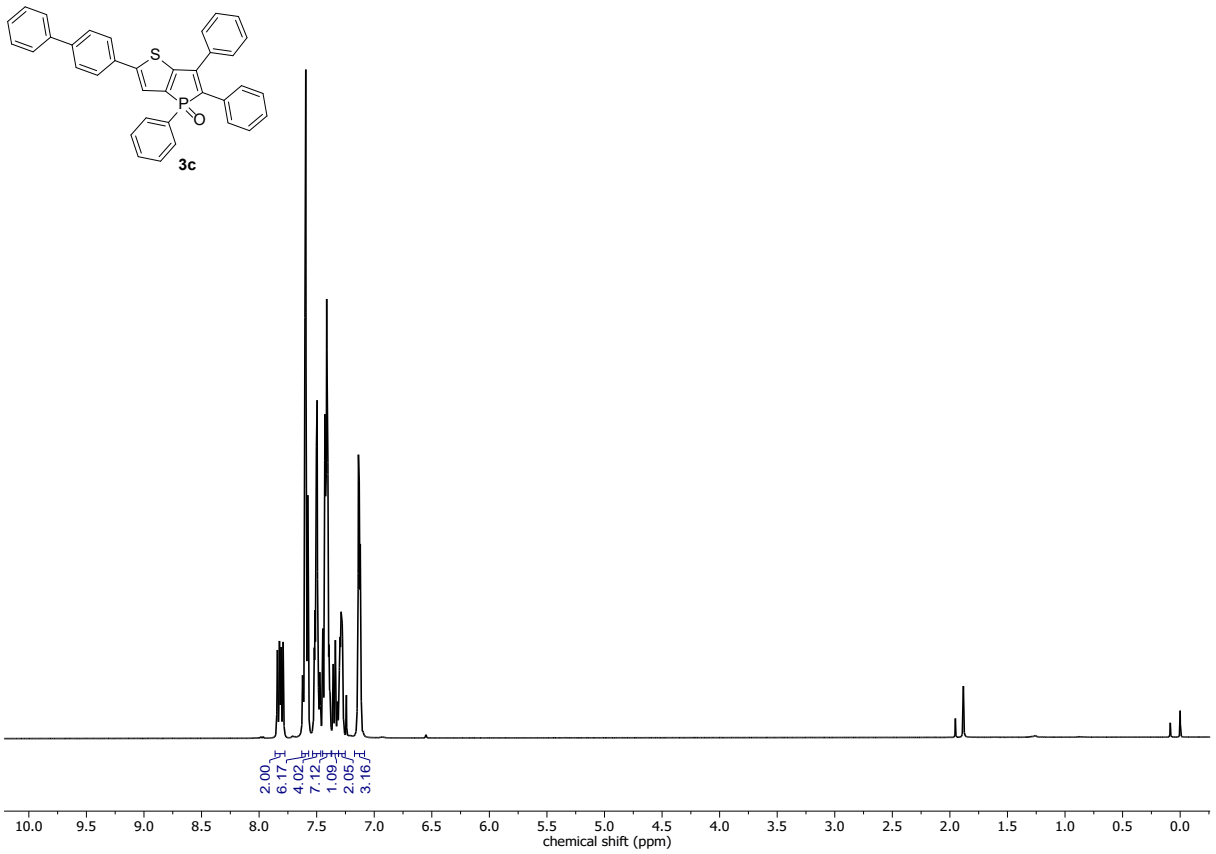

Fig S3.13: ^{1}H NMR spectrum of **3c** in $CDCl_3$.

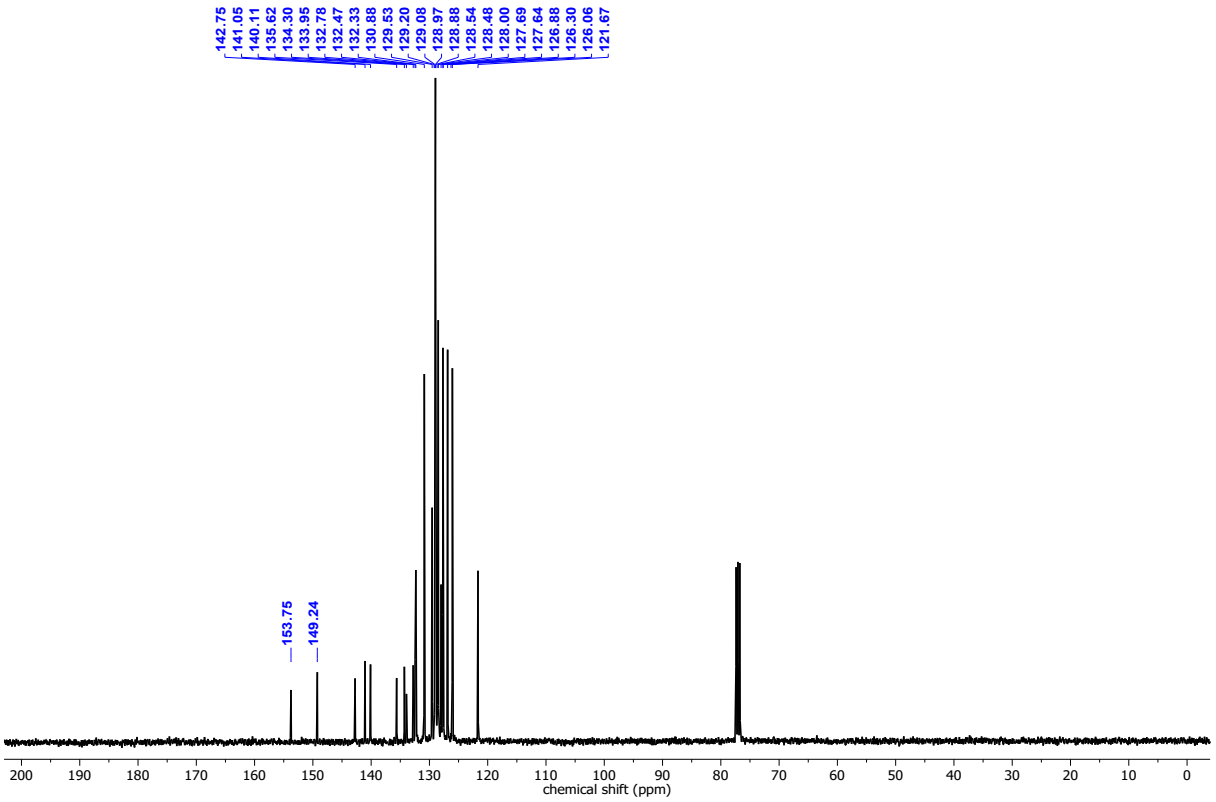

Fig S3.14: $^{13}C\{^{31}P, ^{1}H\}$ NMR spectrum of **3c** in $CDCl_3$.

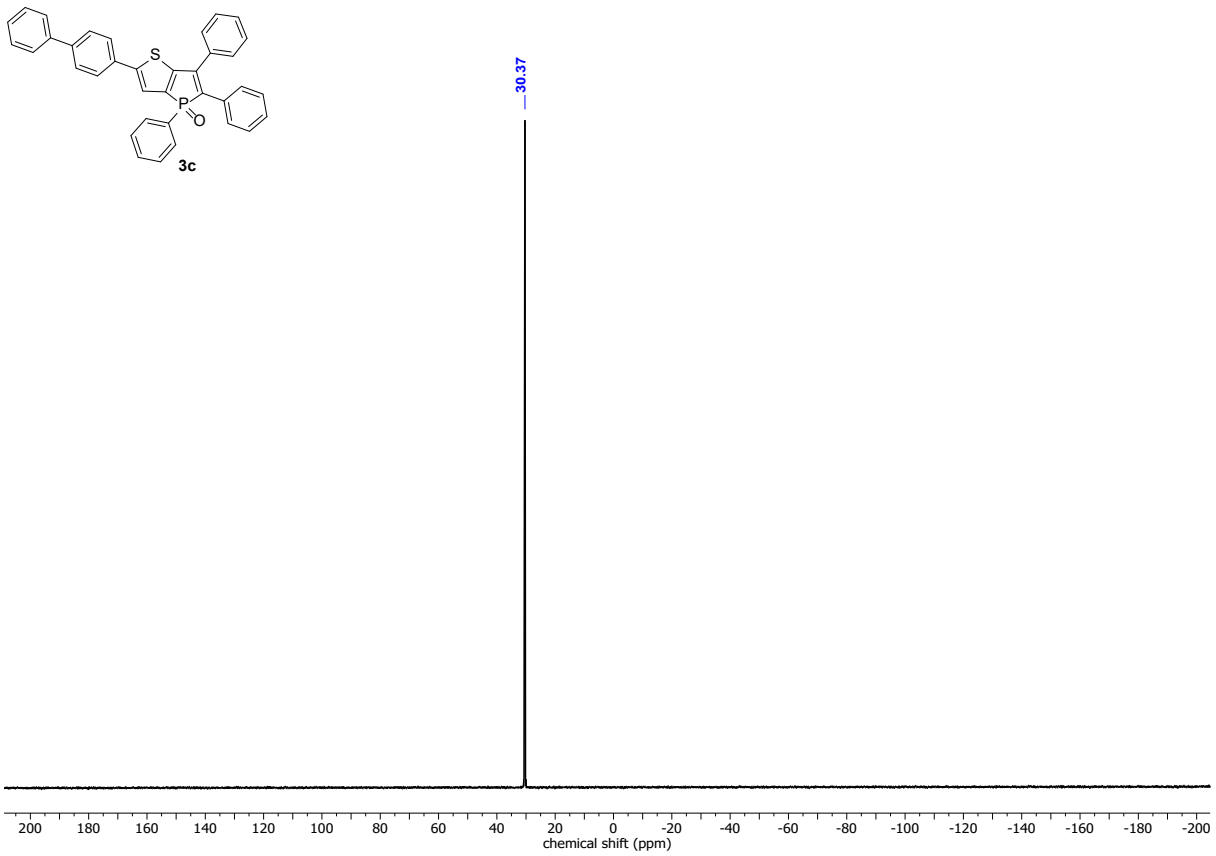

Fig S3.15: $^{31}P\{^{1}H\}$ NMR spectrum of **3c** in $CDCl_3$.

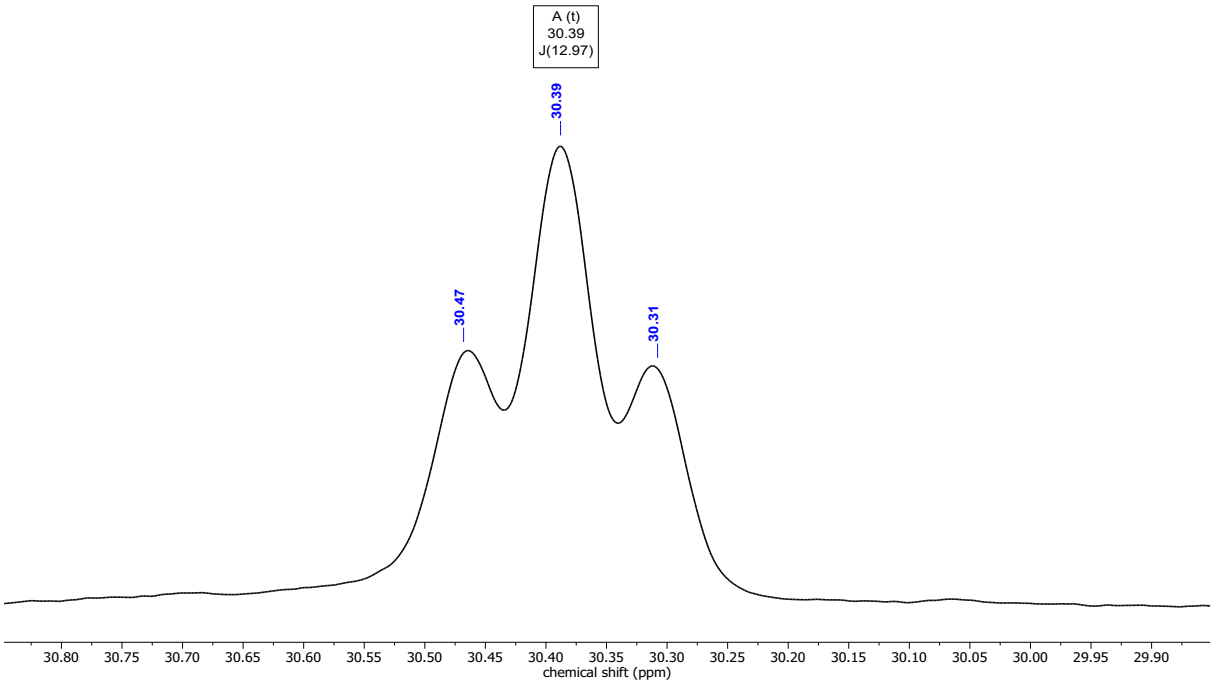

Fig S3.16: Details of the ^{31}P NMR spectrum of **3c** in $CDCl_3$.

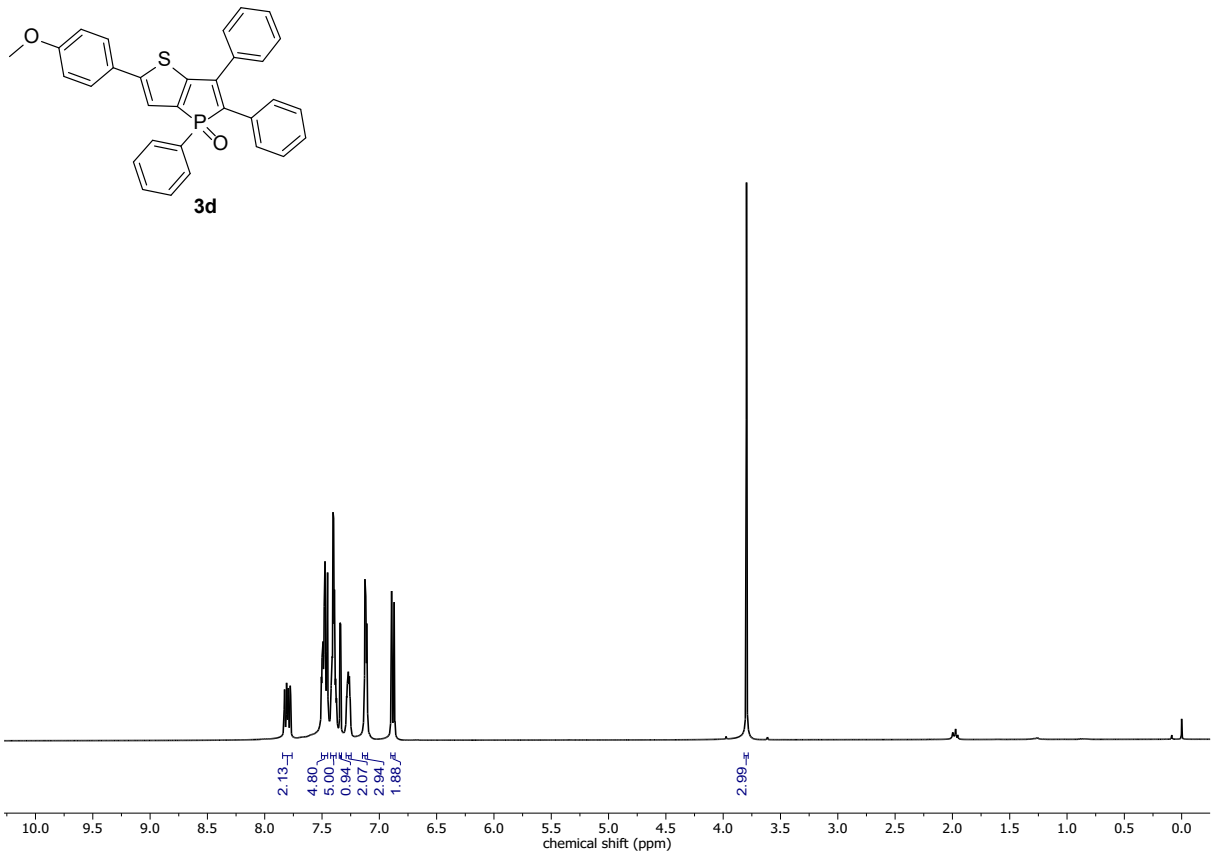

Fig S3.17: ^{1}H NMR spectrum of **3d** in $CDCl_3$.

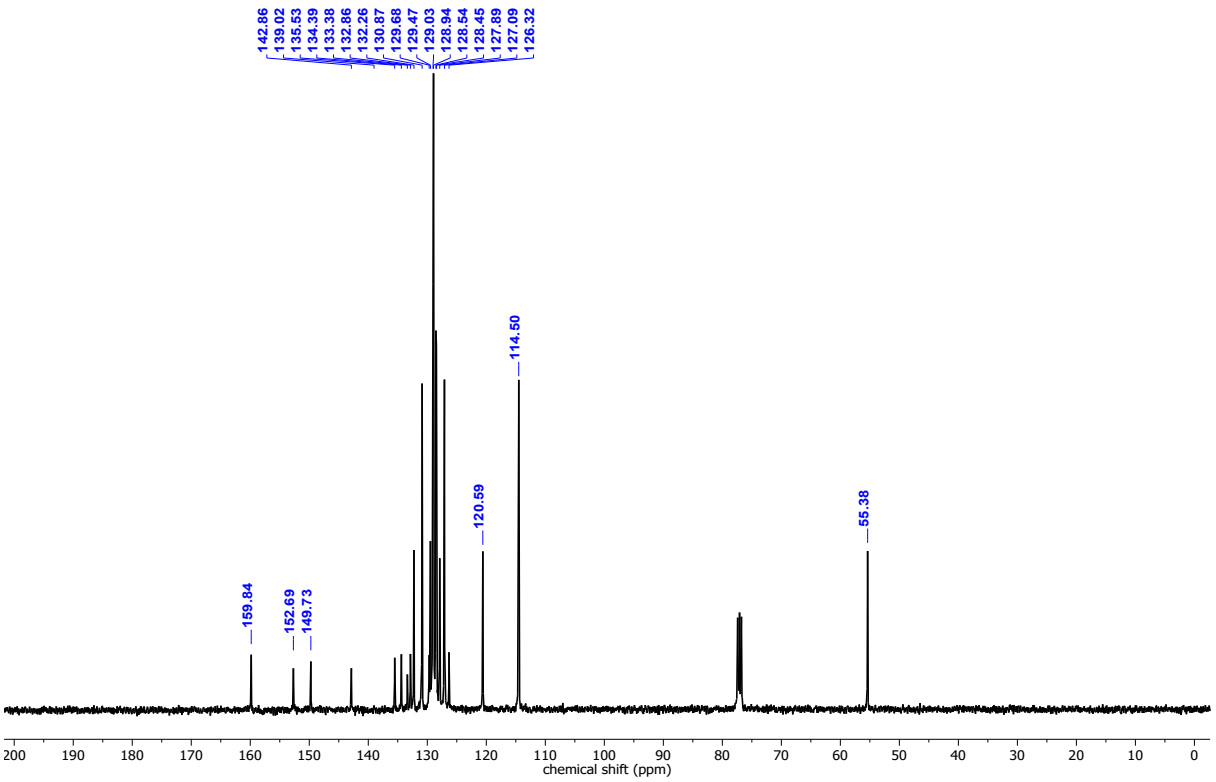

Fig S3.18: $^{13}C\{^{31}P, ^{1}H\}$ NMR spectrum of **3d** in $CDCl_3$.

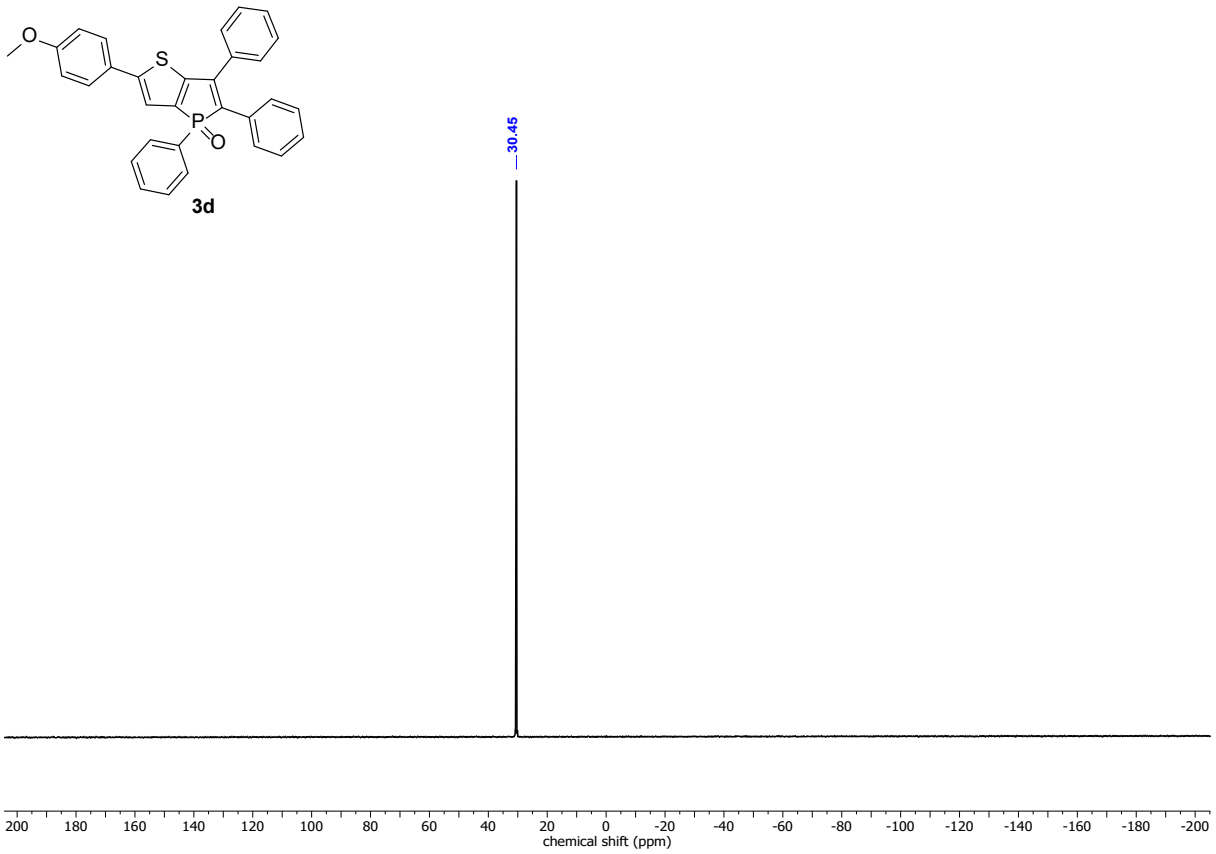

Fig S3.19: $^{31}P\{^{1}H\}$ NMR spectrum of **3d** in $CDCl_3$.

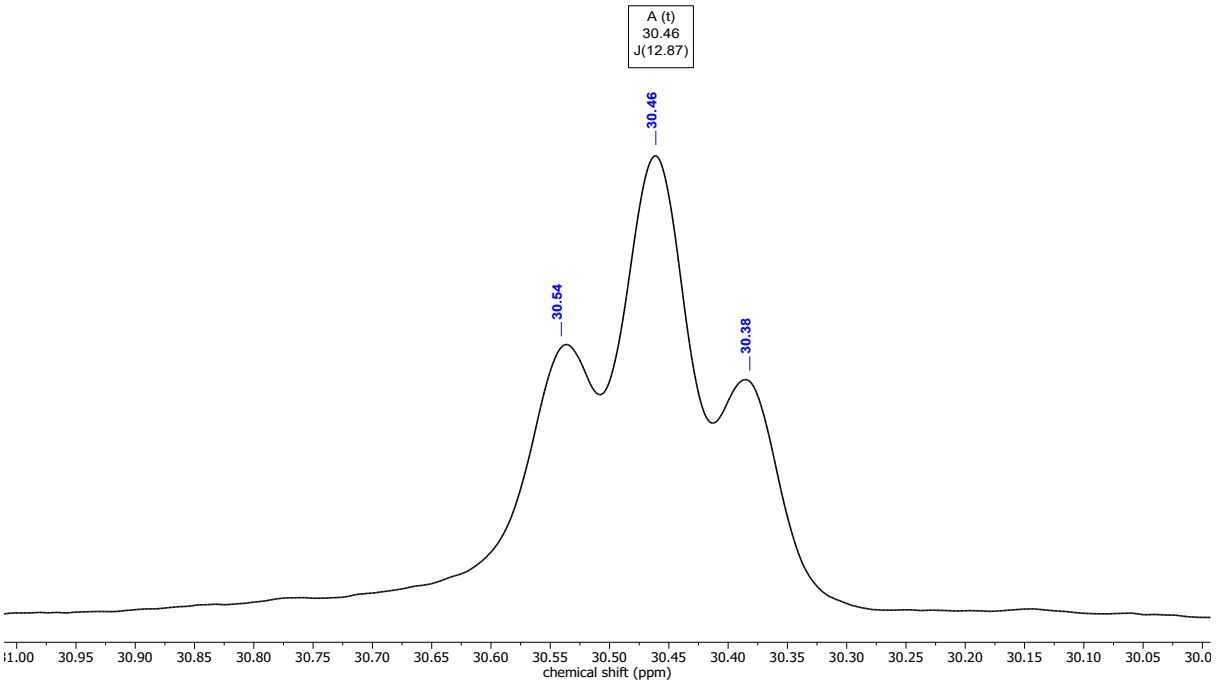

Fig S3.20: Details of the ^{31}P NMR spectrum of **3d** in $CDCl_3$.

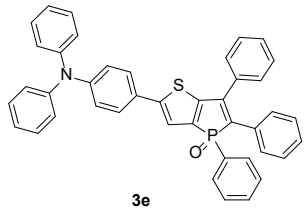

3e

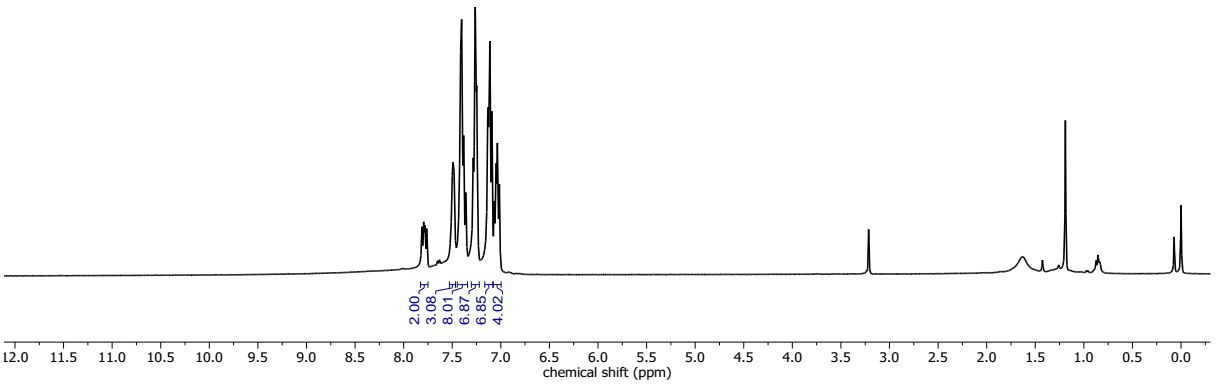

Fig S3.21: ^{1}H NMR spectrum of **3e** in $CDCl_3$.

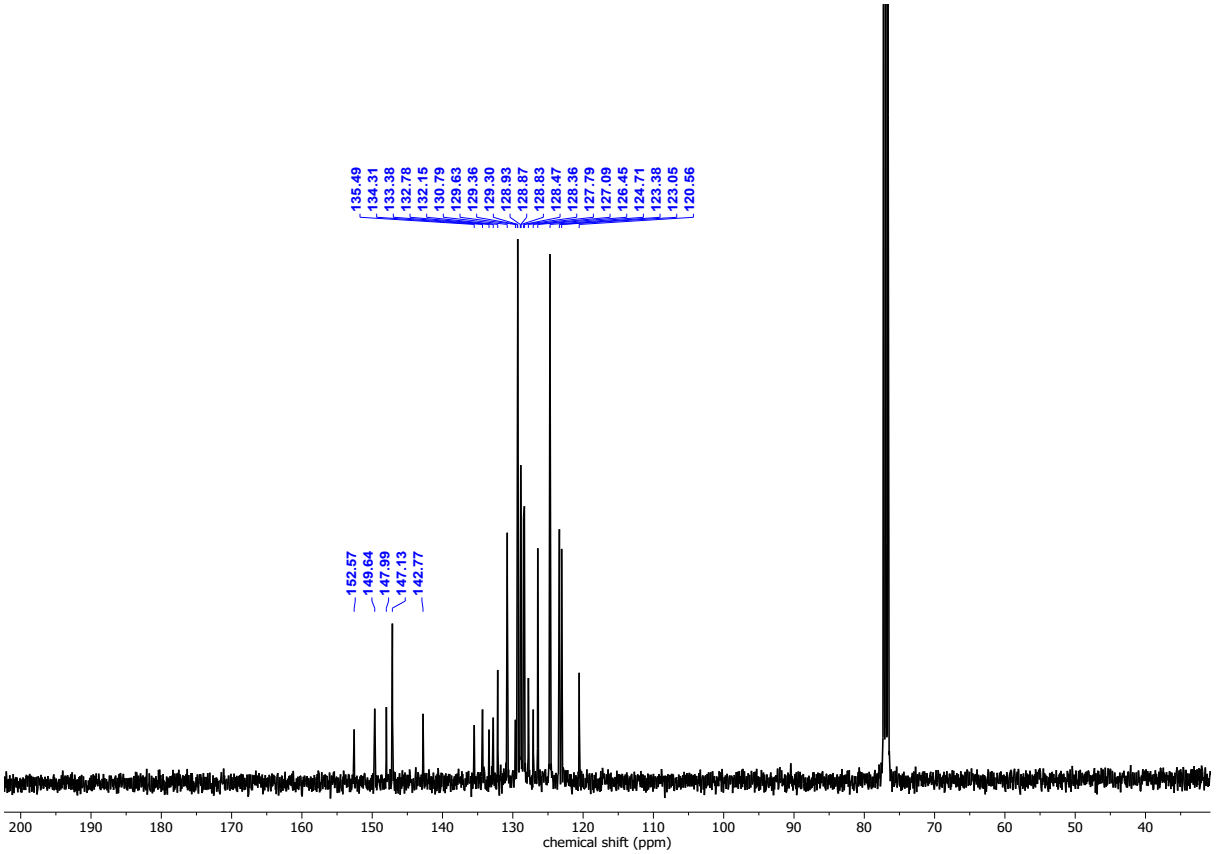

Fig S3.22: $^{13}C\{^{31}P, ^{1}H\}$ NMR spectrum of **3e** in $CDCl_3$.

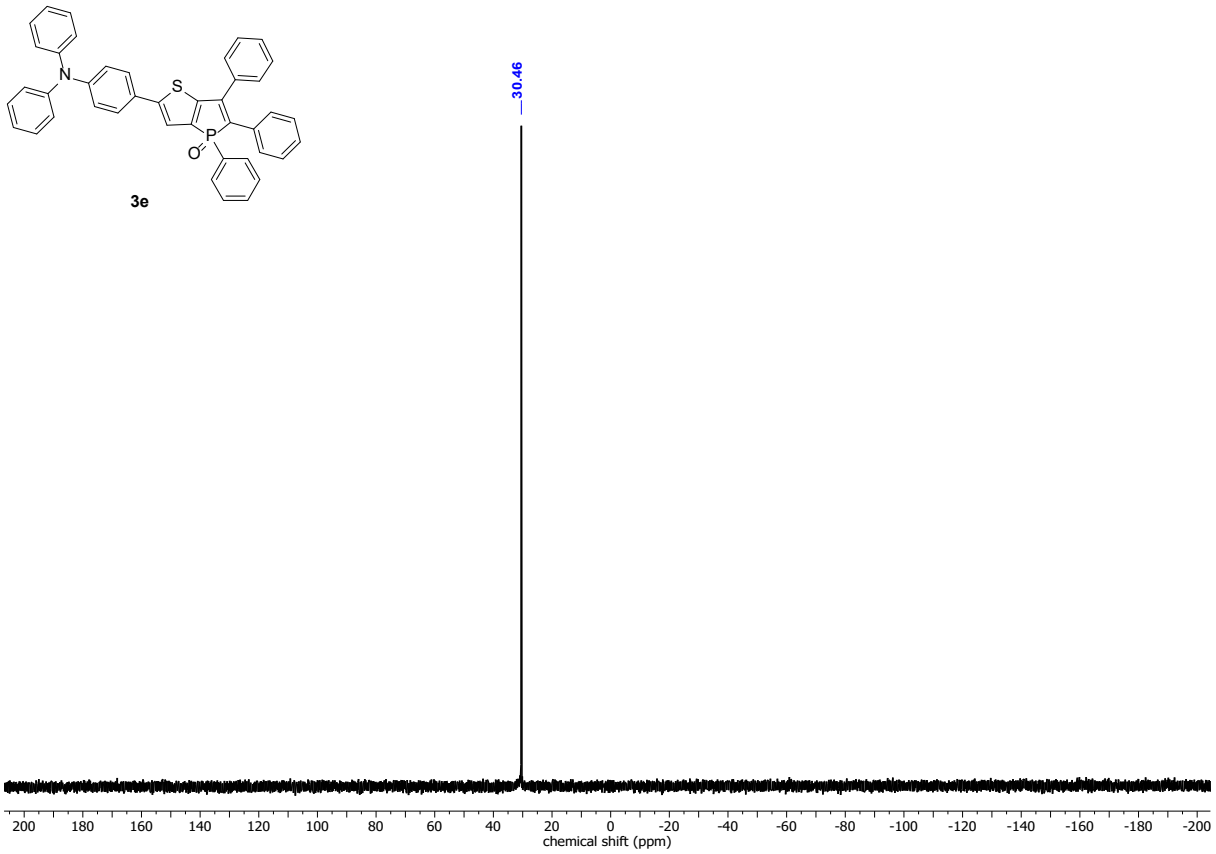

Fig S3.23: $^{31}P\{^{1}H\}$ NMR spectrum of **3e** in $CDCl_3$.

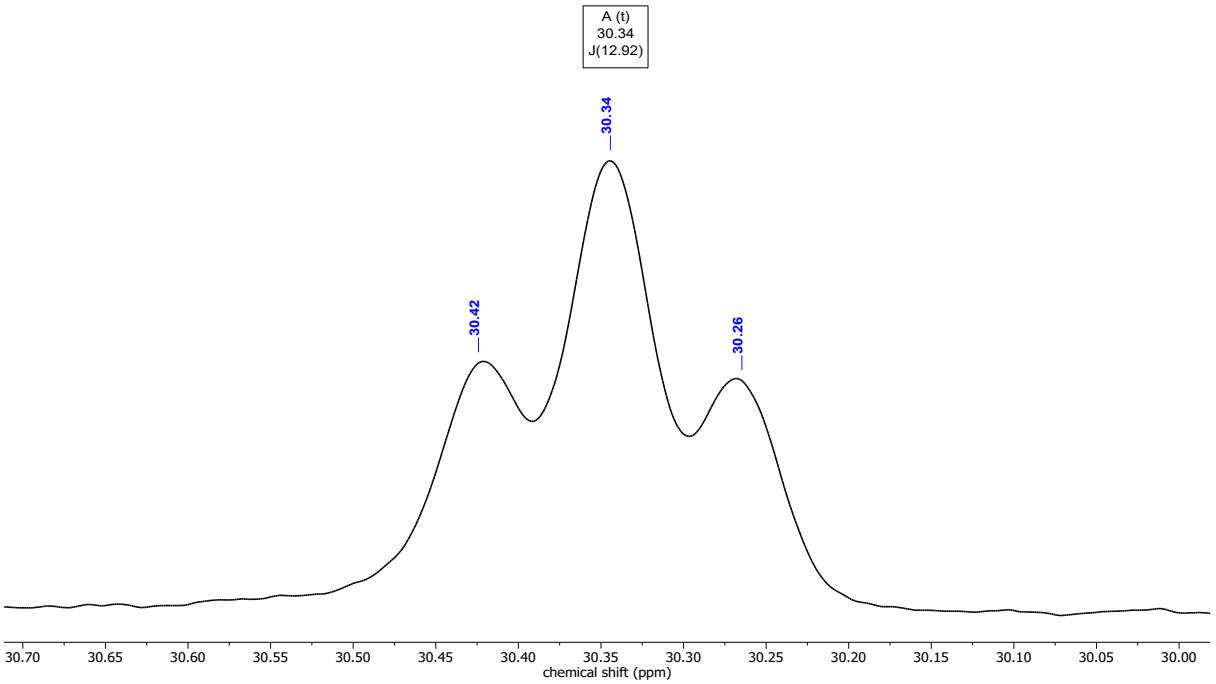

Fig S3.24: Details of the ^{31}P NMR spectrum of **3e** in $CDCl_3$.

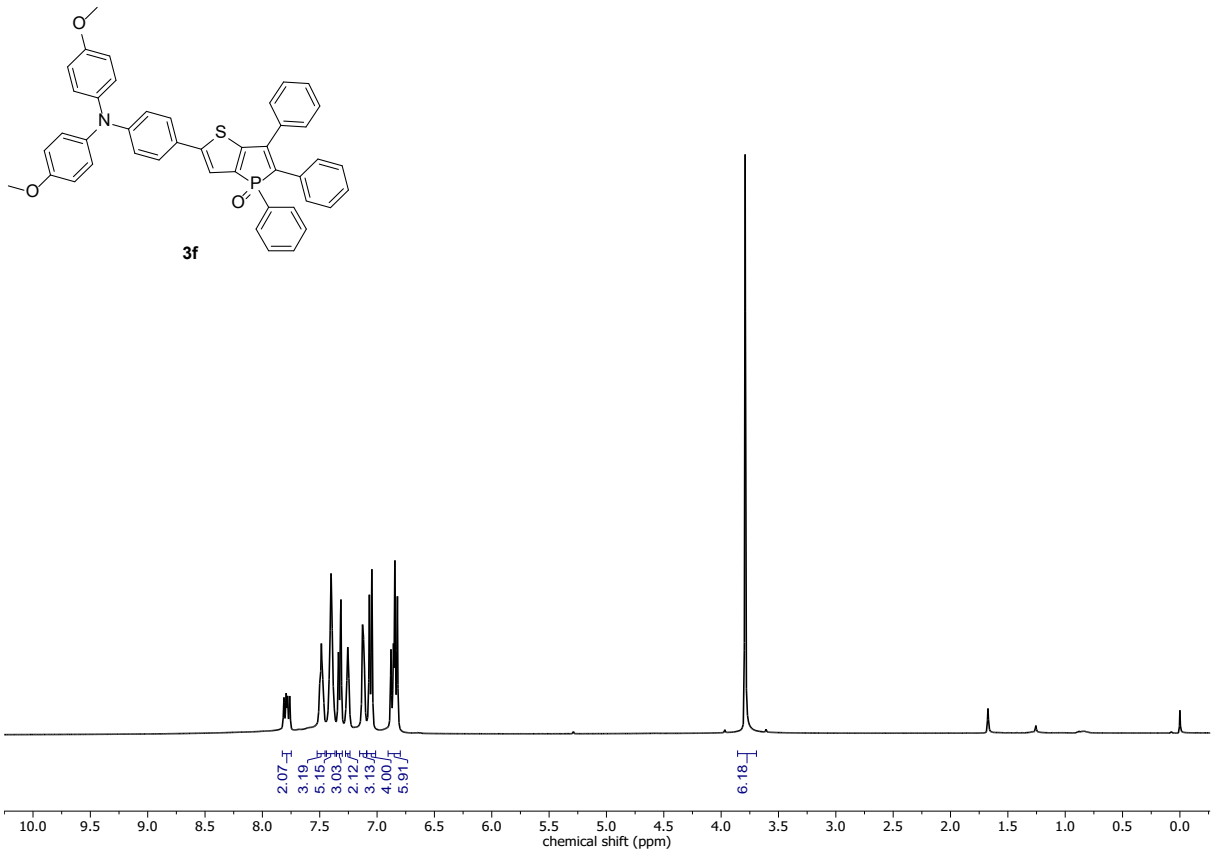

Fig S3.25: ^{1}H NMR spectrum of **3f** in $CDCl_3$.

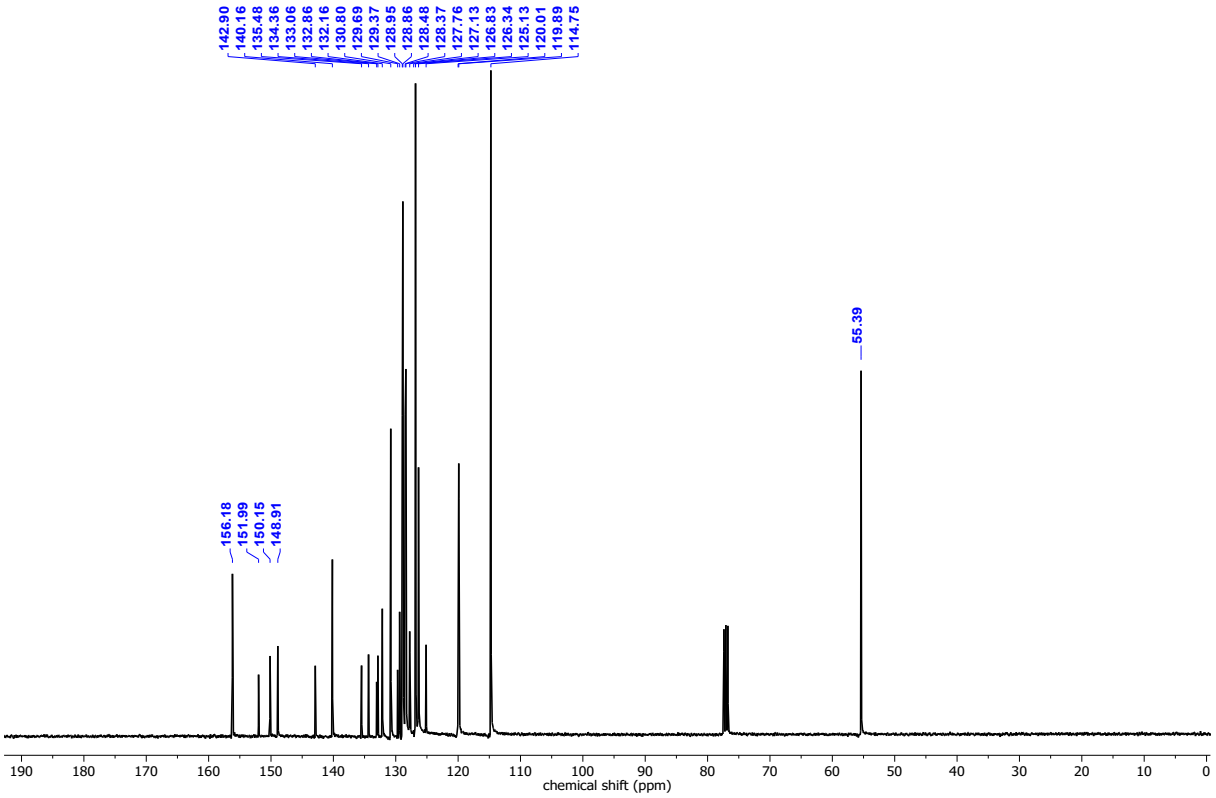

Fig S3.26: $^{13}C\{^{31}P, ^{1}H\}$ NMR spectrum of **3f** in $CDCl_3$.

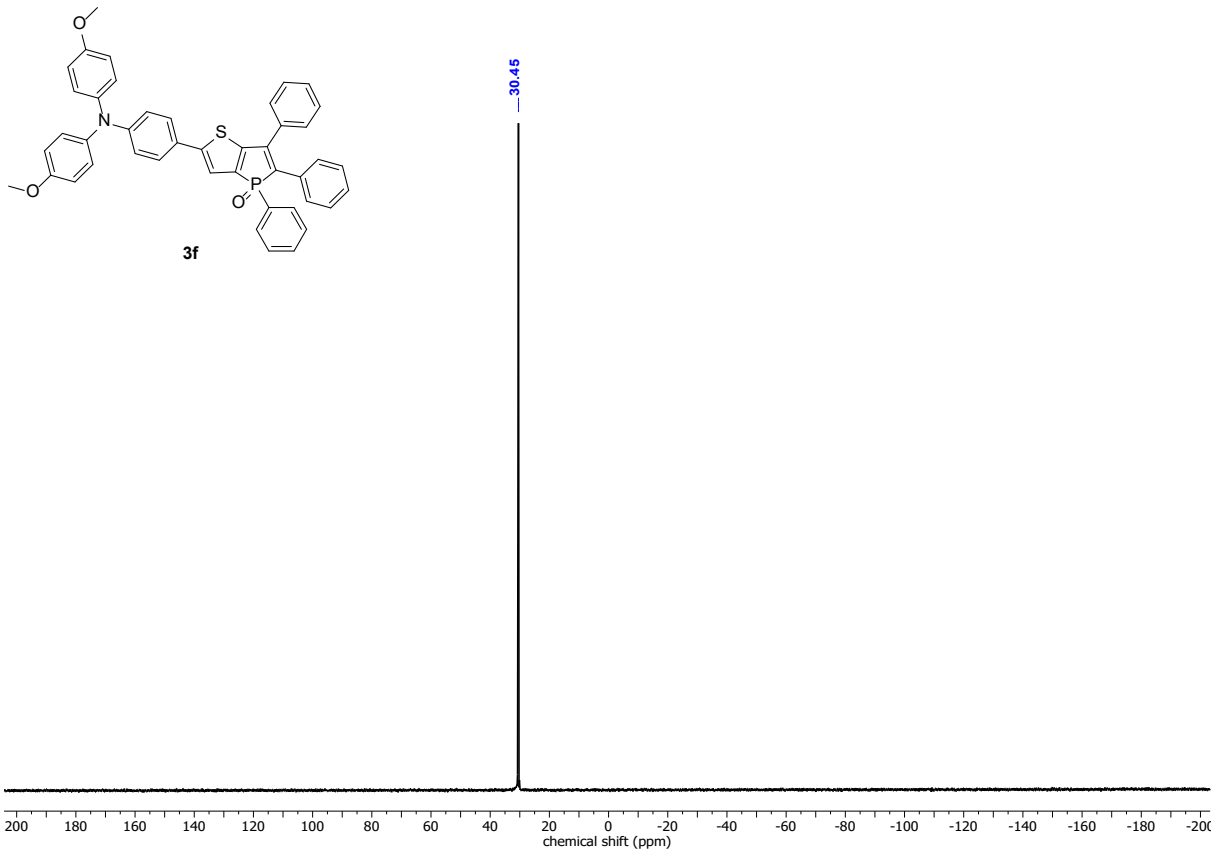

Fig S3.27: $^{31}P\{^{1}H\}$ NMR spectrum of **3f** in $CDCl_3$.

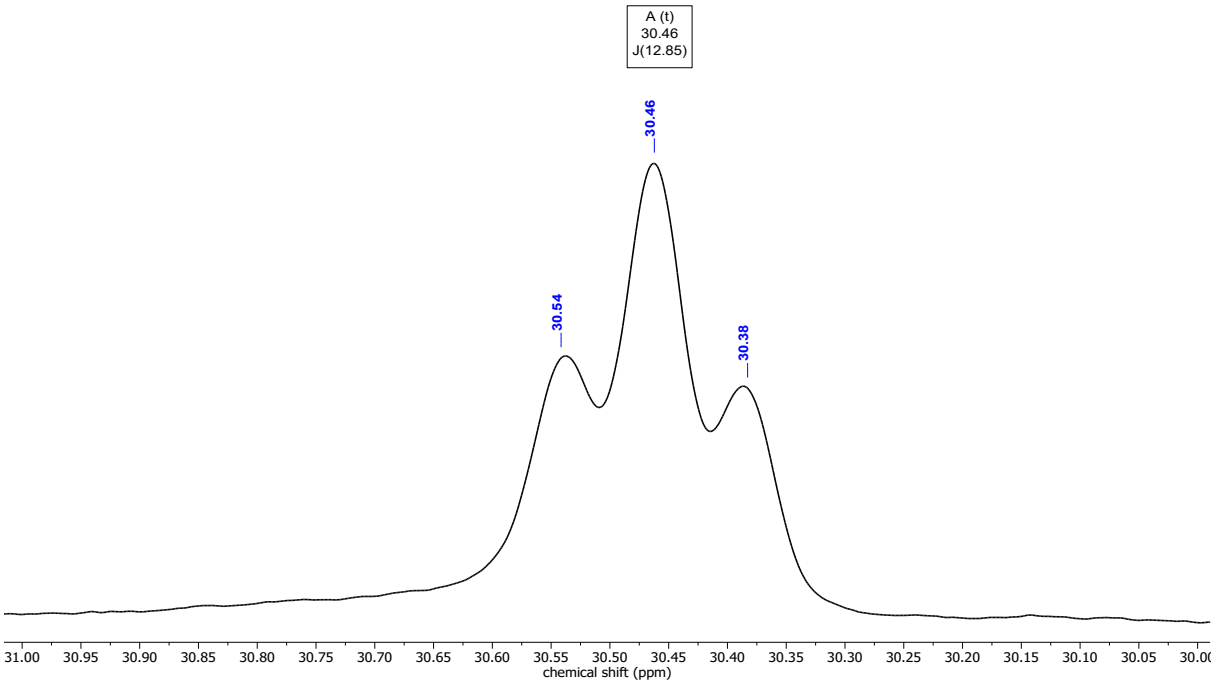

Fig S3.28: Details of the ^{31}P NMR spectrum of **3f** in $CDCl_3$.

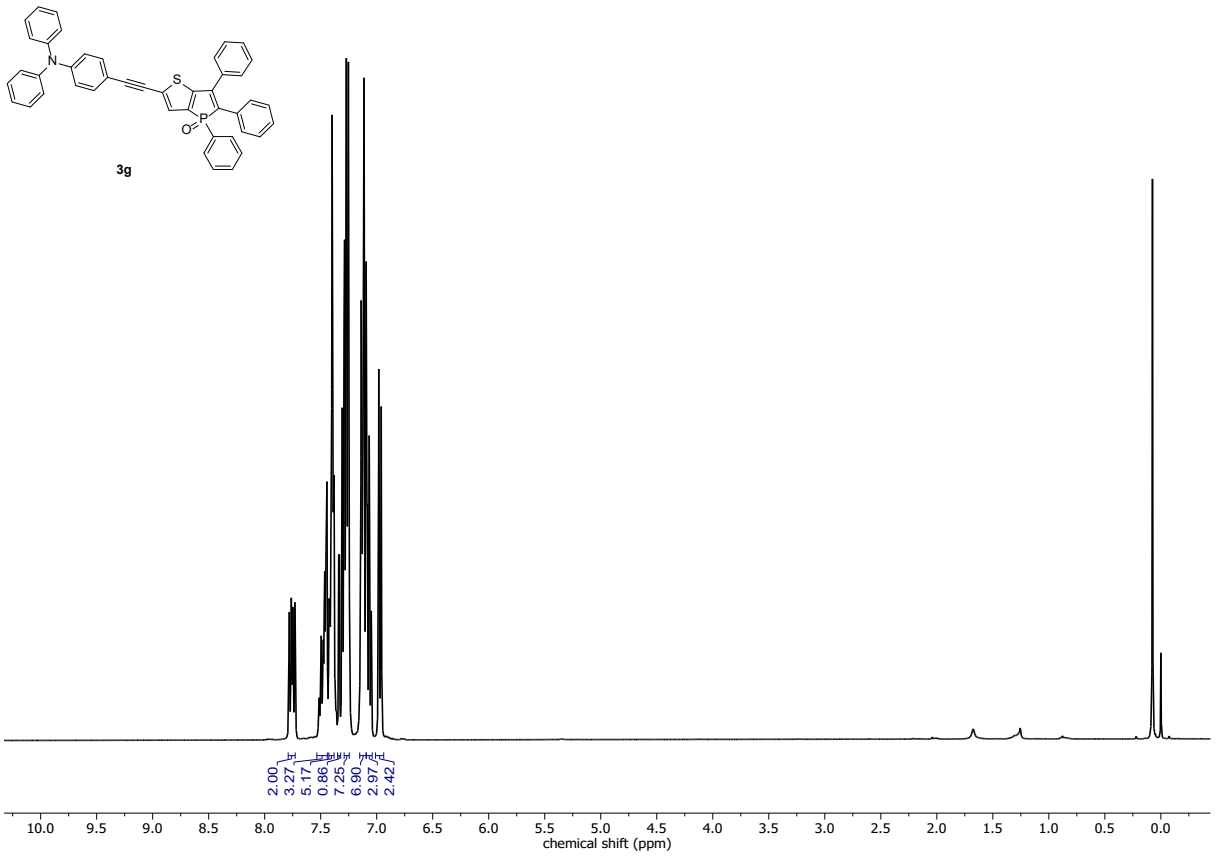

Fig S3.29: ^{1}H NMR spectrum of **3g** in $CDCl_3$.

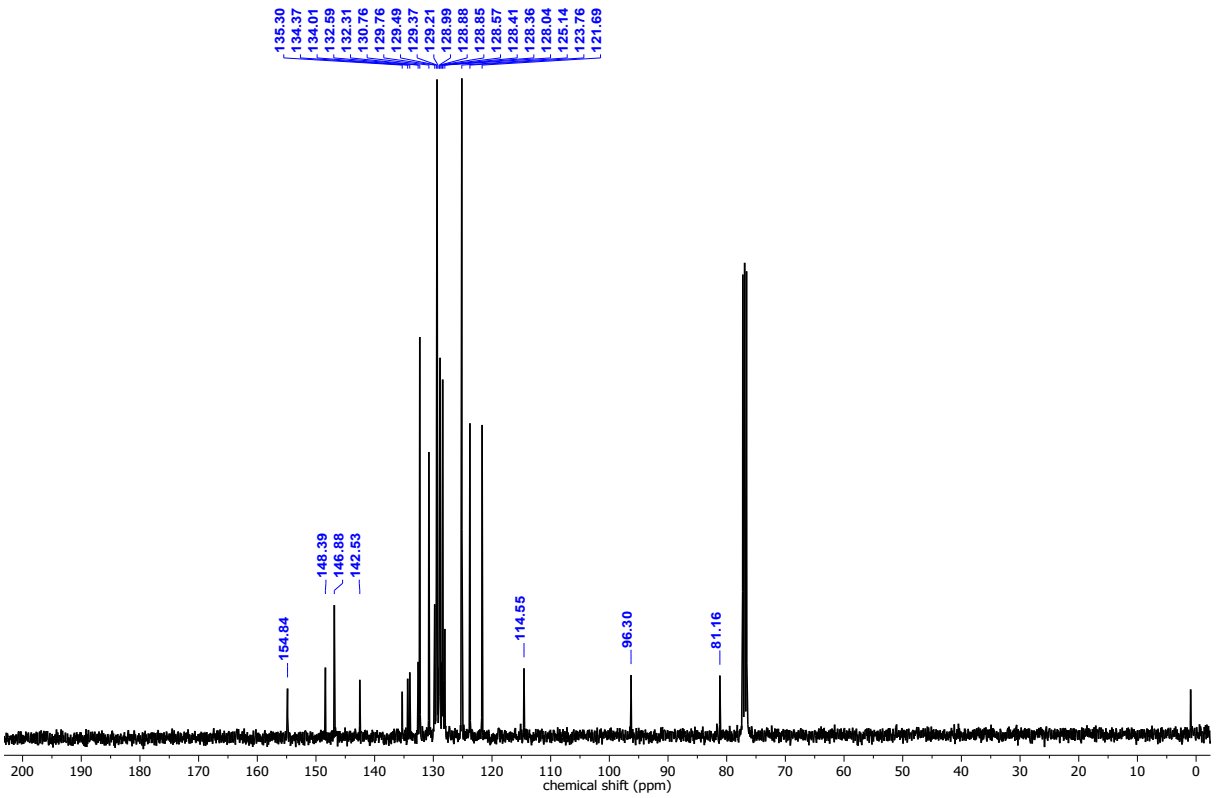

Fig S3.30: $^{13}C\{^{31}P, ^{1}H\}$ NMR spectrum of **3g** in $CDCl_3$.

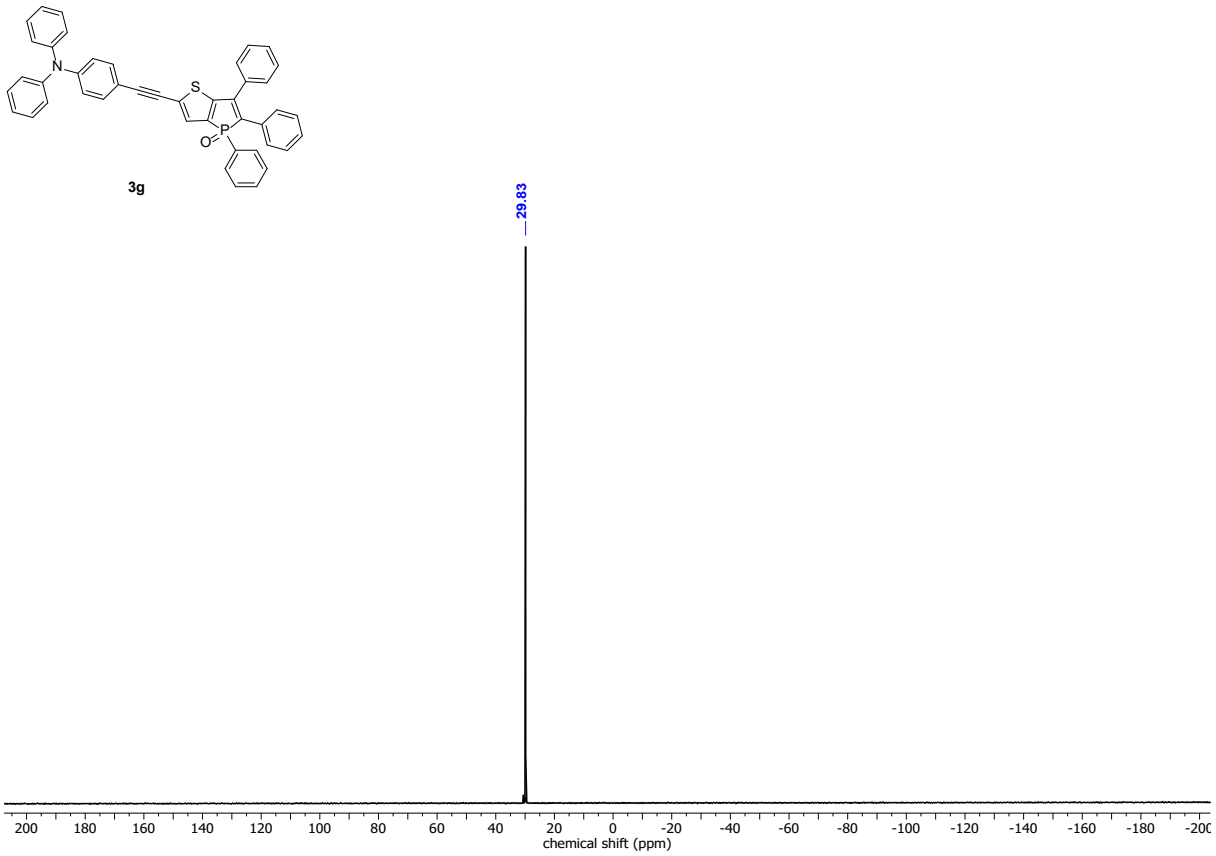

Fig S3.31: $^{31}P\{^{1}H\}$ NMR spectrum of **3g** in $CDCl_3$.

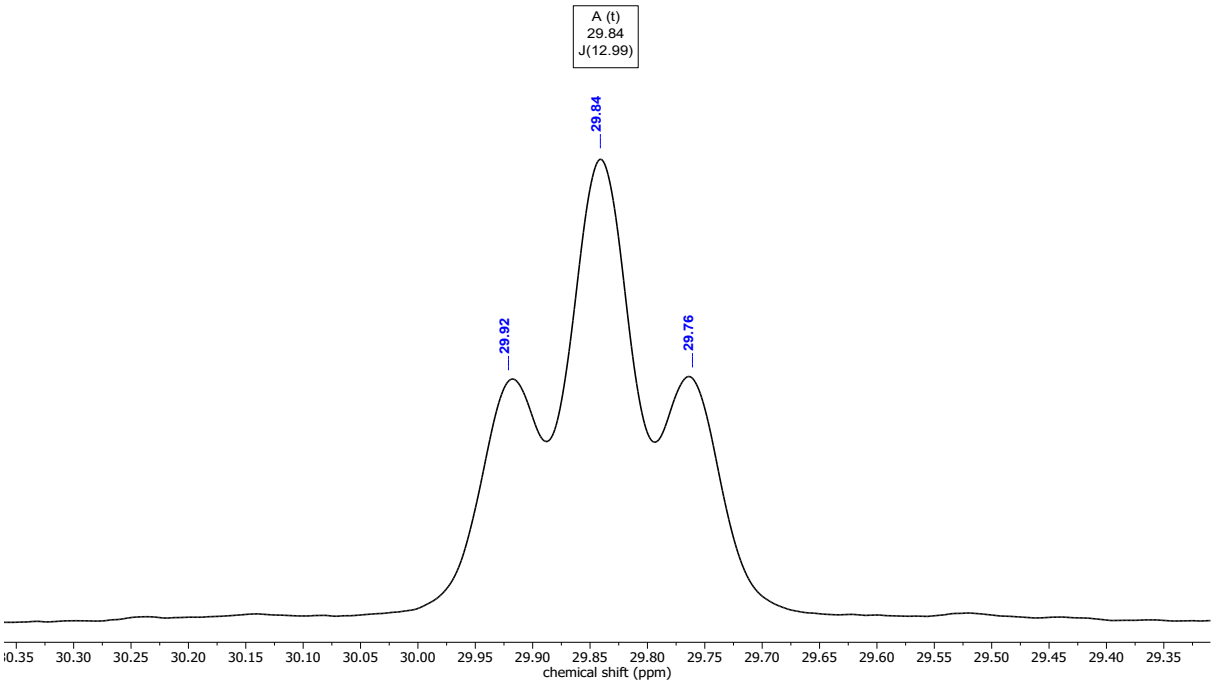

Fig S3.32: Details of the ^{31}P NMR spectrum of **3g** in $CDCl_3$.

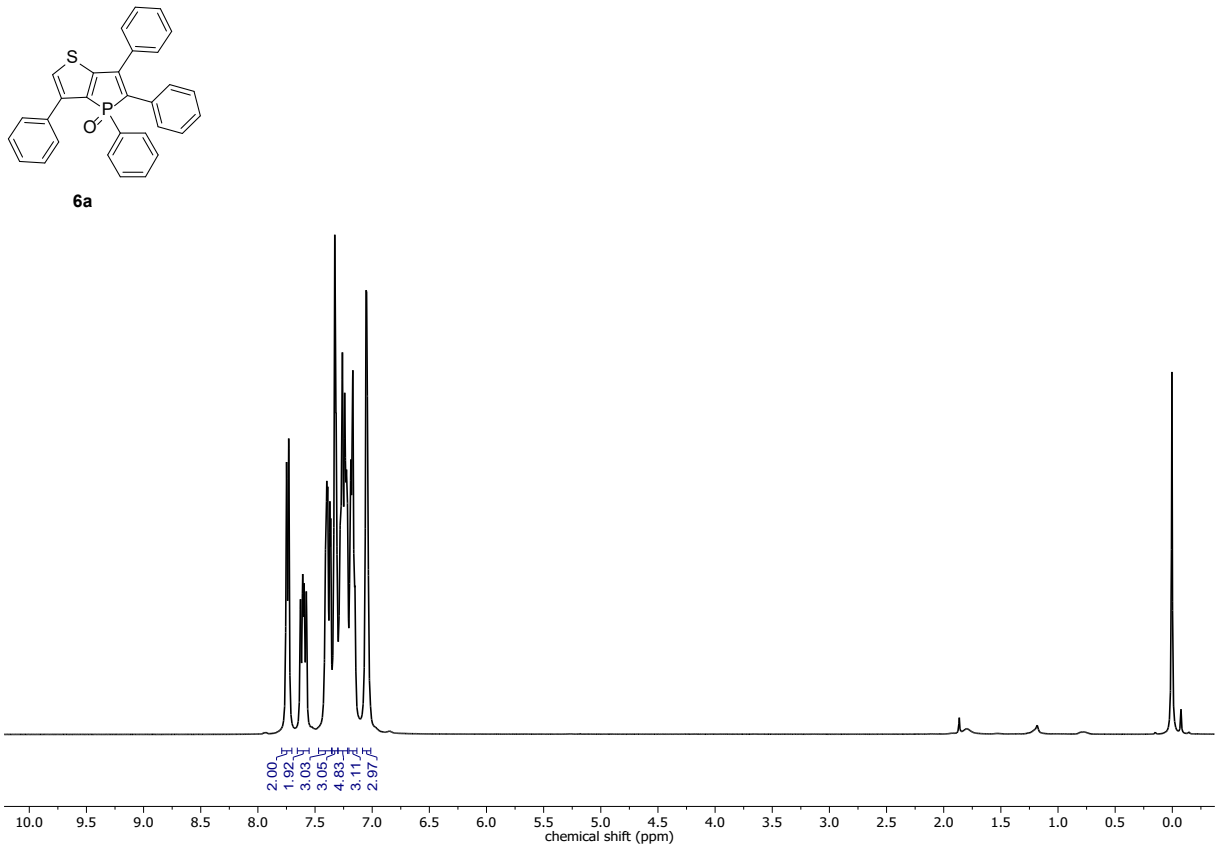

Fig S3.33: ^{1}H NMR spectrum of **6a** in $CDCl_3$.

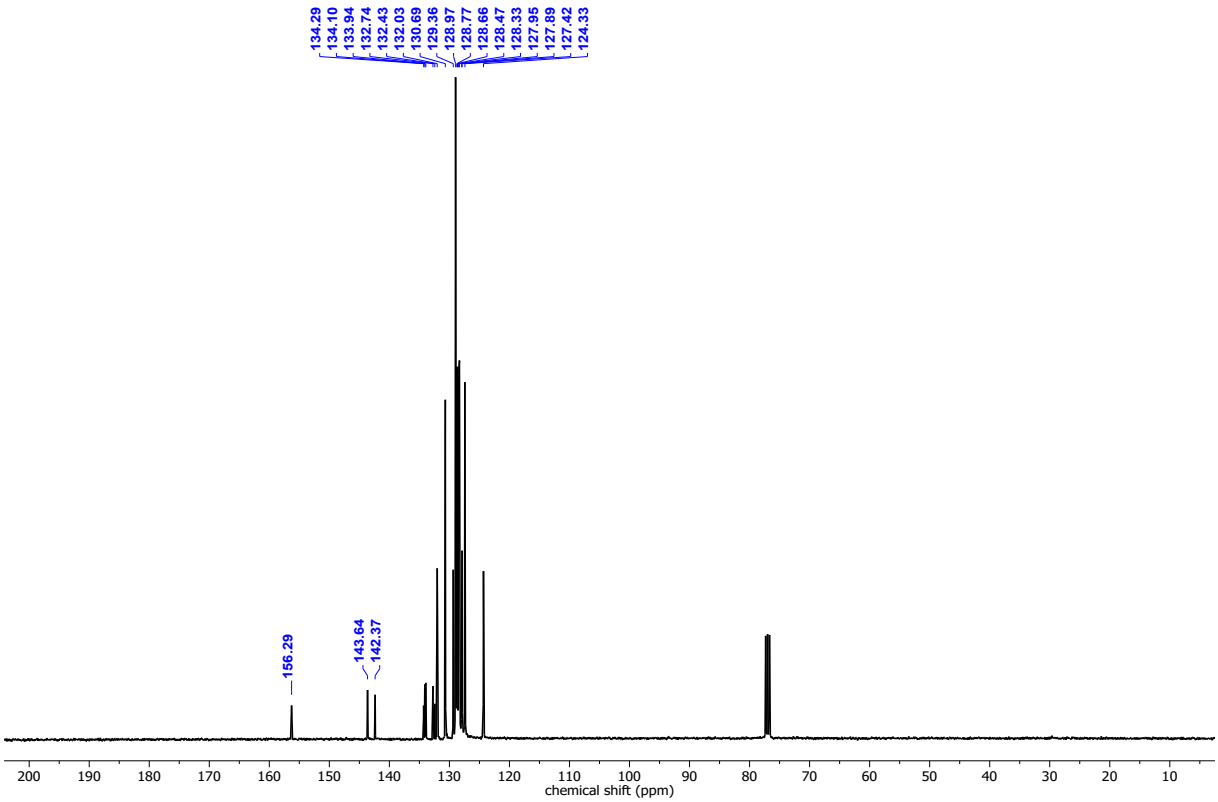

Fig S3.34: $^{13}C\{^{31}P, ^{1}H\}$ NMR spectrum of **6a** in $CDCl_3$.

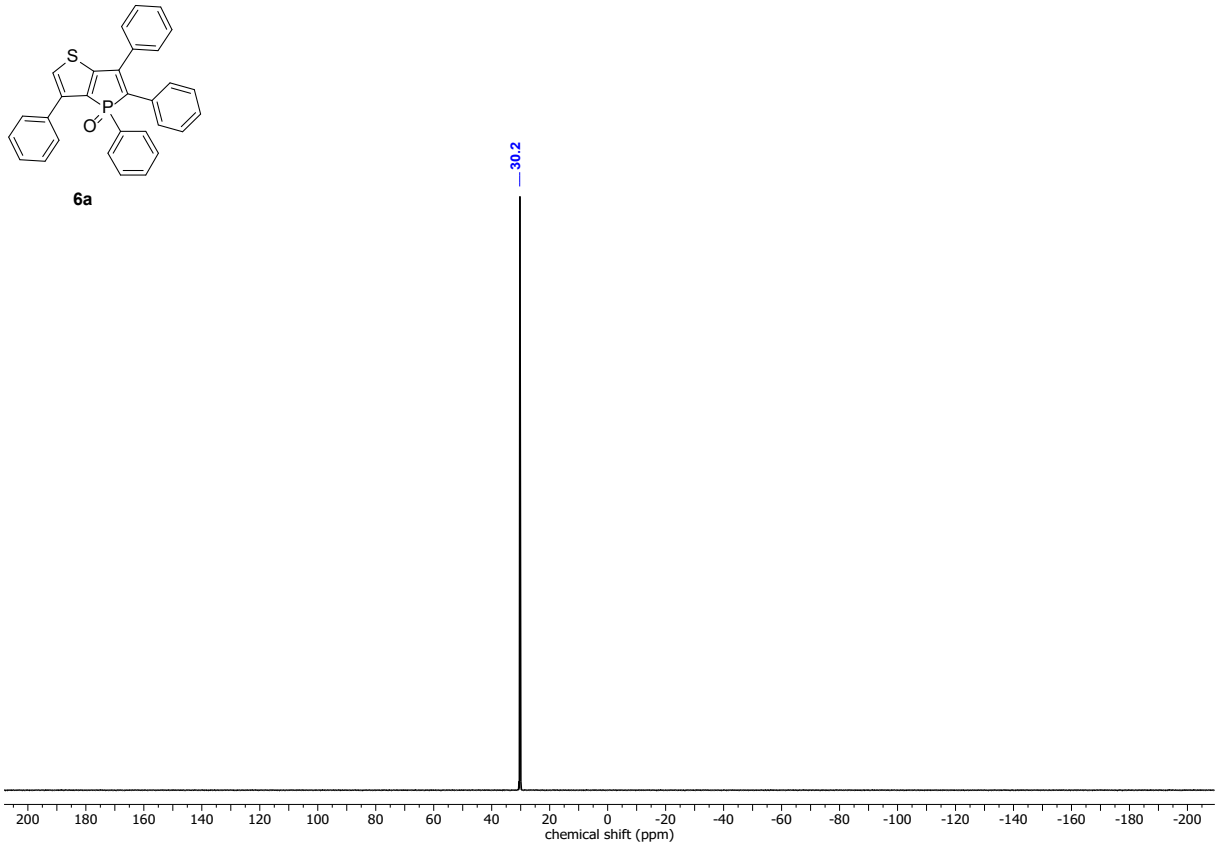

Fig S3.35: $^{31}P\{^{1}H\}$ NMR spectrum of **6a** in $CDCl_3$.

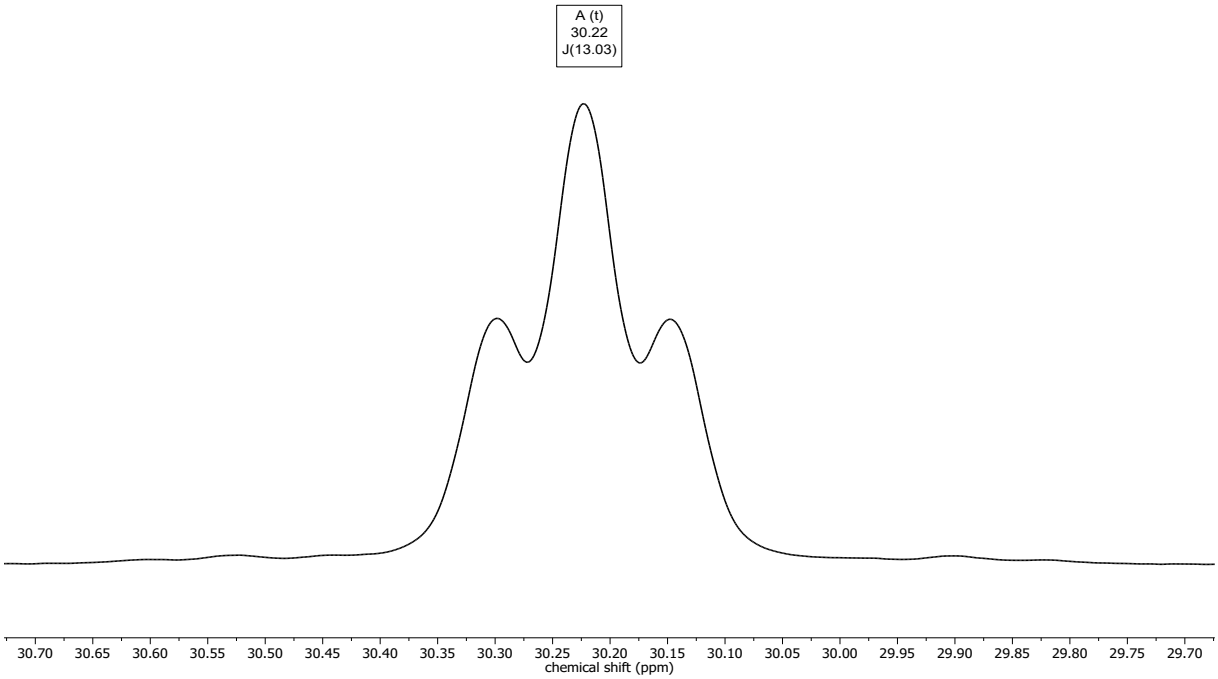

Fig S3.36: Details of the ^{31}P NMR spectrum of **6a** in $CDCl_3$.

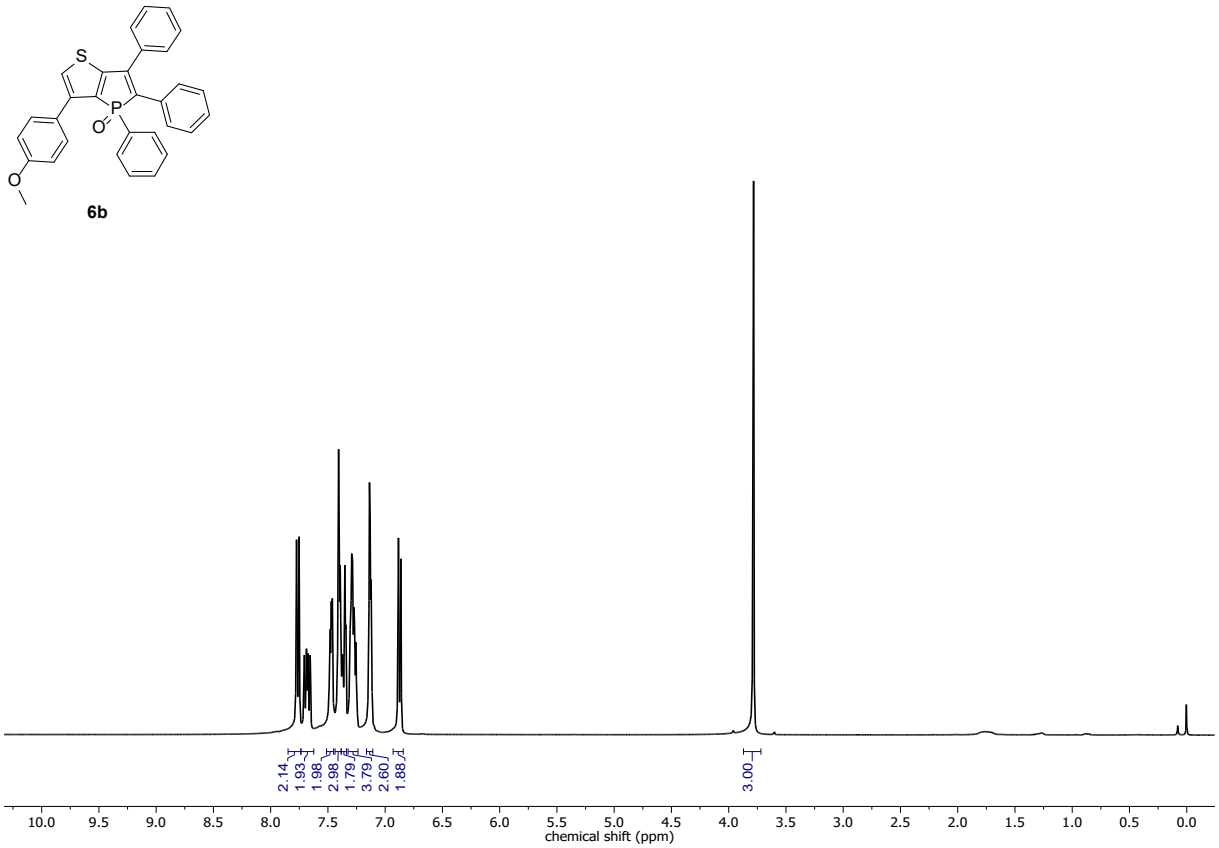

Fig S3.37: ^{1}H NMR spectrum of **6b** in $CDCl_3$.

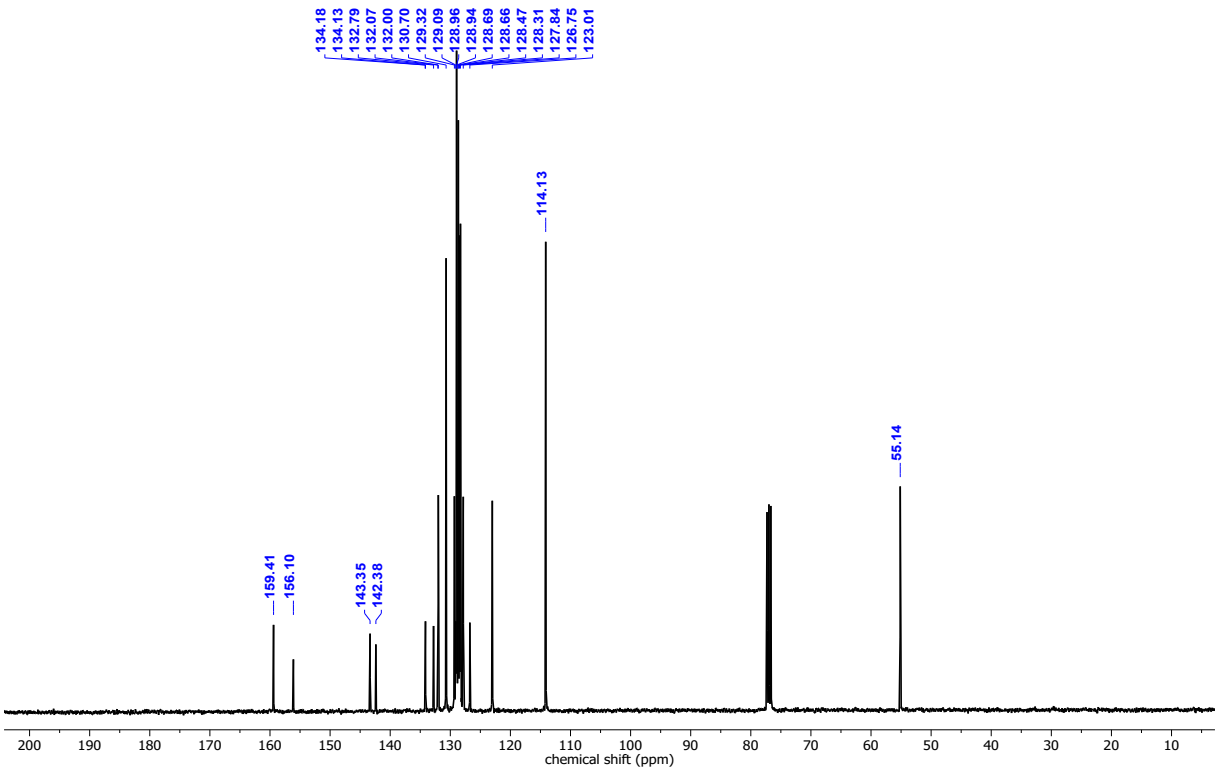

Fig S3.38: $^{13}C\{^{31}P, ^{1}H\}$ NMR spectrum of **6b** in $CDCl_3$.

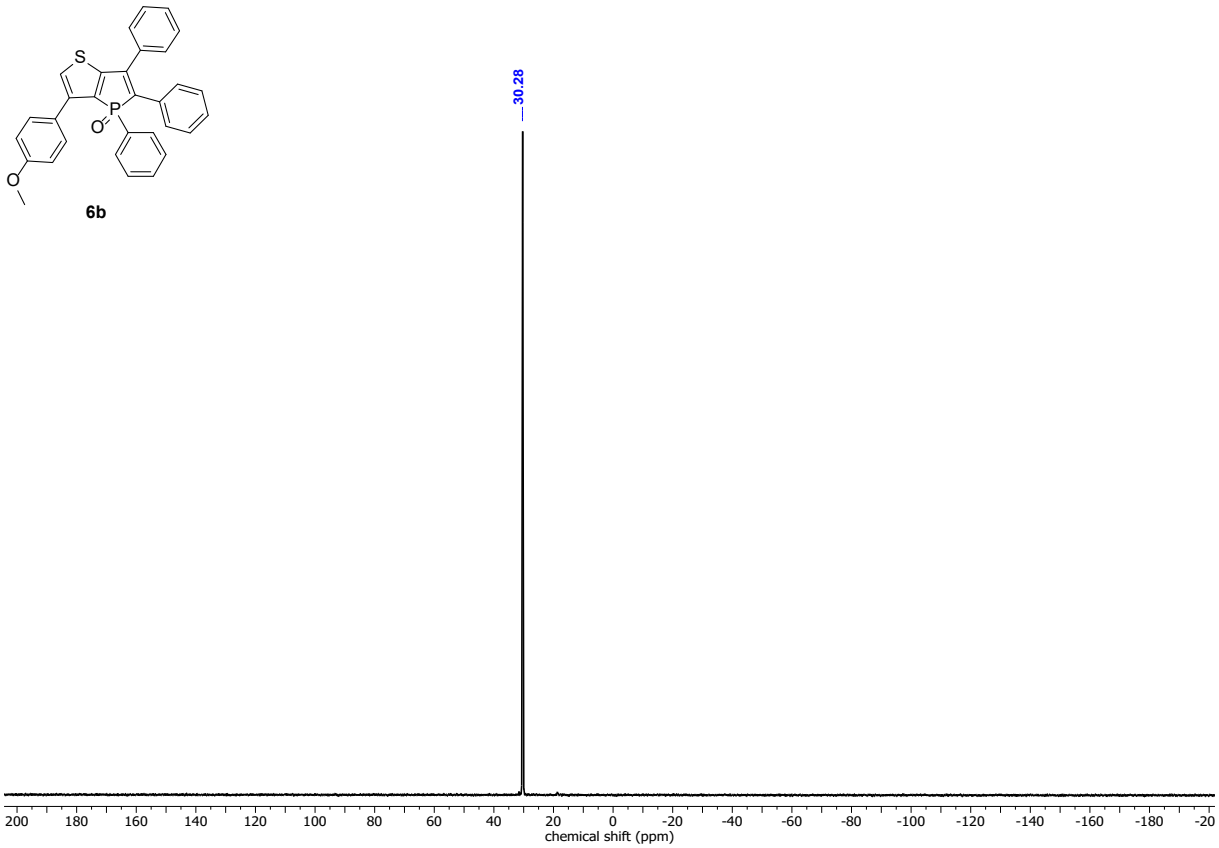

Fig S3.39: $^{31}P\{^{1}H\}$ NMR spectrum of **6b** in $CDCl_3$.

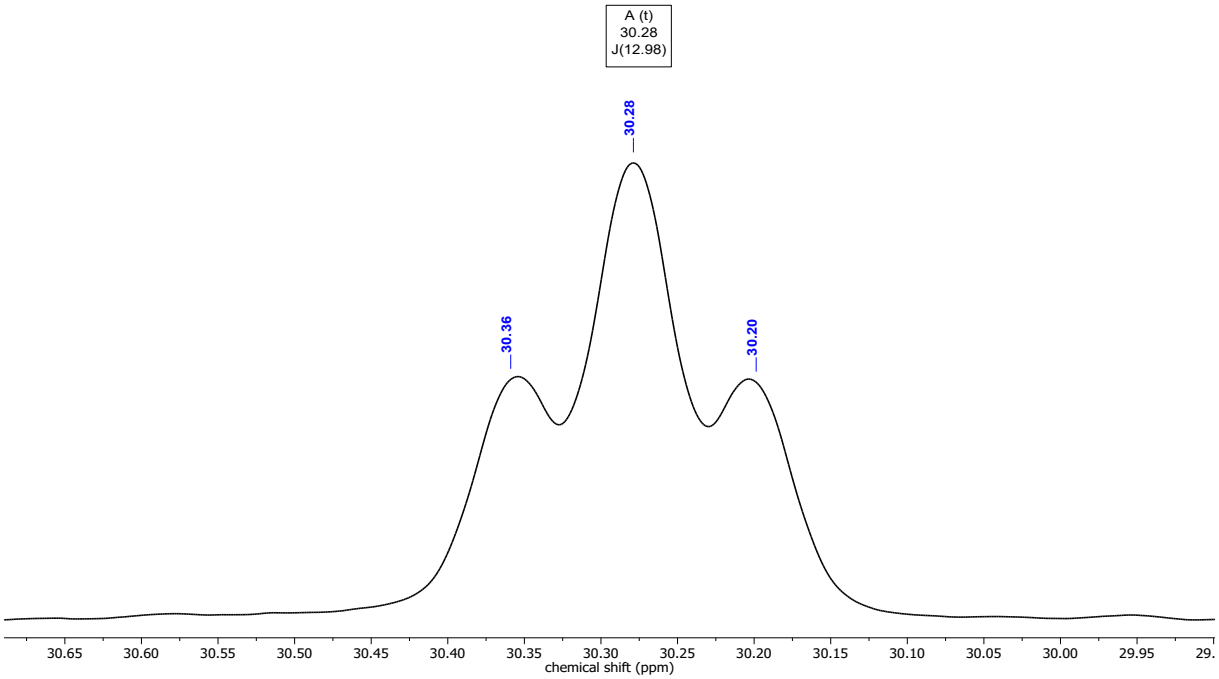

Fig S3.40: Details of the ^{31}P NMR spectrum of **6b** in $CDCl_3$.

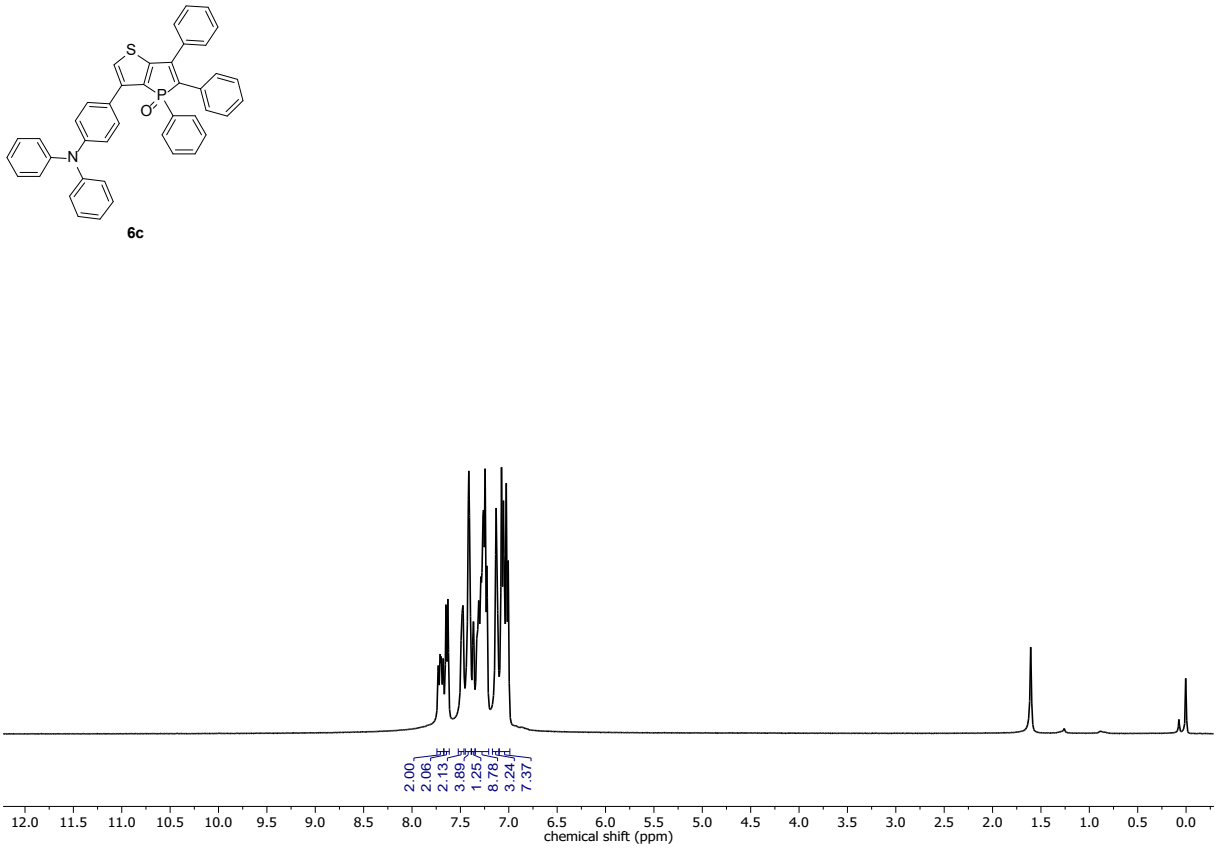

Fig S3.41: ^{1}H NMR spectrum of **6c** in $CDCl_3$.

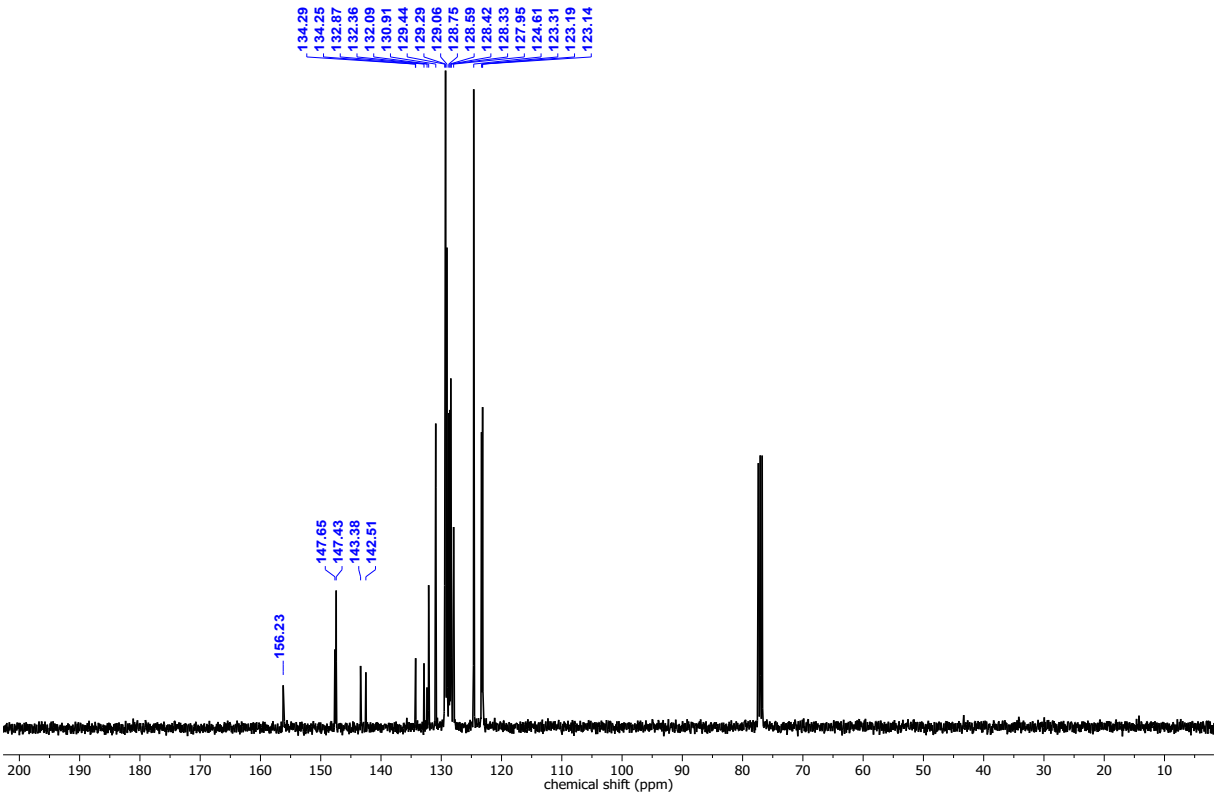

Fig S3.42: $^{13}C\{^{31}P, ^{1}H\}$ NMR spectrum of **6c** in $CDCl_3$.

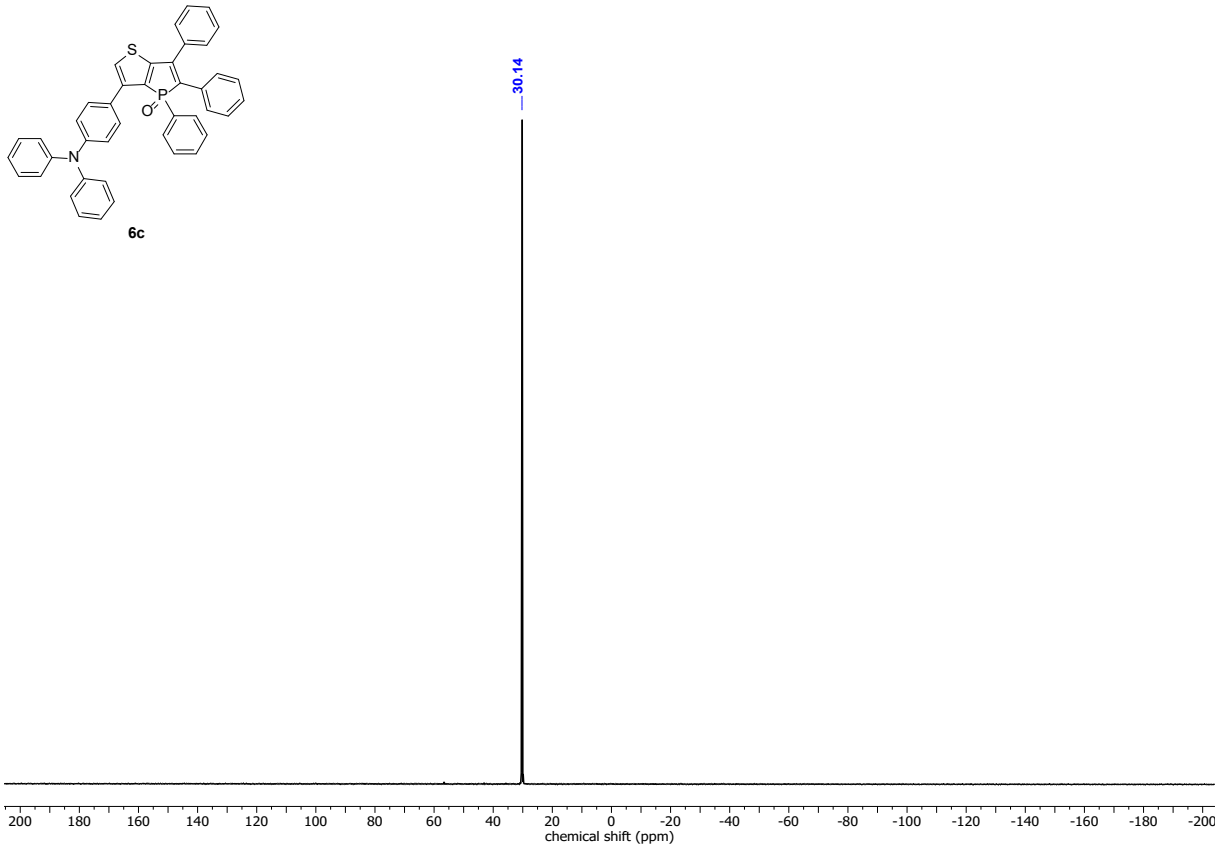

Fig S3.43: $^{31}P\{^{1}H\}$ NMR spectrum of **6c** in $CDCl_3$.

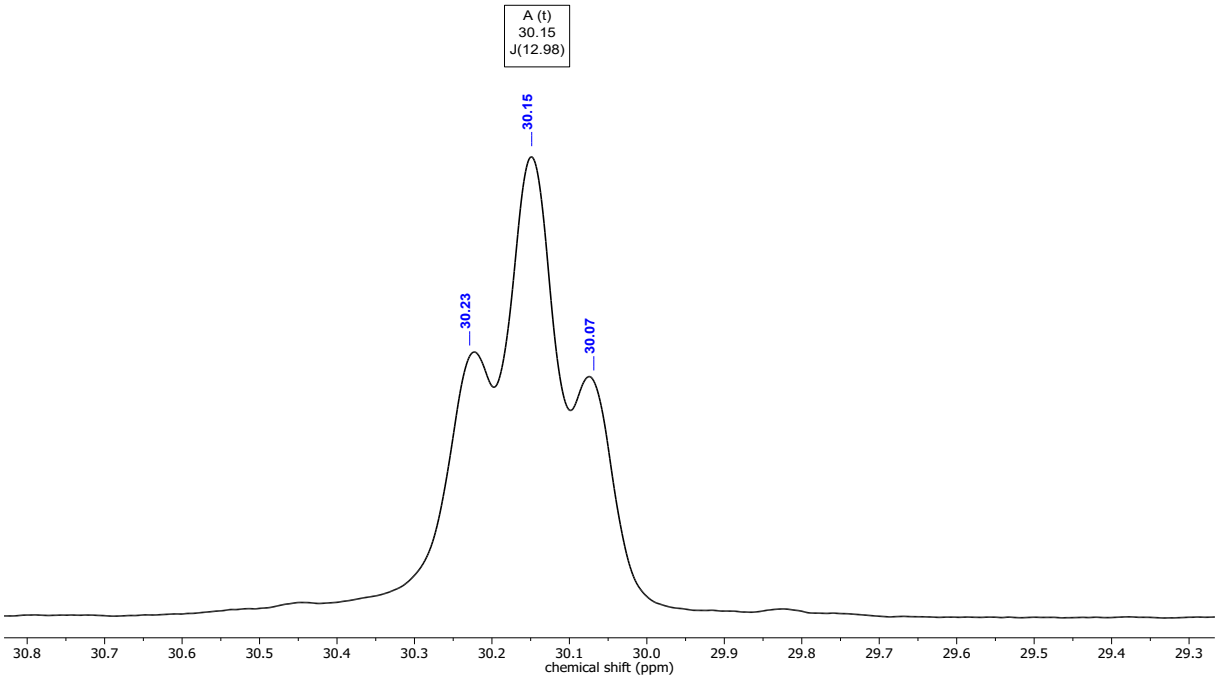

Fig S3.44: Details of the ^{31}P NMR spectrum of **6c** in $CDCl_3$.

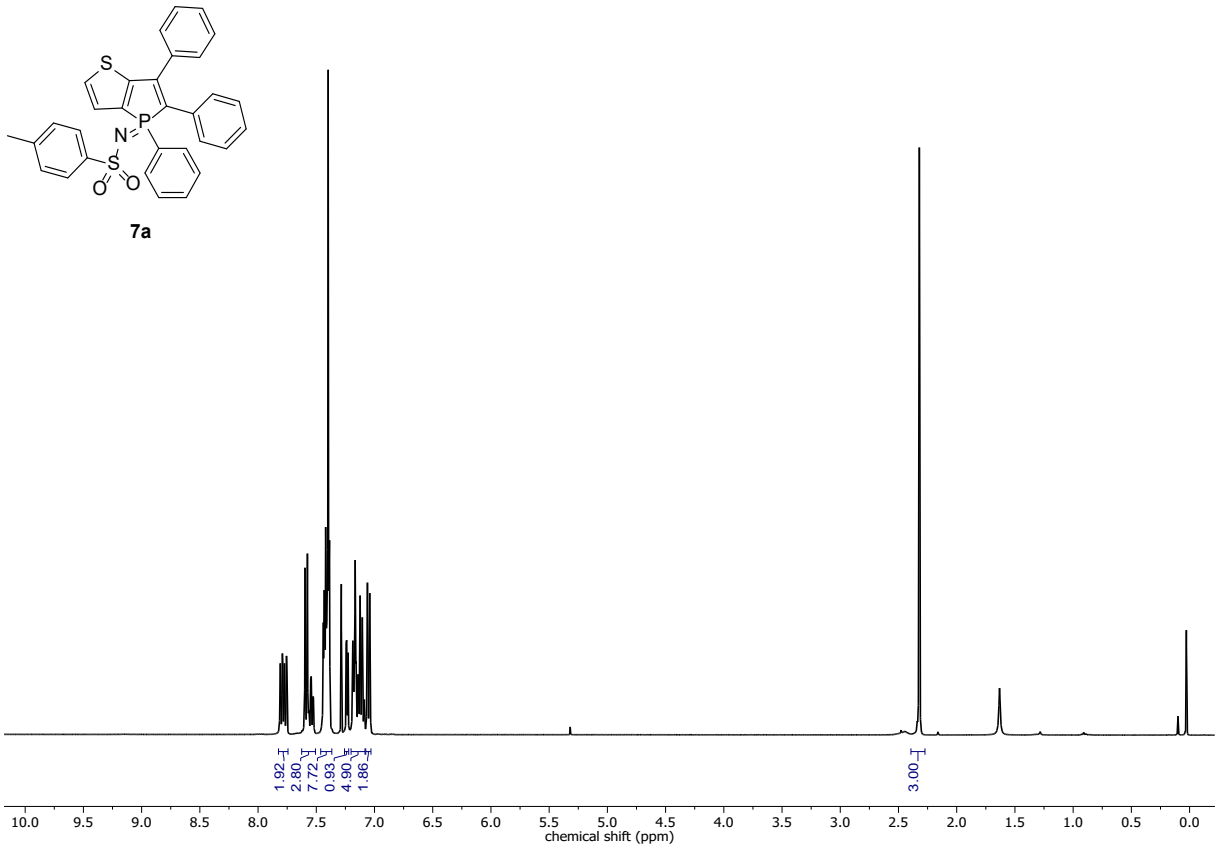

Fig S3.45: ^{1}H NMR spectrum of **7a** in $CDCl_3$

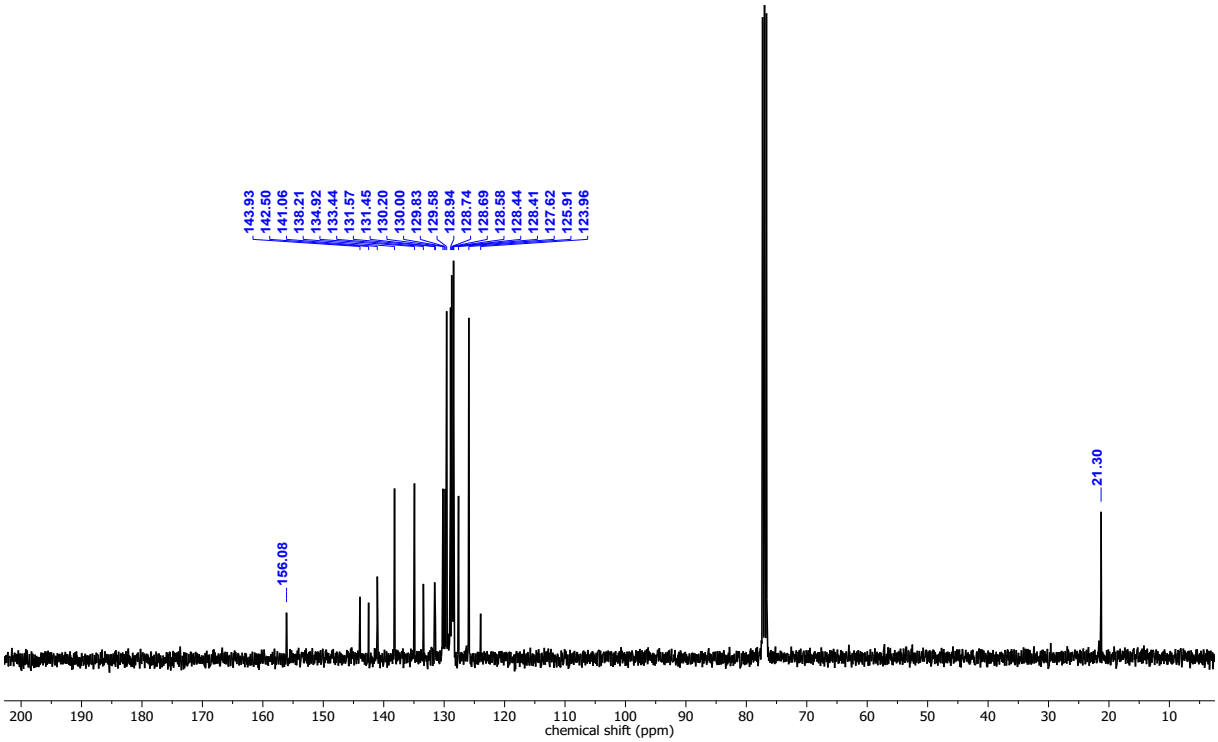

Fig S3.46: $^{13}C\{^{31}P, ^{1}H\}$ NMR spectrum of **7a** in $CDCl_3$.

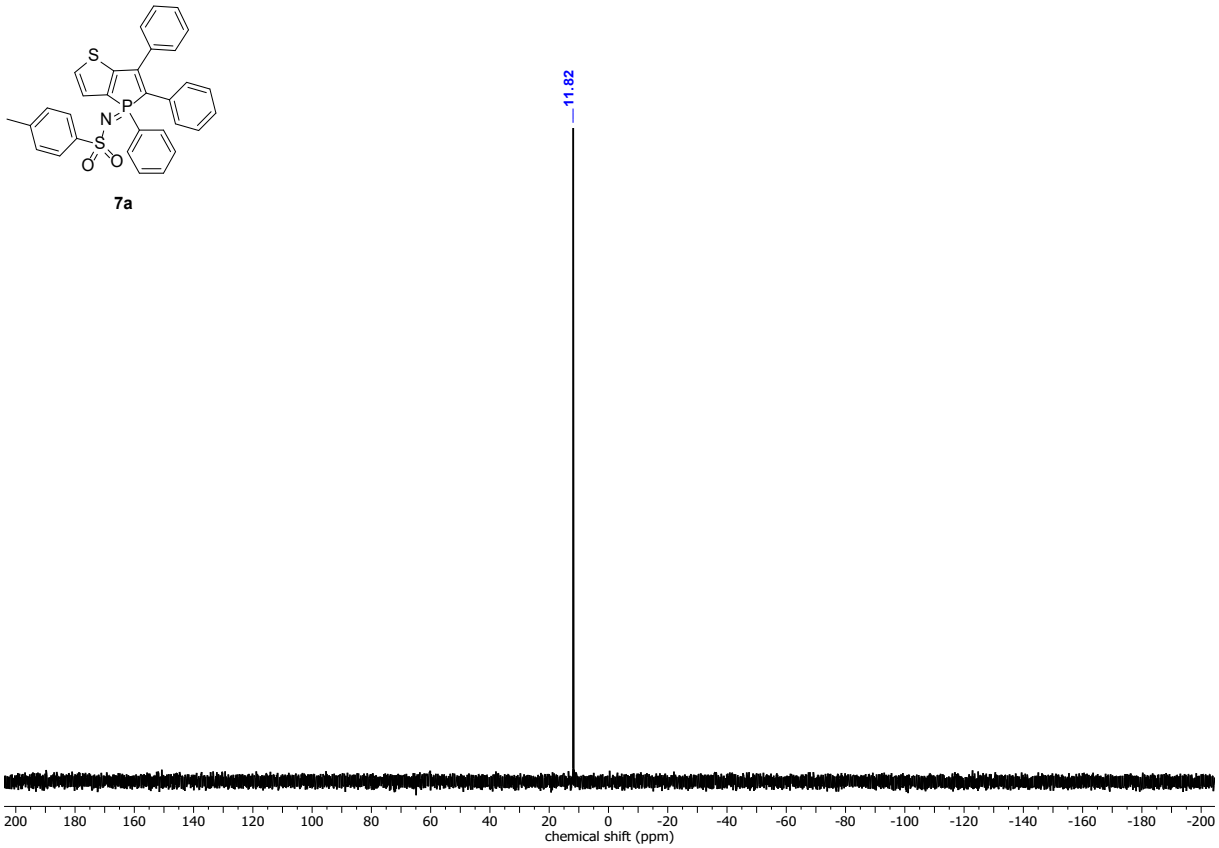

Fig S3.47: $^{31}P\{^{1}H\}$ NMR spectrum of **7a** in $CDCl_3$.

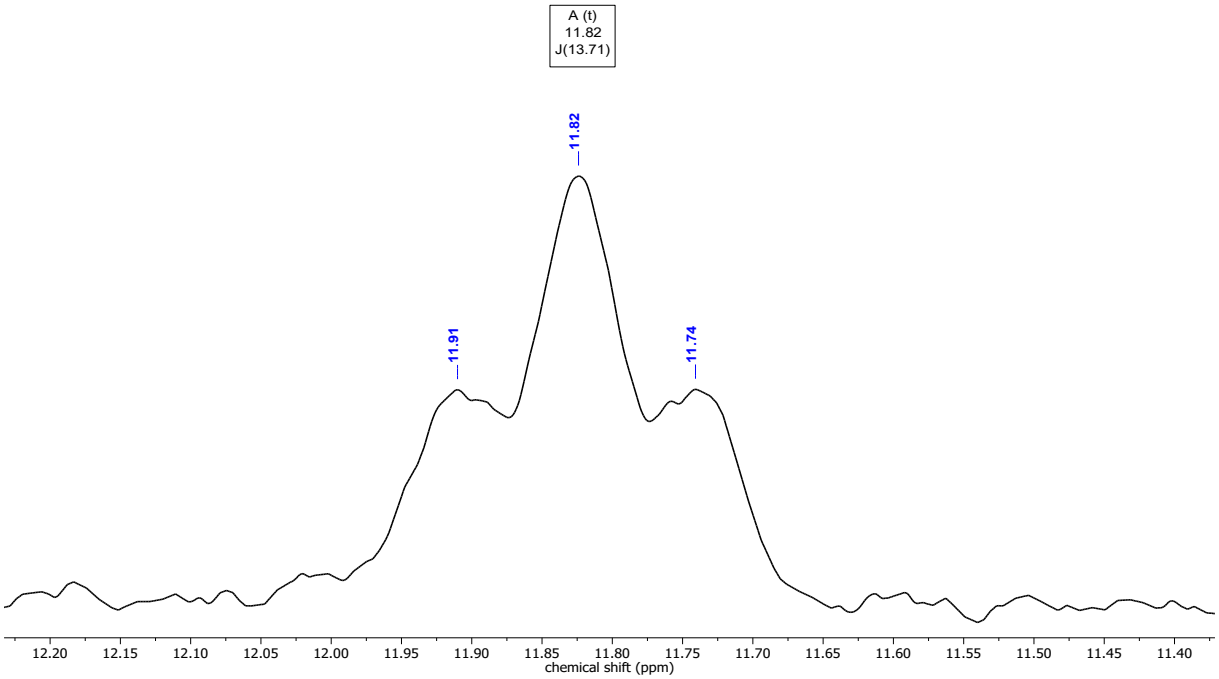

Fig S3.48: Details of the ^{31}P NMR spectrum of **7a** in $CDCl_3$.

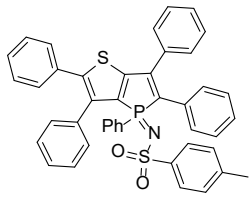

7b

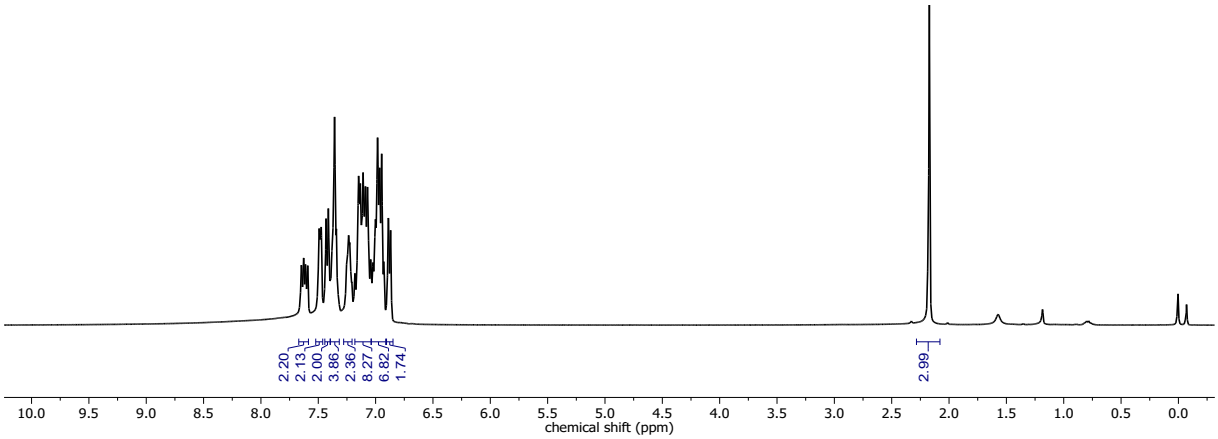

Fig S3.49: ^{1}H NMR spectrum of **7b** in $CDCl_3$.

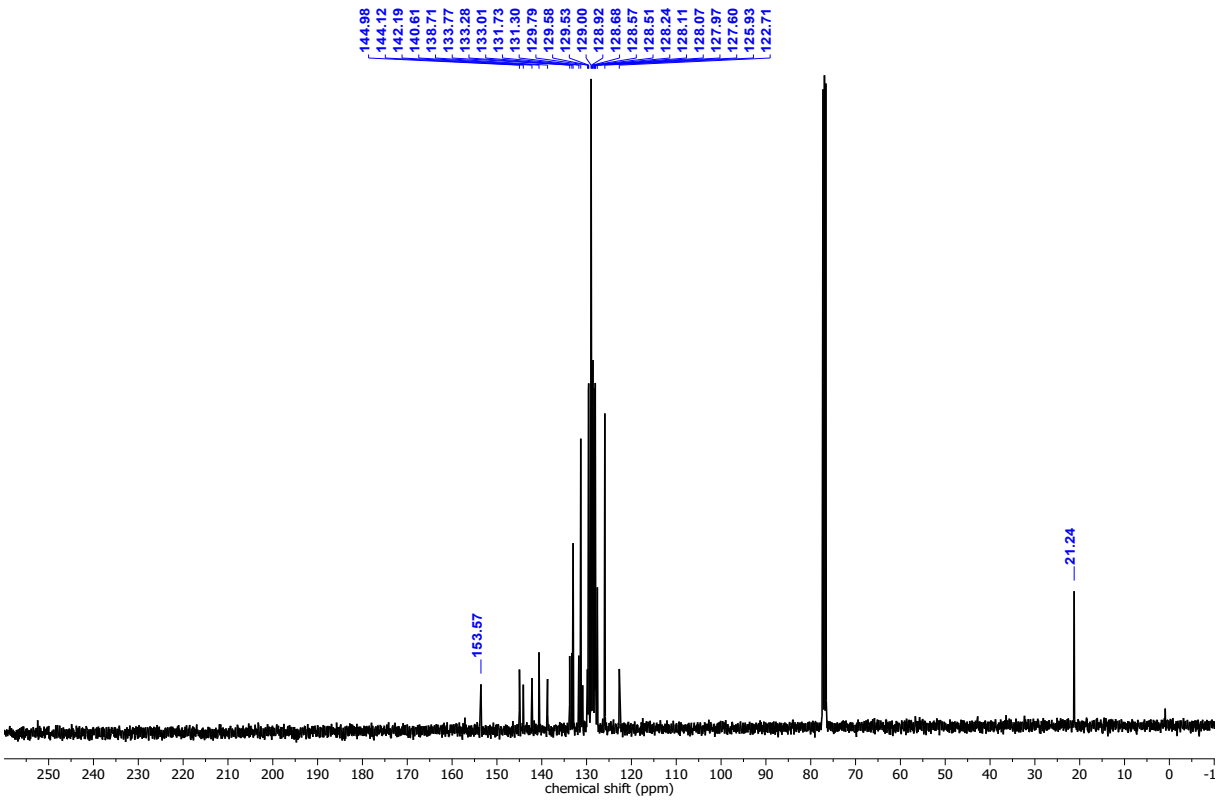

Fig S3.50: $^{13}C\{^{31}P, ^{1}H\}$ NMR spectrum of **7b** in $CDCl_3$.

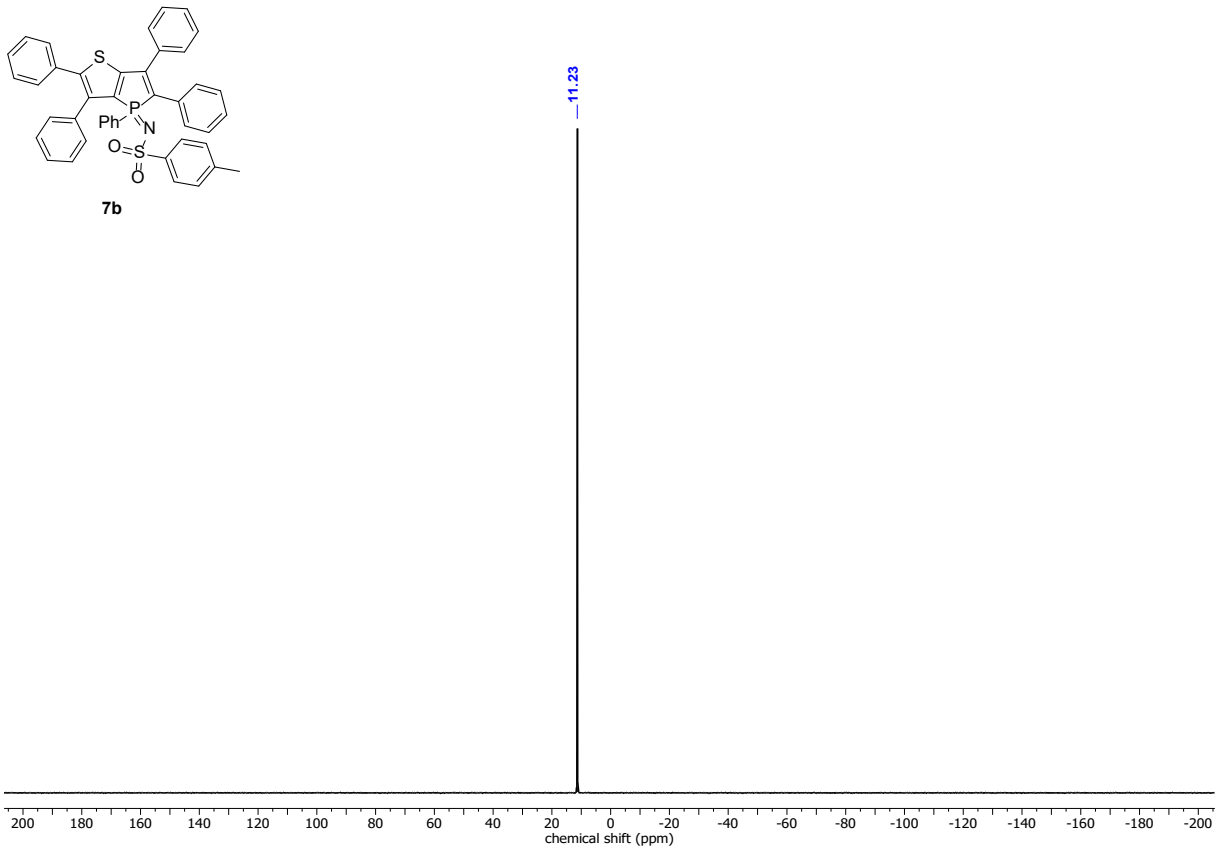

Fig S3.51: $^{31}P\{^{1}H\}$ NMR spectrum of **7b** in $CDCl_3$.

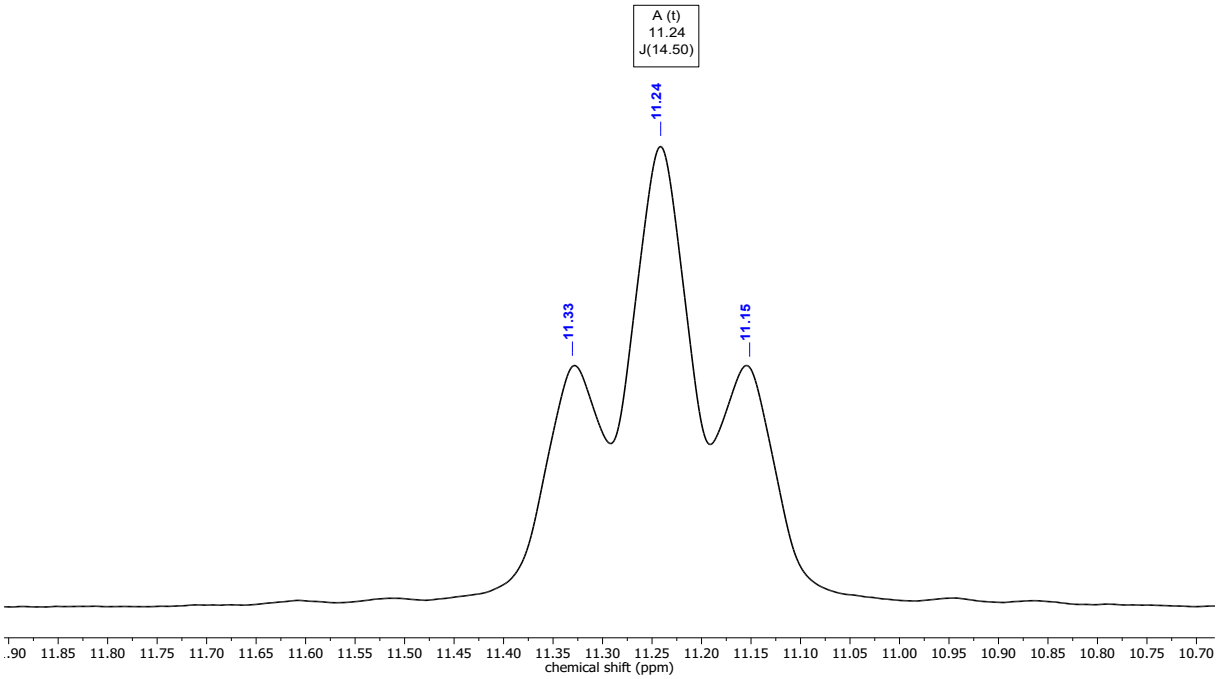

Fig S3.52: Details of the ^{31}P NMR spectrum of **7b** in $CDCl_3$.

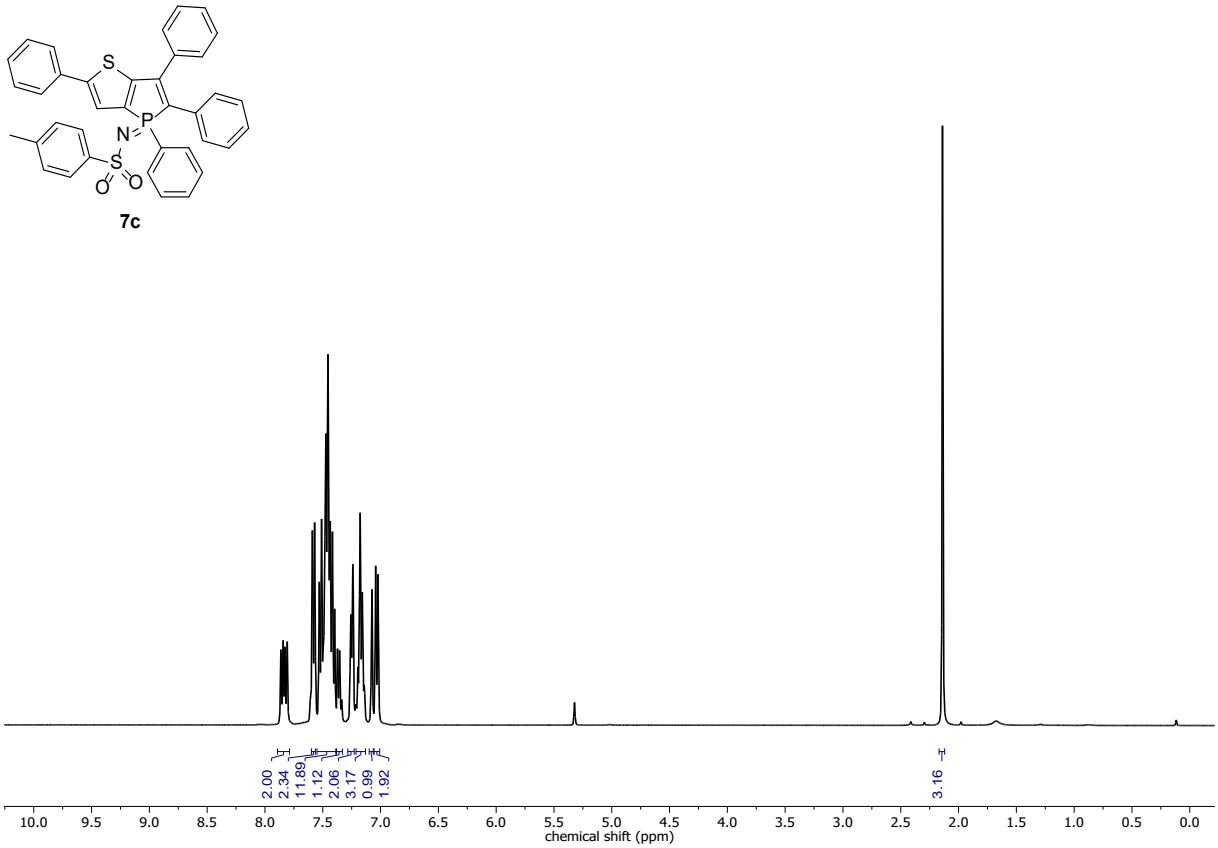

Fig S3.53: ^{1}H NMR spectrum of **7c** in CD_2Cl_2.

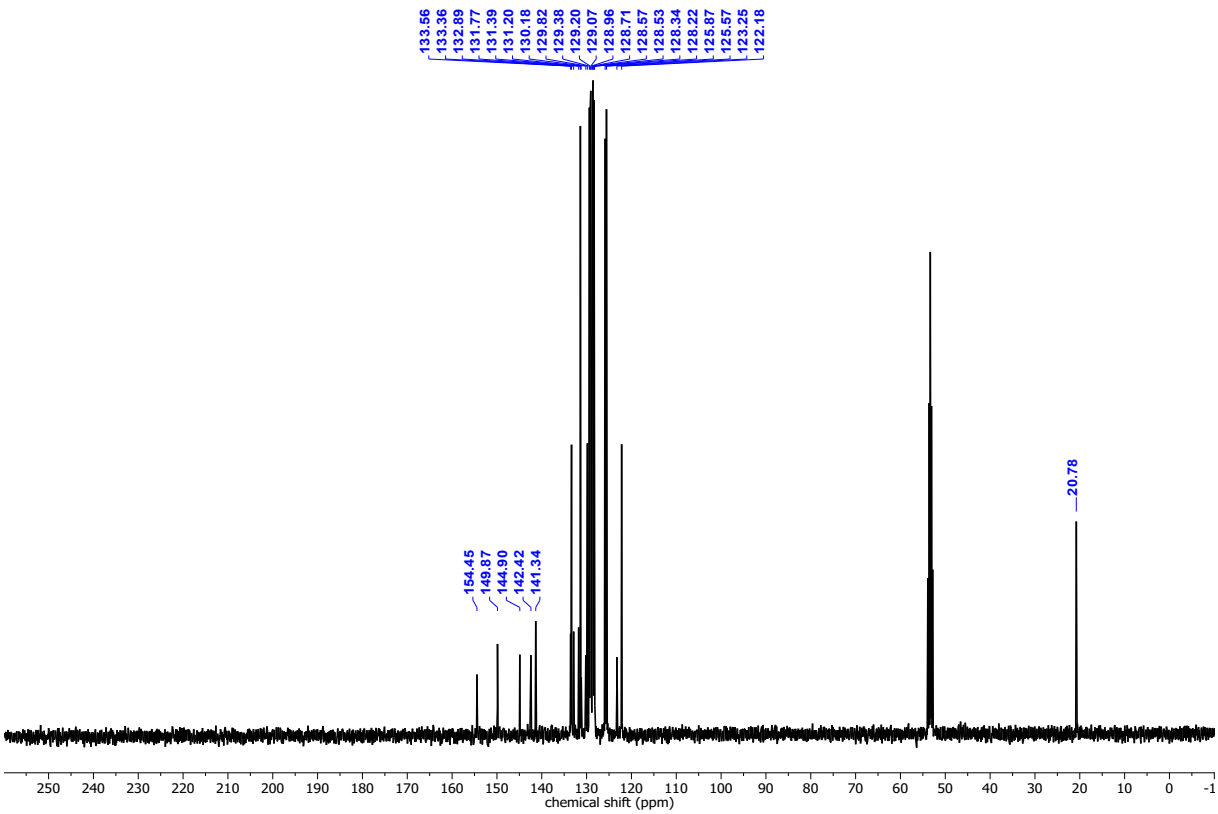

Fig S3.54: $^{13}C\{^{31}P, ^{1}H\}$ NMR spectrum of **7c** in CD_2Cl_2.

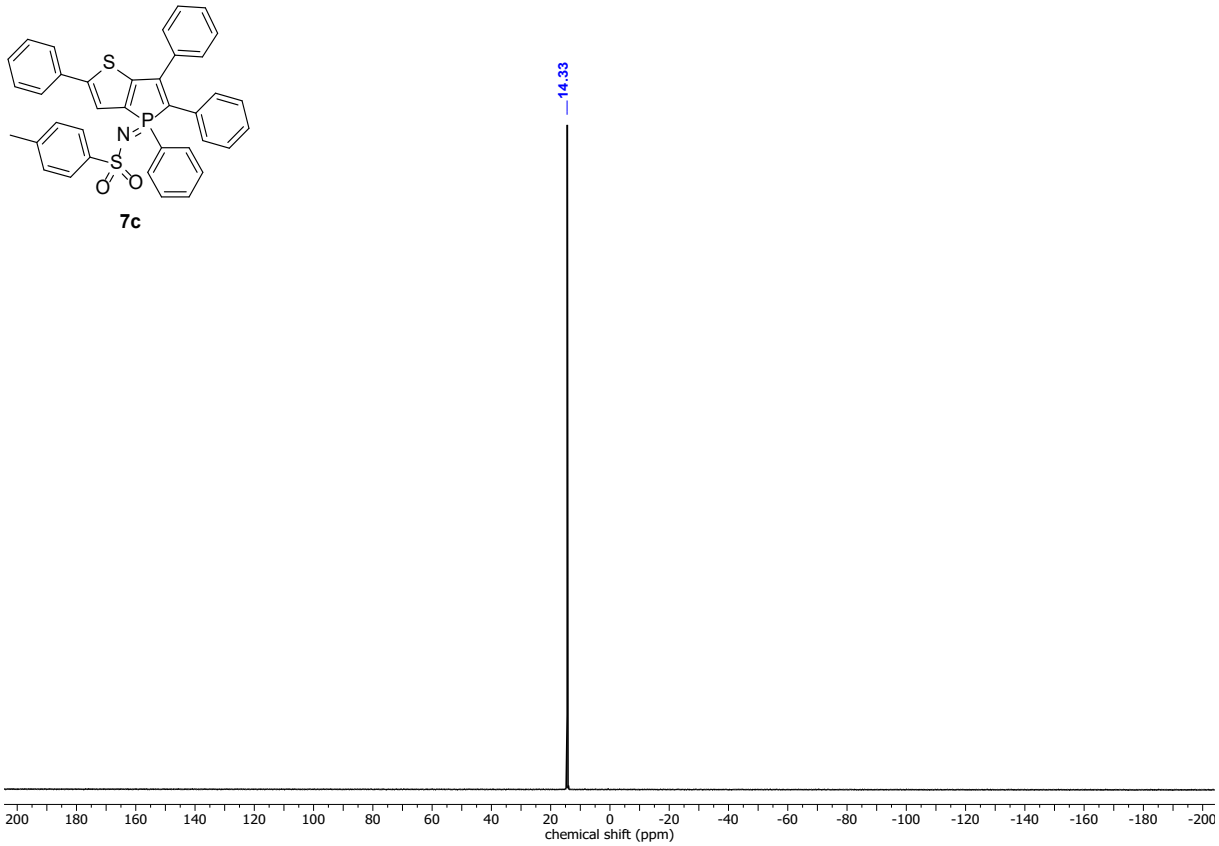

Fig S3.55: $^{31}P\{^{1}H\}$ NMR spectrum of **7c** in CD_2Cl_2.

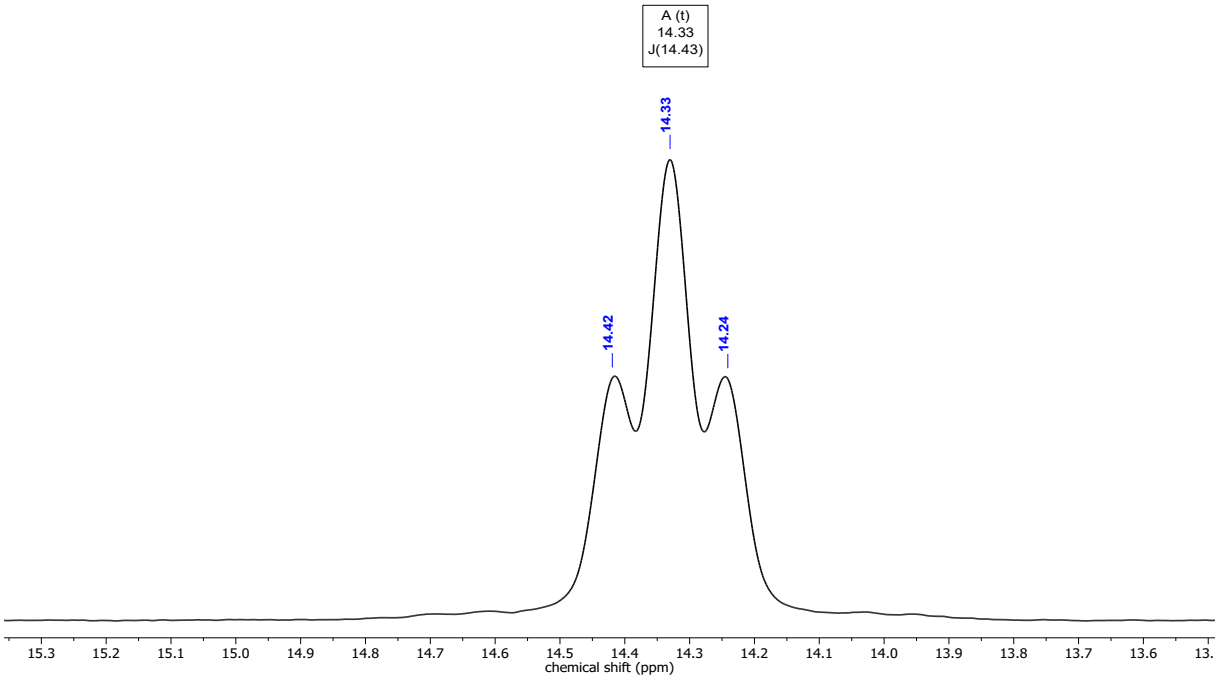

Fig S3.56: Details of the ^{31}P NMR spectrum of **7c** in CD_2Cl_2.

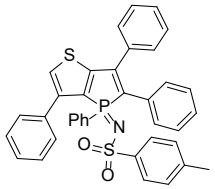

7d

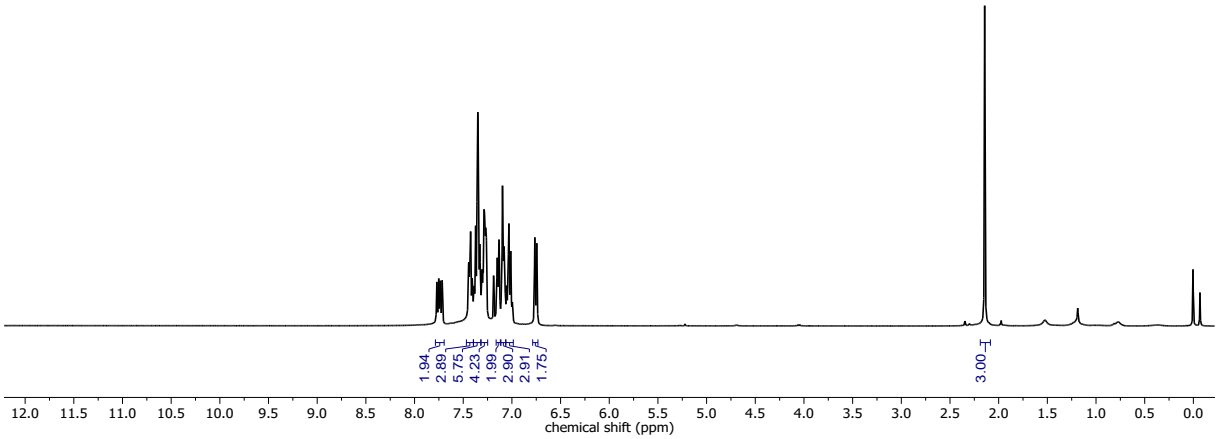

Fig S3.57: ^{1}H NMR spectrum of **7d** in $CDCl_3$

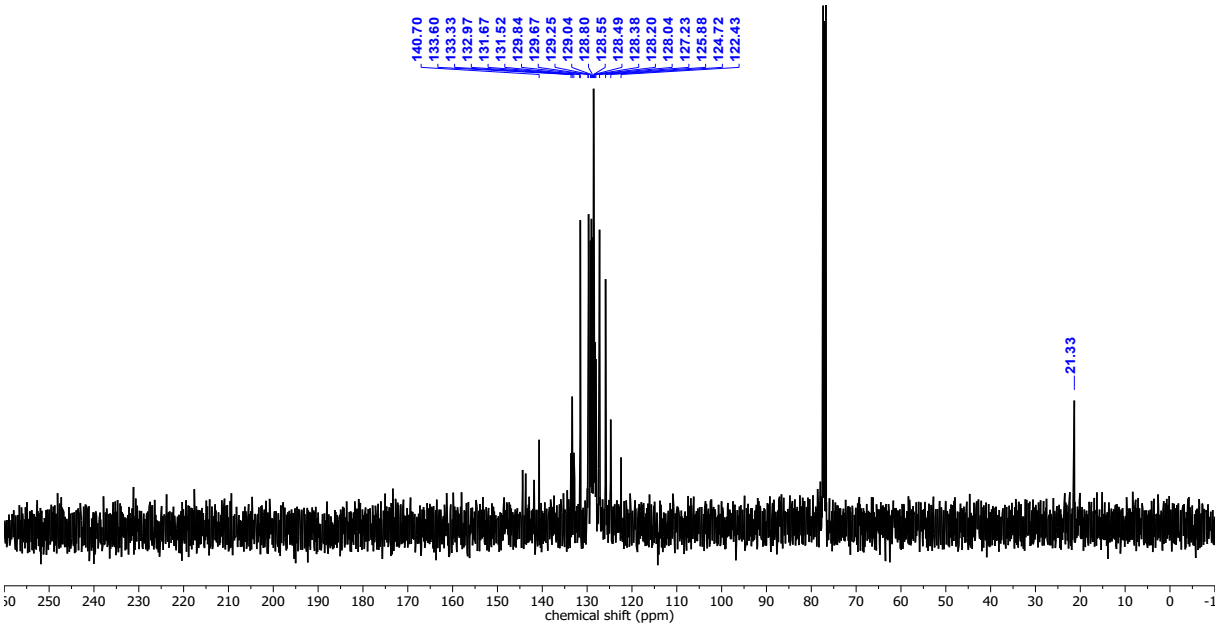

Fig S3.58: $^{13}C\{^{31}P, ^{1}H\}$ NMR spectrum of **7d** in $CDCl_3$.

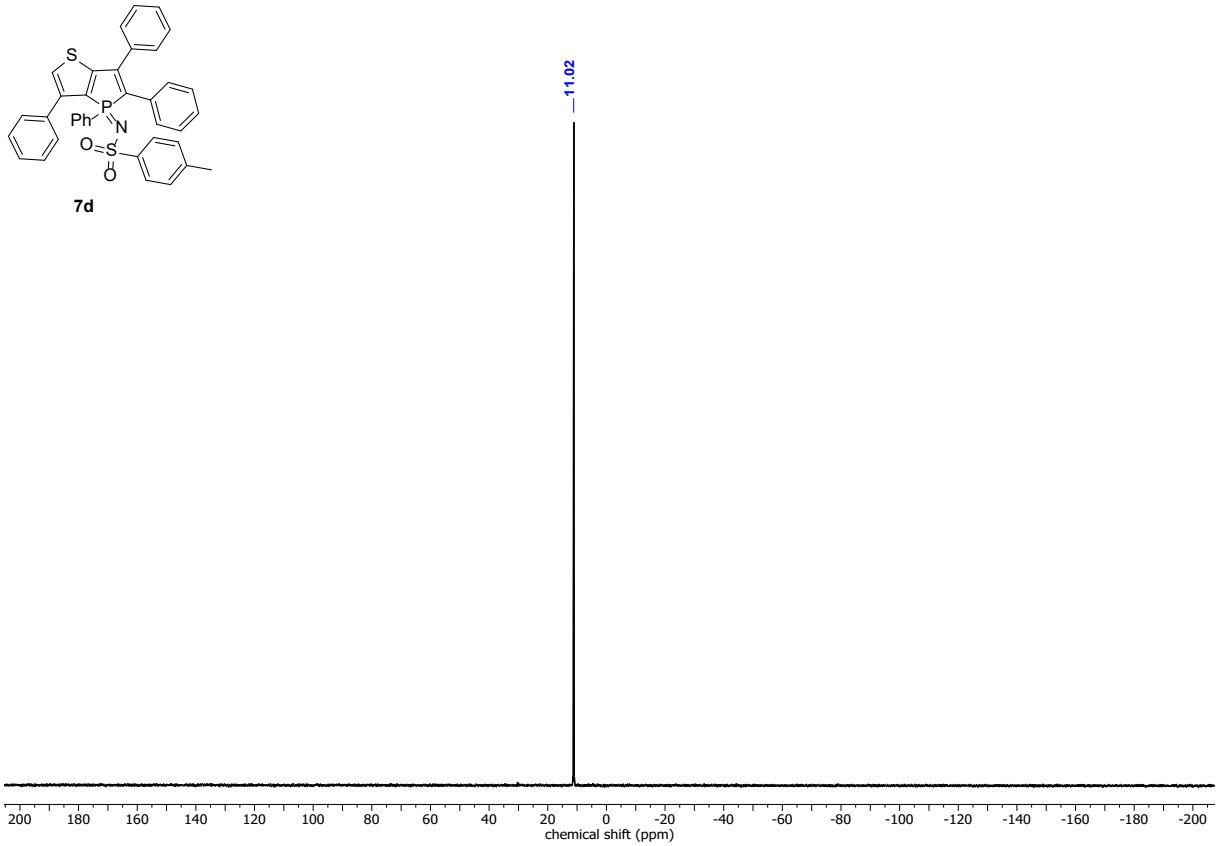

Fig S3.59: $^{31}P\{^{1}H\}$ NMR spectrum of **7d** in $CDCl_3$.

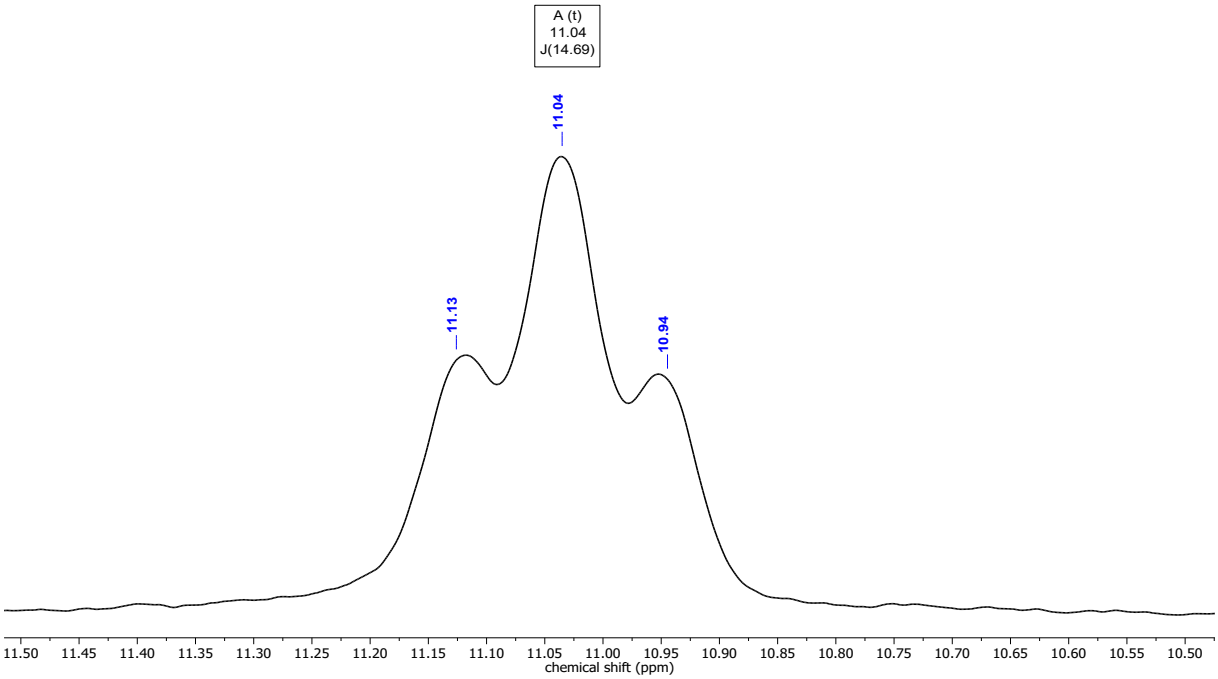

Fig S3.60: Details of the ^{31}P NMR spectrum of **7d** in $CDCl_3$.

4 Crystallographic Data

The data were collected on a Gemini diffractometer (Rigaku Oxford Diffraction) using Mo-Kα radiation (λ = 0.71073 Å) and ω-scan rotation. Data reduction was performed with CrysAlisPro[7] including the program SCALE3 ABSPACK for empirical absorption correction. The structures were solved by dual space methods (SHELXT-2014)[8] and the refinement was performed with SHELXL-2018.[9] Hydrogen atoms for **3f**, **6c**, **7b**, **7d** and disordered fragments of **3c** (disordered $CHCl_3$ solvent molecule) and **7c** (11% fraction of one disordered phenyl substituent (C25 to C30)) were calculated on idealized positions using the riding model, whereas for all other cases hydrogen atoms had been located with a difference-density Fourier map. Structure figures were generated with DIAMOND-4.[10]

CCDC deposition numbers given in Table S4.1-4.3 contains the supplementary crystallographic data for this paper. These data can be obtained free of charge via https://summary.ccdc.cam.ac.uk/structure-summary-form (or from the Cambridge Crystallographic Data Centre, 12 Union Road, Cambridge CB2 1EZ, UK; fax: (+44)1223-336-033; or deposit@ccdc.cam.uk).

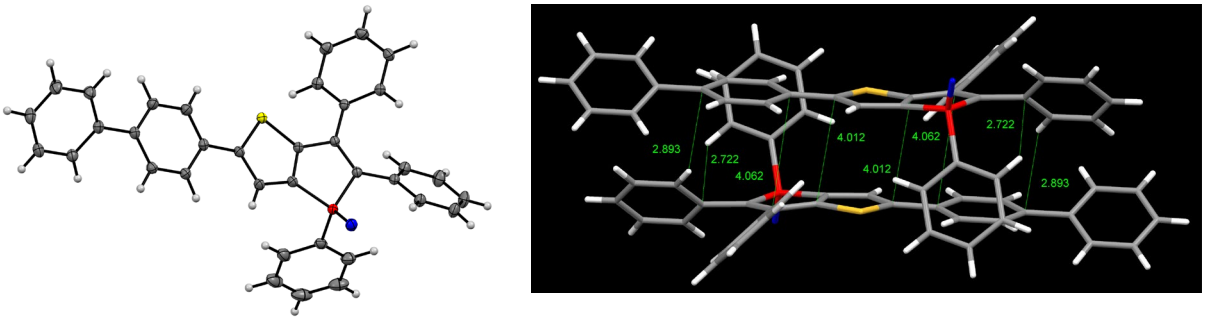

Fig S4.1 Molecular structure of **3c** in the crystal (displacement ellipsoids shown at 50% level) and intermolecular interactions [Å].

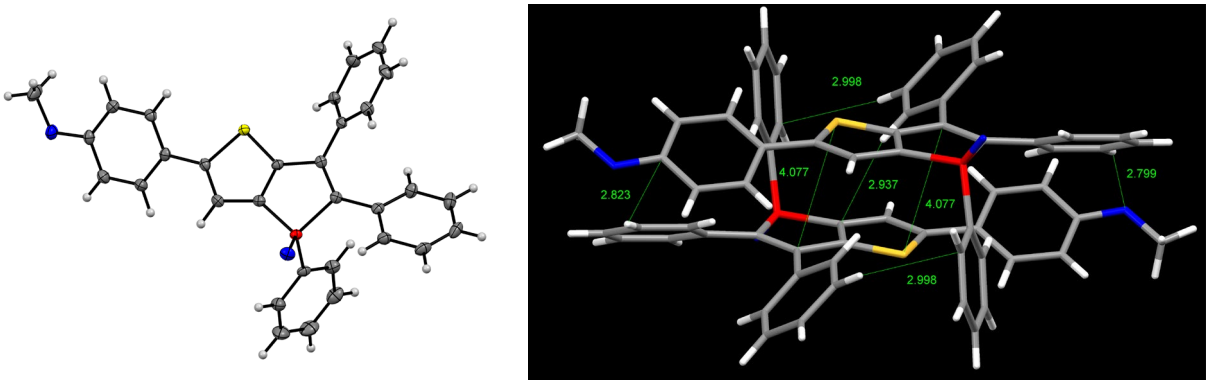

Fig S4.2 Molecular structure of **3d** in the crystal (displacement ellipsoids shown at 50% level) and intermolecular interactions [Å].

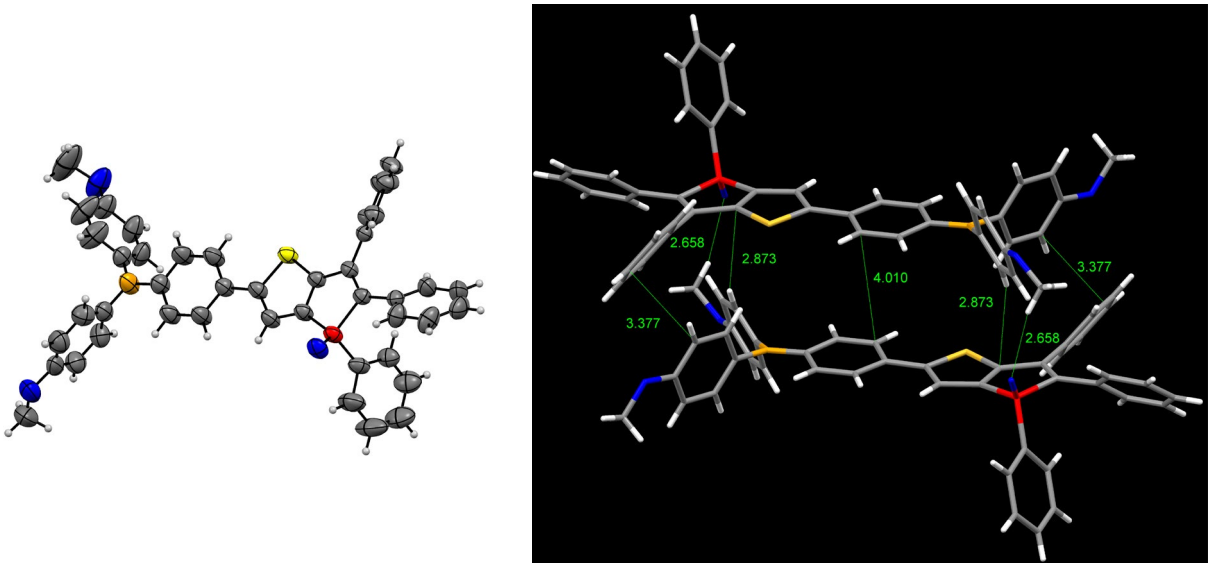

Fig S4.3 Molecular structure of **3f** in the crystal (displacement ellipsoids shown at 50% level) and intermolecular interactions [Å].

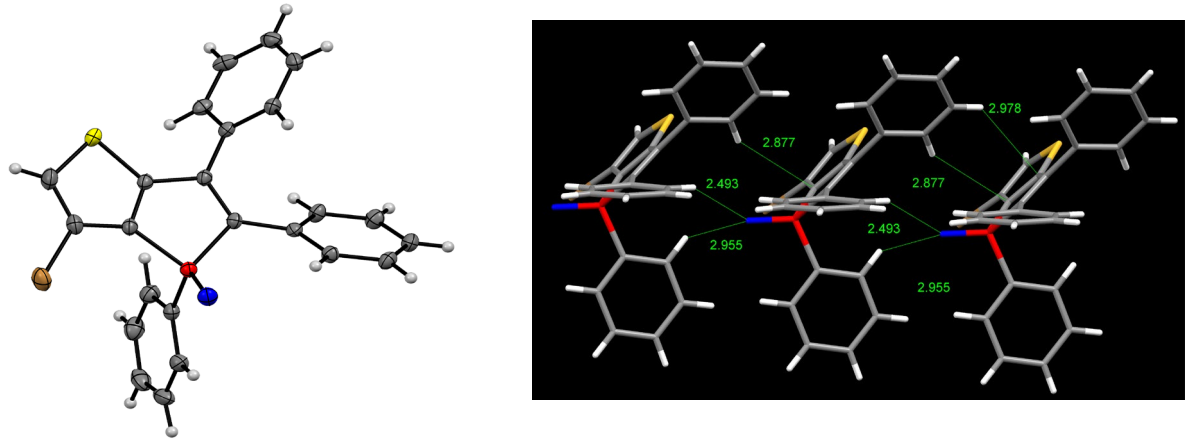

Fig S4.4 Molecular structure of **5** in the crystal (displacement ellipsoids shown at 50% level) and intermolecular interactions [Å].

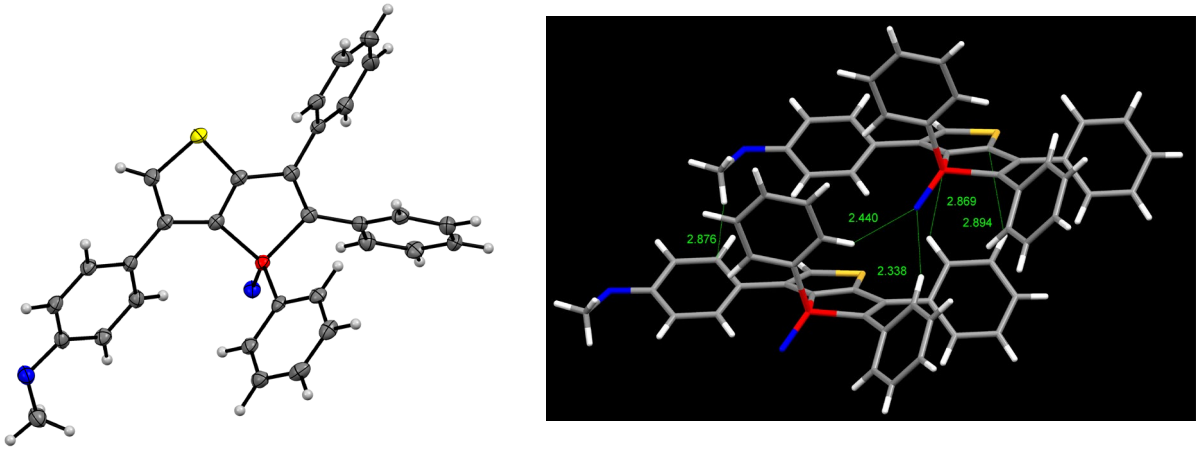

Fig S4.5 Molecular structure of **6b** in the crystal (displacement ellipsoids shown at 50% level) and intermolecular interactions [Å].

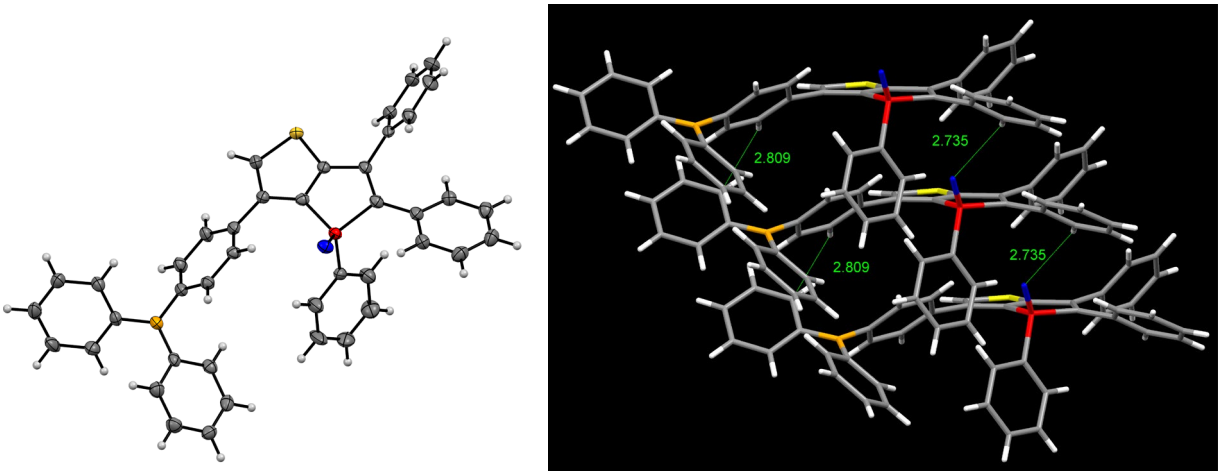

Fig S4.6 Molecular structure of **6c** in the crystal (displacement ellipsoids shown at 50% level) and intermolecular interactions [Å].

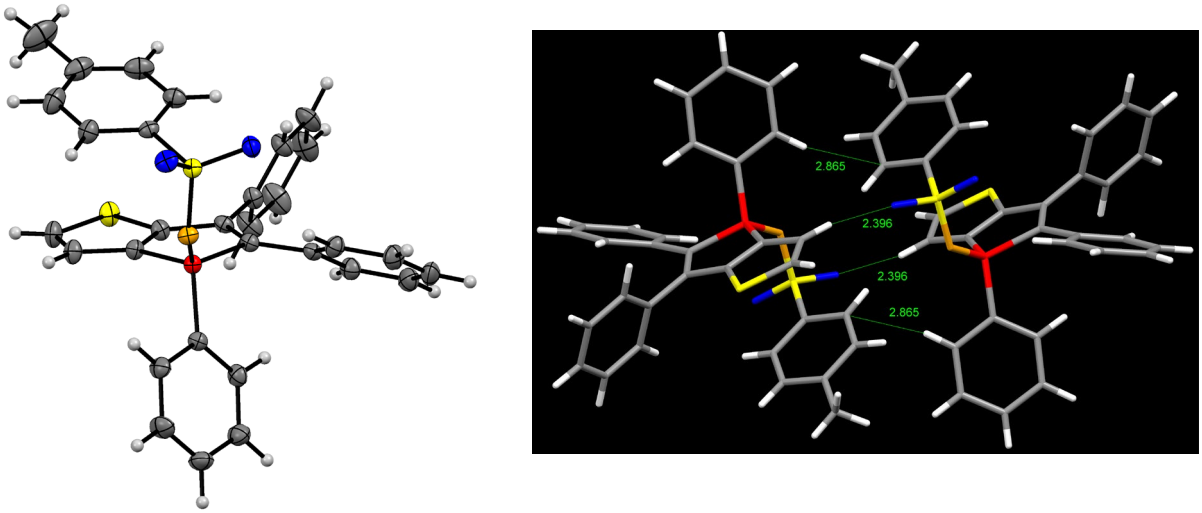

Fig S4.7 Molecular structure of **7a** in the crystal (displacement ellipsoids shown at 50% level) and intermolecular interactions [Å].

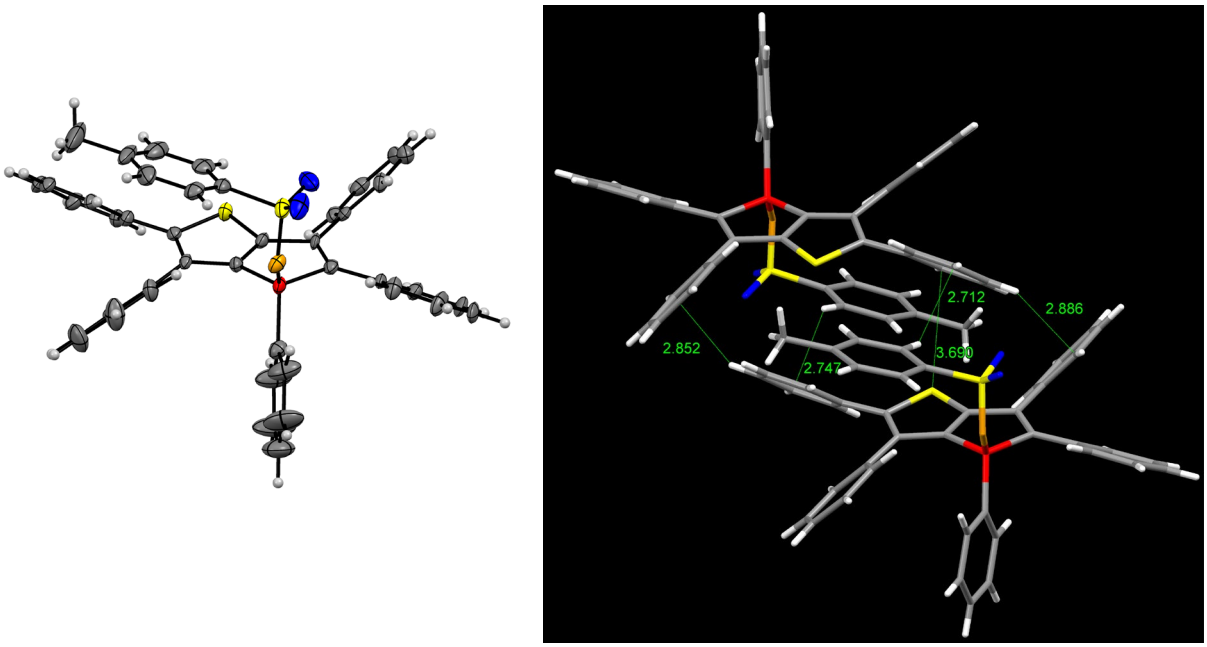

Fig S4.8 Molecular structure of **7b** in the crystal (displacement ellipsoids shown at 50% level) and intermolecular interactions [Å].

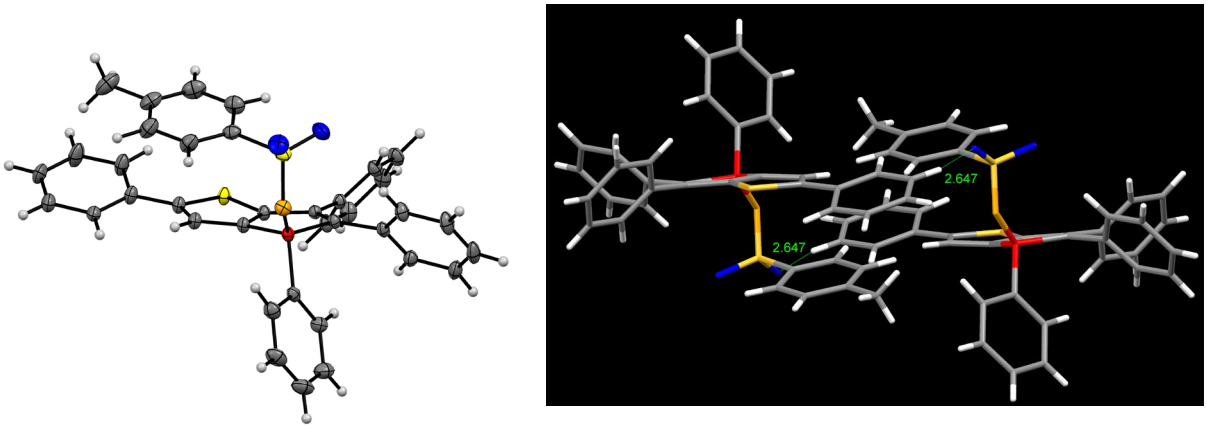

Fig S4.9 Molecular structure of **7c** in the crystal (displacement ellipsoids shown at 50% level) and intermolecular interactions [Å].

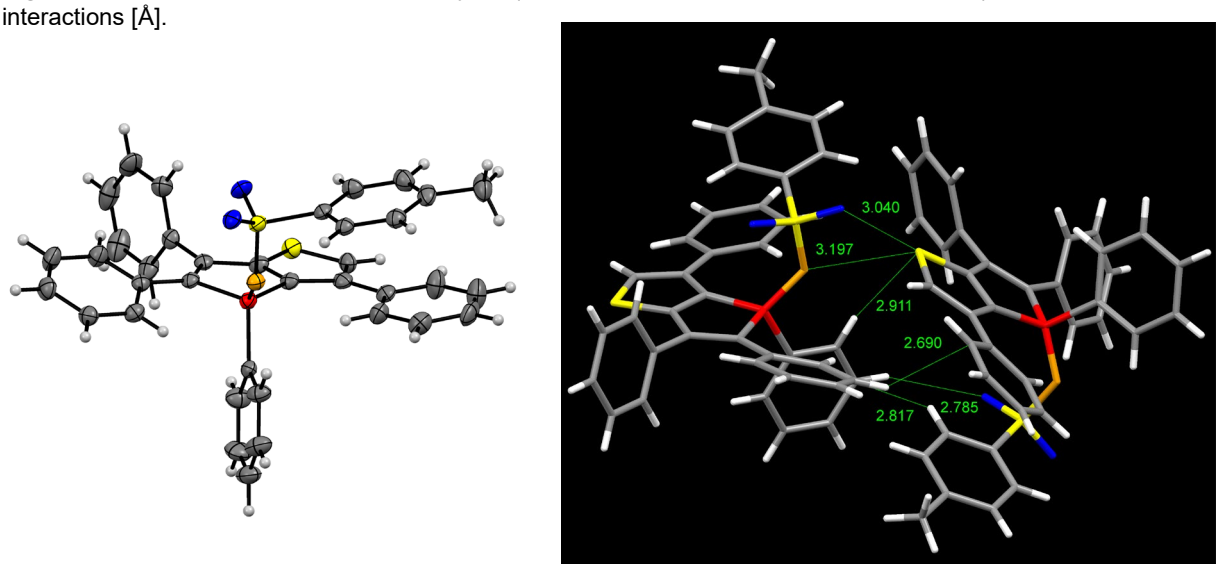

Fig S4.10 Molecular structure of **7d** in the crystal (displacement ellipsoids shown at 50% level) and intermolecular interactions [Å].

Table S.4.1 Fundamental structure parameters

Compound	**3c**	**3d**	**3f**	**5**
Empirical formula	$C_{37}H_{26}Cl_3OPS$	$C_{31}H_{23}O_2PS$	$C_{44}H_{34}NO_3PS$	$C_{24}H_{16}BrOPS$
Formula weight	655.96	490.52	687.75	463.31
Temperature [K]	130(2)	130(2)	297(2)	130(2)
Wavelength [pm]	71.073	71.073	71.073	71.073
Crystal system	Triclinic	Monoclinic	Triclinic	Monoclinic
Space group	$P\,\bar{1}$	*P* 2_1/*n*	$P\,\bar{1}$	*I* 2/*a*
Unit cell dimensions				
a [pm]	965.93(3)	1441.75(3)	1181.86(4)	1665.28(6)
b [pm]	1125.39(5)	814.27(2)	1289.85(5)	634.41(2)
c [pm]	1511.55(5)	2145.51(5)	1408.45(6)	3822.89(12)
α [deg]	104.159(3)	90	76.183(3)	90
β [deg]	95.593(3)	102.225(2)	70.981(4)	95.410(3)
γ [deg]	93.673(3)	90	63.505(4)	90
Volume [nm^3]	1.5790(1)	2.4617(1)	1.8056(1)	4.0208(2)
Z	2	4	2	8
$\rho_{(calculated)}$ [Mg/m^3]	1.380	1.324	1.265	1.531
μ [mm^{-1}]	0.437	0.224	0.176	2.240
F(000)	676	1024	720	1872
Crystal size [mm^3]	0.33 · 0.30 · 0.18	0.44 · 0.12 · 0.04	0.24 · 0.17 · 0.07	0.39 · 0.14 · 0.02
Θ_{Min} / Θ_{Max} [deg]	2.406 / 32.397	2.683 / 30.890	2.475 / 27.327	2.457 / 30.608
Index ranges	-14 ≤ h ≤ 14 -16 ≤ k ≤ 16 -21 ≤ l ≤ 22	-19 ≤ h ≤ 19 -11 ≤ k ≤ 11 -30 ≤ l ≤ 30	-15 ≤ h ≤ 15 -16 ≤ k ≤ 16 -18 ≤ l ≤ 18	-22 ≤ h ≤ 23 -9 ≤ k ≤ 8 -54 ≤ l ≤ 54
Reflections collected	30979	27337	30385	19164
Indp. reflections (R_{int})	10405 (0.0309)	6929 (0.0454)	7379 (0.0345)	5591 (0.0446)
Completeness (Θ_{Max})	99.9 % (30.51)	100.0 % (28.29)	99.9 % (25.35)	100.0 % (28.29)
T_{Max} / T_{Min}	1.00000 / 0.99143	1.00000 / 0.99183	1.00000 / 0.97285	1.00000 / 0.75054
Restraints / parameters	13 / 515	0 / 408	91 / 508	0 / 317
Gof on F^2	1.015	1.035	1.012	1.046
R1 / wR2 (I>2σ(I))	0.0482, 0.1137	0.0484, 0.0960	0.0462, 0.1048	0.0433, 0.0879
R1 / wR2 (all data)	0.0645, 0.1250	0.0680, 0.1041	0.0800, 0.1217	0.0639, 0.0963
Residual electron density [$e \cdot Å^{-3}$]	0.464 / -0.916	0.389 / -0.372	0.176 / -0.218	0.604 / -0.512
Comments	-	-	†[1]	-
CCDC No	2302468	2302469	2302470	2302471

Table S.4.2 Fundamental structure parameters

Compound	**6b**	**6c**	**7a**	**7b**
Empirical formula	$C_{31}H_{23}O_2PS$	$C_{42}H_{30}NOPS$	$C_{31}H_{24}NO_2PS_2$	$C_{43.50}H_{33}ClNO_2P\ S_2$
Formula weight	490.52	627.70	537.60	732.25
Temperature [K]	130(2)	130(2)	130(2)	130(2)
Wavelength [pm]	71.073	71.073	71.073	71.073
Crystal system	Monoclinic	Monoclinic	Monoclinic	Monoclinic
Space group	*P* $2_1/c$	*P* 2_1	*I* 2/*a*	*P* $2_1/n$
Unit cell dimensions				
a [pm]	857.05(2)	2303.80(3)	1748.94(3)	1891.94(6)
b [pm]	620.37(1)	585.63(1)	1461.65(3)	1279.23(3)
c [pm]	4498.2(1)	4682.47(5)	2104.13(4)	2999.0(1)
α [deg]	90	90	90	90
β [deg]	90.949(2)	98.810(1)	104.428(2)	95.030(3)
γ [deg]	90	90	90	90
Volume [nm^3]	2.39130(9)	6.2429(2)	5.20923(18)	7.2302(4)
Z	4	8	8	8
$\rho_{(calculated)}$ [Mg/m^3]	1.362	1.336	1.371	1.345
μ [mm^{-1}]	0.230	0.192	0.296	0.305
F(000)	1024	2624	2240	3048
Crystal size [mm^3]	0.50 · 0.21 · 0.14	0.64 · 0.24 · 0.09	0.46 · 0.15 · 0.06	0.40 · 0.25 · 0.04
Θ_{Min} / Θ_{Max} [deg]	2.377 / 26.736	1.907 / 26.707	2.405 / 30.627	2.228 / 27.195
Index ranges	-10 ≤ h ≤ 10 -7 ≤ k ≤ 7 -56 ≤ l ≤ 56	-26 ≤ h ≤ 28 -7 ≤ k ≤ 7 -57 ≤ l ≤ 59	-24 ≤ h ≤ 24 -19 ≤ k ≤ 20 -28 ≤ l ≤ 30	-24 ≤ h ≤ 24 -16 ≤ k ≤ 16 -36 ≤ l ≤ 34
Reflections collected	21279	64488	35040	44165
Indp. reflections (R_{int})	4748 (0.0437)	24154 (0.0374)	7397 (0.0490)	14606 (0.0929)
Completeness (Θ_{Max})	100.0 % (25.35)	99.8 % (25.35)	100.0 % (28.29)	99.9 % (25.35)
T_{Max} / T_{Min}	1.00000 / 0.87616	1.00000 / 0.97176	1.00000 / 0.85505	1.00000 / 0.97957
Restraints / parameters	6 / 408	1 / 1658	0 / 430	0 / 912
Gof on F^2	1.181	1.055	1.044	1.066
R1 / wR2 (I>2σ(I))	0.0594, 0.1215	0.0544, 0.1271	0.0490, 0.1090	0.1005, 0.2040
R1 / wR2 (all data)	0.0654, 0.1243	0.0653, 0.1346	0.0663, 0.1173	0.1750, 0.2427
Residual electron density [$e \cdot Å^{-3}$]	0.364 / -0.426	0.769 / -0.349	0.763 / -0.382	0.655 / -0.897
Comments	-	†[2]	-	-
CCDC No	2302472	2302473	2302474	2302475

Table S.4.3 Fundamental structure parameters

Compound	**7c**	**7d**
Empirical formula	$C_{37}H_{28}NO_2PS_2$	$C_{37}H_{28}NO_2PS_2$
Formula weight	613.69	613.69
Temperature [K]	130(2)	130(2)
Wavelength [pm]	71.073	71.073
Crystal system	Triclinic	Triclinic
Space group	$P\,\bar{1}$	$P\,\bar{1}$
Unit cell dimensions		
a [pm]	962.52(2)	1430.48(6)
b [pm]	1007.76(2)	2072.90(9)
c [pm]	1585.93(4)	2087.35(9)
α [deg]	85.546(2)	96.716(4)
β [deg]	80.509(2)	91.419(4)
γ [deg]	81.965(2)	92.987(4)
Volume [nm^3]	1.50003(6)	6.1357(5)
Z	2	8
$\rho_{(calculated)}$ [Mg/m^3]	1.359	1.329
μ [mm^{-1}]	0.267	0.261
F(000)	640	2560
Crystal size [mm^3]	0.51 · 0.23 · 0.18	0.35 · 0.26 · 0.25
Θ_{Min} / Θ_{Max} [deg]	2.345 / 34.820	1.966 / 26.711
Index ranges	-15 ≤ h ≤ 15 -16 ≤ k ≤ 16 -25 ≤ l ≤ 25	-17 ≤ h ≤ 17 -25 ≤ k ≤ 25 -26 ≤ l ≤ 26
Reflections collected	47897	29655
Indp. reflections (R_{int})	12299 (0.0341)	29655 (0.0370)
Completeness (Θ_{Max})	100.0 % (33.14)	99.6 % (25.35)
T_{Max} / T_{Min}	1.00000 / 0.99374	1.00000 / 0.90126
Restraints / parameters	21 / 516	0 / 1554
Gof on F^2	1.021	0.906
R1 / wR2 (I>2σ(I))	0.0448, 0.1092	0.0477, 0.0979
R1 / wR2 (all data)	0.0599, 0.1188	0.0806, 0.1057
Residual electron density [e·Å^{-3}]	0.505 / -0.371	0.399 / -0.411
Comments	-	†[3]
CCDC No	2302476	-

†[1]: At deep temperatures -143°C (130K) reflections of an incommensurate modulated structure are detectable. These studies are not finished yet and the results will be published separately. †[2]: Racemic twin. Twin domain ratio 0.51(8) : 0.49(8). †[3]: Two component twin. Twin law by rows $\bar{1}00, 00\bar{1}, 0\bar{1}0$; Twin domain ratio 0.6290(5) : 0.3710(5). Details of the disordered room temperature and the completely ordered twinned deep temperature phase will be published separately.

5 Photophysical Properties

5.1 Summary of Photoluminescence Properties

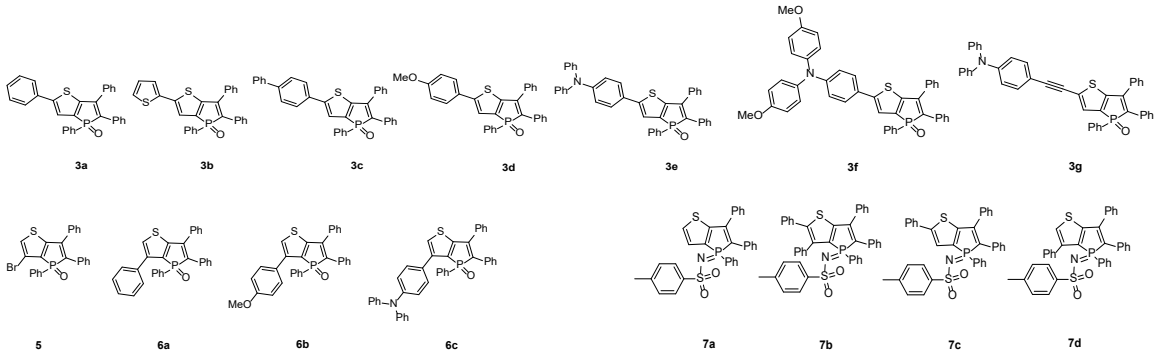

Fig S5.1 Structures of thienophospholes **3-7**.

Table S5.1 Summary of photoluminescence properties in liquid CH_2Cl_2 solutions at rt.

	λ_{abs} [nm]	ε [± 3%] [10^3 L mol^{-1}cm^{-1}]	λ_{em} [nm]	τ [ns][a]	$\Phi_{F(IS)}$ (±2) [%][b]	$k_{r(rt)}$ [10^7 s^{-1}][c]	$k_{nr(rt)}$ [10^7 s^{-1}][c]
3a[d]	248, 308, 408	20.4, 11.9, 14.0	567	**0.229 ± 0.002**	2	< 17.5	427 < k_{nr} < 436
3b	256, 420	20.0, 13.7	584	**0.42 ± 0.01** 0.47 ± 0.05 (77 %) 0.26 ± 0.09 (23 %)	3	7 ± 5	231 ± 11
3c	265, 311, 416	19.5, 17.0, 15.1	572	**0.447 ± 0.003**	4	9 ± 5	214 ± 6
3d	256, 419	22.5, 14.4	593	**0.254 ± 0.004**	2	< 15.8	385 < k_{nr} < 393
3e	273, 323, 444	30.0, 26.0, 24.3	649	**2.36 ± 0.01**	25	10.6 ± 0.9	32 ± 2
3f	288, 343, 458	23.2, 21.3, 19.5	703	**0.89 ± 0.02** 5 ± 1 (2 %) 0.828 ± 0.007 (98 %)	7	8 ± 2	104 ± 5
3g	297, 348, 432	24.1, 27.4, 23.4	634	**4.618 ± 0.005**	60	13.0 ± 0.4	8.7 ± 0.5
5	248, 379	17.9, 8.1	522	**0.51 ± 0.01** 4.51 ± 0.03 (7 %) 0.214 ± 0.002 (93 %)	2	< 8.0	193 < k_{nr} < 201
6a	250, 386	28.8, 6.6	525	**0.50 ± 0.02** 4.60 ± 0.02 (7 %) 0.175 ± 0.005 (93 %)	2	< 8.3	198 < k_{nr} < 211
6b	258, 392	40.0, 8.9	530	**0.214 ± 0.003** 0.6 ± 0.2 (3 %) 0.203 ± 0.004 (97 %)	2	< 19	459 < k_{nr} < 474
6c	242, 337, 400	33.5, 25.3	640	**0.238 ± 0.004** 2.1 ± 0.4 (1 %) 0.231 ± 0.004 (99 %)	3	13 ± 9	407 ± 16

[a] For multiexponential decays, the amplitude-weighted average lifetimes (τ_{av_amp}) are shown along with the different decay components and the relative amplitude in parentheses.[11] [b] $\Phi_{F(IS)}$ was obtained using a calibrated integrating sphere system [c] The decay rate constants are determined according to $k_r = 1/\tau_r = \Phi_F/\tau_{obs}$ and $k_{nr} = 1\text{-}\Phi_F/\tau_r$.[11] [d] The photoluminescence properties of **3a** have been previously reported in MeCN solution at rt.[2]

Table S5.2 Summary of photoluminescence properties in frozen glassy matrix in CH_2Cl_2-MeOH (1:1) at 77 K.

Compound	λ_{ex} [nm]	λ_{em} [nm]	$\tau_{(77\ K)}$ [ns][a]
3a[b]	373	552	**8.435 ± 0.009** 9.12 ± 0.04 (60 %) 7.39 ± 0.08 (40 %)
3b	373	568	**8.46 ± 0.01** 8.87 ± 0.07 (86 %) 6.0 ± 0.4 (14 %)
3c	373	557	**6.82 ± 0.02** 7.01 ± 0.04 (94 %) 4.0 ± 0.8 (6 %)
3d	373	579	**7.550 ± 0.009** 7.91 ± 0.05 (88 %) 4.9 ± 0.4 (12 %)
3e	373	425, 615	**1.89 ± 0.03** 1.2 ± 0.1 (33 %) 2.26 ± 0.05 (67 %) **6.10 ± 0.02** 6.308 ± 0.007 (95 %) 2.2 ± 0.2 (5 %)
3f	373	412, 645	**0.87 ± 0.02** 1.57 ± 0.07 (26 %) 0.63 ± 0.04 (74 %) **5.89 ± 0.02** 6.21 ± 0.03 (87 %) 3.8 ± 0.3 (13 %)
3g	373	590	**4.810 ± 0.006** 5.49 ± 0.04 (35 %) 4.45 ± 0.3 (65 %)
5	373	515	**11.33 ± 0.02** 11.70 ± 0.05 (93 %) 6.2 ± 0.7 (7 %)
6a	373	510	**10.67 ± 0.02** 11.10 ± 0.06 (92 %) 5.5 ± 0.7 (8 %)
6b	373	515	**10.35 ± 0.02** 10.82 ± 0.06 (87 %) 7.2 ± 0.4 (13 %)
6c	373	570	**3.22 ± 0.06** 7.3 ± 0.2 (19 %) 3.1 ± 0.2 (47 %) 1.1 ± 0.1 (34 %)

[a] For multiexponential decays, the amplitude-weighted average lifetimes (τ_{av_amp}) are shown along with the different decay components and the relative amplitude in parentheses.[11] [b] The photoluminescence properties of **3a** have been previously reported in frozen glassy matrix in butyronitrile at 77 K.[2]

Table S5.3 Summary of photoluminescence properties in the solid state at rt.

Compound	λ_{em} [nm]	τ [ns][a]	$\Phi_{F(solid)}$ [± 2%][b]	$k_{r(solid)}$ [10^7 s^{-1}][c]	$k_{nr(solid)}$ [10^7 s^{-1}][c]
3a[d]	548	**6.17 ± 0.02** 6.61 ± 0.02 (86 %) 3.5 ± 0.2 (14 %)	75	12.2 ± 0.4	4.1 ± 0.4
3b	596	**7.16 ± 0.04** 8.17 ± 0.07 (70 %) 4.1 ± 0.2 (30 %)	20	2.8 ± 0.3	11.2 ± 0.4
3c	566	**3.81 ± 0.03** 4.66 ± 0.06 (66 %) 2.1 ± 0.1 (34 %)	51	13.4 ± 0.6	12.9 ± 0.8
3d	585	**8.72 ± 0.02** 8.98 ± 0.04 (93 %) 5.1 ± 0.6 (7 %)	61	7.0 ± 0.2	4.5 ± 0.3
3e	646	**1.91 ± 0.06** 3.7 ± 0.3 (26 %) 1.8 ± 0.3 (43 %) 0.6 ± 0.1 (31 %)	16	8 ± 1	44 ± 3
3f	649	**4.43 ± 0.02** 5.04 ± 0.06 (75 %) 2.6 ± 0.2 (25 %)	52	11.7 ± 0.5	10.8 ± 0.6
3g	591	**1.54 ± 0.04** 3.3 ± 0.1 (22 %) 1.5 ± 0.2 (36 %) 0.64 ± 0.08 (42 %)	27	18 ± 2	47 ± 4
5	492	**5.09 ± 0.02** 6.15 ± 0.07 (63 %) 3.3 ± 0.1 (37 %)	45	8.8 ± 0.4	10.8 ± 0.5
6a	508	**5.67 ± 0.02** 6.66 ± 0.03 (71 %) 3.23 ± 0.08 (29 %)	40	7.1 ± 0.4	10.6 ± 0.4
6b	499	**6.46 ± 0.02** 7.16 ± 0.08 (79 %) 3.8 ± 0.3 (21 %)	65	10.1 ± 0.3	5.4 ± 0.4
6c	547	**3.64 ± 0.02** 3.0 ± 0.1 (70 %) 5.1 ± 0.2 (30 %)	16	4.4 ± 0.6	23.1 ± 0.7
7a	543	**8.47 ± 0.03** 8.87 ± 0.04 (92 %) 3.9 ± 0.5 (8 %)	58	6.9 ± 0.3	5.0 ± 0.3
7b	561	**7.55 ± 0.02** 7.97 ± 0.07 (88 %) 4.5 ± 0.5 (12 %)	75	9.9 ± 0.3	3.3 ± 0.3
7c	570	**9.21 ± 0.02** 10.7 ± 0.1 (69 %) 5.9 ± 0.3 (31 %)	84	9.1 ± 0.2	1.7 ± 0.3
7d	521	**7.13 ± 0.02** 7.80 ± 0.07 (82 %) 4.2 ± 0.3 (18 %)	75	10.5 ± 0.3	3.5 ± 0.3

[a] For multiexponential decays, the amplitude-weighted average lifetimes (τ_{av_amp}) are shown along with the different decay components and the relative amplitude in parentheses.[11] [b] Φ_F of solids at RT were obtained using a calibrated integrating sphere with a suitable sample holder. [c] The decay rate constants are determined according to $k_r = 1/\tau_r = \Phi_F/\tau_{obs}$ and $k_{nr} = 1\text{-}\Phi_F/\tau_r$.[11] [d] The photoluminescence properties of **3a** have been previously reported in solid state at rt.[2]

5.2 Summary of Photoluminescence Properties in CH_2Cl_2 Solution at rt

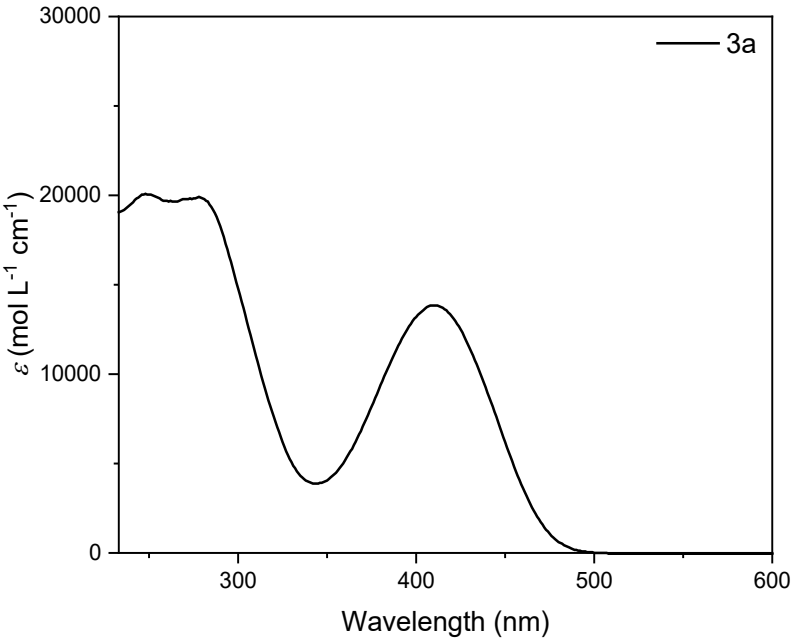

Figure S5.2.1: Absorption spectrum of **3a** in liquid CH_2Cl_2 solution at rt.

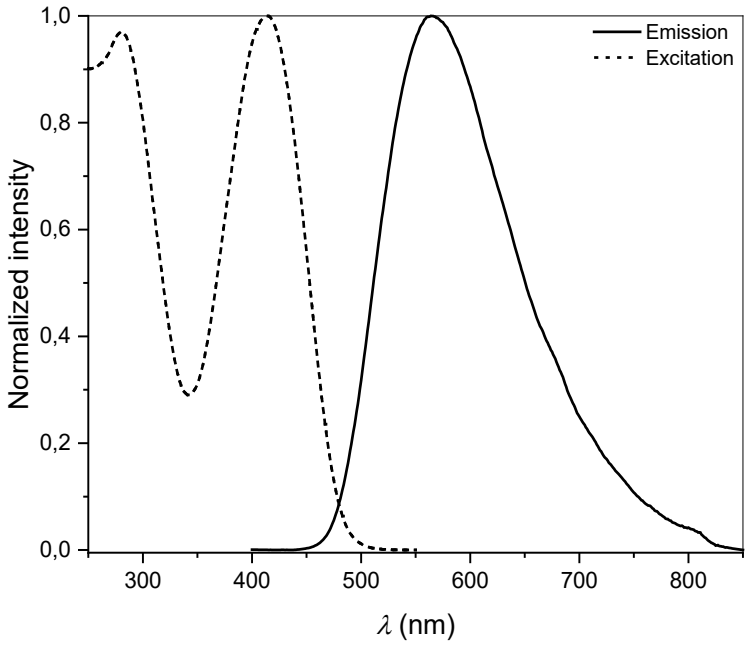

Figure S5.2.2: Normalized emission (solid line, λ_{exc} = 320.0 nm) and excitation (dashed line, λ_{obs} = 580.0 nm) sw of **3a** in liquid CH_2Cl_2 solution at rt.

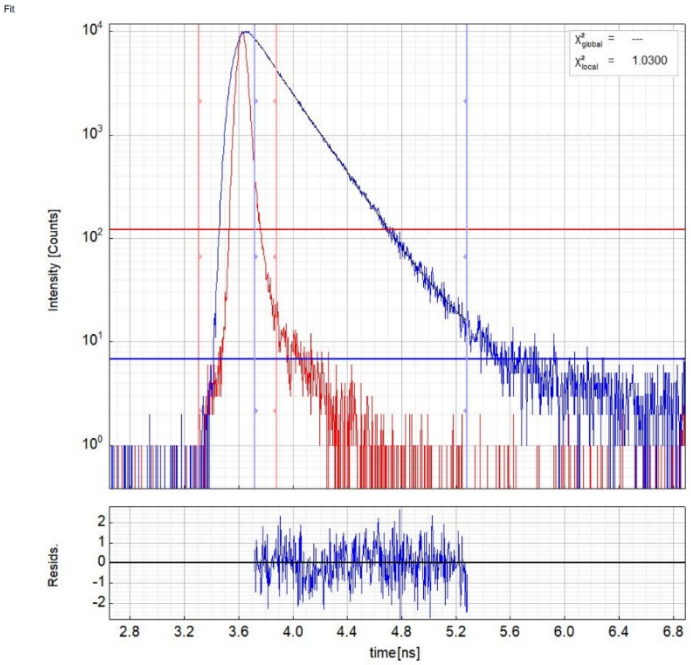

Parameter	Value	Δ
A_1[kCnts/Chnl]	13.86	±0.26
τ_1[ns]	0.2294	±0.0015
I_1[kCnts]	795	±17
A_{Rel1}[%]	100.0	---
$Bkgr_{Dec}$[kCnts]	0.0068	±0.0014
$Bkgr_{IRF}$[Cnts/Chnl]	122	±24
$Shift_{IRF}$[ps]	21.0	±4.2
A_{Scatt}[kCnts]	- 144	±52
τ_{AvInt}[ns]	0.2294	±0.0015
τ_{AvAmp}[ns]	0.2294	±0.0015

Figure S5.2.3: Left - Raw (experimental) time-resolved photoluminescence decay (blue) of **3a** in liquid CH_2Cl_2 solution at rt including the residuals (air-equilibrated, λ_{exc} = 373.0 nm, λ_{det} = 565.0 nm) and the IRF (red). Right - Fitting parameters including pre-exponential factors and confidence limits.

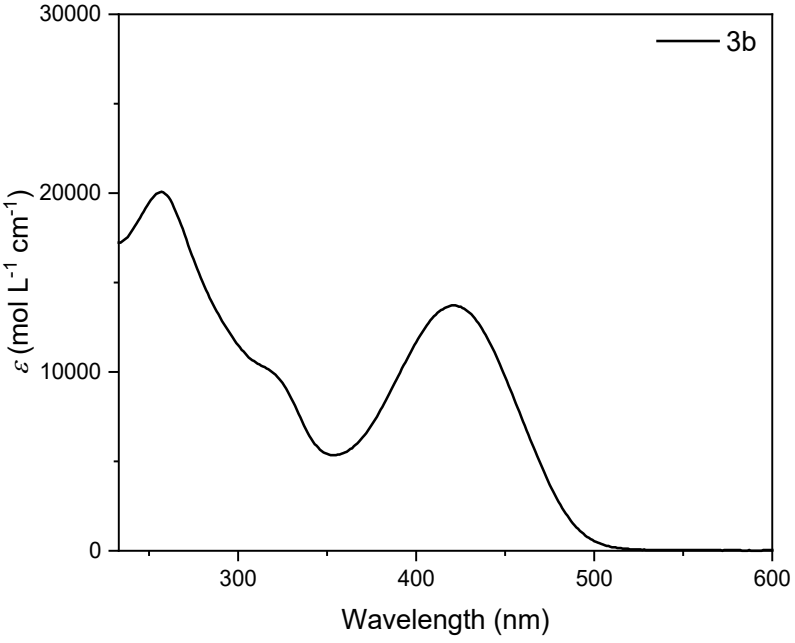

Figure S5.2.4: Absorption spectrum of **3b** in liquid CH_2Cl_2 solution at rt.

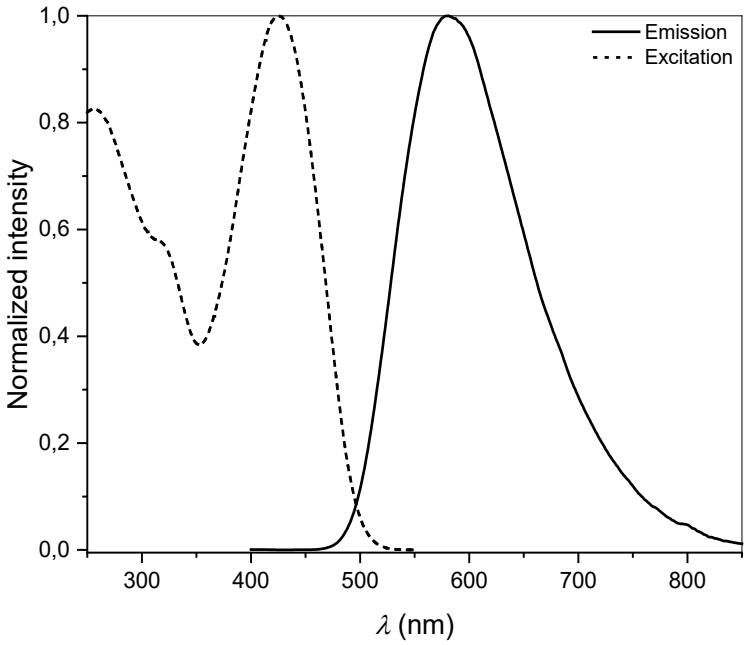

Figure S5.2.5: Normalized emission (solid line, λ_{exc} = 320.0 nm) and excitation (dashed line, λ_{obs} = 580.0 nm) spectra of **3b** in liquid CH_2Cl_2 solution at rt.

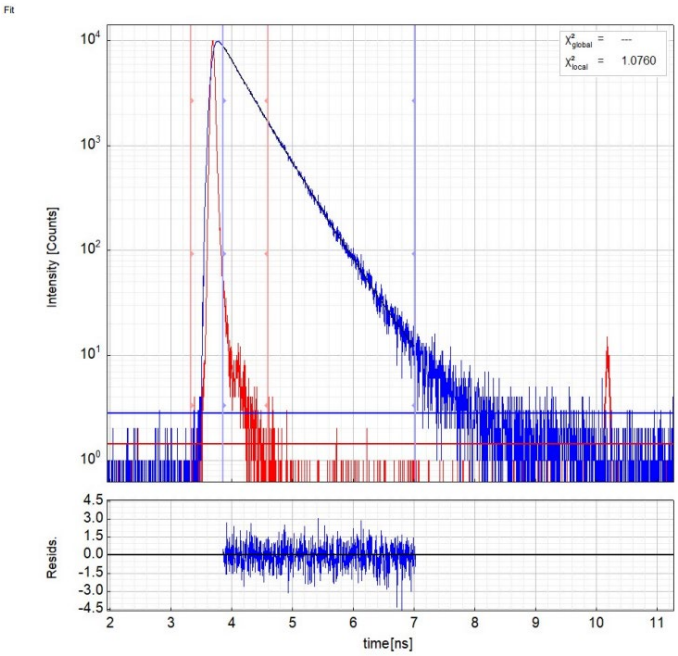

Parameter	Value	Δ
A_1[kCnts/Chnl]	10.9	±4.4
τ_1[ns]	0.471	±0.045
I_1[kCnts]	1 280	±440
A_{Rel1}[%]	77	±30
A_2[kCnts/Chnl]	3.4	±4.1
τ_2[ns]	0.256	±0.094
I_2[kCnts]	220	±440
A_{Rel2}[%]	24	±30
$Bkgr_{Dec}$[kCnts]	0.0029	±0.0022
$Bkgr_{IRF}$[Cnts/Chnl]	1.5	±3.6
$Shift_{IRF}$[ps]	-1.5	±3.3
A_{Scatt}[kCnts]	-1 230	±540
τ_{AvInt}[ns]	0.4399	±0.0043
τ_{AvAmp}[ns]	0.420	±0.011

Figure S5.2.6: Left - Raw (experimental) time-resolved photoluminescence decay (blue) of **3b** in liquid CH_2Cl_2 solution at rt including the residuals (air-equilibrated, λ_{exc} = 373.0 nm, λ_{det} = 580.0 nm) and the IRF (red). Right - Fitting parameters including pre-exponential factors and confidence limits.

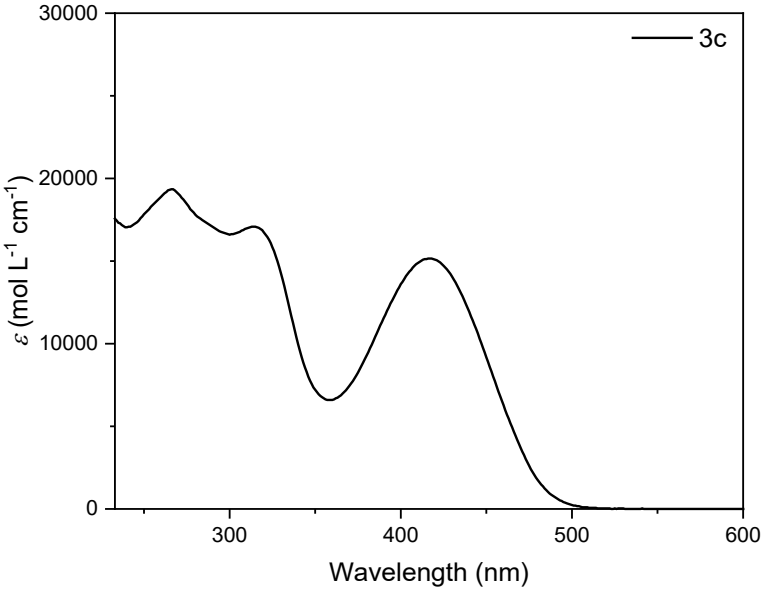

Figure S5.2.7: Absorption spectrum of **3c** in liquid CH_2Cl_2 solution at rt.

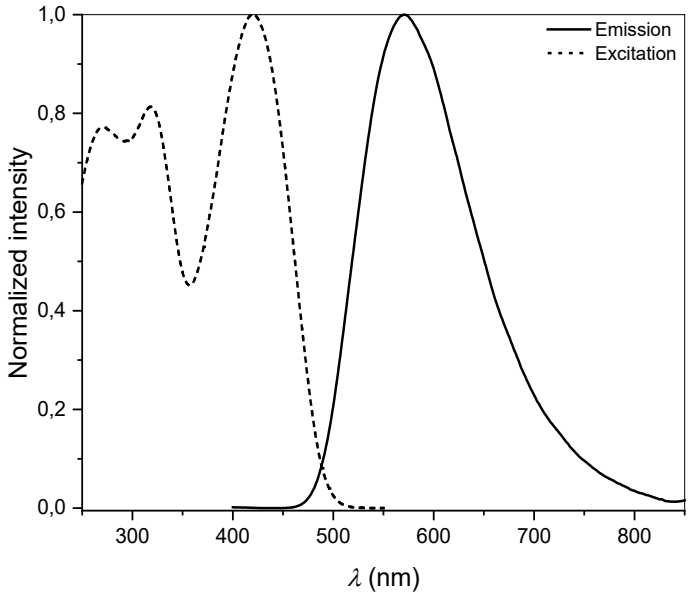

Figure S5.2.8: Normalized emission (solid line, λ_{exc} = 320.0 nm) and excitation (dashed line, λ_{obs} = 580.0 nm) spectra of **3c** in liquid CH_2Cl_2 solution at rt.

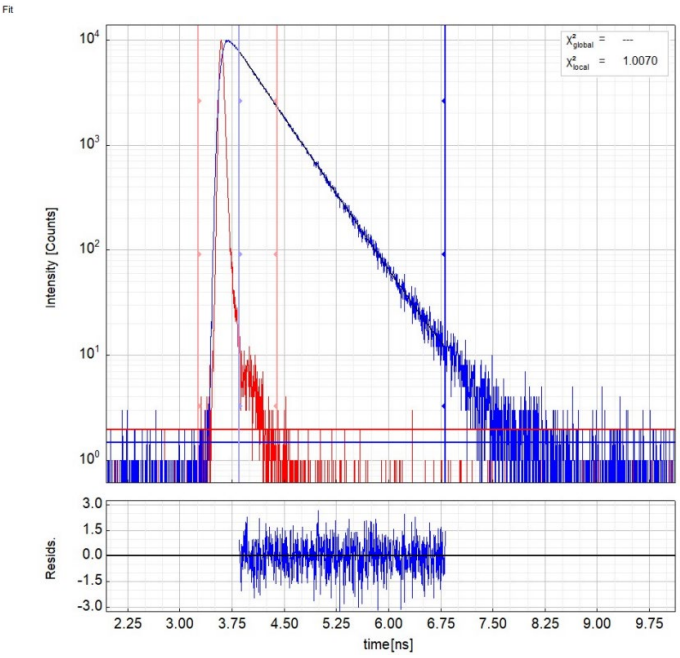

Parameter	Value	Δ
A_1[kCnts/Chnl]	13.78	±0.26
τ_1[ns]	0.4470	±0.0026
I_1[kCnts]	1 539	±29
A_{Rel1}[%]	100.0	---
$Bkgr_{Dec}$[kCnts]	0.0015	±0.0010
$Bkgr_{IRF}$[Cnts/Chnl]	2.0	±4.6
$Shift_{IRF}$[ps]	-28.1	±8.7
A_{Scatt}[kCnts]	800	±1 500
τ_{AvInt}[ns]	0.4470	±0.0026
τ_{AvAmp}[ns]	0.4470	±0.0026

Figure S5.2.9: Left - Raw (experimental) time-resolved photoluminescence decay (blue) of **3c** in liquid CH_2Cl_2 solution at rt including the residuals (air-equilibrated, λ_{exc} = 373.0 nm, λ_{det} = 570.0 nm) and the IRF (red). Right - Fitting parameters including pre-exponential factors and confidence limits.

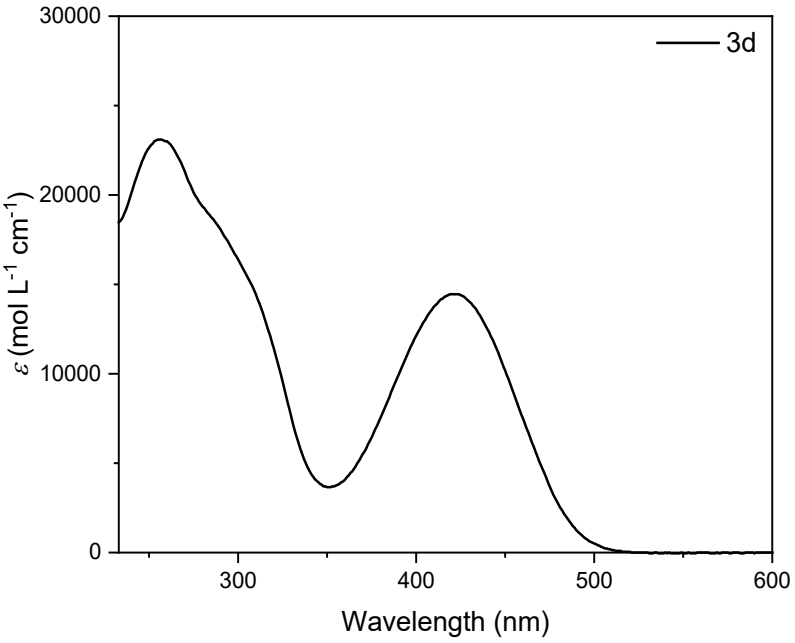

Figure S5.2.10: Absorption spectrum of **3d** in liquid CH_2Cl_2 solution at rt.

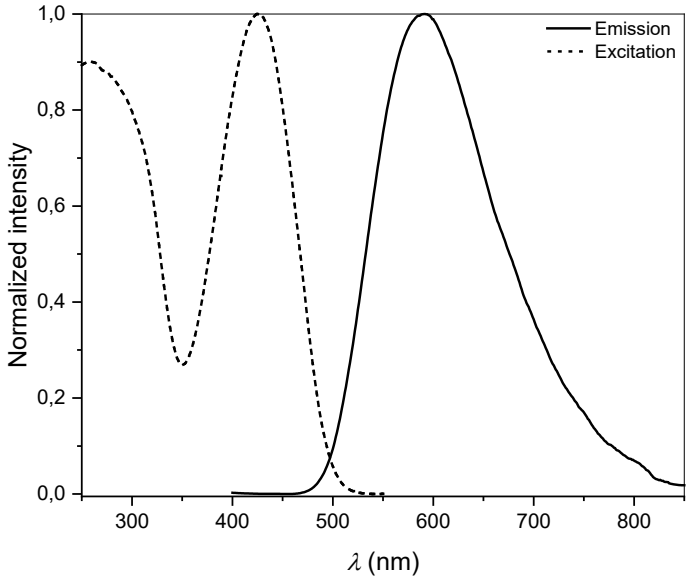

Figure S5.2.11: Normalized emission (solid line, λ_{exc} = 320.0 nm) and excitation (dashed line, λ_{obs} = 580.0 nm) spectra of **3d** in liquid CH_2Cl_2 solution at rt.

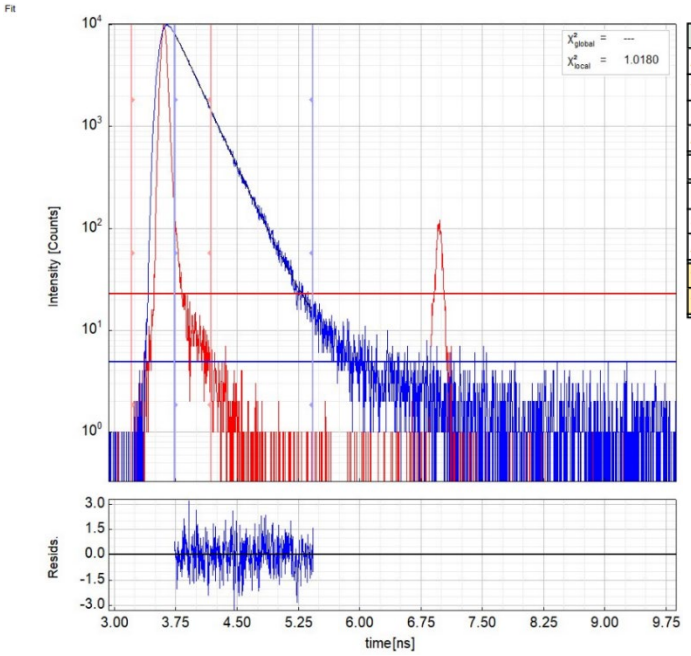

Parameter	Value	Δ
A_1[kCnts/Chnl]	14.27	±0.25
τ_1[ns]	0.2544	±0.0036
I_1[kCnts]	907	±11
A_{Rel1}[%]	100.0	---
$Bkgr_{Dec}$[kCnts]	0.0049	±0.0014
$Bkgr_{IRF}$[Cnts/Chnl]	23	±11
$Shift_{IRF}$[ps]	12.2	±2.8
A_{Scatt}[kCnts]	- 450	±190
τ_{AvInt}[ns]	0.2544	±0.0036
τ_{AvAmp}[ns]	0.2544	±0.0036

Figure S5.2.12: Left - Raw (experimental) time-resolved photoluminescence decay (blue) of **3d** in liquid CH_2Cl_2 solution at rt including the residuals (air-equilibrated, λ_{exc} = 373.0 nm, λ_{det} = 590.0 nm) and the IRF (red). Right - Fitting parameters including pre-exponential factors and confidence limits.

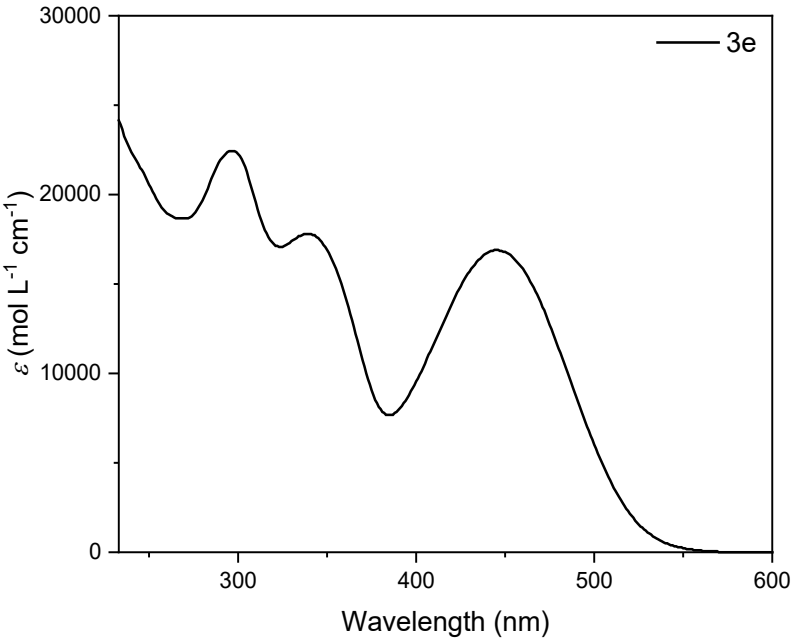

Figure S5.2.13: Absorption spectrum of **3e** in liquid CH_2Cl_2 solution at rt.

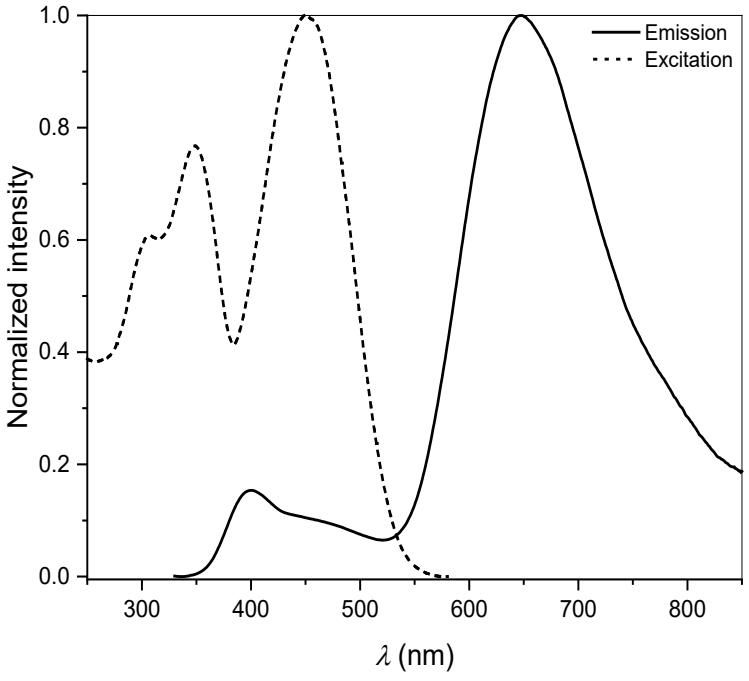

Figure S5.2.14: Normalized emission (solid line, λ_{exc} = 320.0 nm) and excitation (dashed line, λ_{obs} = 600.0 nm) spectra of **3e** in liquid CH_2Cl_2 solution at rt.

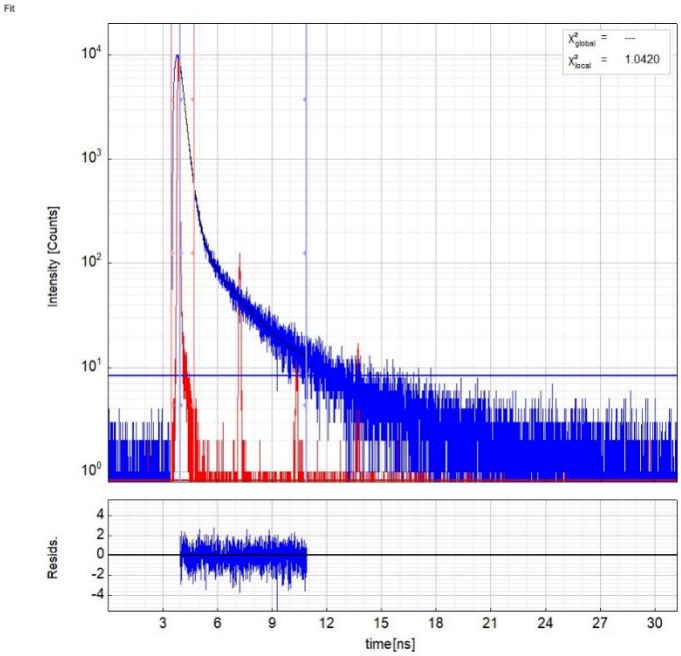

Parameter	Value	Δ
A_1[kCnts/Chnl]	0.270	±0.013
τ_1[ns]	1.712	±0.064
I_1[kCnts]	115.3	±2.0
A_{Rel1}[%]	2.1	±0.2
A_2[kCnts/Chnl]	12.87	±0.28
τ_2[ns]	0.2454	±0.0022
I_2[kCnts]	790	±15
A_{Rel2}[%]	98.0	±0.2
$Bkgr_{Dec}$[kCnts]	0.0084	±0.0010
$Bkgr_{IRF}$[Cnts/Chnl]	0.9	±4.2
$Shift_{IRF}$[ps]	116.3	±4.3
A_{Scatt}[kCnts]	- 400	±130
τ_{AvInt}[ns]	0.4322	±0.0088
τ_{AvAmp}[ns]	0.2755	±0.0029

Figure S5.2.15: Left - Raw (experimental) time-resolved photoluminescence decay (blue) of **3e** in liquid CH_2Cl_2 solution at rt including the residuals (air-equilibrated, λ_{exc} = 373.0 nm, λ_{det} = 500.0 nm) and the IRF (red). Right - Fitting parameters including pre-exponential factors and confidence limits.

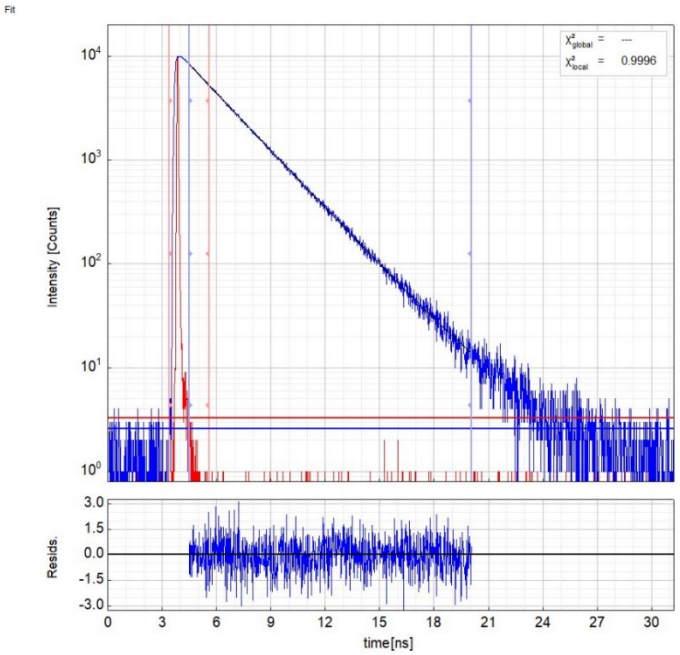

Parameter	Value	Δ
A_1[kCnts/Chnl]	11.11	±0.25
τ_1[ns]	2.3609	±0.0078
I_1[kCnts]	1 639	±36
A_{Rel1}[%]	100.0	---
$Bkgr_{Dec}$[kCnts]	0.0026	±0.0009
$Bkgr_{IRF}$[Cnts/Chnl]	3.3	±3.4
$Shift_{IRF}$[ps]	144	±43
A_{Scatt}[kCnts]	- 320	±780
τ_{AvInt}[ns]	2.3609	±0.0078
τ_{AvAmp}[ns]	2.3609	±0.0078

Figure S5.2.16: Left - Raw (experimental) time-resolved photoluminescence decay (blue) of **3e** in liquid CH_2Cl_2 solution at rt including the residuals (air-equilibrated, λ_{exc} = 373.0 nm, λ_{det} = 650.0 nm) and the IRF (red). Right - Fitting parameters including pre-exponential factors and confidence limits.

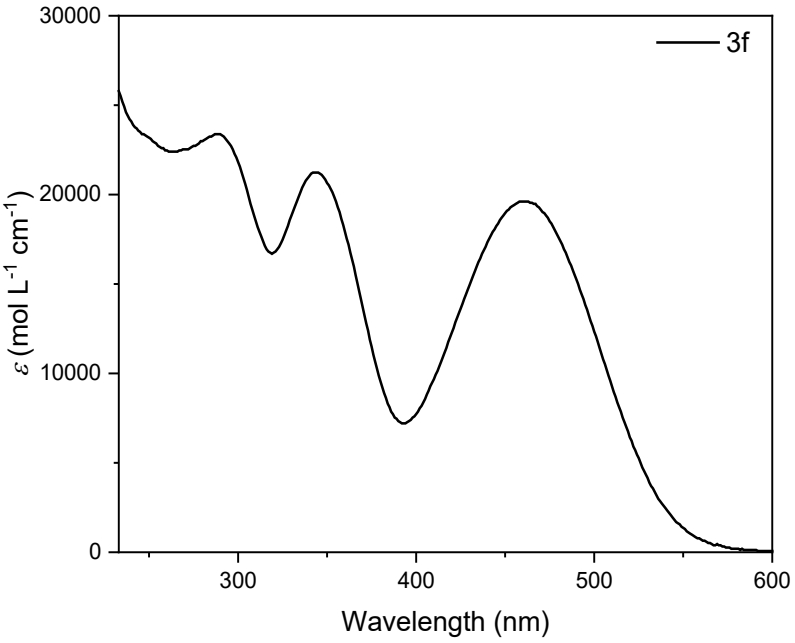

Figure S5.2.17: Absorption spectrum of **3f** in liquid CH_2Cl_2 solution at rt.

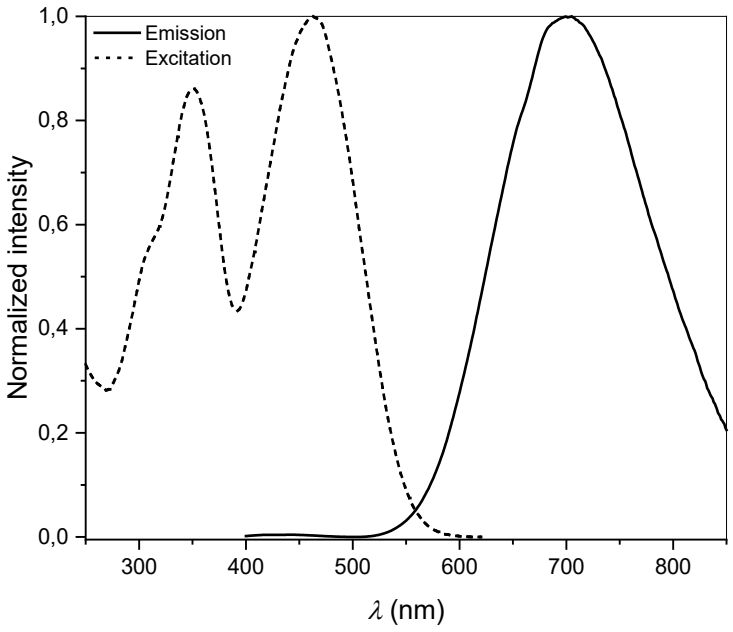

Figure S5.2.18: Normalized emission (solid line, λ_{exc} = 320.0 nm) and excitation (dashed line, λ_{obs} = 650.0 nm) spectra of **3f** in liquid CH_2Cl_2 solution at rt.

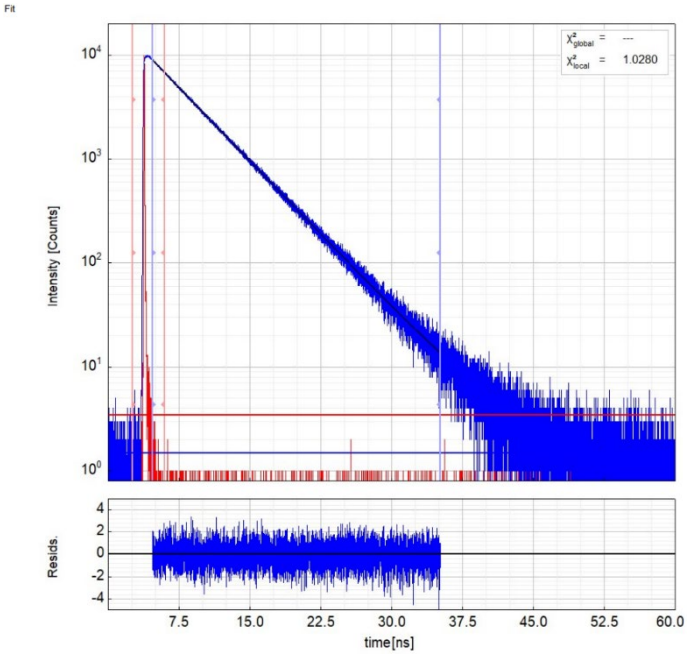

Parameter	Value	Δ
A_1[kCnts/Chnl]	10.969	±0.090
τ_1[ns]	4.6179	±0.0047
I_1[kCnts]	12 670	±120
A_{Rel1}[%]	100.0	---
$Bkgr_{Dec}$[kCnts]	0.0015	±0.0004
$Bkgr_{IRF}$[Cnts/Chnl]	3.5	±1.4
$Shift_{IRF}$[ps]	119	±26
A_{Scatt}[kCnts]	-1 200	±1 300
τ_{AvInt}[ns]	4.6179	±0.0047
τ_{AvAmp}[ns]	4.6179	±0.0047

Figure S5.2.19: Left - Raw (experimental) time-resolved photoluminescence decay (blue) of **3f** in liquid CH_2Cl_2 solution at rt including the residuals (air-equilibrated, λ_{exc} = 373.0 nm, λ_{det} = 700.0 nm) and the IRF (red). Right - Fitting parameters including pre-exponential factors and confidence limits.

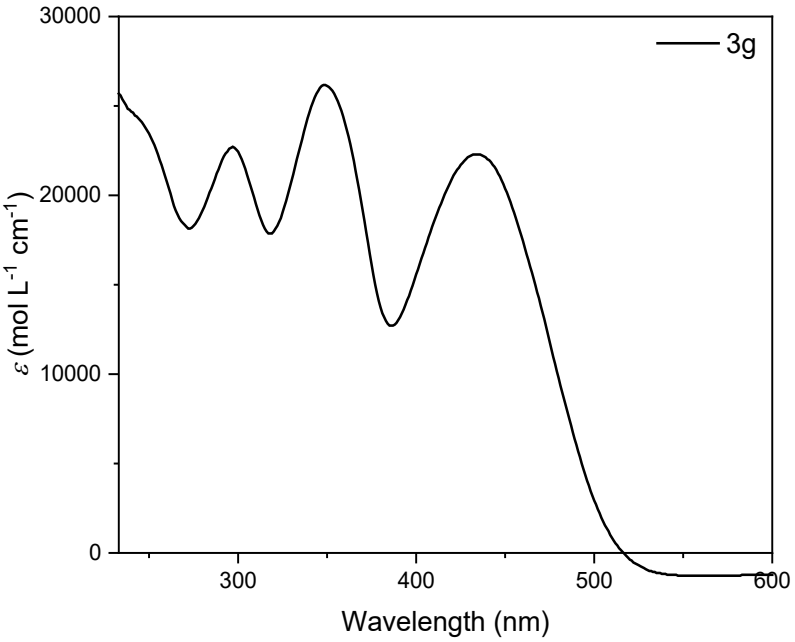

Figure S5.2.20: Absorption spectrum of **3g** in liquid CH_2Cl_2 solution at rt.

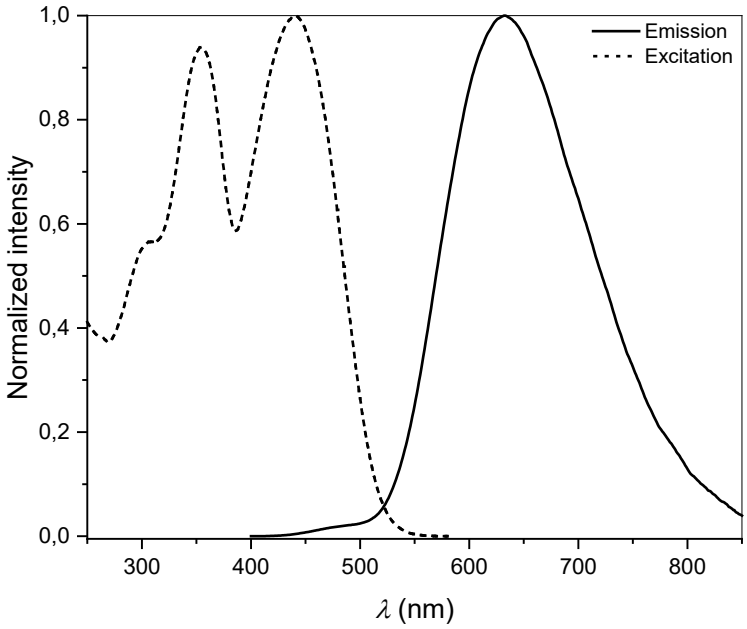

Figure S5.2.21: Normalized emission (solid line, λ_{exc} = 320.0 nm) and excitation (dashed line, λ_{obs} = 600.0 nm) spectra of **3g** in liquid CH_2Cl_2 solution at rt.

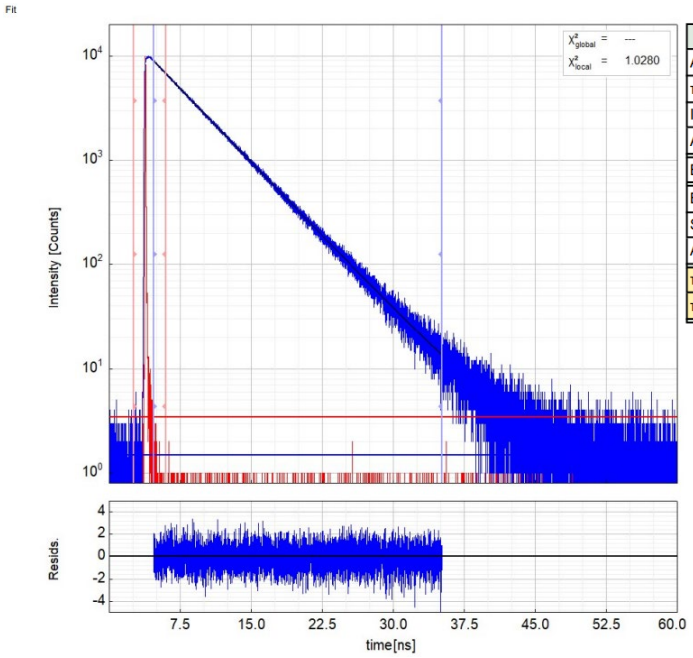

Parameter	Value	Δ
A_1[kCnts/Chnl]	10.969	±0.090
τ_1[ns]	4.6179	±0.0047
I_1[kCnts]	12 670	±120
A_{Rel1}[%]	100.0	---
$Bkgr_{Dec}$[kCnts]	0.0015	±0.0004
$Bkgr_{IRF}$[Cnts/Chnl]	3.5	±1.4
$Shift_{IRF}$[ps]	119	±26
A_{Scatt}[kCnts]	-1 200	±1 300
τ_{AvInt}[ns]	4.6179	±0.0047
τ_{AvAmp}[ns]	4.6179	±0.0047

Figure S5.2.22: Left - Raw (experimental) time-resolved photoluminescence decay (blue) of **3g** in liquid CH_2Cl_2 solution at rt including the residuals (air-equilibrated, λ_{exc} = 373.0 nm, λ_{det} = 630.0 nm) and the IRF (red). Right - Fitting parameters including pre-exponential factors and confidence limits.

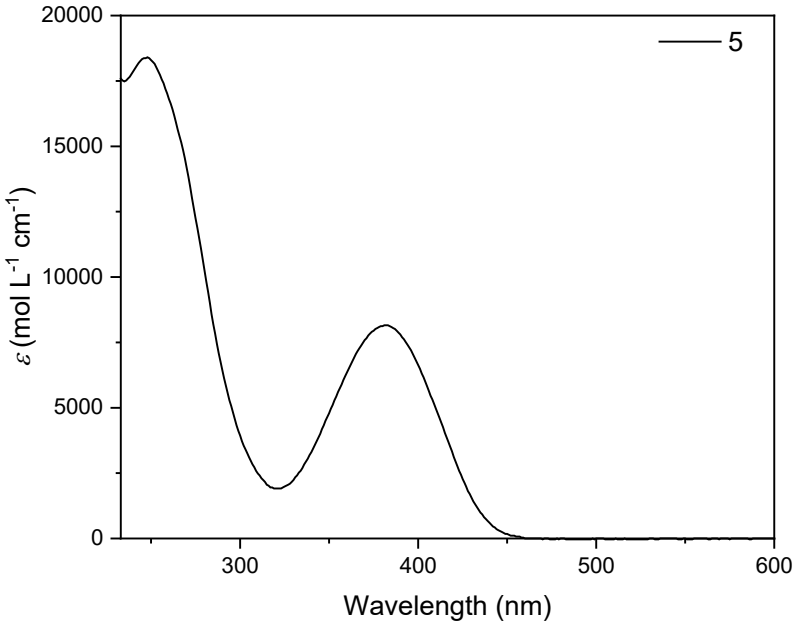

Figure S5.2.23: Absorption spectrum of **5** in liquid CH_2Cl_2 solution at rt.

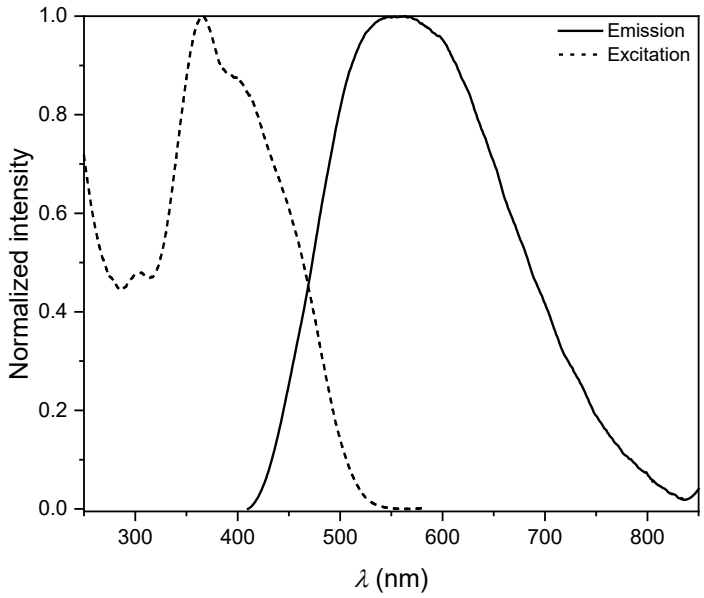

Figure S5.2.24: Normalized emission (solid line, λ_{exc} = 320.0 nm) and excitation (dashed line, λ_{obs} = 600.0 nm) spectra of **5** in liquid CH_2Cl_2 solution at rt.

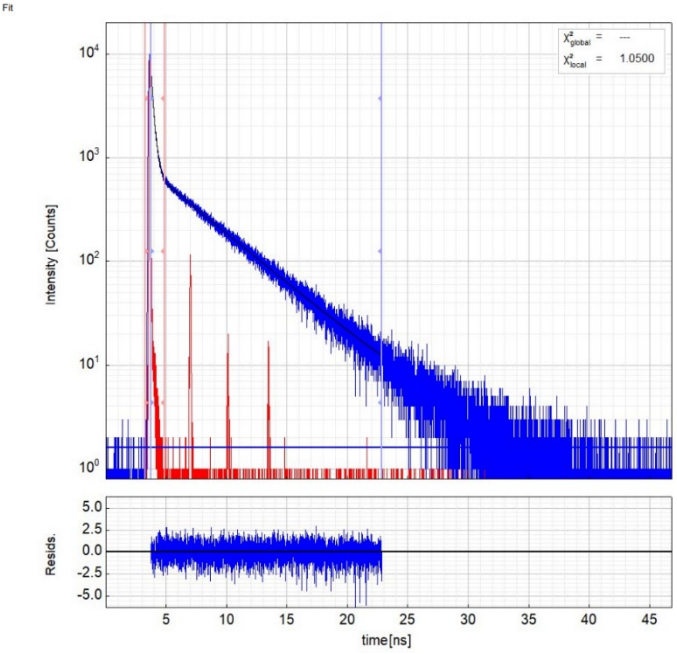

Parameter	Value	Δ
A_1[kCnts/Chnl]	0.7473	±0.0073
τ_1[ns]	4.513	±0.028
I_1[kCnts]	843.1	±5.8
A_{Rel1}[%]	6.8	±0.3
A_2[kCnts/Chnl]	10.27	±0.29
τ_2[ns]	0.2135	±0.0024
I_2[kCnts]	548	±13
A_{Rel2}[%]	93.3	±0.3
$Bkgr_{Dec}$[kCnts]	0.0017	±0.0005
$Bkgr_{IRF}$[Cnts/Chnl]	-5.9	±2.7
$Shift_{IRF}$[ps]	29.6	±4.4
A_{Scatt}[kCnts]	290	±140
τ_{AvInt}[ns]	2.820	±0.028
τ_{AvAmp}[ns]	0.5053	±0.0100

Figure S5.2.25: Left - Raw (experimental) time-resolved photoluminescence decay (blue) of **5** in liquid CH_2Cl_2 solution at rt including the residuals (air-equilibrated, λ_{exc} = 373.0 nm, λ_{det} = 620.0 nm) and the IRF (red). Right - Fitting parameters including pre-exponential factors and confidence limits.

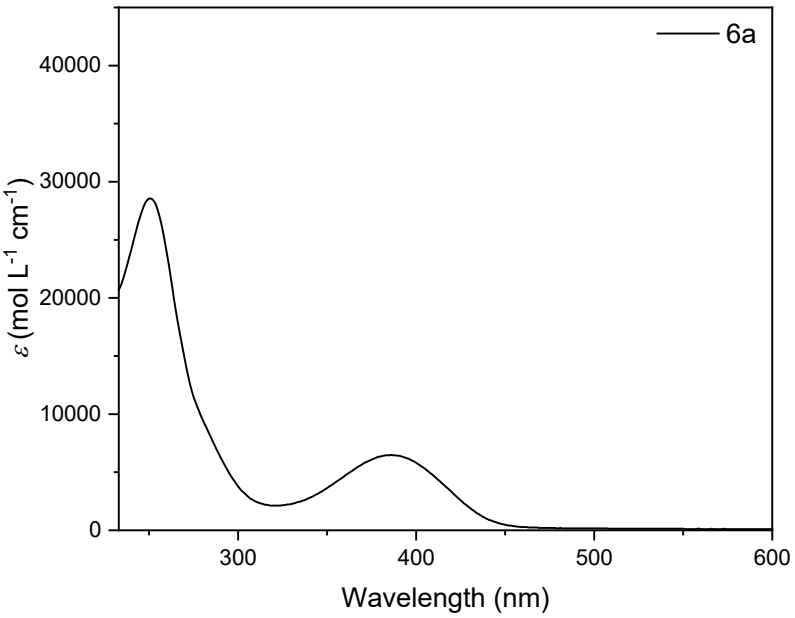

Figure S5.2.26: Absorption spectrum of **6a** in liquid CH_2Cl_2 solution at rt.

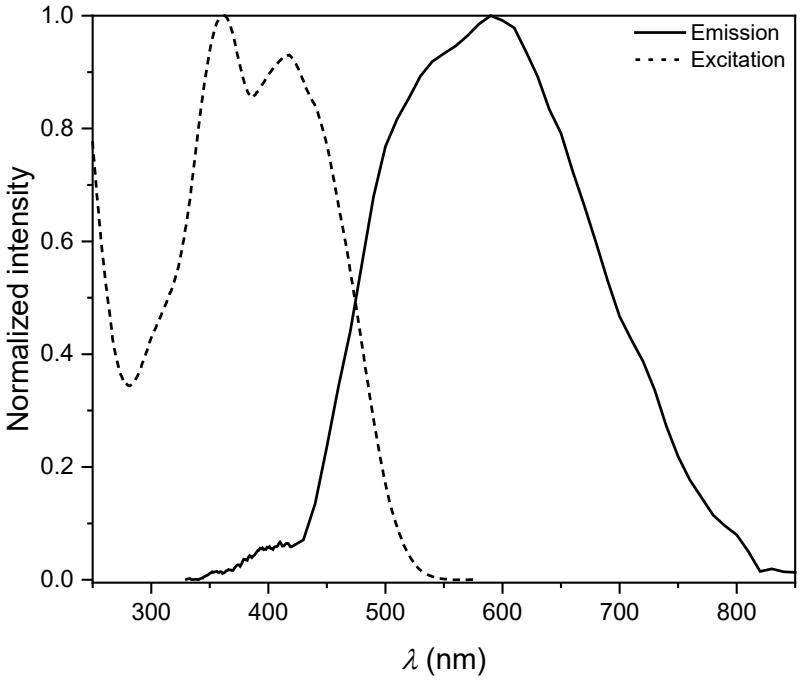

Figure S5.2.27: Normalized emission (solid line, λ_{exc} = 320.0 nm) and excitation (dashed line, λ_{obs} = 600.0 nm) spectra of **6a** in liquid CH_2Cl_2 solution at rt.

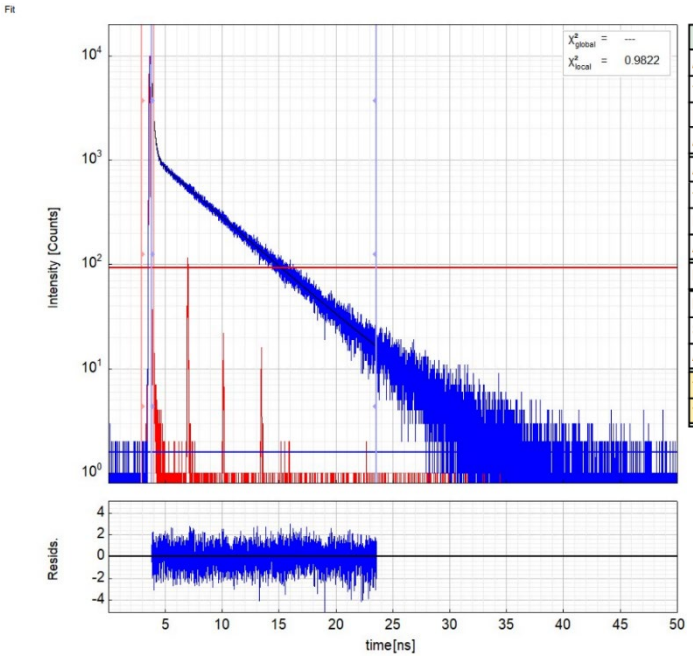

Parameter	Value	Δ
A_1[kCnts/Chnl]	1.284	±0.049
τ_1[ns]	4.600	±0.023
I_1[kCnts]	1 476	±59
A_{Rel1}[%]	7.3	±0.5
A_2[kCnts/Chnl]	16.49	±0.76
τ_2[ns]	0.1749	±0.0050
I_2[kCnts]	722	±36
A_{Rel2}[%]	92.8	±0.5
$Bkgr_{Dec}$[kCnts]	0.0016	±0.0006
$Bkgr_{IRF}$[Cnts/Chnl]	93	±28
$Shift_{IRF}$[ps]	-42.6	±7.5
A_{Scatt}[kCnts]	-24	±94
τ_{AvInt}[ns]	3.147	±0.049
τ_{AvAmp}[ns]	0.495	±0.023

Figure S5.2.28: Left - Raw (experimental) time-resolved photoluminescence decay (blue) of **6a** in liquid CH_2Cl_2 solution at rt including the residuals (air-equilibrated, λ_{exc} = 373.0 nm, λ_{det} = 620.0 nm) and the IRF (red). Right - Fitting parameters including pre-exponential factors and confidence limits.

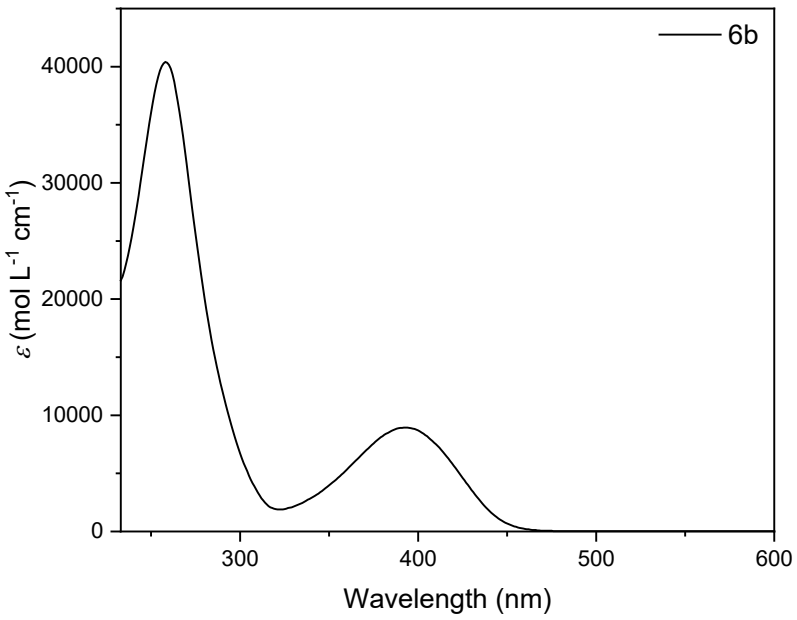

Figure S5.2.29: Absorption spectrum of **6b** in liquid CH_2Cl_2 solution at rt.

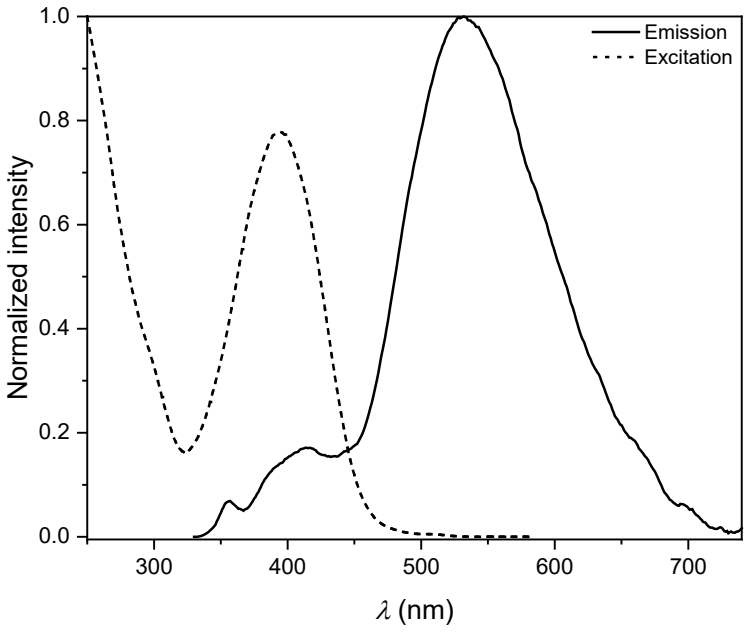

Figure S5.2.30: Normalized emission (solid line, λ_{exc} = 320.0 nm) and excitation (dashed line, λ_{obs} = 600.0 nm) spectra of **6b** in liquid CH_2Cl_2 solution at rt.

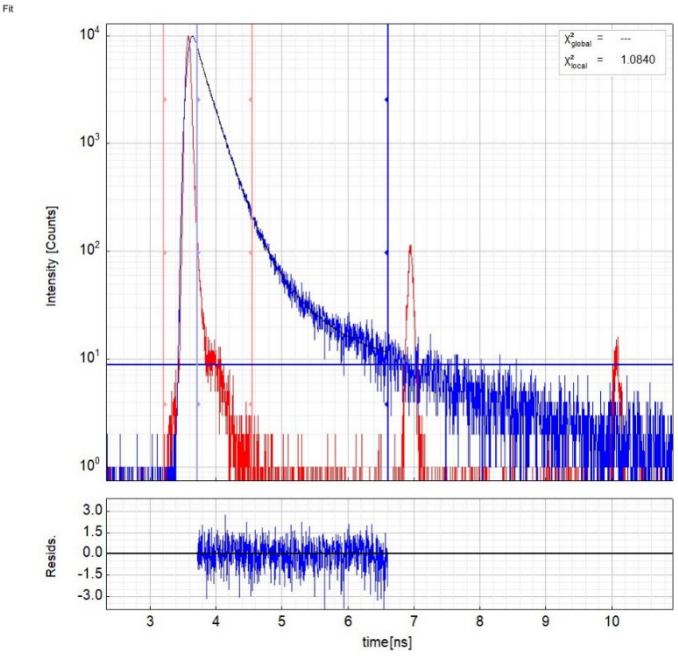

Parameter	Value	Δ
A_1[kCnts/Chnl]	0.38	±0.22
τ_1[ns]	0.62	±0.15
I_1[kCnts]	57	±18
A_{Rel1}[%]	2.6	±1.5
A_2[kCnts/Chnl]	14.02	±0.38
τ_2[ns]	0.2031	±0.0040
I_2[kCnts]	712	±21
A_{Rel2}[%]	97.5	±1.5
$Bkgr_{Dec}$[kCnts]	0.0089	±0.0027
$Bkgr_{IRF}$[Cnts/Chnl]	-0.6	±2.1
$Shift_{IRF}$[ps]	-33.1	±3.0
A_{Scatt}[kCnts]	730	±270
τ_{AvInt}[ns]	0.2337	±0.0053
τ_{AvAmp}[ns]	0.2137	±0.0027

Figure S5.2.31: Left - Raw (experimental) time-resolved photoluminescence decay (blue) of **6b** in liquid CH_2Cl_2 solution at rt including the residuals (air-equilibrated, λ_{exc} = 373.0 nm, λ_{det} = 530.0 nm) and the IRF (red). Right - Fitting parameters including pre-exponential factors and confidence limits.

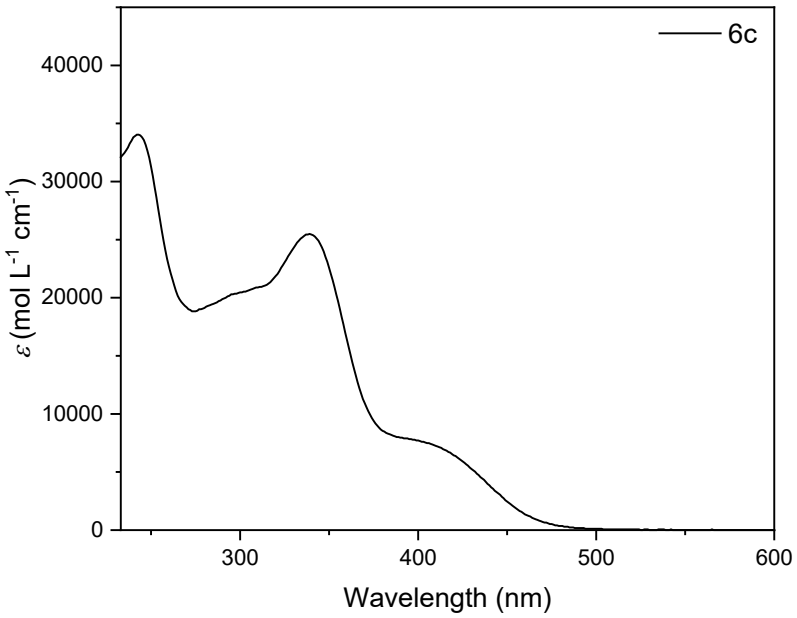

Figure S5.2.32: Absorption spectrum of **6c** in liquid CH_2Cl_2 solution at rt.

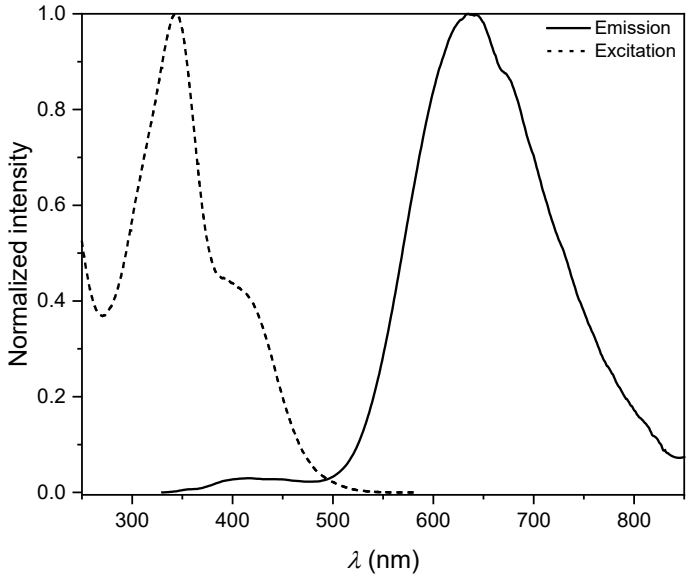

Figure S5.2.33: Normalized emission (solid line, λ_{exc} = 320.0 nm) and excitation (dashed line, λ_{obs} = 600.0 nm) spectra of **6c** in liquid CH_2Cl_2 solution at rt.

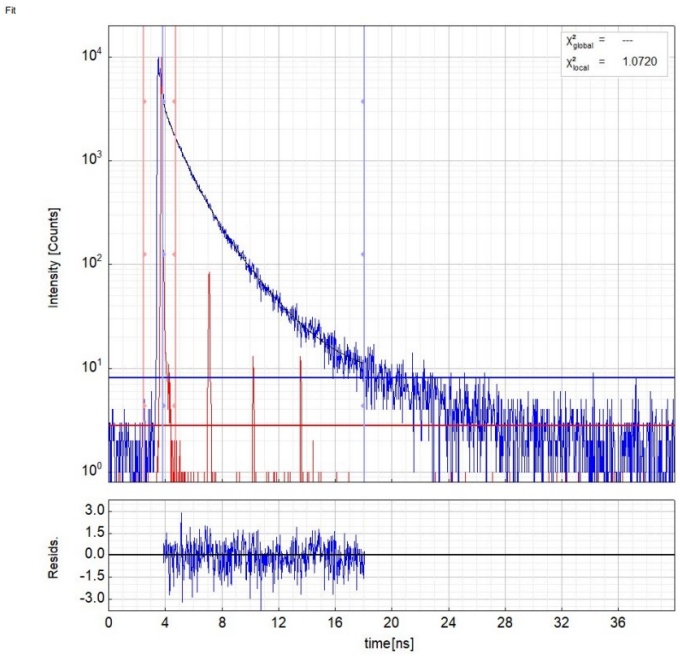

Parameter	Value	Δ
A_1[kCnts/Chnl]	1.02	±0.35
τ_1[ns]	2.48	±0.38
I_1[kCnts]	79	±19
A_{Rel1}[%]	26.8	±8.4
A_2[kCnts/Chnl]	2.77	±0.26
τ_2[ns]	1.02	±0.13
I_2[kCnts]	89	±18
A_{Rel2}[%]	73.3	±8.4
$Bkgr_{Dec}$[kCnts]	0.0081	±0.0022
$Bkgr_{IRF}$[Cnts/Chnl]	2.8	±7.4
$Shift_{IRF}$[ps]	139	±30
A_{Scatt}[kCnts]	210	±190
τ_{AvInt}[ns]	1.706	±0.060
τ_{AvAmp}[ns]	1.410	±0.057

Figure S5.2.23: Left - Raw (experimental) time-resolved photoluminescence decay (blue) of **6c** in liquid CH_2Cl_2 solution at rt including the residuals (air-equilibrated, λ_{exc} = 373.0 nm, λ_{det} = 400.0 nm) and the IRF (red). Right - Fitting parameters including pre-exponential factors and confidence limits.

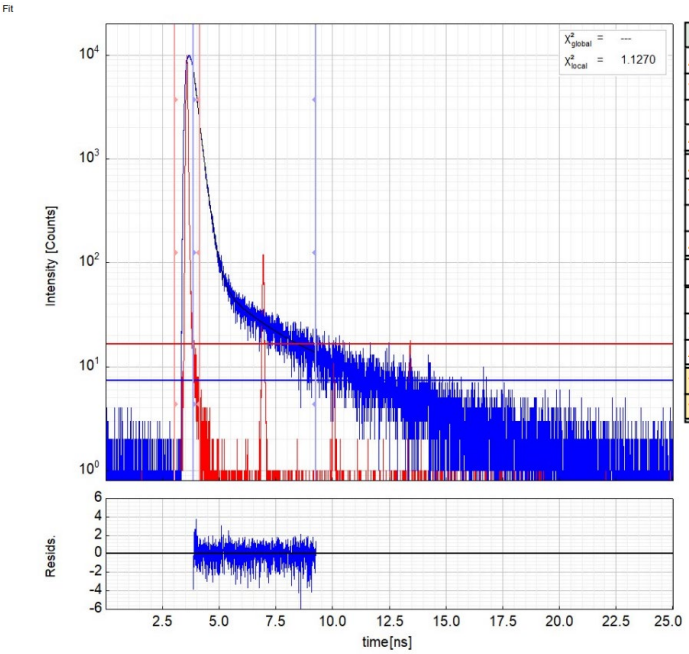

Parameter	Value	Δ
A_1[kCnts/Chnl]	0.095	±0.012
τ_1[ns]	2.13	±0.40
I_1[kCnts]	50.0	±4.7
A_{Rel1}[%]	0.4	±0.1
A_2[kCnts/Chnl]	25.32	±0.73
τ_2[ns]	0.2312	±0.0035
I_2[kCnts]	1 464	±27
A_{Rel2}[%]	99.7	±0.1
$Bkgr_{Dec}$[kCnts]	0.0074	±0.0031
$Bkgr_{IRF}$[Cnts/Chnl]	16.4	±7.8
$Shift_{IRF}$[ps]	-46.2	±3.7
A_{Scatt}[kCnts]	-1 600	±1 400
τ_{AvInt}[ns]	0.294	±0.022
τ_{AvAmp}[ns]	0.2382	±0.0042

Figure S5.2.34: Left - Raw (experimental) time-resolved photoluminescence decay (blue) of **6c** in liquid CH_2Cl_2 solution at rt including the residuals (air-equilibrated, λ_{exc} = 373.0 nm, λ_{det} = 640.0 nm) and the IRF (red). Right - Fitting parameters including pre-exponential factors and confidence limits.

5.3 Summary of Photoluminescence Properties in Frozen CH_2Cl_2-MeOH 1:1 Glassy Matrix at 77 K

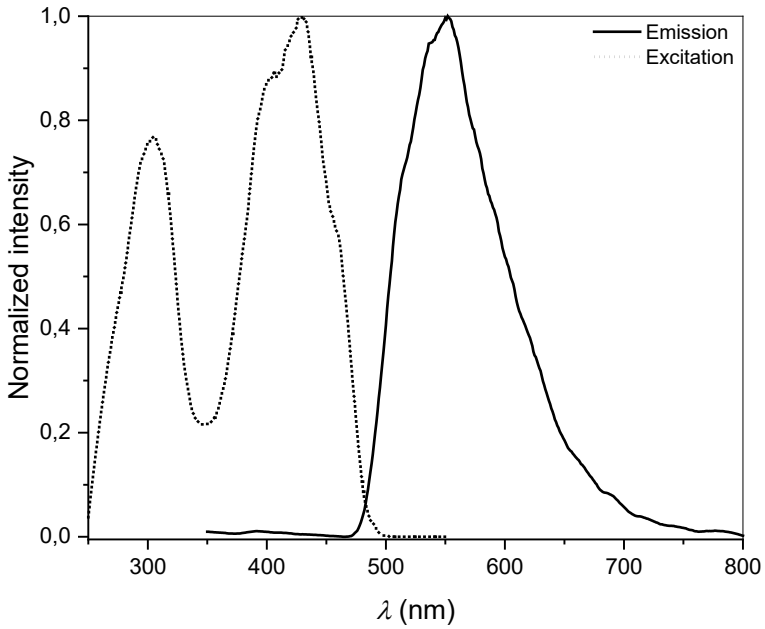

Figure S5.3.1: Normalized emission (solid line, λ_{exc} = 320.0 nm) and excitation (dashed line, λ_{obs} = 580.0 nm) spectra of **3a** in a frozen CH_2Cl_2-MeOH 1:1 glassy matrix at 77 K.

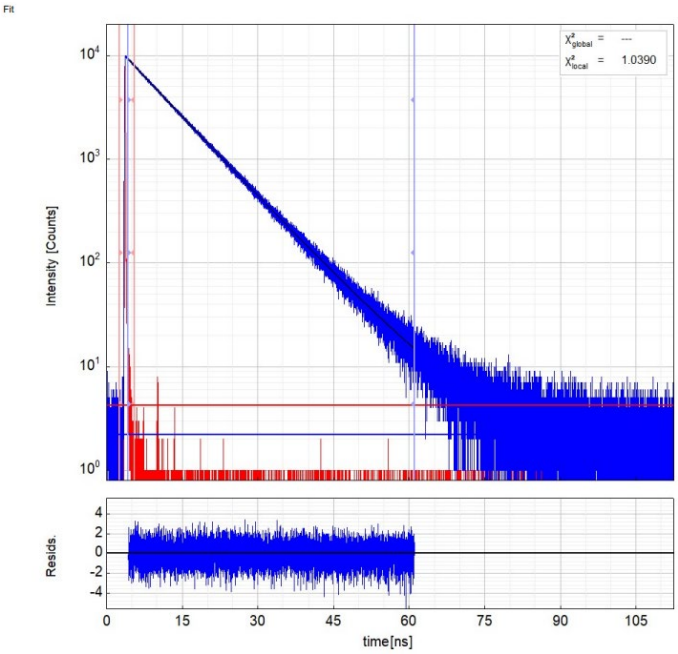

Parameter	Value	Δ
A_1[kCnts/Chnl]	6.060	±0.066
τ_1[ns]	9.116	±0.041
I_1[kCnts]	13 810	±160
A_{Rel1}[%]	60.5	±0.7
A_2[kCnts/Chnl]	3.957	±0.080
τ_2[ns]	7.394	±0.079
I_2[kCnts]	7 320	±170
A_{Rel2}[%]	39.6	±0.7
$Bkgr_{Dec}$[kCnts]	0.0022	±0.0004
$Bkgr_{IRF}$[Cnts/Chnl]	4.3	±3.6
$Shift_{IRF}$[ps]	29	±28
A_{Scatt}[kCnts]	- 500	±2 200
τ_{AvInt}[ns]	8.5189	±0.0071
τ_{AvAmp}[ns]	8.4349	±0.0094

Figure S5.3.2: Left - Raw (experimental) time-resolved photoluminescence decay (blue) of **3a** in a frozen CH_2Cl_2-MeOH 1:1 glassy matrix at 77 K including the residuals (λ_{exc} = 373.0 nm, λ_{det} = 560.0 nm) and the IRF (red). Right - Fitting parameters including pre-exponential factors and confidence limits.

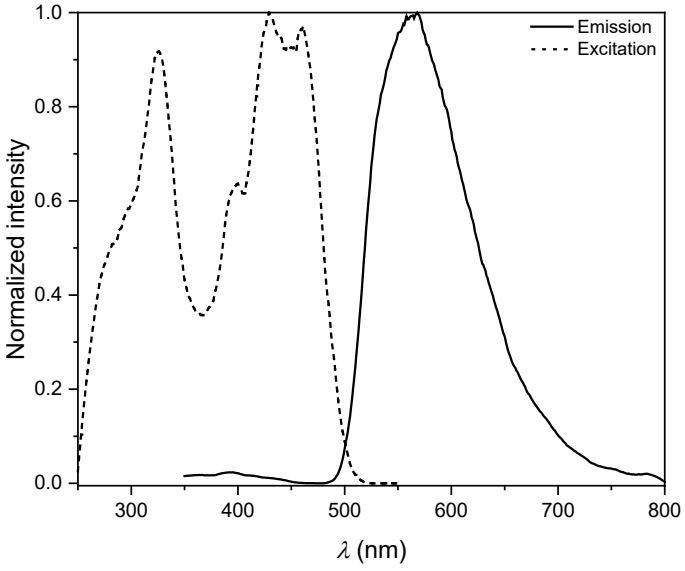

Figure S5.3.3: Normalized emission (solid line, λ_{exc} = 320.0 nm) and excitation (dashed line, λ_{obs} = 580.0 nm) spectra of **3b** in a frozen CH_2Cl_2-MeOH 1:1 glassy matrix at 77 K.

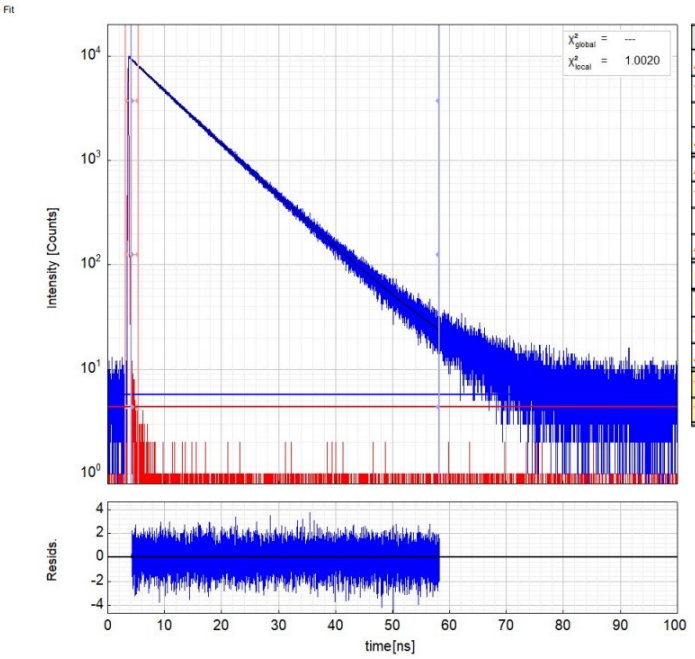

Parameter	Value	Δ
A_1[kCnts/Chnl]	8.57	±0.38
τ_1[ns]	8.872	±0.066
I_1[kCnts]	19 000	±680
A_{Rel1}[%]	85.7	±3.9
A_2[kCnts/Chnl]	1.44	±0.40
τ_2[ns]	6.03	±0.38
I_2[kCnts]	2 170	±700
A_{Rel2}[%]	14.4	±3.9
$Bkgr_{Dec}$[kCnts]	0.0058	±0.0005
$Bkgr_{IRF}$[Cnts/Chnl]	4.4	±2.0
$Shift_{IRF}$[ps]	-5.8	±9.7
A_{Scatt}[kCnts]	-1 400	±1 900
τ_{AvInt}[ns]	8.5801	±0.0082
τ_{AvAmp}[ns]	8.463	±0.012

Figure S5.3.4: Left - Raw (experimental) time-resolved photoluminescence decay (blue) of **3b** in a frozen CH_2Cl_2-MeOH 1:1 glassy matrix at 77 K including the residuals (λ_{exc} = 373.0 nm, λ_{det} = 560.0 nm) and the IRF (red). Right - Fitting parameters including pre-exponential factors and confidence limits.

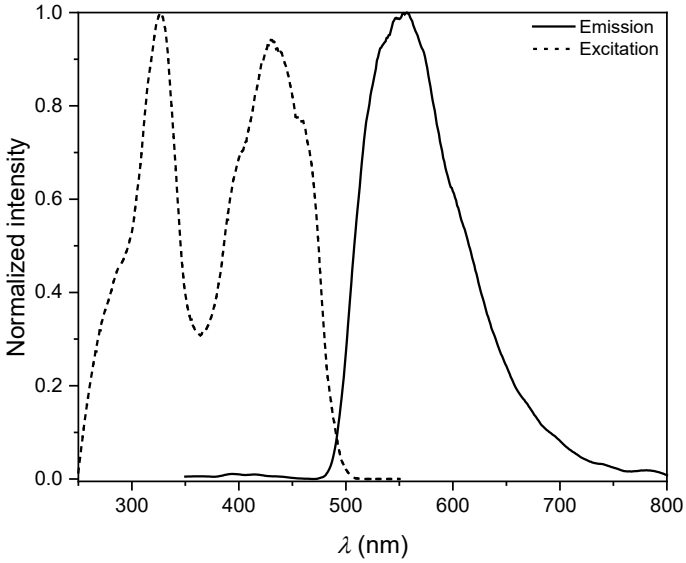

Figure S5.3.5: Normalized emission (solid line, λ_{exc} = 320.0 nm) and excitation (dashed line, λ_{obs} = 580.0 nm) spectra of **3c** in a frozen CH_2Cl_2-MeOH 1:1 glassy matrix at 77 K.

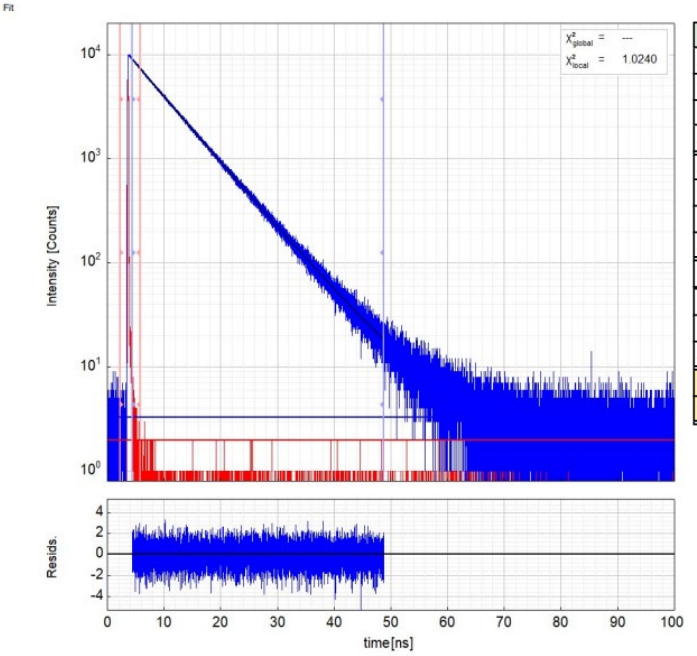

Parameter	Value	Δ
A_1[kCnts/Chnl]	9.51	±0.22
τ_1[ns]	7.008	±0.043
I_1[kCnts]	16 660	±290
A_{Rel1}[%]	93.8	±2.1
A_2[kCnts/Chnl]	0.64	±0.22
τ_2[ns]	4.01	±0.83
I_2[kCnts]	640	±320
A_{Rel2}[%]	6.3	±2.1
$Bkgr_{Dec}$[kCnts]	0.0033	±0.0005
$Bkgr_{IRF}$[Cnts/Chnl]	2.0	±2.8
$Shift_{IRF}$[ps]	31	±20
A_{Scatt}[kCnts]	800	±2 900
τ_{AvInt}[ns]	6.8972	±0.0087
τ_{AvAmp}[ns]	6.820	±0.022

Figure S5.3.6: Left - Raw (experimental) time-resolved photoluminescence decay (blue) of **3c** in a frozen CH_2Cl_2-MeOH 1:1 glassy matrix at 77 K including the residuals (λ_{exc} = 373.0 nm, λ_{det} = 560.0 nm) and the IRF (red). Right - Fitting parameters including pre-exponential factors and confidence limits.

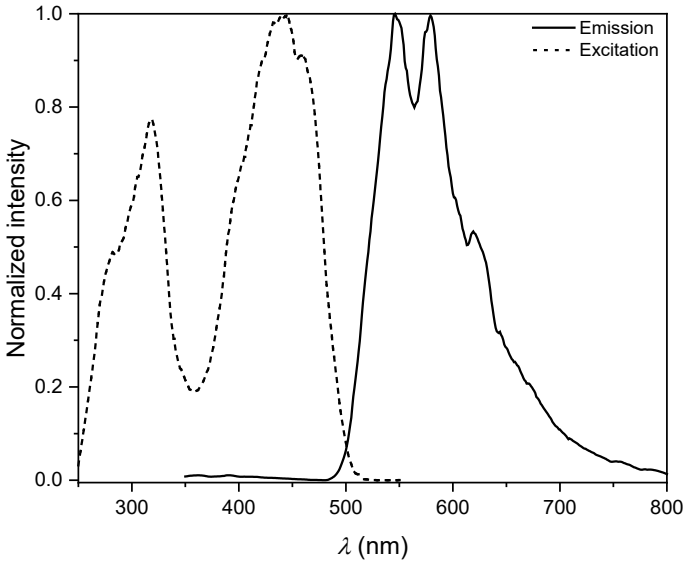

Figure S5.3.7: Normalized emission (solid line, λ_{exc} = 320.0 nm) and excitation (dashed line, λ_{obs} = 580.0 nm) spectra of **3d** in a frozen CH_2Cl_2-MeOH 1:1 glassy matrix at 77 K.

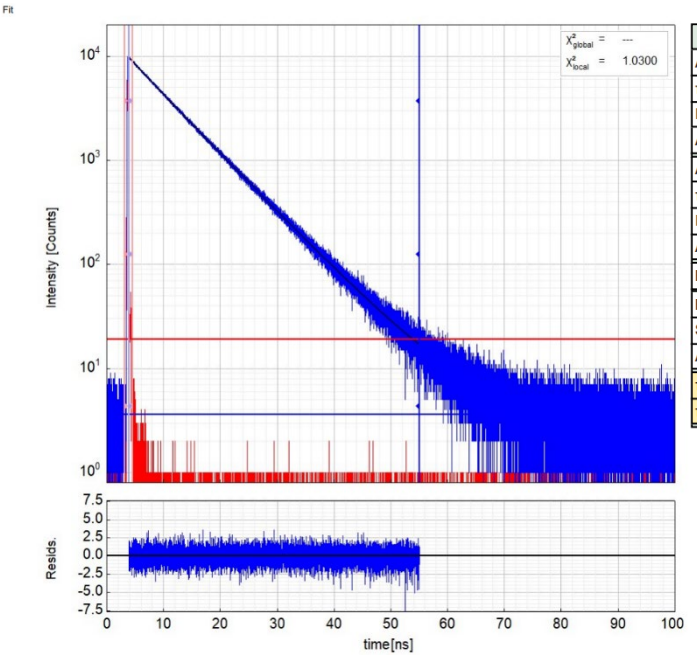

Parameter	Value	Δ
A_1[kCnts/Chnl]	9.06	±0.26
τ_1[ns]	7.907	±0.046
I_1[kCnts]	17 900	±400
A_{Rel1}[%]	88.2	±2.4
A_2[kCnts/Chnl]	1.22	±0.26
τ_2[ns]	4.89	±0.36
I_2[kCnts]	1 490	±400
A_{Rel2}[%]	11.9	±2.4
$Bkgr_{Dec}$[kCnts]	0.0036	±0.0004
$Bkgr_{IRF}$[Cnts/Chnl]	19	±11
$Shift_{IRF}$[ps]	14	±17
A_{Scatt}[kCnts]	400	±440
τ_{AvInt}[ns]	7.6755	±0.0065
τ_{AvAmp}[ns]	7.5497	±0.0090

Figure S5.3.8: Left - Raw (experimental) time-resolved photoluminescence decay (blue) of **3d** in a frozen CH_2Cl_2-MeOH 1:1 glassy matrix at 77 K including the residuals (λ_{exc} = 373.0 nm, λ_{det} = 560.0 nm) and the IRF (red). Right - Fitting parameters including pre-exponential factors and confidence limits.

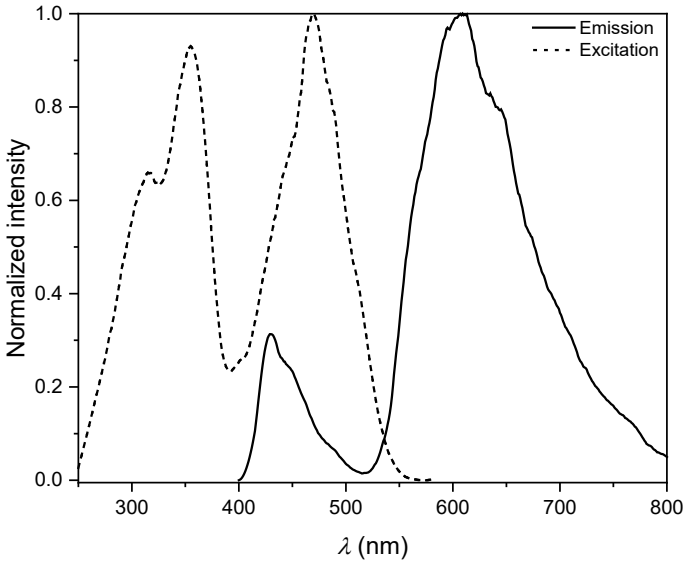

Figure S5.3.9: Normalized emission (solid line, λ_{exc} = 320.0 nm) and excitation (dashed line, λ_{obs} = 600.0 nm) spectra of **3e** in a frozen CH_2Cl_2-MeOH 1:1 glassy matrix at 77 K.

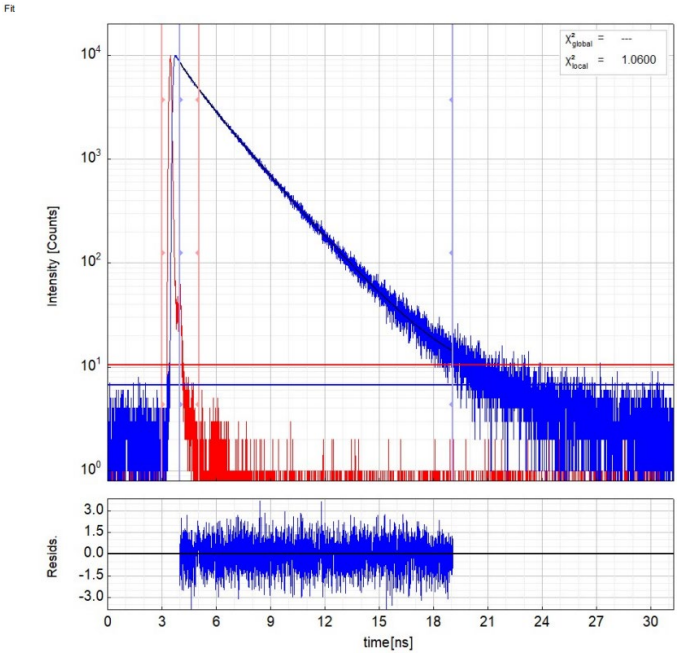

Parameter	Value	Δ
A_1[kCnts/Chnl]	3.78	±0.55
τ_1[ns]	1.15	±0.14
I_1[kCnts]	1 090	±300
A_{Rel1}[%]	33.0	±5.1
A_2[kCnts/Chnl]	7.71	±0.63
τ_2[ns]	2.258	±0.050
I_2[kCnts]	4 350	±270
A_{Rel2}[%]	67.1	±5.1
$Bkgr_{Dec}$[kCnts]	0.0067	±0.0009
$Bkgr_{IRF}$[Cnts/Chnl]	10.4	±9.4
$Shift_{IRF}$[ps]	- 200.4	±6.5
A_{Scatt}[kCnts]	870	±530
τ_{AvInt}[ns]	2.036	±0.011
τ_{AvAmp}[ns]	1.891	±0.026

Figure S5.3.10: Left - Raw (experimental) time-resolved photoluminescence decay (blue) of **3e** in a frozen CH_2Cl_2-MeOH 1:1 glassy matrix at 77 K including the residuals (λ_{exc} = 373.0 nm, λ_{det} = 425.0 nm) and the IRF (red). Right - Fitting parameters including pre-exponential factors and confidence limits.

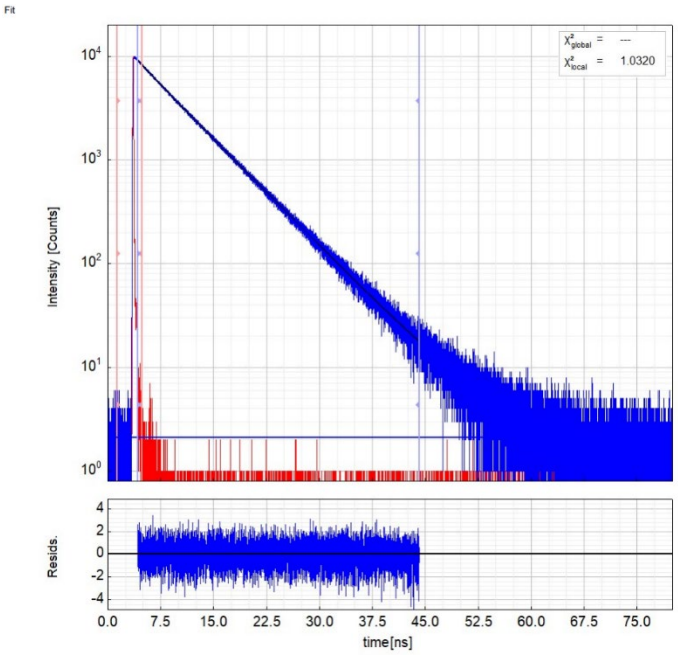

Parameter	Value	Δ
A_1[kCnts/Chnl]	9.547	±0.023
τ_1[ns]	6.3081	±0.0066
I_1[kCnts]	15 055	±37
A_{Rel1}[%]	94.9	±0.3
A_2[kCnts/Chnl]	0.520	±0.026
τ_2[ns]	2.17	±0.17
I_2[kCnts]	281	±30
A_{Rel2}[%]	5.2	±0.3
$Bkgr_{Dec}$[kCnts]	0.0022	±0.0001
$Bkgr_{IRF}$[Cnts/Chnl]	-6.1	±1.3
$Shift_{IRF}$[ps]	-1.7	±8.8
A_{Scatt}[kCnts]	- 260	±210
τ_{AvInt}[ns]	6.2322	±0.0050
τ_{AvAmp}[ns]	6.095	±0.023

Figure S5.3.11: Left - Raw (experimental) time-resolved photoluminescence decay (blue) of **3e** in a frozen CH_2Cl_2-MeOH 1:1 glassy matrix at 77 K including the residuals (λ_{exc} = 373.0 nm, λ_{det} = 615.0 nm) and the IRF (red). Right - Fitting parameters including pre-exponential factors and confidence limits.

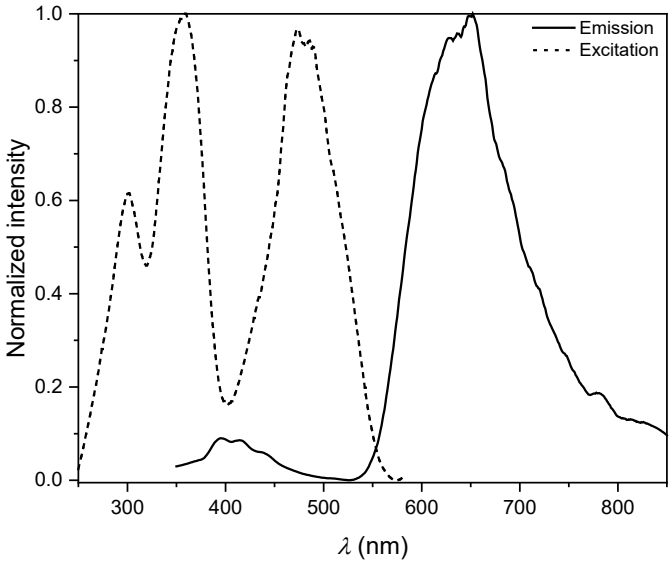

Figure S5.3.12: Normalized emission (solid line, λ_{exc} = 320.0 nm) and excitation (dashed line, λ_{obs} = 600.0 nm) spectra of **3f** in a frozen CH_2Cl_2-MeOH 1:1 glassy matrix at 77 K.

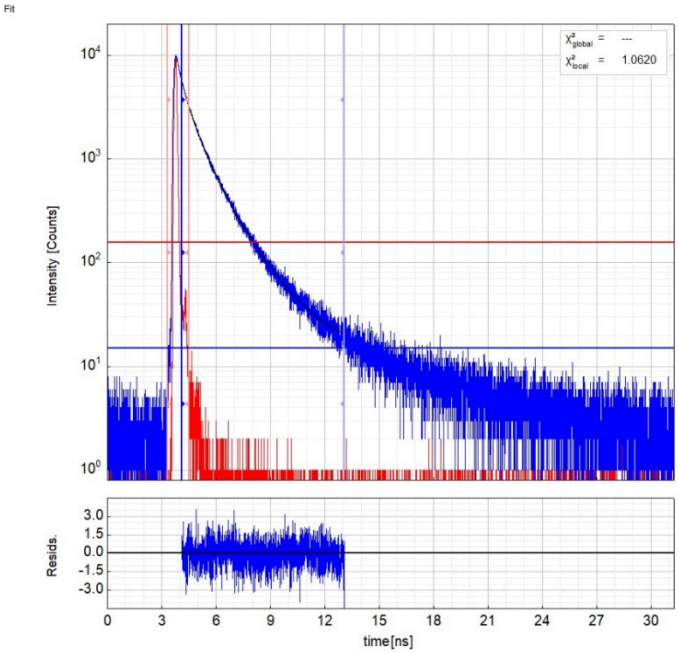

Parameter	Value	Δ
A_1[kCnts/Chnl]	2.49	±0.27
τ_1[ns]	1.568	±0.067
I_1[kCnts]	973	±65
A_{Rel1}[%]	25.8	±2.6
A_2[kCnts/Chnl]	7.16	±0.35
τ_2[ns]	0.630	±0.037
I_2[kCnts]	1 130	±110
A_{Rel2}[%]	74.3	±2.6
$Bkgr_{Dec}$[kCnts]	0.0151	±0.0014
$Bkgr_{IRF}$[Cnts/Chnl]	158	±29
$Shift_{IRF}$[ps]	52	±22
A_{Scatt}[kCnts]	-8	±98
τ_{AvInt}[ns]	1.065	±0.017
τ_{AvAmp}[ns]	0.871	±0.022

Figure S5.3.13: Left - Raw (experimental) time-resolved photoluminescence decay (blue) of **3f** in a frozen CH_2Cl_2-MeOH 1:1 glassy matrix at 77 K including the residuals (λ_{exc} = 373.0 nm, λ_{det} = 412.0 nm) and the IRF (red). Right - Fitting parameters including pre-e xponential factors and confidence limits.

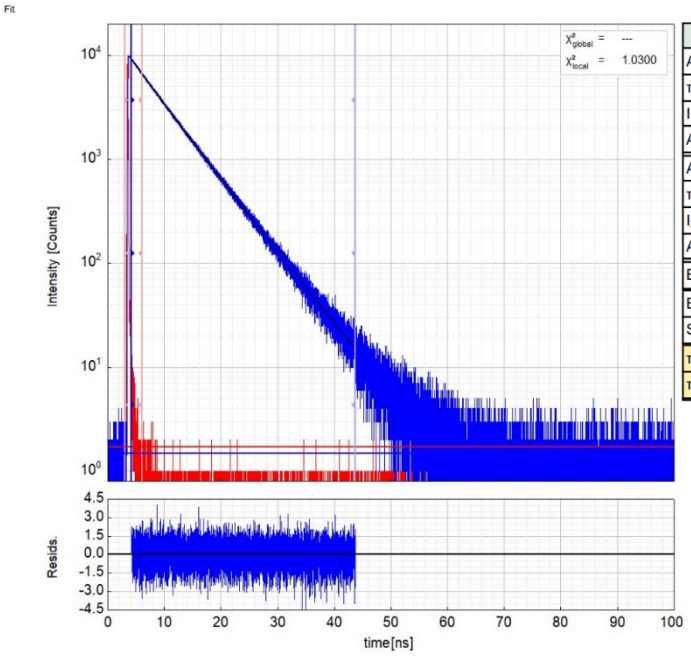

Parameter	Value	Δ
A_1[kCnts/Chnl]	9.06	±0.17
τ_1[ns]	6.209	±0.031
I_1[kCnts]	14 060	±190
A_{Rel1}[%]	87.2	±2.1
A_2[kCnts/Chnl]	1.34	±0.23
τ_2[ns]	3.75	±0.25
I_2[kCnts]	1 250	±290
A_{Rel2}[%]	12.9	±2.1
$Bkgr_{Dec}$[kCnts]	0.0015	±0.0004
$Bkgr_{IRF}$[Cnts/Chnl]	1.8	±2.6
$Shift_{IRF}$[ps]	- 119	±79
τ_{AvInt}[ns]	6.0069	±0.0059
τ_{AvAmp}[ns]	5.892	±0.018

Figure S5.3.14: Left - Raw (experimental) time-resolved photoluminescence decay (blue) of **3f** in a frozen CH_2Cl_2-MeOH 1:1 glassy matrix at 77 K including the residuals (λ_{exc} = 373.0 nm, λ_{det} = 645.0 nm) and the IRF (red). Right - Fitting parameters including pre-exponential factors and confidence limits.

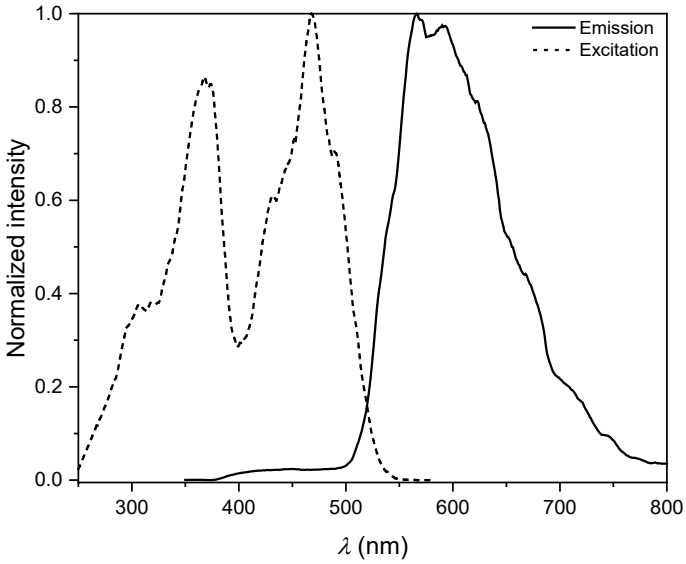

Figure S5.3.15: Normalized emission (solid line, λ_{exc} = 320.0 nm) and excitation (dashed line, λ_{obs} = 600.0 nm) spectra of **3g** in a frozen CH_2Cl_2-MeOH 1:1 glassy matrix at 77 K.

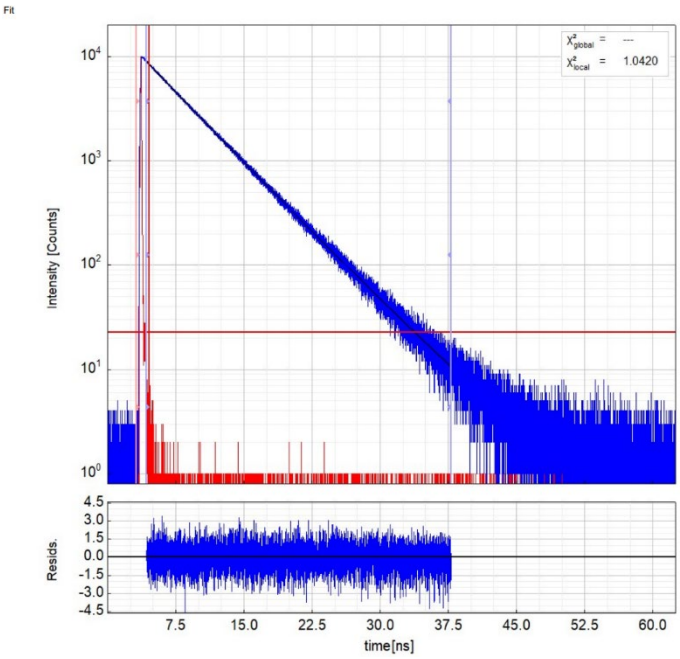

Parameter	Value	Δ
A_1[kCnts/Chnl]	3.625	±0.072
τ_1[ns]	5.490	±0.044
I_1[kCnts]	4 980	±110
A_{Rel1}[%]	34.7	±0.7
A_2[kCnts/Chnl]	6.847	±0.096
τ_2[ns]	4.450	±0.030
I_2[kCnts]	7 620	±120
A_{Rel2}[%]	65.4	±0.7
$Bkgr_{Dec}$[kCnts]	0.0005	±0.0005
$Bkgr_{IRF}$[Cnts/Chnl]	22.8	±9.9
$Shift_{IRF}$[ps]	15	±32
A_{Scatt}[kCnts]	- 250	±560
τ_{AvInt}[ns]	4.8606	±0.0051
τ_{AvAmp}[ns]	4.8097	±0.0055

Figure S5.3.16: Left - Raw (experimental) time-resolved photoluminescence decay (blue) of **3g** in a frozen CH_2Cl_2-MeOH 1:1 glassy matrix at 77 K including the residuals (λ_{exc} = 373.0 nm, λ_{det} = 590.0 nm) and the IRF (red). Right - Fitting parameters including pre-exponential factors and confidence limits.

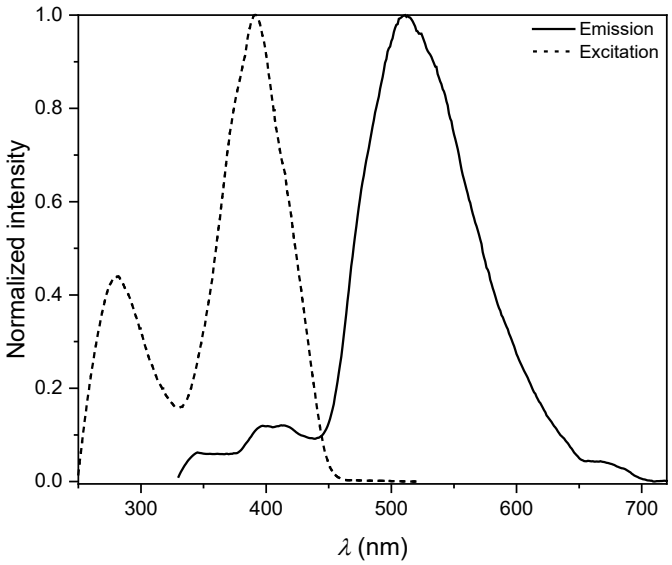

Figure S5.3.17: Normalized emission (solid line, λ_{exc} = 320.0 nm) and excitation (dashed line, λ_{obs} = 550.0 nm) spectra of **5** in a frozen CH_2Cl_2-MeOH 1:1 glassy matrix at 77 K.

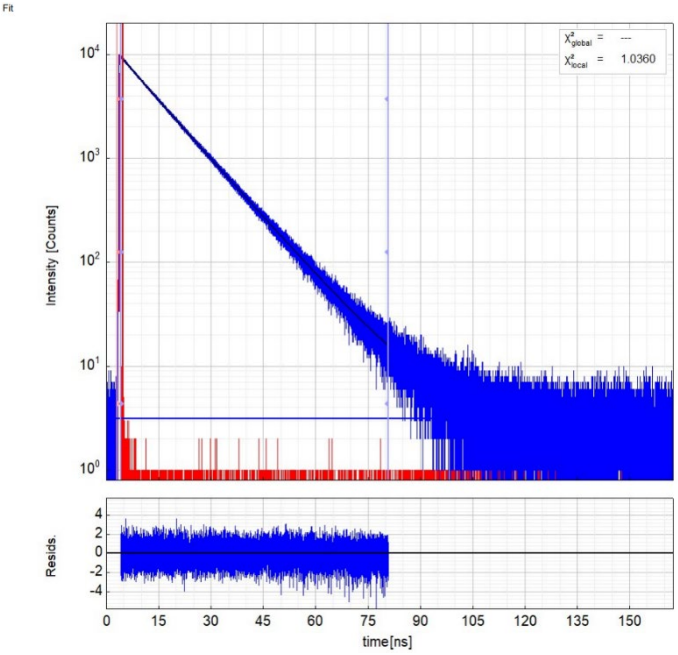

Parameter	Value	Δ
A_1[kCnts/Chnl]	9.28	±0.16
τ_1[ns]	11.704	±0.045
I_1[kCnts]	27 150	±340
A_{Rel1}[%]	93.3	±1.3
A_2[kCnts/Chnl]	0.68	±0.14
τ_2[ns]	6.19	±0.66
I_2[kCnts]	1 050	±310
A_{Rel2}[%]	6.8	±1.3
$Bkgr_{Dec}$[kCnts]	0.0032	±0.0004
$Bkgr_{IRF}$[Cnts/Chnl]	-3.8	±4.8
$Shift_{IRF}$[ps]	-32.1	±6.0
A_{Scatt}[kCnts]	2 200	±2 100
τ_{AvInt}[ns]	11.4986	±0.0094
τ_{AvAmp}[ns]	11.329	±0.017

Figure S5.3.18: Left - Raw (experimental) time-resolved photoluminescence decay (blue) of **5** in a frozen CH_2Cl_2-MeOH 1:1 glassy matrix at 77 K including the residuals (λ_{exc} = 373.0 nm, λ_{det} = 515.0 nm) and the IRF (red). Right - Fitting parameters including pre-exponential factors and confidence limits.

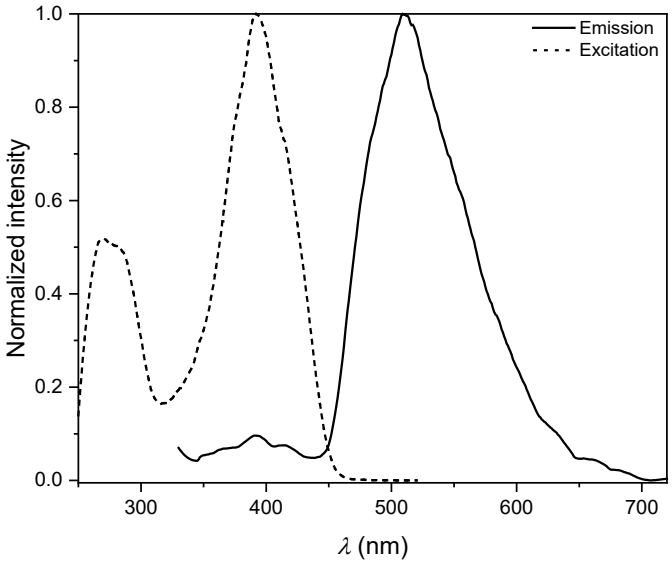

Figure S5.3.19: Normalized emission (solid line, λ_{exc} = 320.0 nm) and excitation (dashed line, λ_{obs} = 550.0 nm) spectra of **6a** in a frozen CH_2Cl_2-MeOH 1:1 glassy matrix at 77 K.

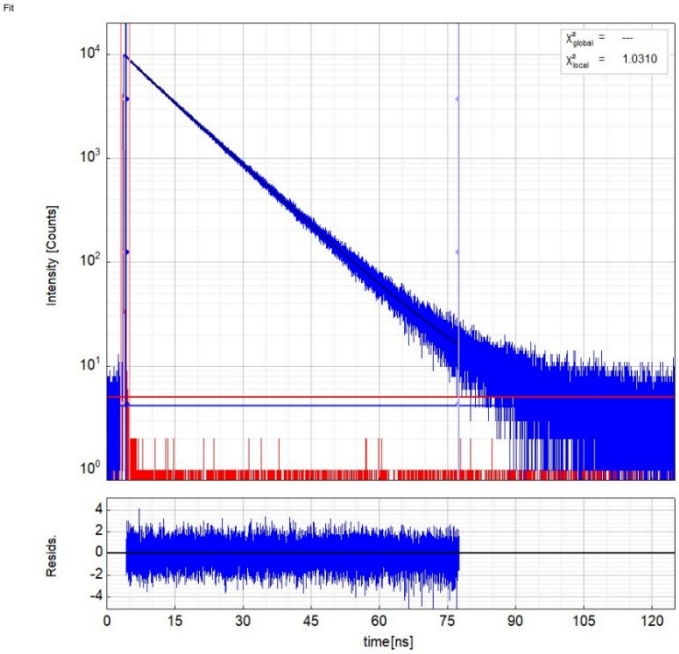

Parameter	Value	Δ
A_1[kCnts/Chnl]	9.37	±0.17
τ_1[ns]	11.104	±0.057
I_1[kCnts]	25 990	±350
A_{Rel1}[%]	92.3	±1.5
A_2[kCnts/Chnl]	0.79	±0.16
τ_2[ns]	5.46	±0.70
I_2[kCnts]	1 080	±330
A_{Rel2}[%]	7.8	±1.5
$Bkgr_{Dec}$[kCnts]	0.0042	±0.0004
$Bkgr_{IRF}$[Cnts/Chnl]	5.1	±4.1
$Shift_{IRF}$[ps]	-18	±19
A_{Scatt}[kCnts]	-1 900	±3 100
τ_{AvInt}[ns]	10.880	±0.012
τ_{AvAmp}[ns]	10.665	±0.024

Figure S5.3.20: Left - Raw (experimental) time-resolved photoluminescence decay (blue) of **6a** in a frozen CH_2Cl_2-MeOH 1:1 glassy matrix at 77 K including the residuals (λ_{exc} = 373.0 nm, λ_{det} = 510.0 nm) and the IRF (red). Right - Fitting parameters including pre-exponential factors and confidence limits.

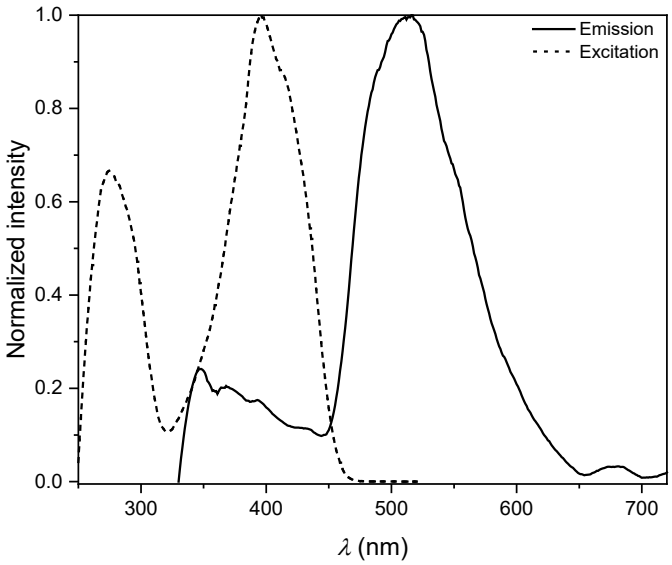

Figure S5.3.21: Normalized emission (solid line, λ_{exc} = 320.0 nm) and excitation (dashed line, λ_{obs} = 550.0 nm) spectra of **6b** in a frozen CH_2Cl_2-MeOH 1:1 glassy matrix at 77 K.

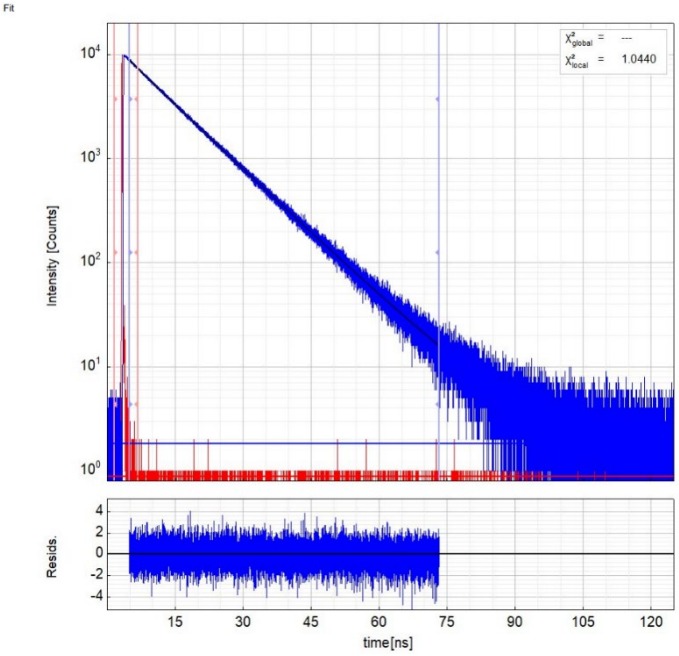

Parameter	Value	Δ
A_1[kCnts/Chnl]	9.06	±0.29
τ_1[ns]	10.820	±0.058
I_1[kCnts]	24 490	±620
A_{Rel1}[%]	87.3	±2.4
A_2[kCnts/Chnl]	1.33	±0.25
τ_2[ns]	7.16	±0.38
I_2[kCnts]	2 380	±590
A_{Rel2}[%]	12.8	±2.4
$Bkgr_{Dec}$[kCnts]	0.0019	±0.0004
$Bkgr_{IRF}$[Cnts/Chnl]	0.9	±2.2
$Shift_{IRF}$[ps]	- 368	±24
A_{Scatt}[kCnts]	- 900	±6 700
τ_{AvInt}[ns]	10.4959	±0.0083
τ_{AvAmp}[ns]	10.352	±0.018

Figure S5.3.22: Left - Raw (experimental) time-resolved photoluminescence decay (blue) of **6b** in a frozen CH_2Cl_2-MeOH 1:1 glassy matrix at 77 K including the residuals (λ_{exc} = 373.0 nm, λ_{det} = 515.0 nm) and the IRF (red). Right - Fitting parameters including pre-exponential factors and confidence limits.

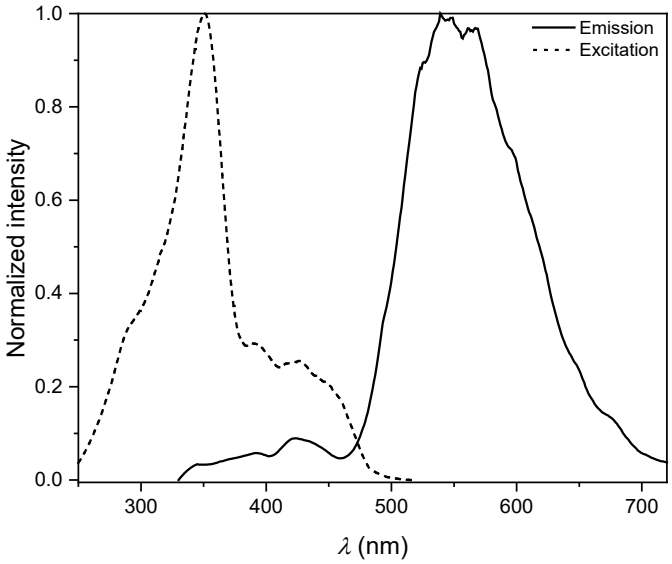

Figure S5.3.23: Normalized emission (solid line, λ_{exc} = 320.0 nm) and excitation (dashed line, λ_{obs} = 550.0 nm) spectra of **6c** in a frozen CH_2Cl_2-MeOH 1:1 glassy matrix at 77 K.

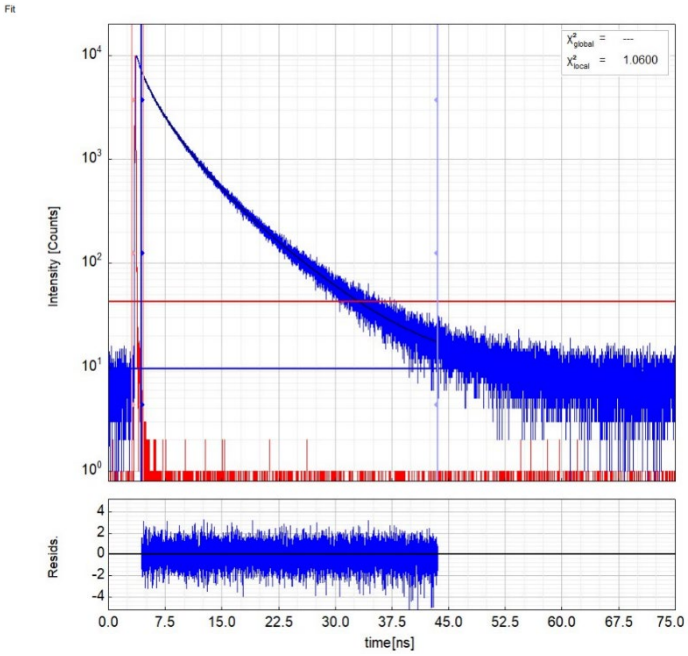

Parameter	Value	Δ
A_1[kCnts/Chnl]	2.04	±0.17
τ_1[ns]	7.28	±0.20
I_1[kCnts]	3 700	±210
A_{Rel1}[%]	18.8	±1.5
A_2[kCnts/Chnl]	5.13	±0.20
τ_2[ns]	3.11	±0.17
I_2[kCnts]	3 990	±190
A_{Rel2}[%]	47.5	±1.4
A_3[kCnts/Chnl]	3.66	±0.29
τ_3[ns]	1.12	±0.13
I_3[kCnts]	1 020	±170
A_{Rel3}[%]	33.8	±2.3
$Bkgr_{Dec}$[kCnts]	0.0096	±0.0008
$Bkgr_{IRF}$[Cnts/Chnl]	43	±18
$Shift_{IRF}$[ps]	-52	±31
A_{Scatt}[kCnts]	250	±320
τ_{AvInt}[ns]	4.647	±0.031
τ_{AvAmp}[ns]	3.215	±0.061

Figure S5.3.24: Left - Raw (experimental) time-resolved photoluminescence decay (blue) of **6c** in a frozen CH_2Cl_2-MeOH 1:1 glassy matrix at 77 K including the residuals (λ_{exc} = 373.0 nm, λ_{det} = 570.0 nm) and the IRF (red). Right - Fitting parameters including pre-exponential factors and confidence limits.

5.4 Summary of Photoluminescence Properties in the Solid State at rt

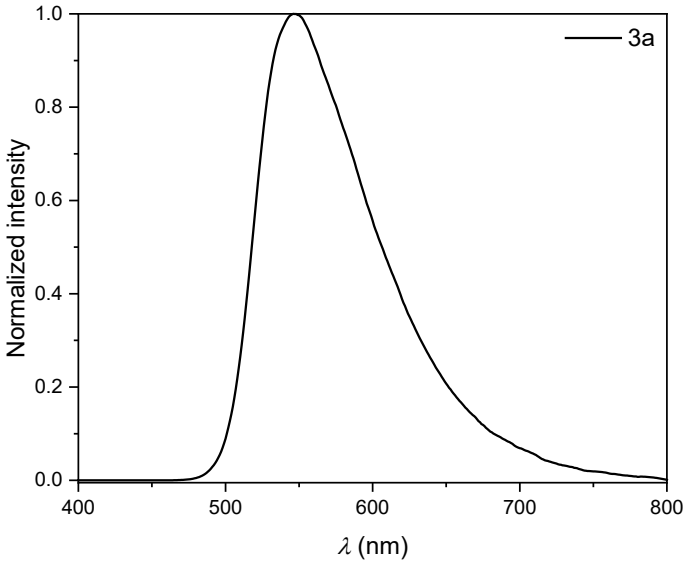

Figure S5.4.1: Normalized emission spectrum of **3a** in solid state at rt (λ_{exc} = 350.0 nm).

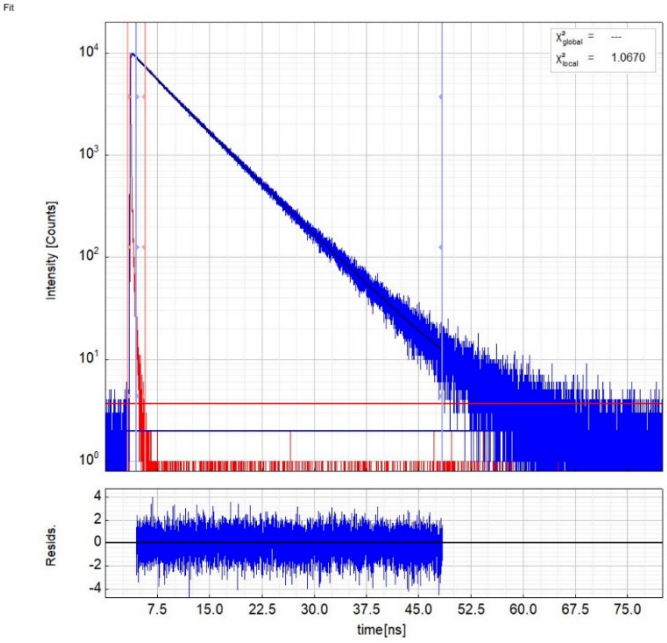

Parameter	Value	Δ
A_1[kCnts/Chnl]	9.03	±0.11
τ_1[ns]	6.607	±0.023
I_1[kCnts]	14 910	±130
A_{Rel1}[%]	86.0	±1.2
A_2[kCnts/Chnl]	1.48	±0.12
τ_2[ns]	3.49	±0.19
I_2[kCnts]	1 290	±170
A_{Rel2}[%]	14.1	±1.2
$Bkgr_{Dec}$[kCnts]	0.0020	±0.0004
$Bkgr_{IRF}$[Cnts/Chnl]	3.7	±2.8
$Shift_{IRF}$[ps]	-6	±59
τ_{AvInt}[ns]	6.3588	±0.0066
τ_{AvAmp}[ns]	6.169	±0.019

Figure S5.4.2: Left - Raw (experimental) time-resolved photoluminescence decay (blue) of **3a** in solid state at rt including the residuals (λ_{exc} = 373.0 nm, λ_{det} = 550.0 nm) and the IRF (red). Right - Fitting parameters including pre-exponential factors and confidence limits.

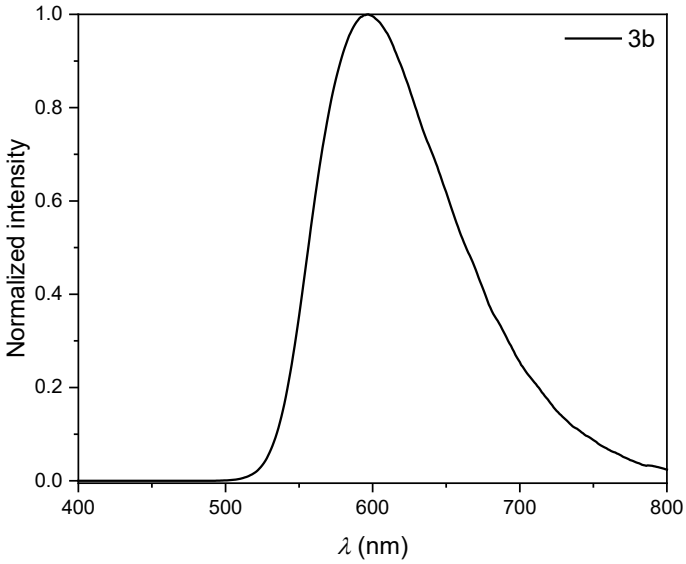

Figure S5.4.1: Normalized emission spectrum of **3b** in solid state at rt (λ_{exc} = 350.0 nm).

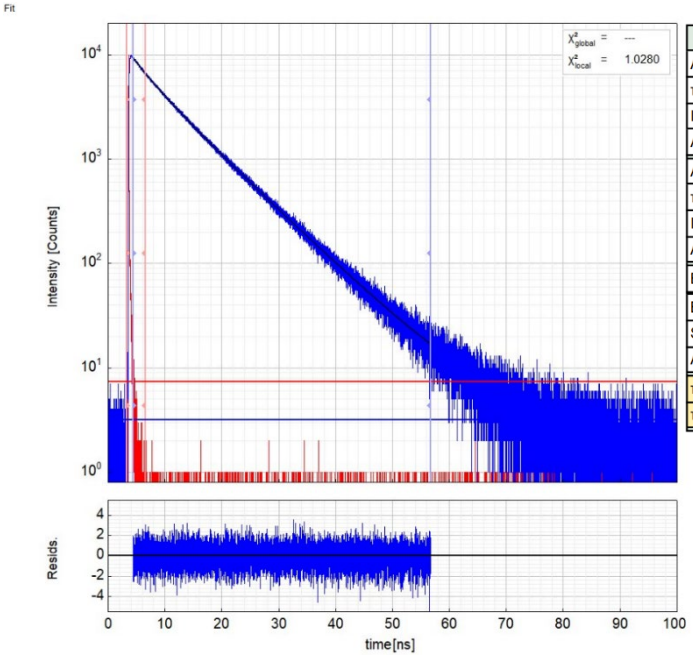

Parameter	Value	Δ
A_1[kCnts/Chnl]	7.48	±0.19
τ_1[ns]	8.467	±0.070
I_1[kCnts]	15 830	±260
A_{Rel1}[%]	70.2	±1.7
A_2[kCnts/Chnl]	3.18	±0.19
τ_2[ns]	4.08	±0.20
I_2[kCnts]	3 240	±340
A_{Rel2}[%]	29.9	±1.7
$Bkgr_{Dec}$[kCnts]	0.0032	±0.0006
$Bkgr_{IRF}$[Cnts/Chnl]	7.4	±1.2
$Shift_{IRF}$[ps]	-24	±31
A_{Scatt}[kCnts]	150	±480
τ_{AvInt}[ns]	7.721	±0.017
τ_{AvAmp}[ns]	7.157	±0.037

Figure S5.4.2: Left - Raw (experimental) time-resolved photoluminescence decay (blue) of **3b** in solid state at rt including the residuals (λ_{exc} = 373.0 nm, λ_{det} = 600.0 nm) and the IRF (red). Right - Fitting parameters including pre-exponential factors and confidence limits.

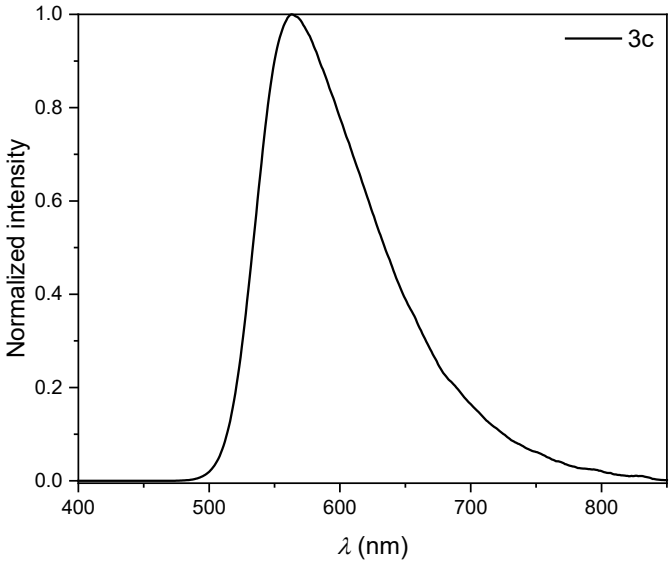

Figure S5.4.1: Normalized emission spectrum of **3c** in solid state at rt (λ_{exc} = 350.0 nm).

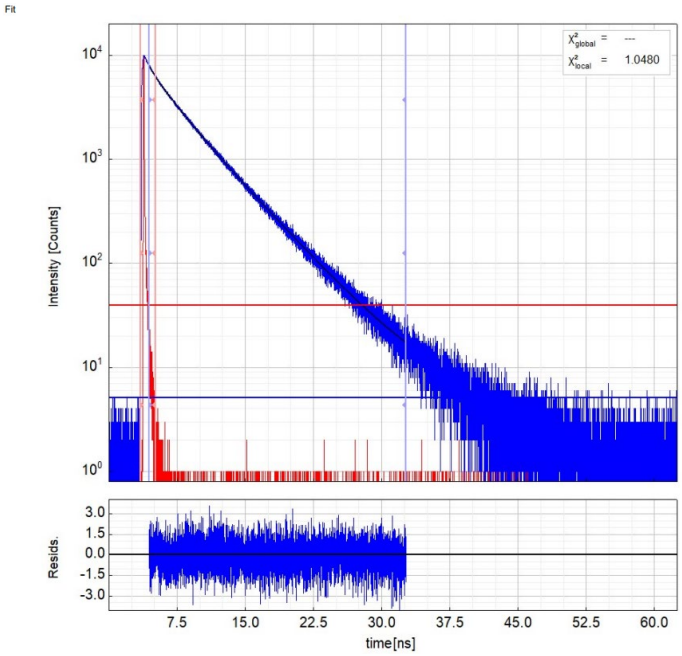

Parameter	Value	Δ
A_1[kCnts/Chnl]	6.51	±0.24
τ_1[ns]	4.664	±0.056
I_1[kCnts]	7 580	±200
A_{Rel1}[%]	66.0	±2.2
A_2[kCnts/Chnl]	3.36	±0.23
τ_2[ns]	2.14	±0.13
I_2[kCnts]	1 800	±230
A_{Rel2}[%]	34.1	±2.2
$Bkgr_{Dec}$[kCnts]	0.0052	±0.0008
$Bkgr_{IRF}$[Cnts/Chnl]	39.5	±4.7
$Shift_{IRF}$[ps]	191	±31
A_{Scatt}[kCnts]	- 180	±160
τ_{AvInt}[ns]	4.181	±0.014
τ_{AvAmp}[ns]	3.805	±0.028

Figure S5.4.2: Left - Raw (experimental) time-resolved photoluminescence decay (blue) of **3c** in solid state at rt including the residuals (λ_{exc} = 373.0 nm, λ_{det} = 560.0 nm) and the IRF (red). Right - Fitting parameters including pre-exponential factors and confidence limits.

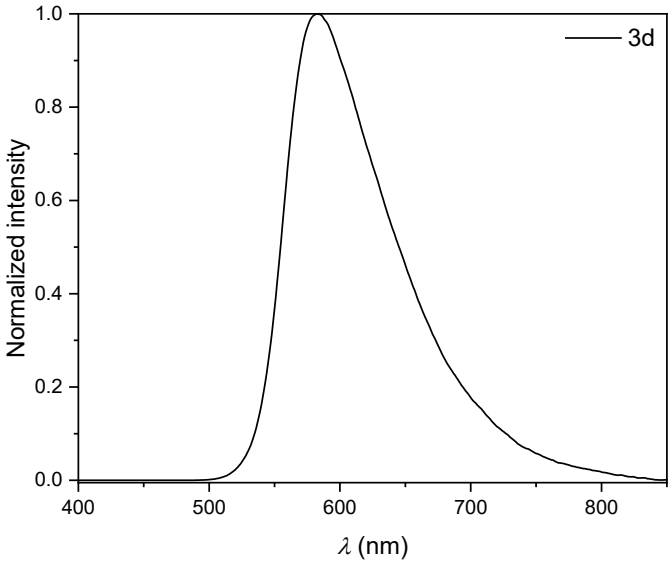

Figure S5.4.1: Normalized emission spectrum of **3d** in solid state at rt (λ_{exc} = 350.0 nm).

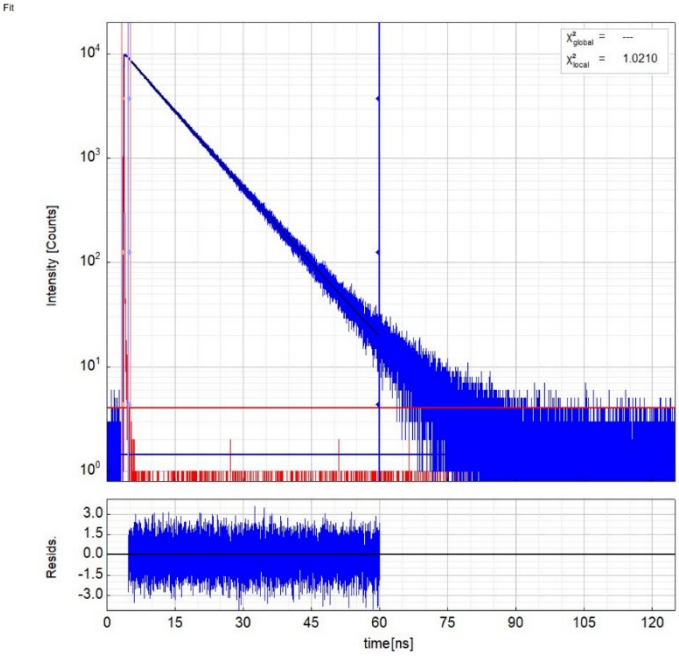

Parameter	Value	Δ
A_1[kCnts/Chnl]	9.68	±0.16
τ_1[ns]	8.976	±0.040
I_1[kCnts]	21 720	±280
A_{Rel1}[%]	93.3	±1.6
A_2[kCnts/Chnl]	0.71	±0.17
τ_2[ns]	5.13	±0.56
I_2[kCnts]	910	±310
A_{Rel2}[%]	6.8	±1.6
$Bkgr_{Dec}$[kCnts]	0.0015	±0.0004
$Bkgr_{IRF}$[Cnts/Chnl]	4.1	±3.0
$Shift_{IRF}$[ps]	54	±33
A_{Scatt}[kCnts]	900	±3 700
τ_{AvInt}[ns]	8.8221	±0.0074
τ_{AvAmp}[ns]	8.715	±0.015

Figure S5.4.2: Left - Raw (experimental) time-resolved photoluminescence decay (blue) of **3d** in solid state at rt including the residuals (λ_{exc} = 373.0 nm, λ_{det} = 580.0 nm) and the IRF (red). Right - Fitting parameters including pre-exponential factors and confidence limits.

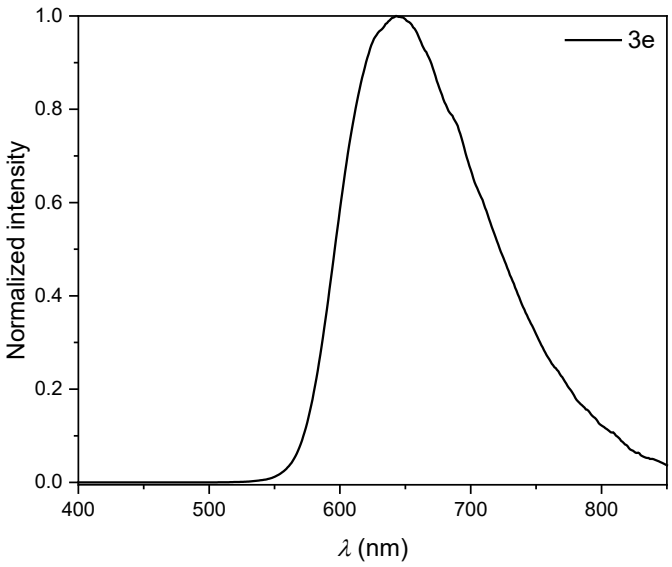

Figure S5.4.1: Normalized emission spectrum of **3e** in solid state at rt (λ_{exc} = 350.0 nm).

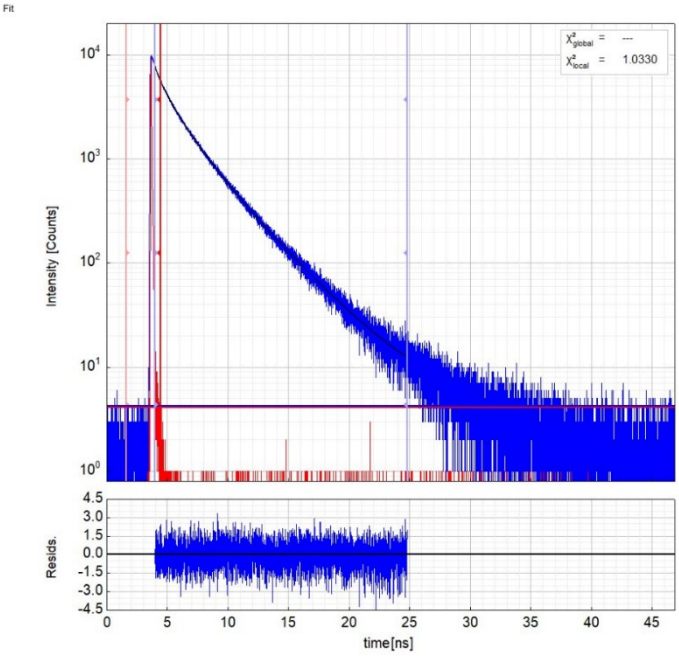

Parameter	Value	Δ
A_1[kCnts/Chnl]	2.55	±0.75
τ_1[ns]	3.69	±0.34
I_1[kCnts]	2 350	±550
A_{Rel1}[%]	25.7	±7.2
A_2[kCnts/Chnl]	4.28	±0.33
τ_2[ns]	1.81	±0.30
I_2[kCnts]	1 940	±450
A_{Rel2}[%]	43.2	±3.3
A_3[kCnts/Chnl]	3.09	±0.44
τ_3[ns]	0.60	±0.12
I_3[kCnts]	470	±160
A_{Rel3}[%]	31.2	±4.9
$Bkgr_{Dec}$[kCnts]	0.0042	±0.0016
$Bkgr_{IRF}$[Cnts/Chnl]	5	±15
$Shift_{IRF}$[ps]	-6.0	±3.9
A_{Scatt}[kCnts]	1 900	±1 600
τ_{AvInt}[ns]	2.621	±0.035
τ_{AvAmp}[ns]	1.914	±0.063

Figure S5.4.2: Left - Raw (experimental) time-resolved photoluminescence decay (blue) of **3e** in solid state at rt including the residuals (λ_{exc} = 373.0 nm, λ_{det} = 645.0 nm) and the IRF (red). Right - Fitting parameters including pre-exponential factors and confidence limits.

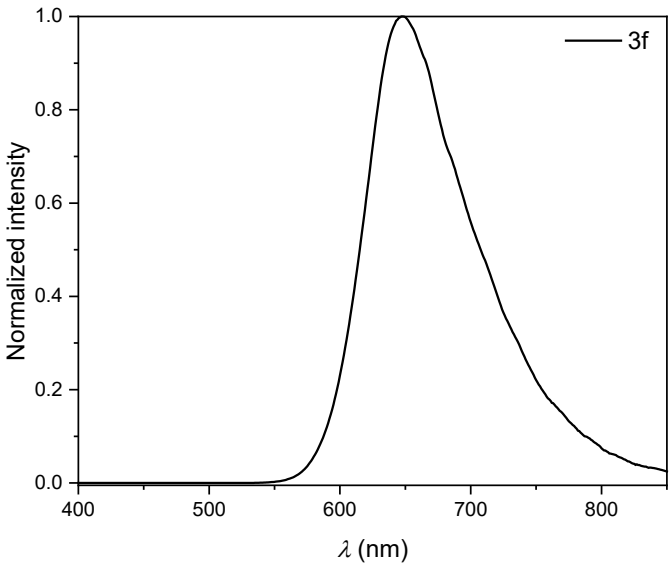

Figure S5.4.1: Normalized emission spectrum of **3f** in solid state at rt (λ_{exc} = 350.0 nm).

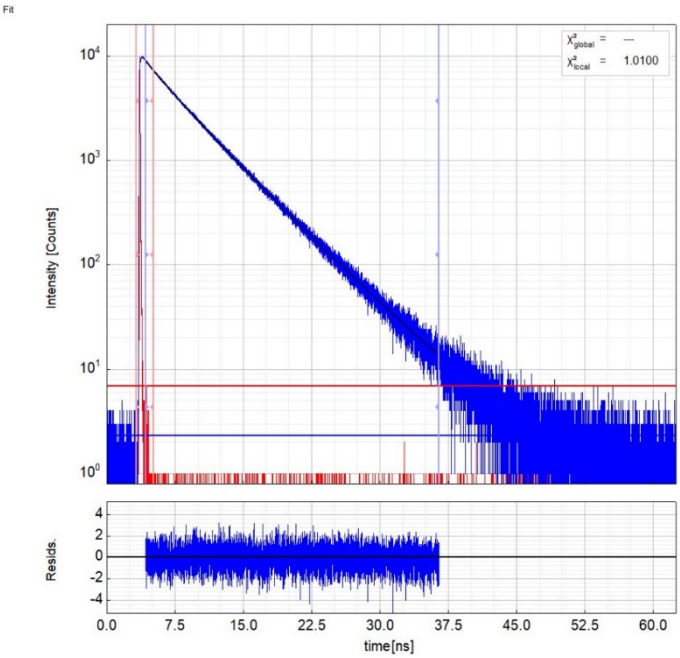

Parameter	Value	Δ
A_1[kCnts/Chnl]	7.94	±0.34
τ_1[ns]	5.036	±0.057
I_1[kCnts]	10 000	±320
A_{Rel1}[%]	74.8	±3.1
A_2[kCnts/Chnl]	2.69	±0.33
τ_2[ns]	2.63	±0.20
I_2[kCnts]	1 760	±340
A_{Rel2}[%]	25.3	±3.1
$Bkgr_{Dec}$[kCnts]	0.0024	±0.0007
$Bkgr_{IRF}$[Cnts/Chnl]	6.9	±4.9
$Shift_{IRF}$[ps]	-42	±40
A_{Scatt}[kCnts]	180	±860
τ_{AvInt}[ns]	4.675	±0.011
τ_{AvAmp}[ns]	4.427	±0.023

Figure S5.4.2: Left - Raw (experimental) time-resolved photoluminescence decay (blue) of **3f** in solid state at rt including the residuals (λ_{exc} = 373.0 nm, λ_{det} = 650.0 nm) and the IRF (red). Right - Fitting parameters including pre-exponential factors and confidence limits.

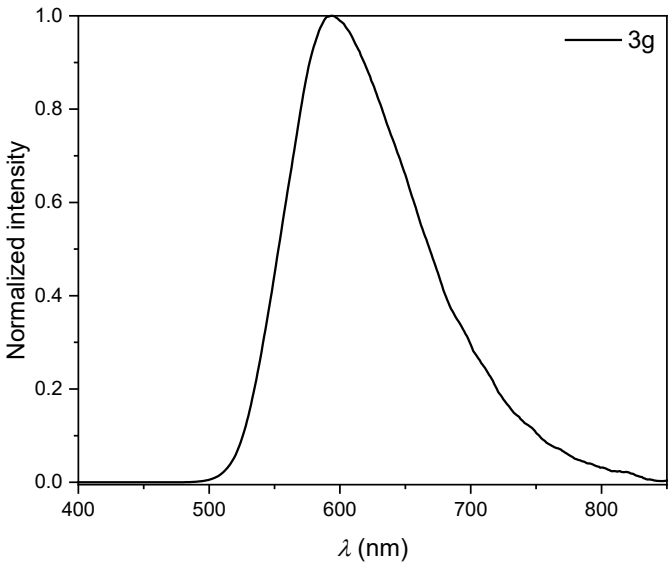

Figure S5.4.1: Normalized emission spectrum of **3g** in solid state at rt (λ_{exc} = 350.0 nm).

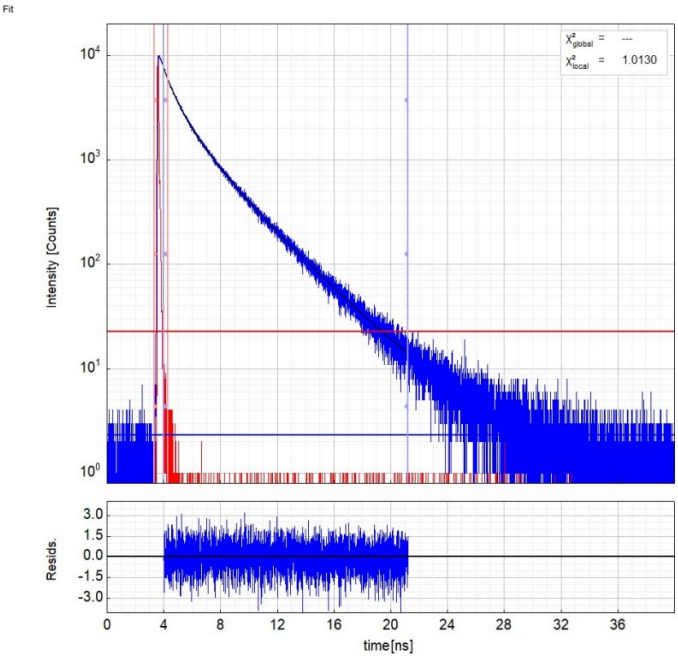

Parameter	Value	Δ
A_1[kCnts/Chnl]	2.43	±0.24
τ_1[ns]	3.318	±0.097
I_1[kCnts]	2 020	±130
A_{Rel1}[%]	22.3	±2.2
A_2[kCnts/Chnl]	3.94	±0.50
τ_2[ns]	1.49	±0.15
I_2[kCnts]	1 470	±110
A_{Rel2}[%]	36.2	±4.0
A_3[kCnts/Chnl]	4.53	±0.60
τ_3[ns]	0.640	±0.080
I_3[kCnts]	730	±170
A_{Rel3}[%]	41.6	±5.2
$Bkgr_{Dec}$[kCnts]	0.0024	±0.0010
$Bkgr_{IRF}$[Cnts/Chnl]	23	±19
$Shift_{IRF}$[ps]	0	±22
A_{Scatt}[kCnts]	- 160	±930
τ_{AvInt}[ns]	2.218	±0.019
τ_{AvAmp}[ns]	1.542	±0.041

Figure S5.4.2: Left - Raw (experimental) time-resolved photoluminescence decay (blue) of **3g** in solid state at rt including the residuals (λ_{exc} = 373.0 nm, λ_{det} = 590.0 nm) and the IRF (red). Right - Fitting parameters including pre-exponential factors and confidence limits.

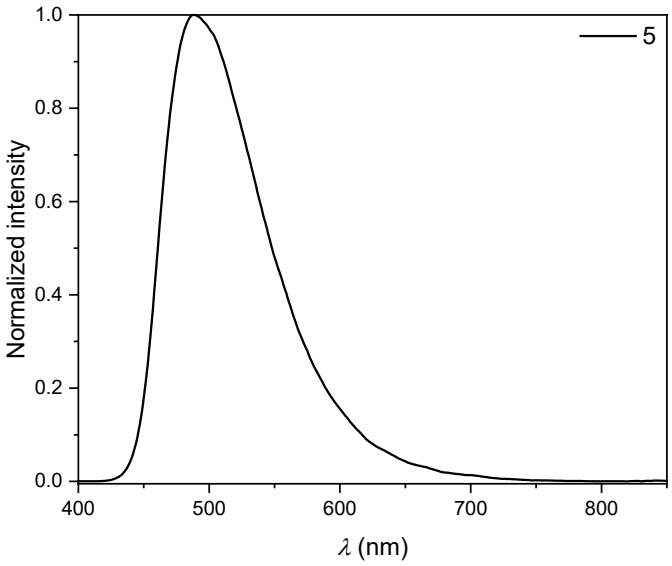

Figure S5.4.1: Normalized emission spectrum of **5** in solid state at rt (λ_{exc} = 350.0 nm).

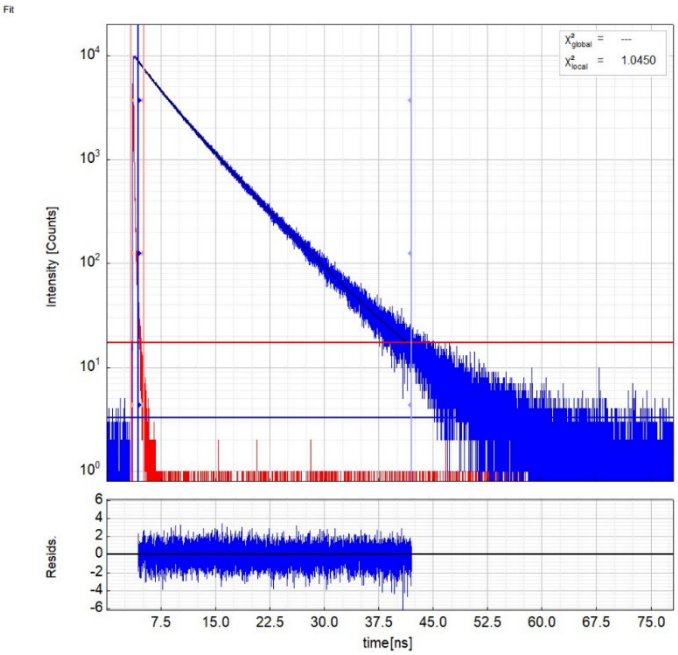

Parameter	Value	Δ
A_1[kCnts/Chnl]	6.61	±0.25
τ_1[ns]	6.154	±0.065
I_1[kCnts]	10 170	±300
A_{Rel1}[%]	63.1	±2.6
A_2[kCnts/Chnl]	3.88	±0.27
τ_2[ns]	3.28	±0.13
I_2[kCnts]	3 180	±340
A_{Rel2}[%]	37.0	±2.6
$Bkgr_{Dec}$[kCnts]	0.0033	±0.0006
$Bkgr_{IRF}$[Cnts/Chnl]	17.5	±5.7
$Shift_{IRF}$[ps]	21	±31
A_{Scatt}[kCnts]	120	±520
τ_{AvInt}[ns]	5.4696	±0.0100
τ_{AvAmp}[ns]	5.091	±0.016

Figure S5.4.2: Left - Raw (experimental) time-resolved photoluminescence decay (blue) of **5** in solid state at rt including the residuals (λ_{exc} = 373.0 nm, λ_{det} = 490.0 nm) and the IRF (red). Right - Fitting parameters including pre-exponential factors and confidence limits.

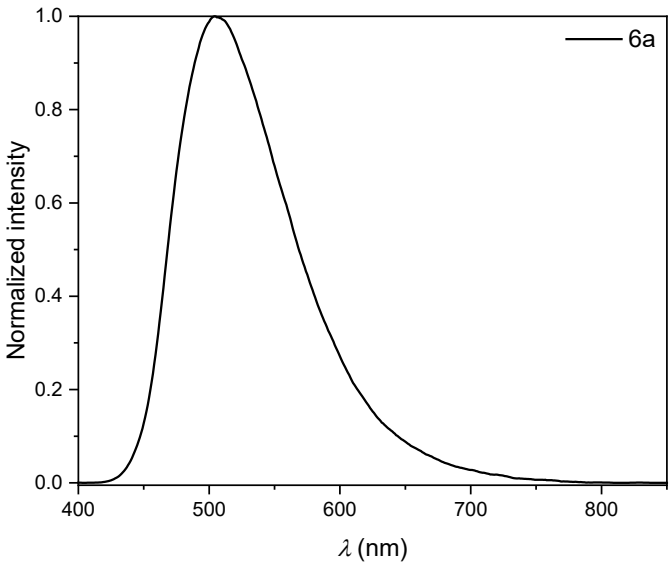

Figure S5.4.1: Normalized emission spectrum of **6a** in solid state at rt (λ_{exc} = 350.0 nm).

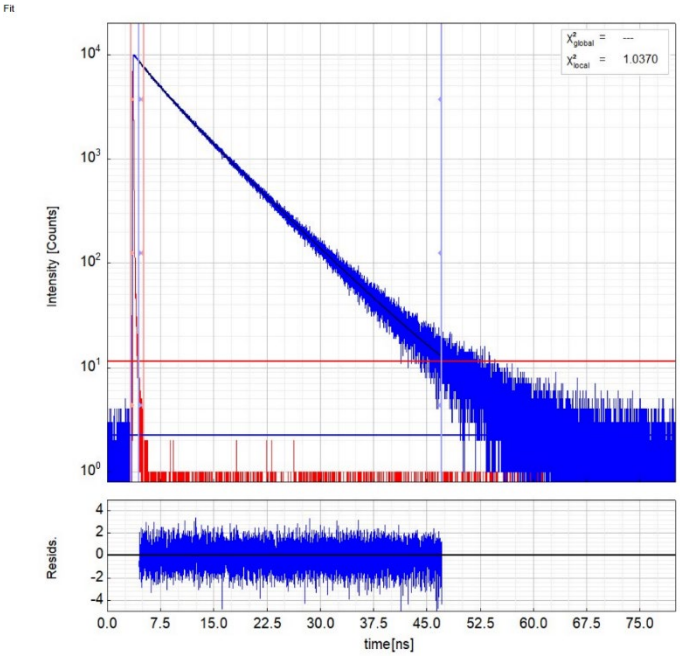

Parameter	Value	Δ
A_1[kCnts/Chnl]	7.353	±0.093
τ_1[ns]	6.658	±0.029
I_1[kCnts]	12 240	±130
A_{Rel1}[%]	71.3	±1.0
A_2[kCnts/Chnl]	2.97	±0.12
τ_2[ns]	3.230	±0.082
I_2[kCnts]	2 400	±150
A_{Rel2}[%]	28.8	±1.0
$Bkgr_{Dec}$[kCnts]	0.0023	±0.0004
$Bkgr_{IRF}$[Cnts/Chnl]	11.5	±4.1
$Shift_{IRF}$[ps]	-2	±34
A_{Scatt}[kCnts]	-30	±700
τ_{AvInt}[ns]	6.0966	±0.0072
τ_{AvAmp}[ns]	5.673	±0.017

Figure S5.4.2: Left - Raw (experimental) time-resolved photoluminescence decay (blue) of **6a** in solid state at rt including the residuals (λ_{exc} = 373.0 nm, λ_{det} = 510.0 nm) and the IRF (red). Right - Fitting parameters including pre-exponential factors and confidence limits.

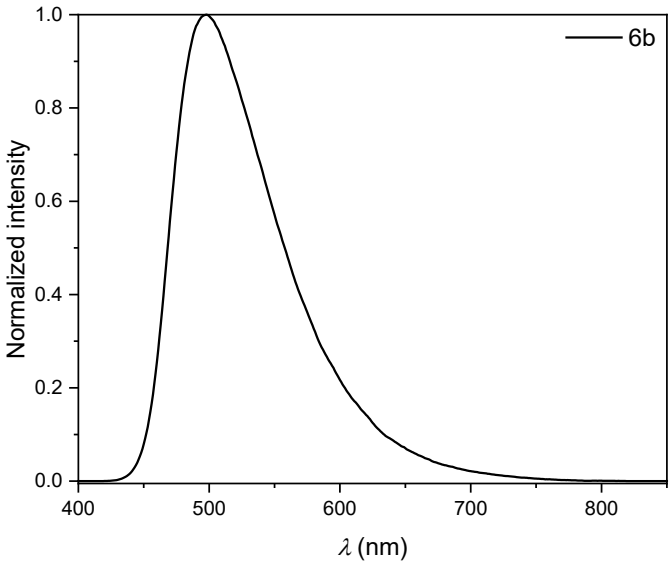

Figure S5.4.1: Normalized emission spectrum of **6b** in solid state at rt (λ_{exc} = 350.0 nm).

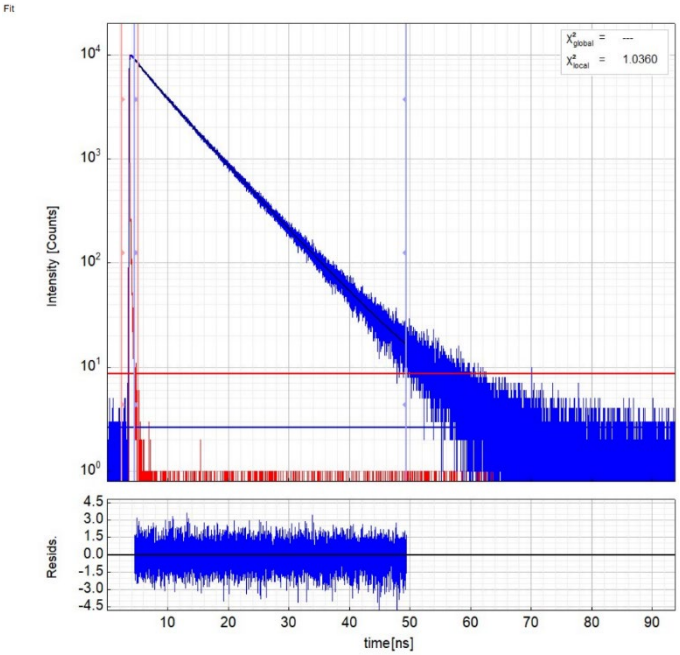

Parameter	Value	Δ
A_1[kCnts/Chnl]	8.40	±0.36
τ_1[ns]	7.161	±0.082
I_1[kCnts]	15 030	±480
A_{Rel1}[%]	79.1	±3.2
A_2[kCnts/Chnl]	2.23	±0.35
τ_2[ns]	3.80	±0.31
I_2[kCnts]	2 120	±500
A_{Rel2}[%]	21.0	±3.2
$Bkgr_{Dec}$[kCnts]	0.0027	±0.0007
$Bkgr_{IRF}$[Cnts/Chnl]	8.7	±3.7
$Shift_{IRF}$[ps]	46	±31
A_{Scatt}[kCnts]	- 350	±980
τ_{AvInt}[ns]	6.746	±0.014
τ_{AvAmp}[ns]	6.455	±0.024

Figure S5.4.2: Left - Raw (experimental) time-resolved photoluminescence decay (blue) of **6b** in solid state at rt including the residuals (λ_{exc} = 373.0 nm, λ_{det} = 500.0 nm) and the IRF (red). Right - Fitting parameters including pre-exponential factors and confidence limits.

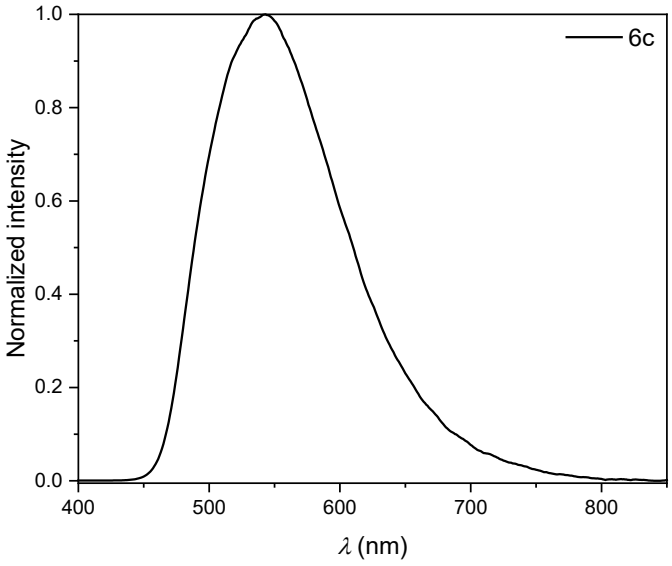

Figure S5.4.1: Normalized emission spectrum of **6c** in solid state at rt (λ_{exc} = 350.0 nm).

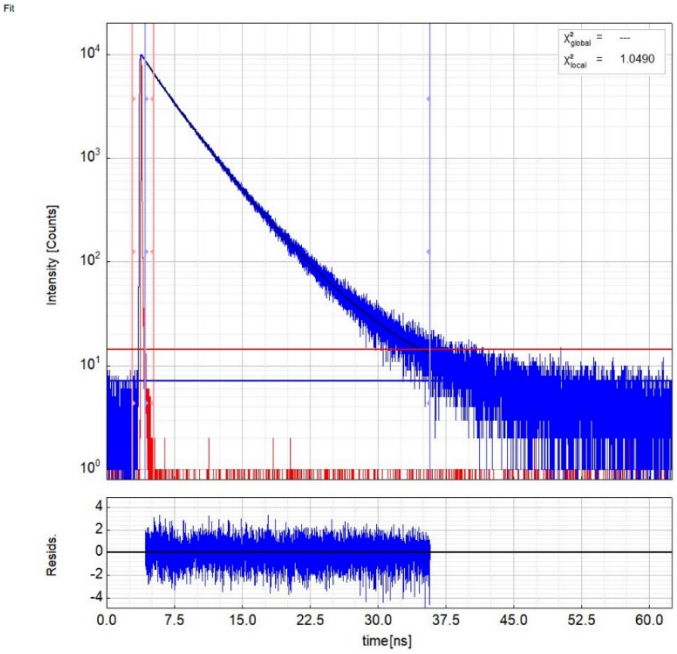

Parameter	Value	Δ
A_1[kCnts/Chnl]	7.12	±0.61
τ_1[ns]	3.00	±0.11
I_1[kCnts]	5 340	±650
A_{Rel1}[%]	70.1	±6.0
A_2[kCnts/Chnl]	3.04	±0.61
τ_2[ns]	5.14	±0.24
I_2[kCnts]	3 900	±610
A_{Rel2}[%]	30.0	±6.0
$Bkgr_{Dec}$[kCnts]	0.0072	±0.0009
$Bkgr_{IRF}$[Cnts/Chnl]	14.4	±2.5
$Shift_{IRF}$[ps]	162	±23
A_{Scatt}[kCnts]	- 340	±360
τ_{AvInt}[ns]	3.898	±0.016
τ_{AvAmp}[ns]	3.635	±0.017

Figure S5.4.2: Left - Raw (experimental) time-resolved photoluminescence decay (blue) of **6c** in solid state at rt including the residuals (λ_{exc} = 373.0 nm, λ_{det} = 650.0 nm) and the IRF (red). Right - Fitting parameters including pre-exponential factors and confidence limits.

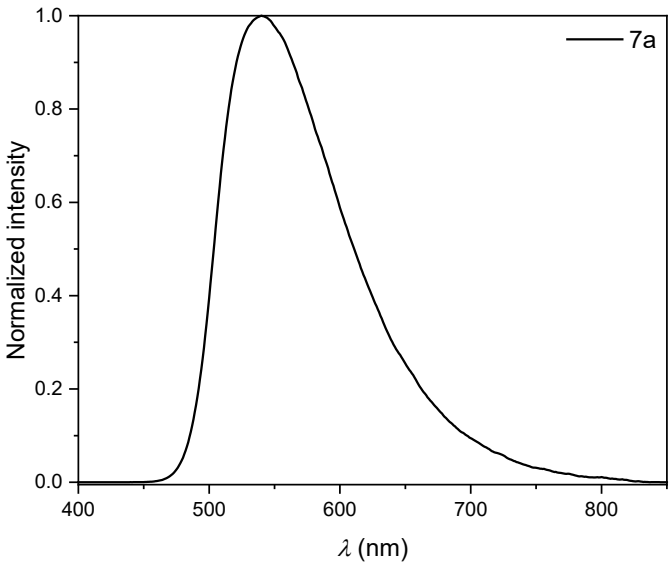

Figure S5.4.1: Normalized emission spectrum of **7a** in solid state at rt (λ_{exc} = 350.0 nm).

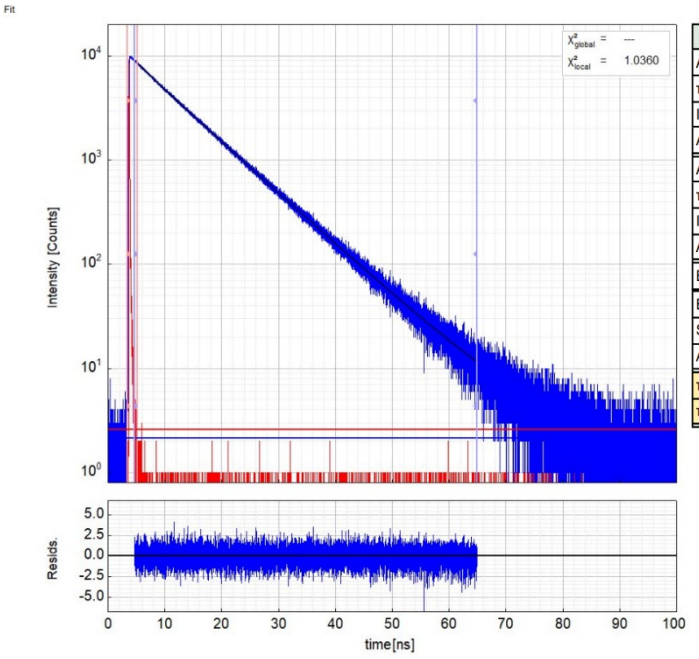

Parameter	Value	Δ
A_1[kCnts/Chnl]	9.37	±0.12
τ_1[ns]	8.871	±0.038
I_1[kCnts]	20 780	±190
A_{Rel1}[%]	92.0	±1.1
A_2[kCnts/Chnl]	0.83	±0.11
τ_2[ns]	3.87	±0.47
I_2[kCnts]	800	±220
A_{Rel2}[%]	8.1	±1.1
$Bkgr_{Dec}$[kCnts]	0.0022	±0.0004
$Bkgr_{IRF}$[Cnts/Chnl]	2.6	±2.5
$Shift_{IRF}$[ps]	75	±11
A_{Scatt}[kCnts]	-2 200	±2 800
τ_{AvInt}[ns]	8.6864	±0.0093
τ_{AvAmp}[ns]	8.467	±0.026

Figure S5.4.2: Left - Raw (experimental) time-resolved photoluminescence decay (blue) of **7a** in solid state at rt including the residuals (λ_{exc} = 373.0 nm, λ_{det} = 540.0 nm) and the IRF (red). Right - Fitting parameters including pre-exponential factors and confidence limits.

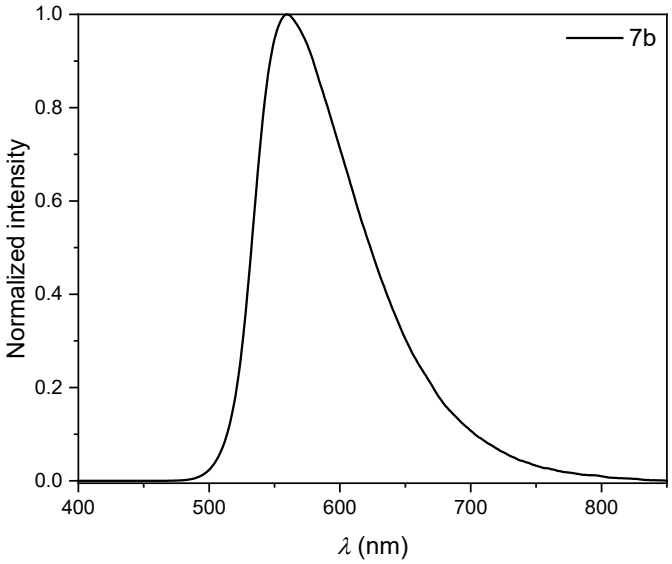

Figure S5.4.1: Normalized emission spectrum of **7b** in solid state at rt (λ_{exc} = 350.0 nm).

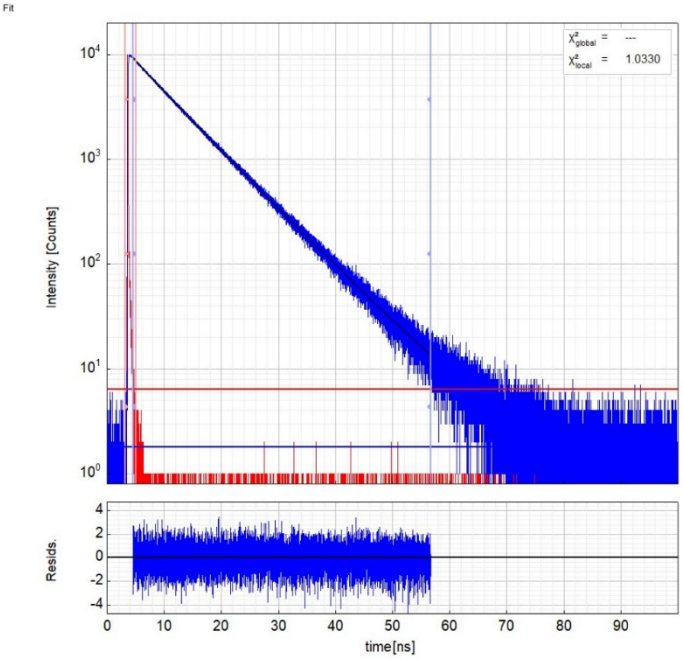

Parameter	Value	Δ
A_1[kCnts/Chnl]	9.39	±0.35
τ_1[ns]	7.965	±0.065
I_1[kCnts]	18 680	±570
A_{Rel1}[%]	88.0	±2.9
A_2[kCnts/Chnl]	1.29	±0.31
τ_2[ns]	4.52	±0.52
I_2[kCnts]	1 460	±490
A_{Rel2}[%]	12.1	±2.9
$Bkgr_{Dec}$[kCnts]	0.0019	±0.0005
$Bkgr_{IRF}$[Cnts/Chnl]	6.4	±6.3
$Shift_{IRF}$[ps]	- 101	±23
A_{Scatt}[kCnts]	1 200	±2 900
τ_{AvInt}[ns]	7.7157	±0.0092
τ_{AvAmp}[ns]	7.549	±0.018

Figure S5.4.2: Left - Raw (experimental) time-resolved photoluminescence decay (blue) of **7b** in solid state at rt including the residuals (λ_{exc} = 373.0 nm, λ_{det} = 560.0 nm) and the IRF (red). Right - Fitting parameters including pre-exponential factors and confidence limits.

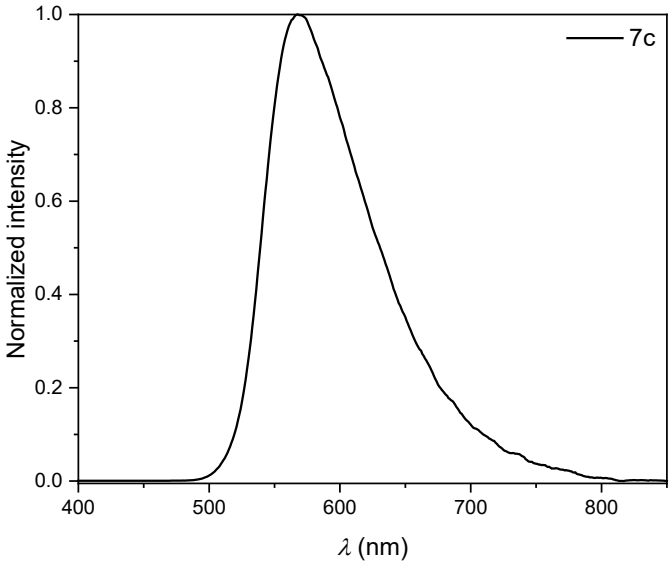

Figure S5.4.1: Normalized emission spectrum of **7c** in solid state at rt (λ_{exc} = 350.0 nm).

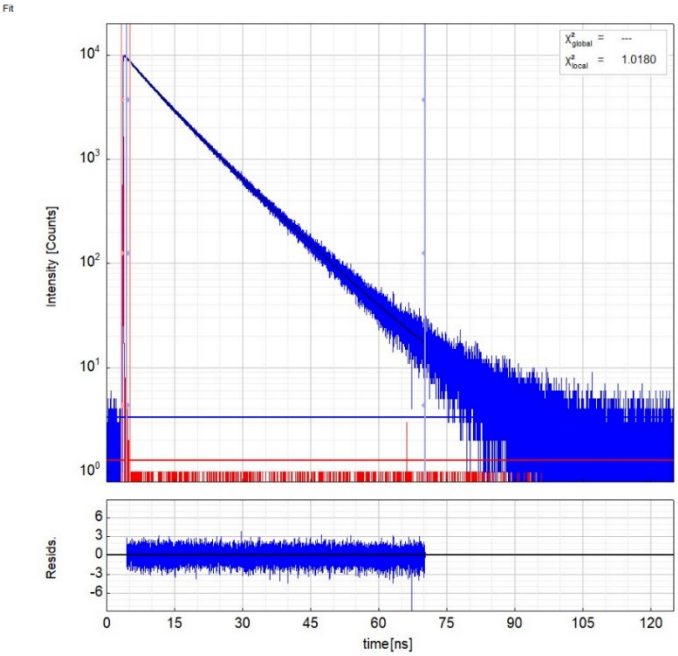

Parameter	Value	Δ
A_1[kCnts/Chnl]	7.11	±0.30
τ_1[ns]	10.68	±0.12
I_1[kCnts]	18 980	±600
A_{Rel1}[%]	69.1	±2.8
A_2[kCnts/Chnl]	3.19	±0.29
τ_2[ns]	5.93	±0.27
I_2[kCnts]	4 710	±620
A_{Rel2}[%]	31.0	±2.8
$Bkgr_{Dec}$[kCnts]	0.0034	±0.0006
$Bkgr_{IRF}$[Cnts/Chnl]	1.3	±1.3
$Shift_{IRF}$[ps]	-8.7	±9.7
A_{Scatt}[kCnts]	-3 100	±3 800
τ_{AvInt}[ns]	9.732	±0.016
τ_{AvAmp}[ns]	9.207	±0.022

Figure S5.4.2: Left - Raw (experimental) time-resolved photoluminescence decay (blue) of **7c** in solid state at rt including the residuals (λ_{exc} = 373.0 nm, λ_{det} = 570.0 nm) and the IRF (red). Right - Fitting parameters including pre-exponential factors and confidence limits.

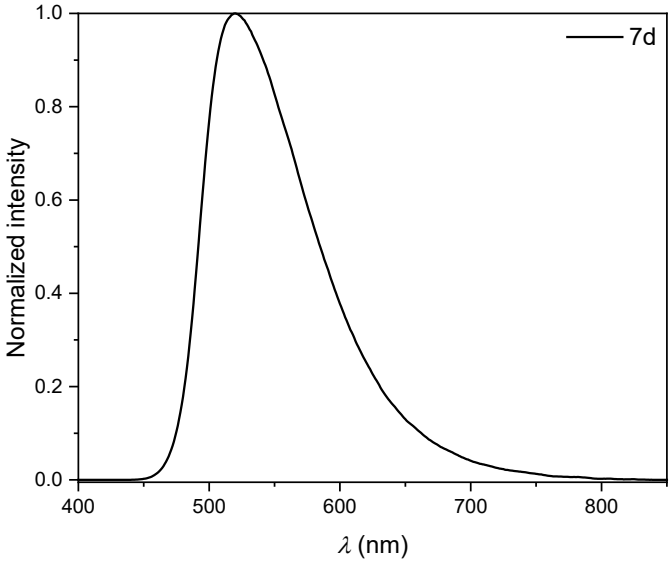

Figure S5.4.1: Normalized emission spectrum of **7d** in solid state at rt (λ_{exc} = 350.0 nm).

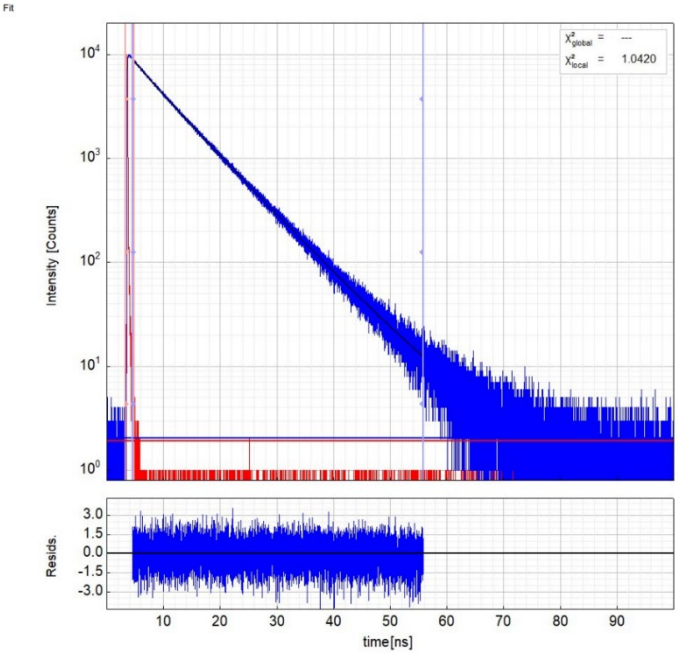

Parameter	Value	Δ
A_1[kCnts/Chnl]	8.44	±0.30
τ_1[ns]	7.795	±0.069
I_1[kCnts]	16 450	±440
A_{Rel1}[%]	81.7	±2.8
A_2[kCnts/Chnl]	1.90	±0.29
τ_2[ns]	4.15	±0.31
I_2[kCnts]	1 960	±440
A_{Rel2}[%]	18.4	±2.8
$Bkgr_{Dec}$[kCnts]	0.0021	±0.0005
$Bkgr_{IRF}$[Cnts/Chnl]	2.0	±2.6
$Shift_{IRF}$[ps]	-39.3	±7.4
A_{Scatt}[kCnts]	3 100	±3 300
τ_{AvInt}[ns]	7.407	±0.011
τ_{AvAmp}[ns]	7.127	±0.019

Figure S5.4.2: Left - Raw (experimental) time-resolved photoluminescence decay (blue) of **7d** in solid state at rt including the residuals (λ_{exc} = 373.0 nm, λ_{det} = 520.0 nm) and the IRF (red). Right - Fitting parameters including pre-exponential factors and confidence limits.

5.5 Solvatochromism

Table S5.5.1 Comparison of the solvent-dependent optical properties of phosphole oxides **3e**, **3g** and **6c** at rt.

Solvent	**3e**			**3g**			**6c**		
	λ_{abs} [nm][a]	λ_{em} [nm][b]	$\Delta\nu$ [cm^{-1}][c]	λ_{abs} [nm][a]	λ_{em} [nm][b]	$\Delta\nu$ [cm^{-1}][c]	λ_{abs} [nm][a]	λ_{em} [nm][b]	$\Delta\nu$ [cm^{-1}][c]
Cyclohexane	437	567	5266	422	552	5581	396	510	5645
THF	441	619	6529	426	599	6765	398	607	8651
CH_2Cl_2	446	641	6834	432	621	7023	399	624	9037
EtOH	449	670	7344	431	644	7674	401	649	9529
DMSO	450	686	7648	431	679	8473	400	n. d.[d]	n. d.[d]

[a] Absorption maxima of the highest wavelength, [b] excited at λ_{abs}, [c] STOKES-Shift (1/ λ_{abs}-1/ λ_{em}), [d] not detectable due to weak fluorescence.

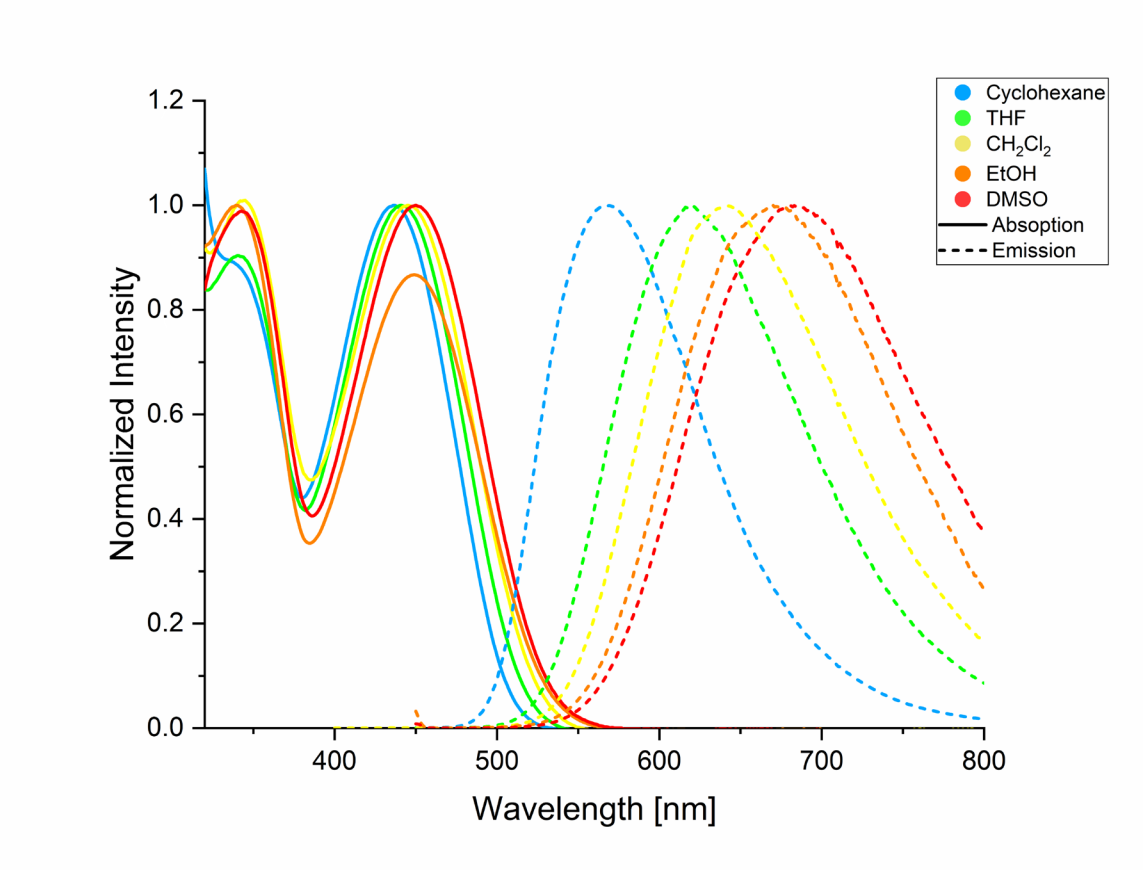

Figure S5.5.1 Absorption and emission spectra of compounds **3e** in selected solvents.

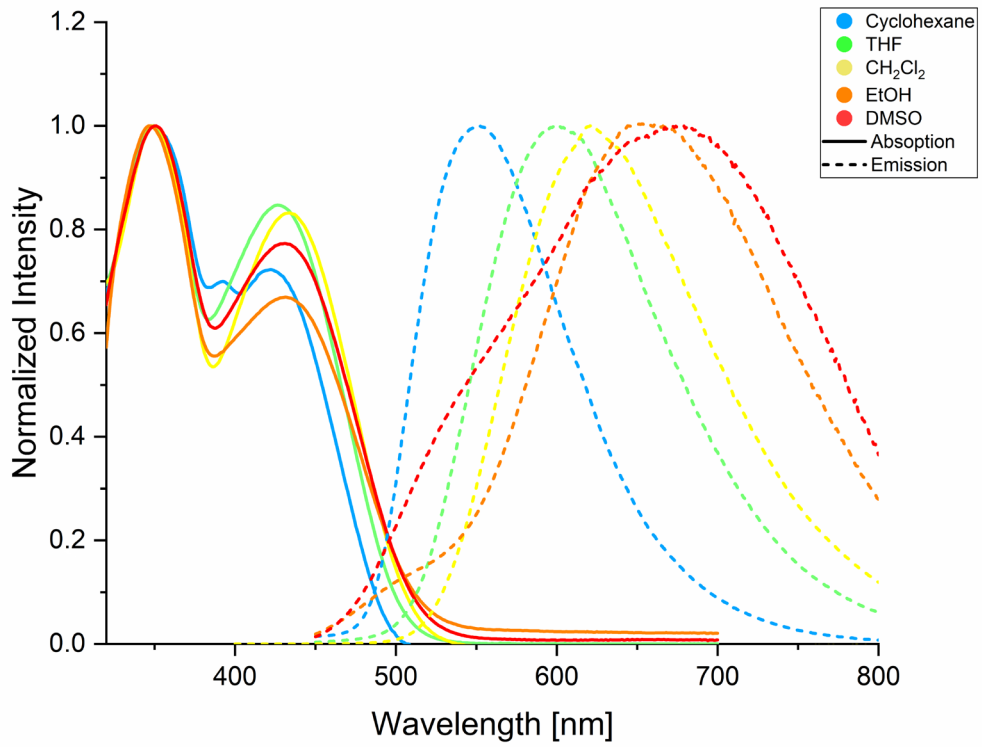

Figure S5.5.2 Absorption and emission spectra of compounds **3g** in selected solvents.

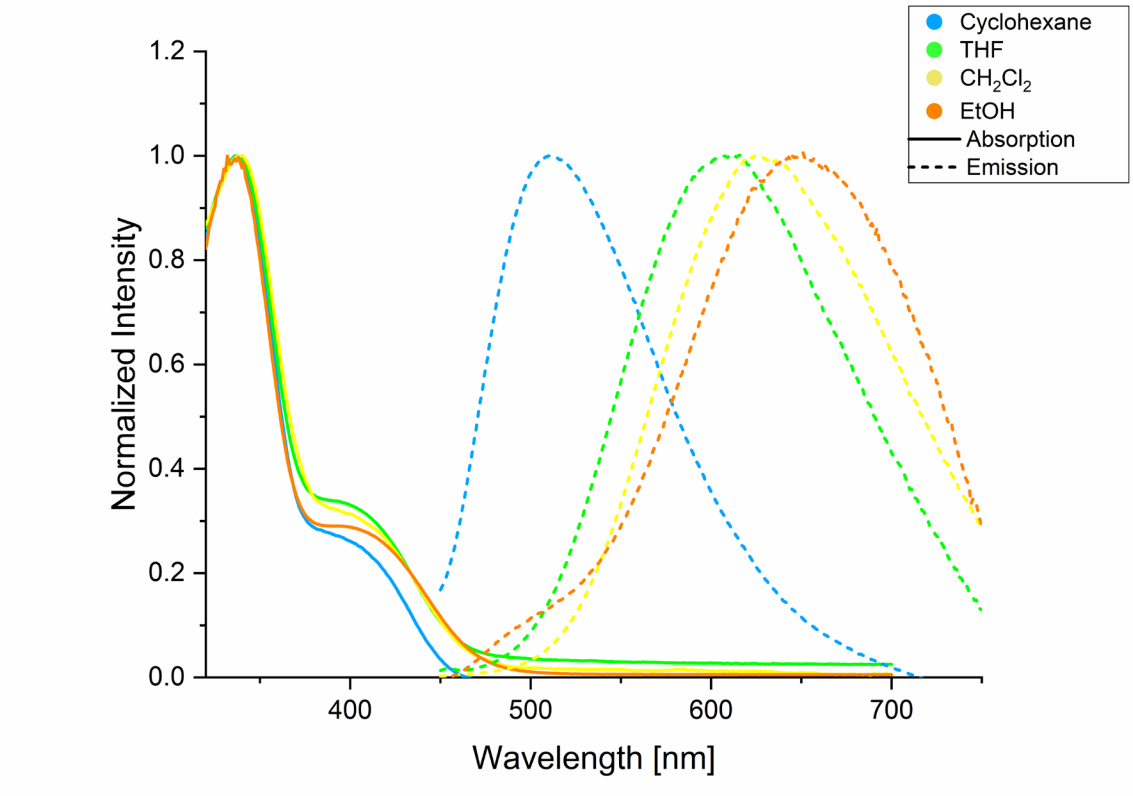

Figure S5.5.3 Absorption and emission spectra of compounds **6c** in selected solvents.

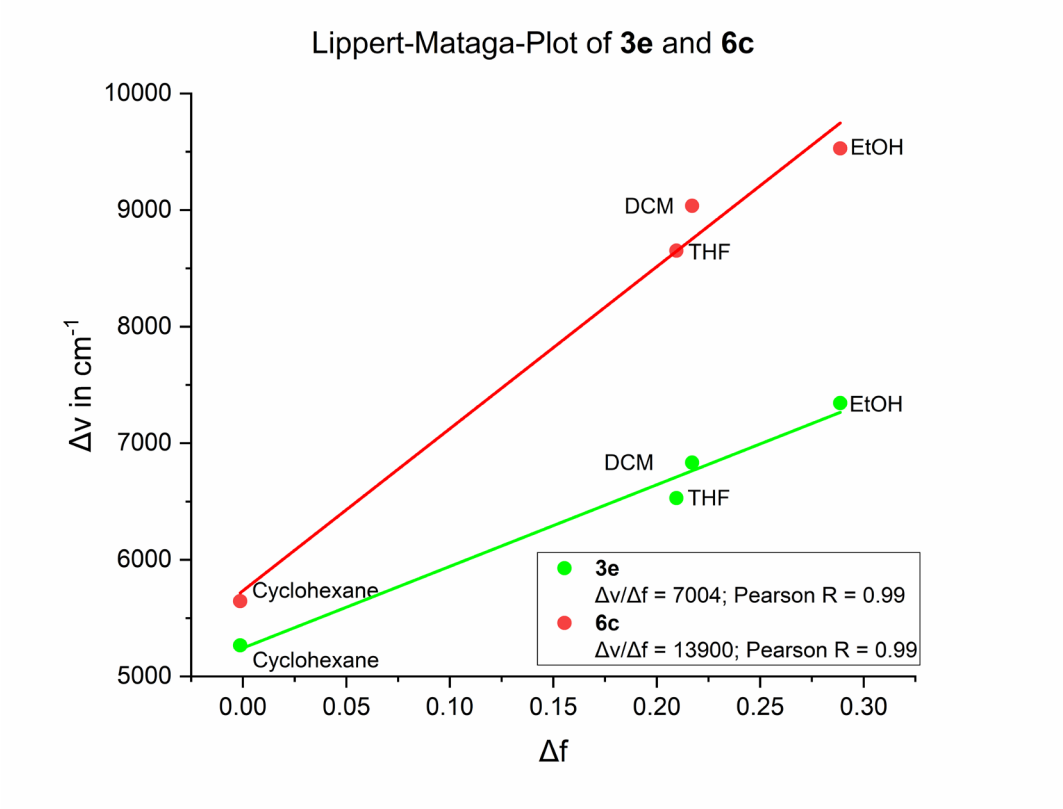

Figure S5.5.4 Lippert-Mataga-Plots of triphenylamine-substituted derivates **3e** and **6c**.

6 Theoretical Calculations

6.1 DFT Calculations

All structure optimizations have been carried out with the quantum mechanical package ORCA 5.0.4[12] using density functional theory. In order to cover for non-covalent interactions (NCI) the r^{2}SCAN-3c[13] functional has been used, incorporating a geometrical counterpoise correction[14] and Grimme's D4[15,16] dispersion correction. For all optimizations, the def2-mTZVPP basis set, the DEFGRID3 according to ORCA's radial grid scheme, as well as tight convergence criteria for optimization and SCF were used. The initial structures have been obtained from experimental crystal structures. The structures will be uploaded to Zenodo for a qualitative estimation of the NCI's the NCIPLOT4[17] program package has been used using a fine grid for the evaluation of the NCI's. For the visualization of molecular structures and orbital plots, an add-on for Blender has been used.[18] For an estimation of the $\pi-\pi$ stacking interactions the tosyl-group has been rotated, resulting in energetically higher conformers (Figure S6.1).

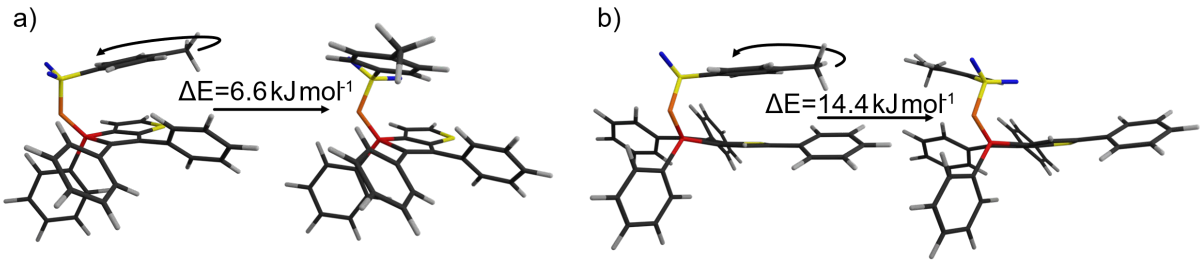

Figure S6.1 Schematic visualization of the rotation of compound a) **7a** and b) **7c.**

The disagreement between experimental and theoretical results (Table S6.1) can probably be deduced to the additional intermolecular interaction present in the experimental crystal data, whereas only intramolecular interactions are present in the gas phase calculations.

Table S6.1 Structural agreement between structure **7a** and **7c**. The angles are measured between the planes resulting from the marked cyclic rings in Figure S6.2 where the distances are marked as well.

		Experiment	R2SCAN-3c
7a	∡	17.26°	9.26°
	d_1	3.316	3.366
	d_2	3.851	3.698
7c	∡	15.87°	5.21°
	d_1	3.365	3.384
	d_2	3.702	3.763

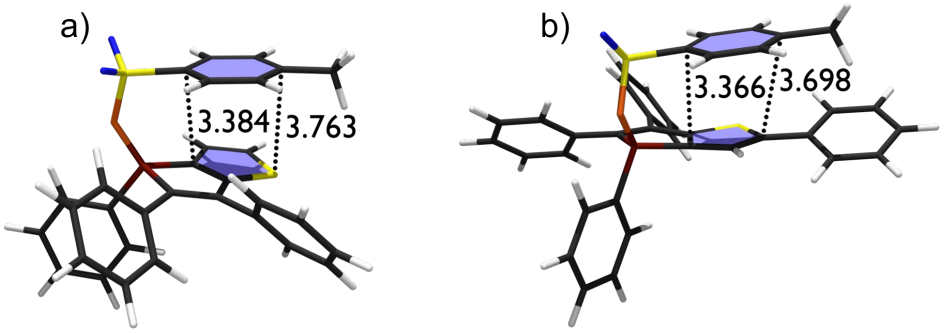

Figure S6.2 Distances shown in Table S6.1 for a) **7a** and b) **7c**. The angles shown in Table S6.1 are measured between the planes marked in blue.

6.2 TDDFT Calculations

The TDDFT calculations have also been carried out using ORCA 5.0.4. For the calculated UV-Vis spectra, ωB97x[19] with the def2-TZVPP basis[20], the def2/J auxiliary basis[21] has been utilized along with the D4 dispersion correction[22,23]. Additionally the CPCM solvation model[24] has been incorporated, employing implicit solvation in CH_2Cl_2.The spectra are obtained from applying a gaussian convolution of 5 nm to the absorption spectrum obtained using the transition electric dipole moments and normalizing the oscillator strength (f_{osc}) to 1. For showing the most relevant transitions, the natural transition orbitals have been plotted, as well as the transition densities.

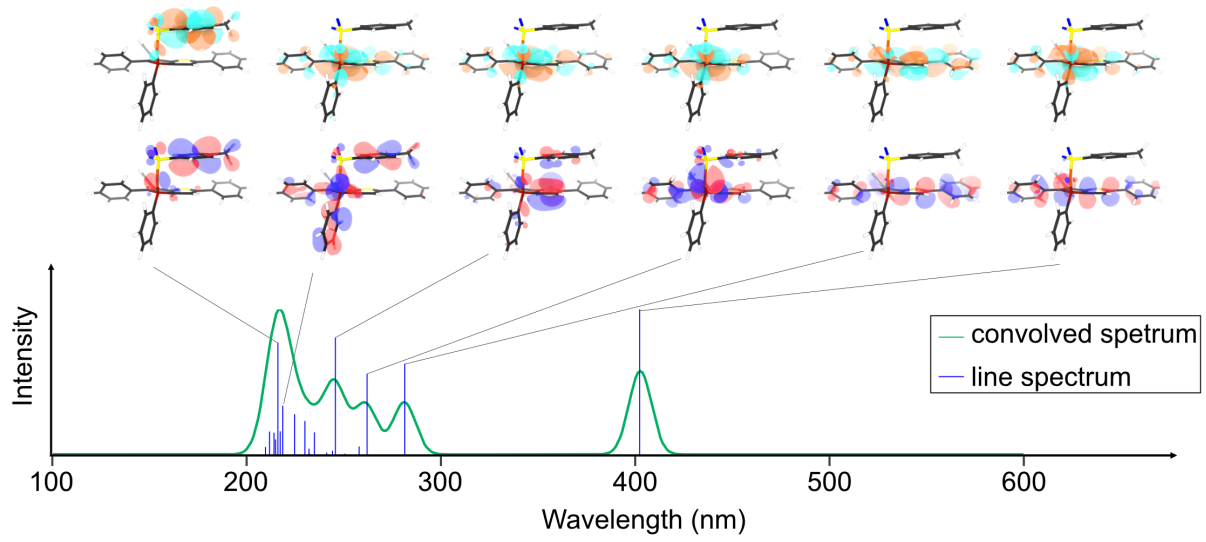

Figure S6.3 Calculated spectrum of **7c** using ωB97x-D4//R2SCAN3c. The natural transition orbitals corresponding to the absorbing state is shown above.

The calculated absorption spectrum for **7c** clearly shows that all major transitions observed result from π→π*. The largest oscillator strength is observed for the π→π* at 402 nm. The absorption nicely agrees with the excitation using blue light.

References

[1] W.-Q. Liu, T. Lei, S. Zhou, X.-L. Yang, J. Li, B. Chen, J. Sivaguru, C.-H. Tung, L.-Z. Wu, *J. Am. Chem. Soc.* **2019**, *141*, 13941–13947.
[2] N. König, Y. Godínez-Loyola, H. Weiske, S. Naumov, P. Lönnecke, R. Tonner-Zech, C. A. Strassert, E. Hey-Hawkins, *Chem. Mater.* **2023**, DOI 10.1021/acs.chemmater.3c01734.
[3] Y.-R. Chen, W.-L. Duan, *J. Am. Chem. Soc.* **2013**, *135*, 16754–16757.
[4] Y. Unoh, K. Hirano, T. Satoh, M. Miura, *Angew. Chem. Int. Ed.* **2013**, *52*, 12975–12979.
[5] N. König, Y. Godínez-Loyola, F. Yang, C. Laube, M. Laue, P. Lönnecke, C. A. Strassert, E. Hey-Hawkins, *Chem. Sci.* **2023**, *14*, 2267–2274.
[6] R. K. Harris, E. D. Becker, S. M. Cabral de Menezes, R. Goodfellow, P. Granger, *Solid State Nucl. Magn. Reson.* **2002**, *22*, 458–483.
[7] Rigaku Oxford Diffraction, CrysAlisPro Software system, Rigaku Corporation, Wroclaw, Poland, **1995-2023**.
[8] G. M. Sheldrick, *Acta Crystallogr. Sect. A Found. Adv.* **2015**, *71*, 3–8.
[9] G. M. Sheldrick, *Acta Crystallogr. Sect. C Struct. Chem.* **2015**, *71*, 3–8.
[10] DIAMOND 4: K. Brandenburg, Version 4.6.8, Crystal Impact GbR, Bonn, Germany, **2022**.
[11] A. Sillen, Y. Engelborghs, *Photochem. Photobiol.* **1998**, *67*, 475–486.
[12] F. Neese, *WIREs Comput. Mol. Sci.* **2022**, *12*, e1606.
[13] S. Grimme, A. Hansen, S. Ehlert, J.-M. Mewes, *J. Chem. Phys.* **2021**, *154*, 064103.
[14] H. Kruse, S. Grimme, *J. Chem. Phys.* **2012**, *136*, 154101.
[15] E. Caldeweyher, C. Bannwarth, S. Grimme, *J. Chem. Phys.* **2017**, *147*, 034112.
[16] E. Caldeweyher, S. Ehlert, A. Hansen, H. Neugebauer, S. Spicher, C. Bannwarth, S. Grimme, *J. Chem. Phys.* **2019**, *150*, 154122.
[17] J. Contreras-García, E. R. Johnson, S. Keinan, R. Chaudret, J.-P. Piquemal, D. N. Beratan, W. Yang, *J. Chem. Theory Comput.* **2011**, *7*, 625–632.
[18] H. Weiske, P. Melix, F. Thiemann, **2024**, DOI 10.5281/ZENODO.10776697.
[19] J.-D. Chai, M. Head-Gordon, *J. Chem. Phys.* **2008**, *128*, DOI 10.1063/1.2834918.
[20] F. Weigend, R. Ahlrichs, *Phys. Chem. Chem. Phys.* **2005**, *7*, 3297–3305.
[21] F. Weigend, *Phys. Chem. Chem. Phys.* **2006**, *8*, 1057.
[22] E. Caldeweyher, S. Ehlert, A. Hansen, H. Neugebauer, S. Spicher, C. Bannwarth, S. Grimme, *J. Chem. Phys.* **2019**, *150*, 154122.
[23] E. Caldeweyher, C. Bannwarth, S. Grimme, *J. Chem. Phys.* **2017**, *147*, 034112.
[24] V. Barone, M. Cossi, *J. Phys. Chem. A* **1998**, *102*, 1995–2001.